NASA Contractor Report 3311

Rotary Balance Data for a Single-Engine Agricultural Airplane Configuration for an Angle-of-Attack Range of 8° to 90°

William Mulcay and Julio Chu

NASA

NASA Contractor Report 3311

Rotary Balance Data for a Single-Engine Agricultural Airplane Configuration for an Angle-of-Attack Range of 8° to 90°

William Mulcay and Julio Chu
Bihrle Applied Research, Inc.
Jericho, New York

NASA

National Aeronautics
and Space Administration

**Scientific and Technical
Information Branch**

1980

SUMMARY

Aerodynamic characteristics obtained in a helical flow envi-
ronment utilizing a rotary balance located in the Langley spin
tunnel are presented in plotted form for a 1/10-scale, single-
engine agricultural airplane model. The configurations tested
include the basic airplane, various wing leading-edge and wing-
tip devices, elevator, aileron and rudder control settings, and
other modifications. Data are presented without analysis for an
angle-of-attack range of 8° to 90°, and clockwise and counter-
clockwise rotations covering an $\frac{\Omega b}{2V}$ range from 0 to .9. This in-
formation is being obtained, along with that of other models, in
order to establish a data base for analysis of the model and full-
scale flight results, and to develop design charts for desirable
stall/spin characteristics.

INTRODUCTION

A wind-tunnel rotary balance measures forces and moments
acting on an airplane model while subjecting it to steady, though
not necessarily equilibrium, spin flow conditions. The need for
these data was recognized early in aircraft development. For ex-
ample, early researchers noted in 1928 that the use of "straight"
force tests conduce to erroneous conclusions when applied to the
spin. NACA investigators at that time developed a "spinning"
balance installed in a 5-foot vertical tunnel; they reasoned that
subjecting all portions of an aircraft model to a constant wind
velocity vector during static force tests was an unsatisfactory
simulation of flow conditions existing in a spin.

In recent years, NASA installed a rotary balance apparatus
in the Langley full-scale tunnel and sponsored studies to deter-
mine the ability of current analytical techniques to compute the

flight motions of current fighter configurations. Again, these studies clearly demonstrated the need to model the effects of spin rotation rate on the aerodynamic characteristics in all phases of the spinning motion. This concern is certainly warranted in the case of the high $\frac{\Omega b}{2V}$ (non-dimensionalized spin rate) values of today's general aviation airplane designs.

These values are high due to high rates of rotation and low rates of descent for low wing-loaded vehicles. Hence, a difference of up to 90° in angle of attack between wing tips and 70° in sideslip angle between nose and tail can be realized.

The NASA Langley Research Center has initiated a broad, general aviation stall/spin research program which includes spin tunnel and free-flight radio control model tests for a number of configurations typical of light, general aviation airplanes. To support these free-flight investigations, a rotary balance facility was developed in the Langley spin tunnel to rapidly identify an airplane's aerodynamic characteristics in a steady spin flow environment. The influence of spin radius, angle of attack, sideslip angle, rate of rotation and control settings on the aerodynamics can be measured, thereby permitting prediction of incipient and developed spin characteristics.

A 1/10-scale, single-engine agricultural airplane model was tested on the wind tunnel rotary balance in the NASA Langley 20-ft. spin tunnel. This report presents the data obtained for the basic configuration, various wing leading-edge and wing-tip devices, elevator, aileron and rudder control settings and other modifications.

SYMBOLS

The units for physical quantities used herein are presented in the International System of Units (SI) and U.S. Customary Units. The measurements were made in the U.S. Customary Units; equivalent dimensions were determined by using the conversion factors given in reference 1.

b	wing span, m (ft)
$\bar{c}$	mean aerodynamic chord, cm (in.)
C_L	lift-force coefficient, $\dfrac{\text{Lift force}}{qS}$
C_N	normal-force coefficient, $\dfrac{\text{Normal force}}{qS}$
C_A	axial-force coefficient, $\dfrac{\text{Axial force}}{qS}$
C_Y	side-force coefficient, $\dfrac{\text{Side force}}{qS}$
C_ℓ	rolling moment coefficient, $\dfrac{\text{Rolling moment}}{qSb}$
C_m	pitching-moment coefficient, $\dfrac{\text{Pitching moment}}{qS\bar{c}}$
C_n	yawing-moment coefficient, $\dfrac{\text{Yawing moment}}{qSb}$
q	free-stream dynamic pressure, N/m^2 (lb/ft^2)
S	wing area, m^2 (ft^2)
V	free-stream velocity, m/sec (ft/sec)
α	angle of attack, deg
β	angle of sideslip, deg
Ω	angular velocity about spin axis, rad/sec
$\dfrac{\Omega b}{2V}$	spin coefficient, positive for clockwise spin
δ_a	aileron deflection, positive when right aileron is down $(\delta_{a_{\text{right}}} - \delta_{a_{\text{left}}})/2$, deg
δ_e	elevator deflection, positive when trailing edge is down, deg
δ_r	rudder deflection, positive when trailing edge is to left, deg

Abbreviations:

cg   center of gravity

LE   leading edge

SR   spin radius

TEST EQUIPMENT

A photograph and sketch of the rotary balance apparatus installed in the Langley 20-Foot Spin Tunnel are shown in figures 1 and 2, respectively. The arm of the balance system rotates about a vertical axis and is mounted on the free end of a horizontal supporting boom, which is hinged at the wall. It is moved from the wall to the center of the tunnel by cables, secured, and then driven by a drive shaft through couplings and gears.

A test model is mounted on a strain gauge balance which is affixed to the bottom of the rotary balance apparatus. Controls located outside the tunnel are used to activate motors on the rig, which position the model to the desired attitude. The angle-of-attack range of the rig is 8 to 90 degrees, and the sideslip angle range is ±15 degrees. The spin radius and lateral displacement motors allow the operator to position the moment center of the balance on the spin axis or at a specific distance from the spin axis. This is done for each combination of angle of attack and sideslip angle. The NASA six-component strain gauge balance mounted inside the model measures the normal, axial, and side forces, and the yawing, rolling, and pitching moments acting about the model body axis. Interactions among the six components are available from previous laboratory calibration tests and are used to correct the raw forces and moments output by the balance strain gauge transducers. For the data presented herein and the practice generally, the force and moment axes of the balance are mounted coincident with the body axes of the air-

plane, with the moment center at the cg location about which
the aerodynamic moments are desired. Electrical current to
and from the balance and to the positioning motors on the rig,
and position-indicating potentiometer voltages are conducted
through slip rings located at the rig head. Examples of how
the rig is positioned for different angles of attack and side-
slip angles are shown in figures 2a and 2b, respectively.

The model can be rotated up to 90 rpm in either direction.
By using different rotational speeds and a specific airflow in
the tunnel, the motions of an airplane in a steady spin can be
simulated. The aerodynamic forces and moments can be measured
at different values of $\frac{\Omega b}{2V}$, including the case of $\frac{\Omega b}{2V} = 0$, where
static aerodynamic data are obtained.

Additional background for this apparatus is given in
reference 2.

The data acquisition, reduction and presentation system for
the rotary balance set-up includes an RPM indicator, a 12-channel
scanner/voltmeter with a 14-bit variable gain analog to digital
converter, and a mini-computer with graphics and a printer. With
this equipment, immediate presentation of data in tabular and/or
plotted form is possible.

TEST PROCEDURES

Rotary aerodynamic data are obtained in two steps. First,
the inertial forces and moments (tares) acting on the model at
different attitudes and rotational speeds are measured. To accom-
plish this, a covered bird cage like structure, which encloses
the model without touching it, is mounted on the upper portion
of the rig and rotates with the model. In this manner, the air
immediately surrounding the model is trapped by the structure
and constrained to rotate with it. As the rig is rotated at the
desired attitude and rate, a pulse voltage from a magnetic

trigger device on the drive shaft begins the data sampling
process. Eighty samples of the 6 balance output channels are
taken over 10 revolutions, with the computer adjusting the
timing, according to the RPM indicator, to sample at 8 fixed
angular positions of the rotating rig. The inertial forces
and moments thus measured are curve-fitted to a least-squares
function of $\frac{\Omega^2}{100}$ and stored for later use on magnetic tape.

For the second step, the covered structure enclosing the
model is removed and the total wind-on forces and moments are
measured. The aerodynamic forces and moments are determined by
subtracting the tare values from the total wind-on values at
each tested RPM and angle of attack. The aerodynamic data are
converted to coefficient form and stored on magnetic tape.

MODEL

A 1/10-scale fiberglass-epoxy, wood and aluminum model of
a typical single-engine configuration used for agricultural pur-
poses was tested in the present study. A three-view drawing of
this model is shown in figure 3, dimensional characteristics of
the model are presented in Table I, and a photograph of the model
installed on the rotary balance located in the Langley 20-Foot
Spin Tunnel is presented in figure 1.

The model was fabricated such that various modifications
could be added. These consisted of a turbine nose, as shown in
figure 4; canopy fairing and a wing-fuselage fillet, shown in
figure 5; an outboard leading-edge wing droop, shown in figure 6;
and a full span leading-edge wing slot, shown in figure 7. In
addition, several wing-tip modifications designed to alter the
characteristics of wing-tip vortex flow were tested. These
consisted of winglets, wing-tip sails and Lockheed Vortex Diffuser
Vanes, as shown in figures 8 and 9. The Lockheed Vortex Diffuser
Vane is patented by the Lockheed-Georgia Aircraft Company.

The model control surfaces could be fixed at any position prior to the test. The maximum deflections for the control surfaces were:

Elevator, deg	27 up, 17 down
Rudder, deg	24 right, 24 left
Aileron, deg	21 up, 17 down

TEST CONDITIONS

The tests were conducted in the spin tunnel at a tunnel velocity of 7.62 m/sec (25ft/sec), which corresponds to a Reynolds number of approximately 120,000 based on the model mean aerodynamic chord. Unless otherwise noted in Table II, all the configurations were tested through an angle-of-attack range of 8 to 35°, with the spin axis in the plane of symmetry of the aircraft at a full-scale distance 152.4 cm (60 in.) forward of the cg location of .26$\bar{c}$. In addition, for some configurations, data were obtained for angles of attack between 30 and 90°, with the spin axis through the cg location. Data were thus obtained at two spin radii for angles of attack of 30 and 35 degrees. At each spin attitude, measurements were obtained for nominal $\frac{\Omega b}{2V}$ values of .1, .2, .3, .4, .5, .6, .7, .8, and .9, in both clockwise and counter-clockwise directions, as well as for $\frac{\Omega b}{2V} = 0$ (static value).

DATA PRESENTATION

Table II identifies the configurations tested and the corresponding appendix figure numbers which present the aerodynamic data. The aerodynamic coefficients plotted vs. $\frac{\Omega b}{2V}$ are presented for each configuration in six sequentially numbered figures in the following order: C_n, C_ℓ, C_m, C_N, C_Y, and C_A. Each figure consists of two pages, which present the subject

aerodynamic coefficient plotted vs $\frac{\Omega b}{2V}$ for the following angles of attack and spin radius:

    a) α = 8, 10, 12, 14, 16 deg   SR = 152.4 cm (60 in.)

    b) α = 18, 20, 25, 30, 35 deg   SR = 152.4 cm (60 in.)

and, in addition, for some configurations noted in Table II:

    c) α = 30, 35, 40, 45, 50 deg   SR = 0

    d) α = 55, 60, 70, 80, 90 deg   SR = 0

All the moment data are presented for a cg location of .26$\bar{c}$.

Lift coefficient plotted vs angle of attack for zero rotation rate is presented in the Appendix for several configurations cited in Table II.

REFERENCES

1. Mechtly, E.A.: The International System of Units - Physical Constants and Conversion Factors. NASA SP-7012, 1973.

2. Bihrle, William, Jr.; Hultberg, Randy S.; and Mulcay, William: Rotary Balance Data for a Typical Single-Engine Low-Wing General Aviation Design for an Angle-of-Attack Range of 30° to 90°. NASA CR-2972, 1978.

TABLE I.- DIMENSIONAL CHARACTERISTICS OF THE BASIC MODEL

Overall length, m (ft) 89 (2.92)

Wing:

    Span, m (ft) 1.35 (4.43)

    Area, m^2 (ft^2) 304 (3.27)

    Root chord, cm (in.). 22.9 (9.0)

    Tip chord, cm (in.) 22.9 (9.0)

    Mean aerodynamic chord, cm (in.). 22.9 (9.0)

    Aspect ratio 6.0

    Dihedral, deg 3.5

    Incidence:

      Root, deg 2.07

      Tip (of constant chord section), deg . . . 0.39

    Airfoil section . . . . NACA 4412

Horizontal tail:

    Span, m (ft) 49 (1.60)

    Area, m^2 (ft^2) . . . . .050 (.54)

    Incidence, deg . . . . -1.55

    Airfoil Section . . . . Flat plate

Vertical tail:

    Area, m^2 (ft^2) . . . . .021 (.222)

    Airfoil section . . . . Flat plate

TABLE II.- CONFIGURATIONS TESTED AND FIGURE INDEX

(Unless noted otherwise, all configurations tested through $\alpha=8$ to $35°$ at SR=152.4 cm (60 in.) and $\beta=0°$.)

FIGURE NO	CONFIGURATION	δ_e deg	δ_a deg	δ_r deg	REMARKS
a,b,c A1-A6	Basic	0	0	0	also $\alpha=30$ to $90°$ at SR=0
A7-A12		17		-24	
A12-A18		-27			
A19-A24			+19		
A25-A30			-19		
A31-A36	Turbine nose	0	0	0	also $\alpha=30$ to $90°$ at SR=0
A37-A42	Canopy fairing				
c A43-A48	Wing-fuselage fillet				
c A49-A54	with outboard LE wing droop				also $\alpha=30$ to $90°$ at SR=0
c A55-A60	with outboard LE wing slat				
a A61-A66	Full-span wing slat				
a A67-A72	Segmented wing slat				
b A73-A78	Winglets				
b A79-A84	Wing tip sails				
b A85-A90	Lockheed Vortex Diffuser Vanes				

a C_L vs. α presented in figure A91.

b C_L vs. α presented in figure A92.

c C_L vs. α presented in figure A93.
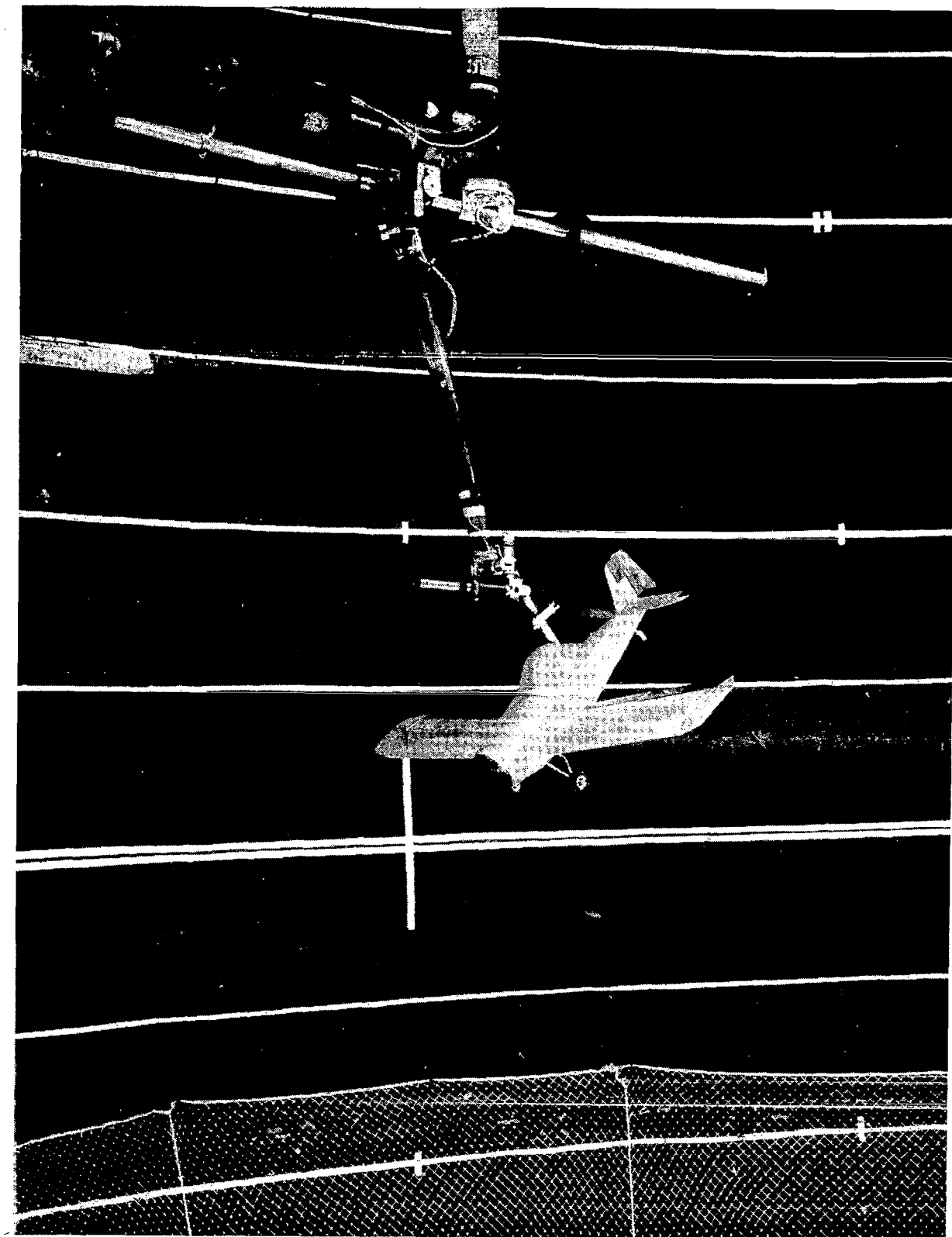
12   Figure 1. - 1/10 - scale model installed on rotary balance apparatus.

A Slip ring housing
B Spin radius offset
   potentiometer
C Lateral offset
   drive gears
D Lateral offset
   potentiometer
E Strut
F Sideslip angle
   potentiometer
G Sideslip angle
   positioning motor

Spin axis

Velocity vector

(b) Front view of model.

Figure 2.- Concluded.

13

A Slip ring housing
B Drive shaft
C Support boom
D Spin radius offset
   potentiometer
E Counterweight
F Strut
G Angle of attack
   positioning motor

Spin axis

Velocity vector

(a) Side view of model.

Figure 2.- Sketch of rotary balance apparatus.
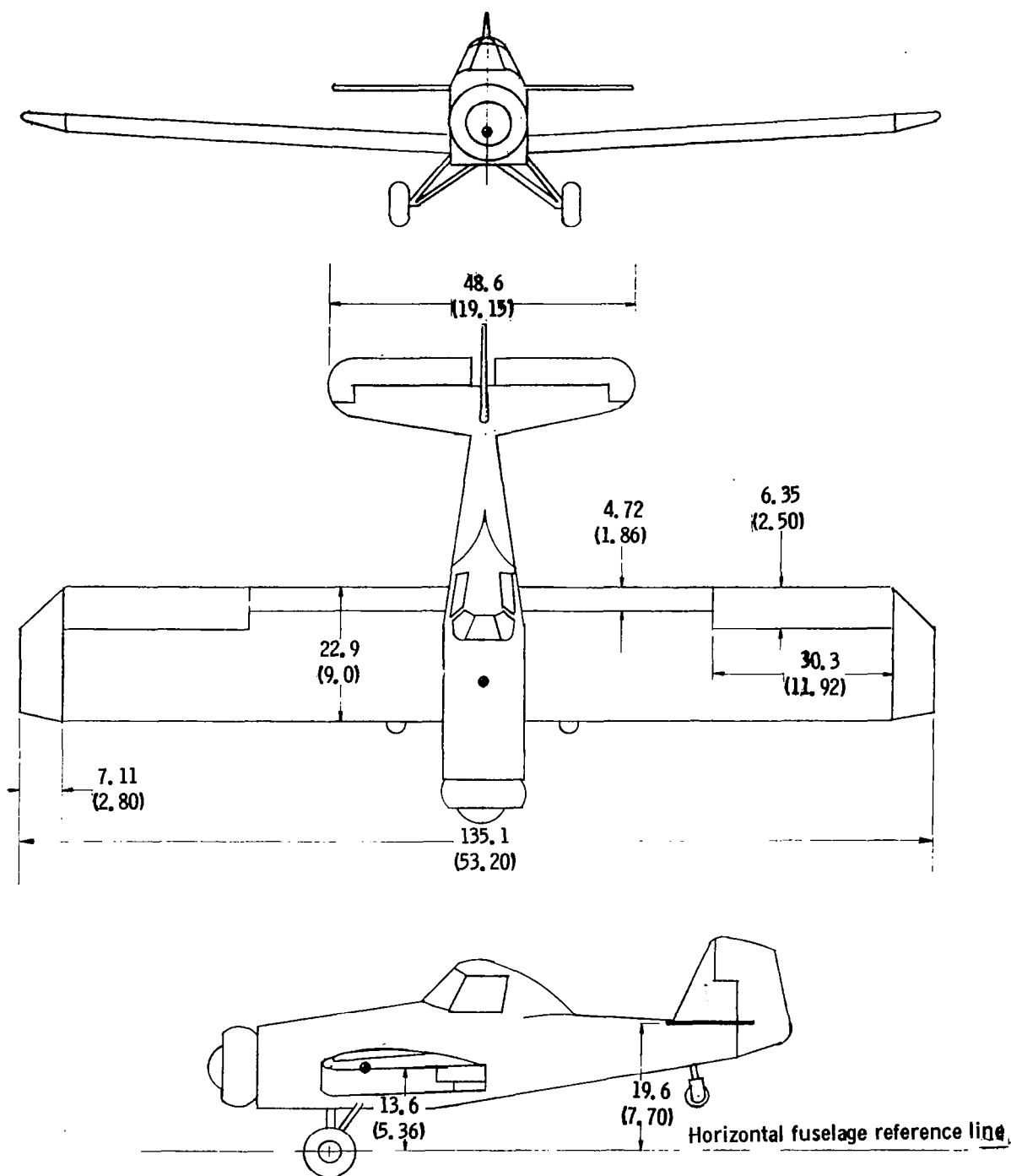
Figure 3. – Three-view of 1/10 – scale basic configuration. Center of gravity positioned at 0.26$\bar{c}$. Dimensions are given in centimeters (inches), model scale.

31.2
(12.28)

.56
(.22)
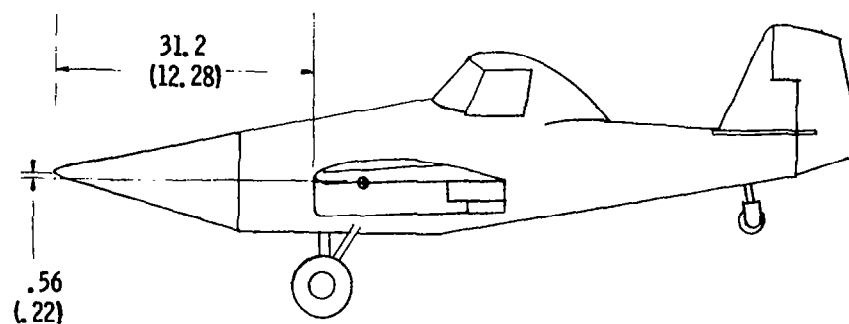
Figure 4. - Turbine nose tested on model. Dimensions are given in centimeters (inches), model scale.
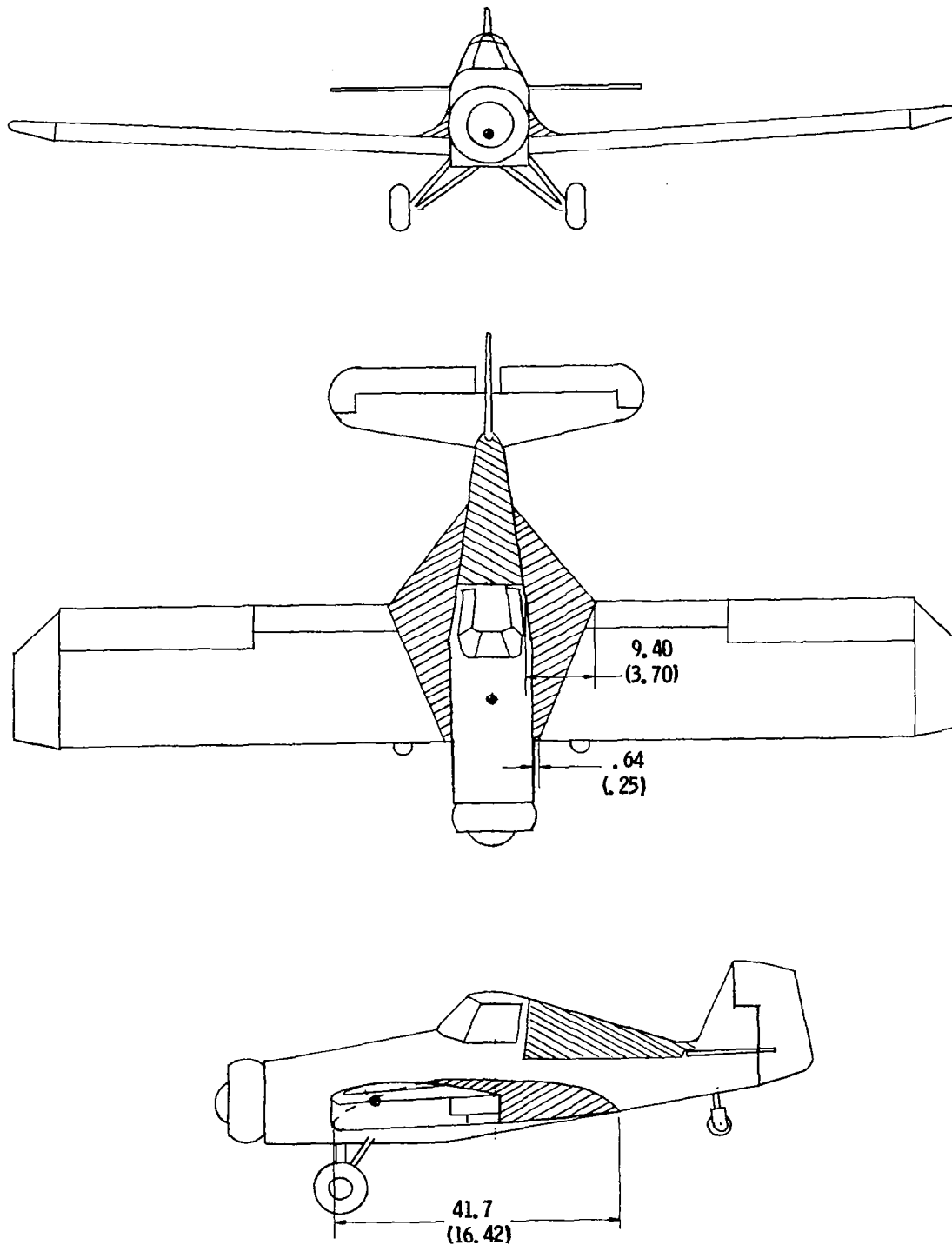
Figure 5. – Canopy fairing and wing-fuselage fillet tested on model.   Dimensions are given in centimeters(inches), model scale.

Fuselage centerline

Wing chord line

26.7
(10.5)

26.7
(10.5)

.03C
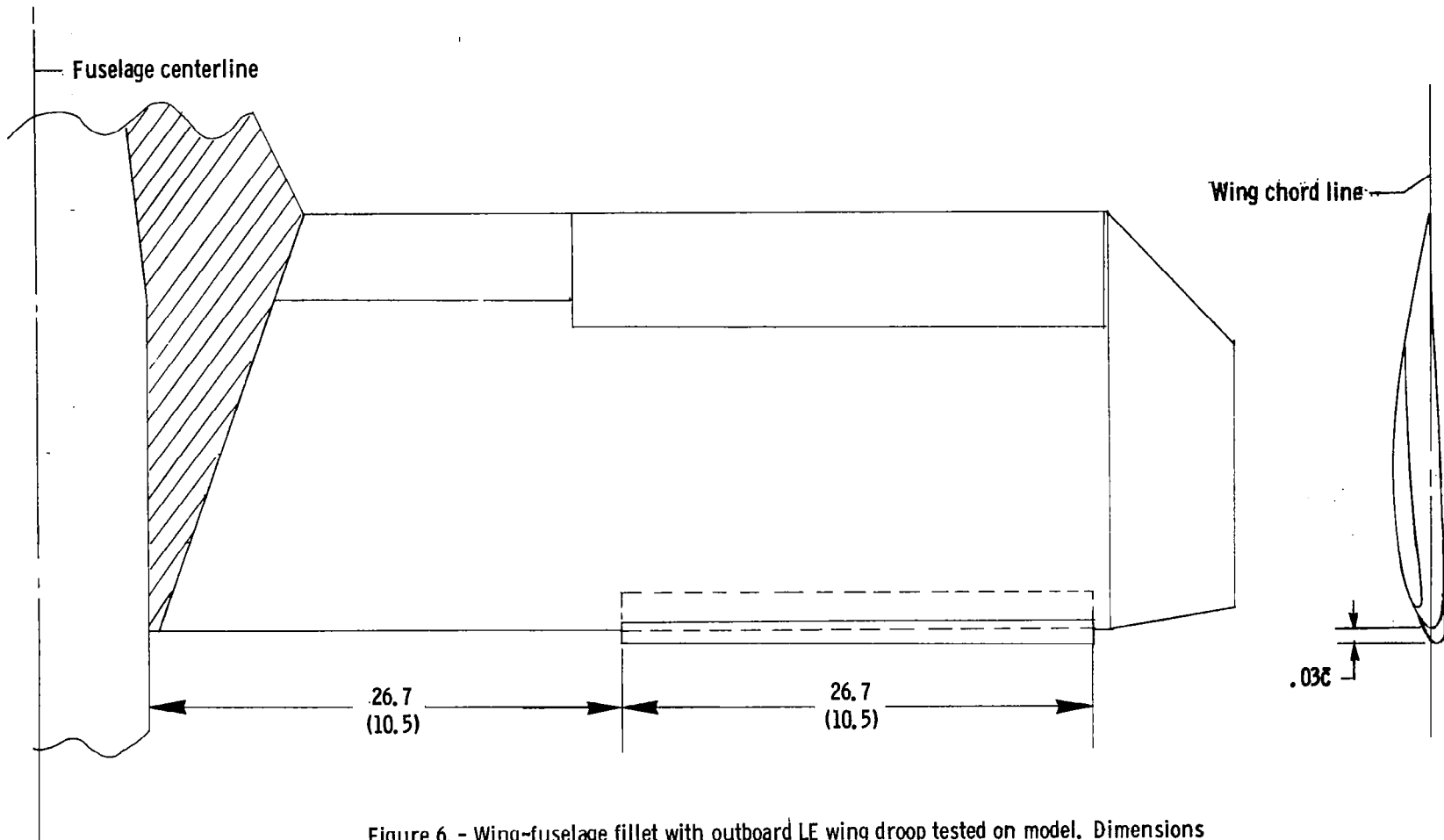
Figure 6. – Wing-fuselage fillet with outboard LE wing droop tested on model. Dimensions
are given in centimeters (inches), model scale.
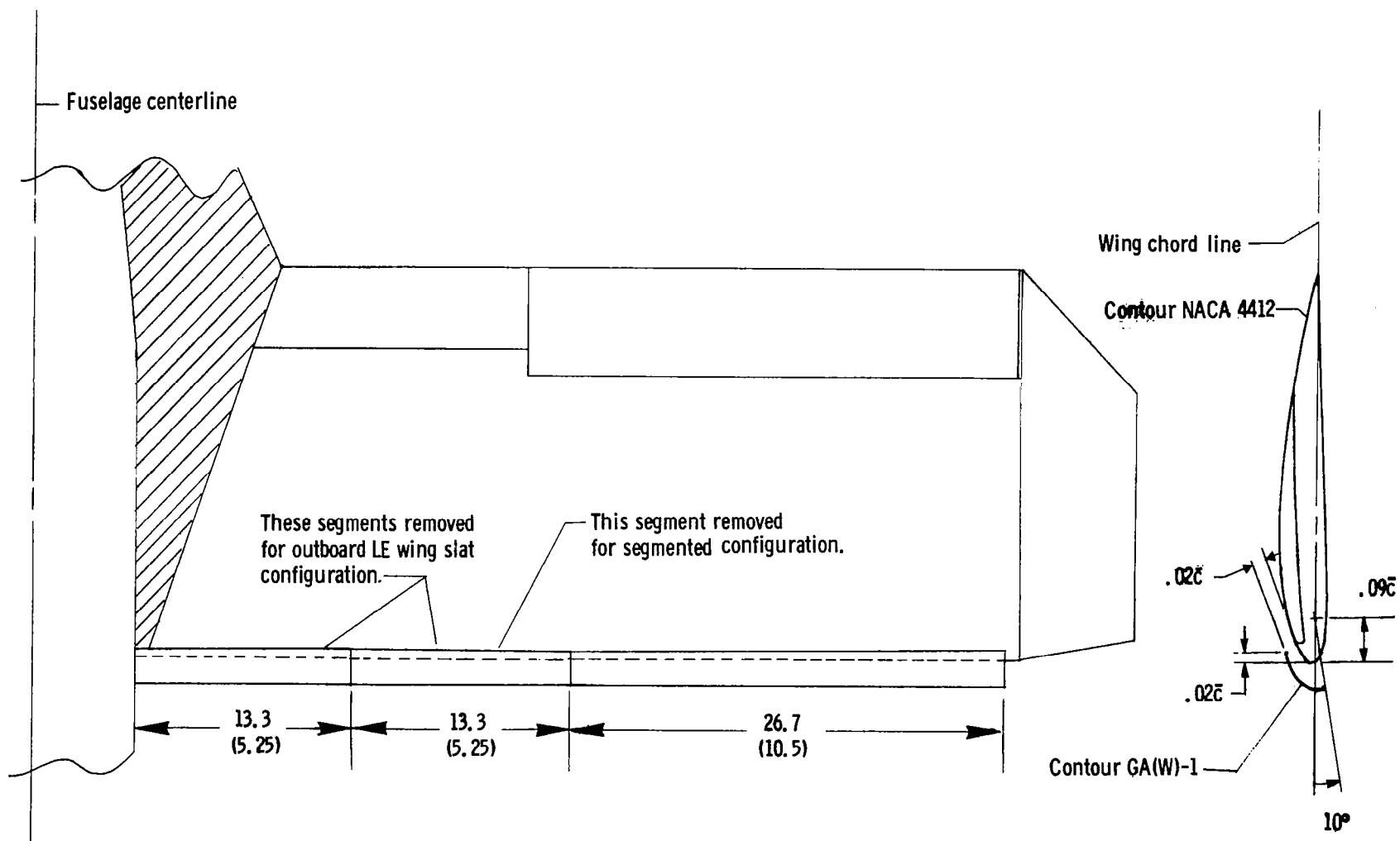
Figure 7. - Wing-fuselage fillet and LE wing slat configurations tested on model. Dimensions are given in centimeters(inches), model scale.

10°

8.51
-(3.35)-

15.2
(5.98)

12.5°

22.9   15.2
(9.0)   (5.98)

Winglet wing tip

Standard wing tip   Modified GA(W)-2 section
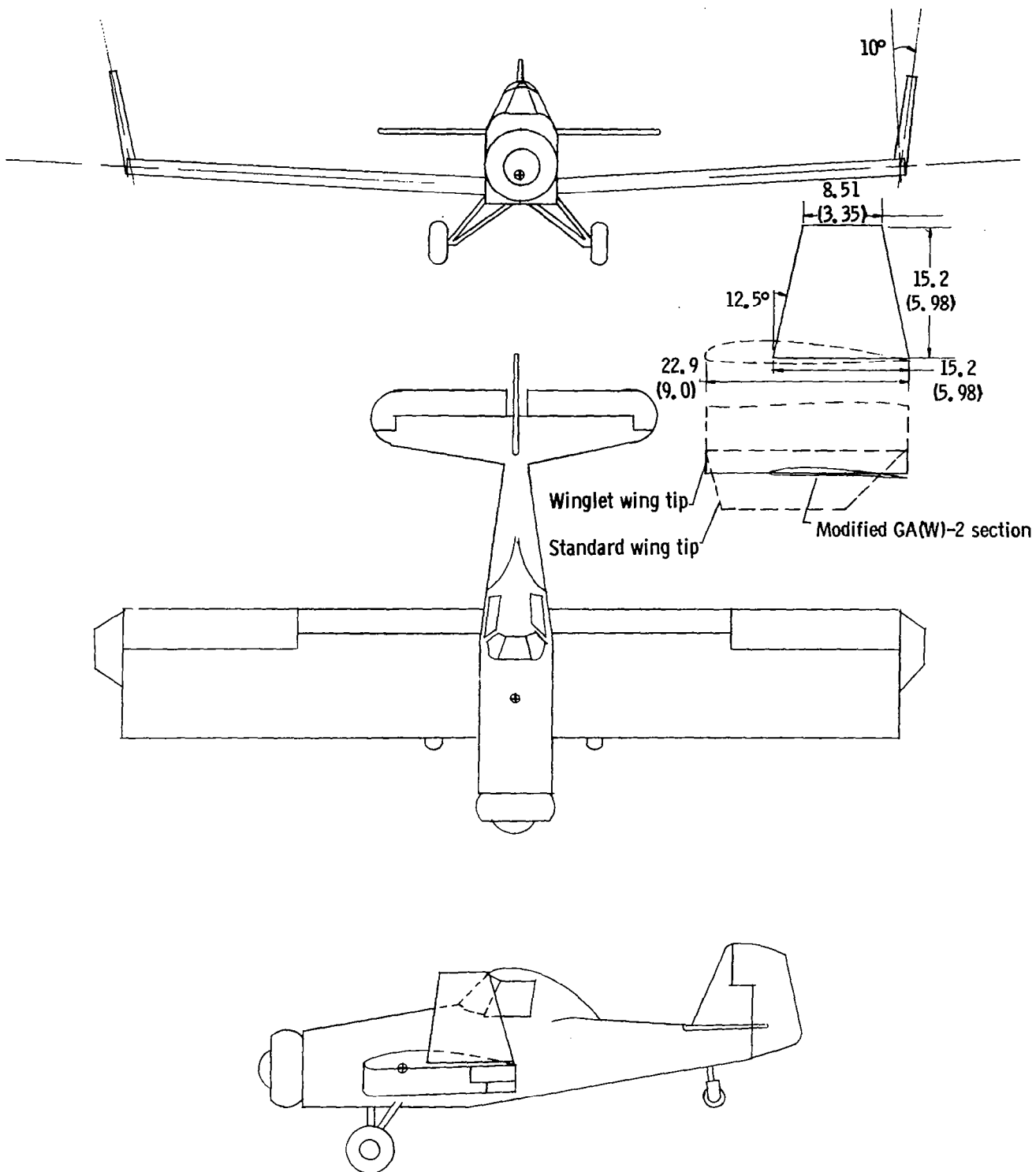
Figure 8. – Winglet installation tested on model. Dimensions are given in centimeters (inches), model scale.

1, 68
(.66)

4, 19
(1, 65)

4, 19
(1, 65)

4, 19
(1, 65)

3, 66
(1, 44)

10° sail chord line
at base

11, 2
(4, 40)

15°   15°   15°

9, 37
(3, 69)

2, 74
(1, 08)
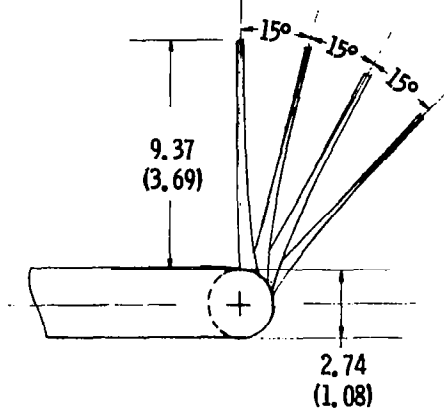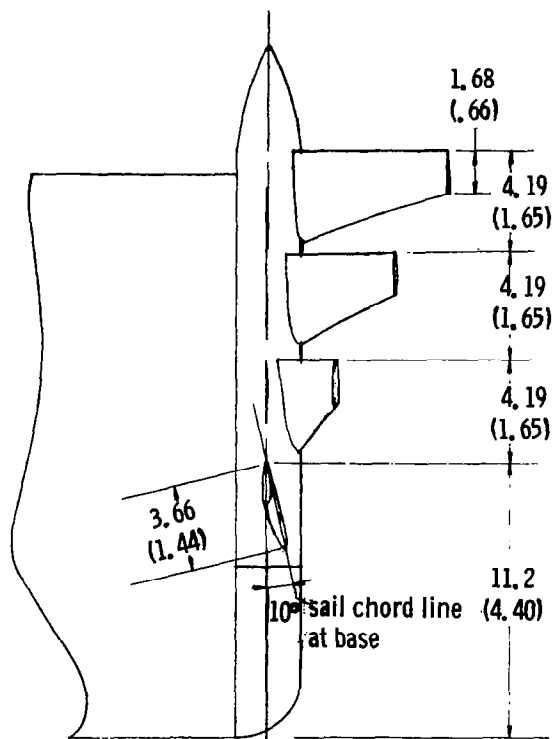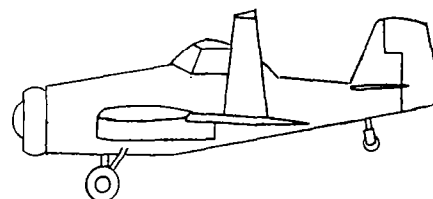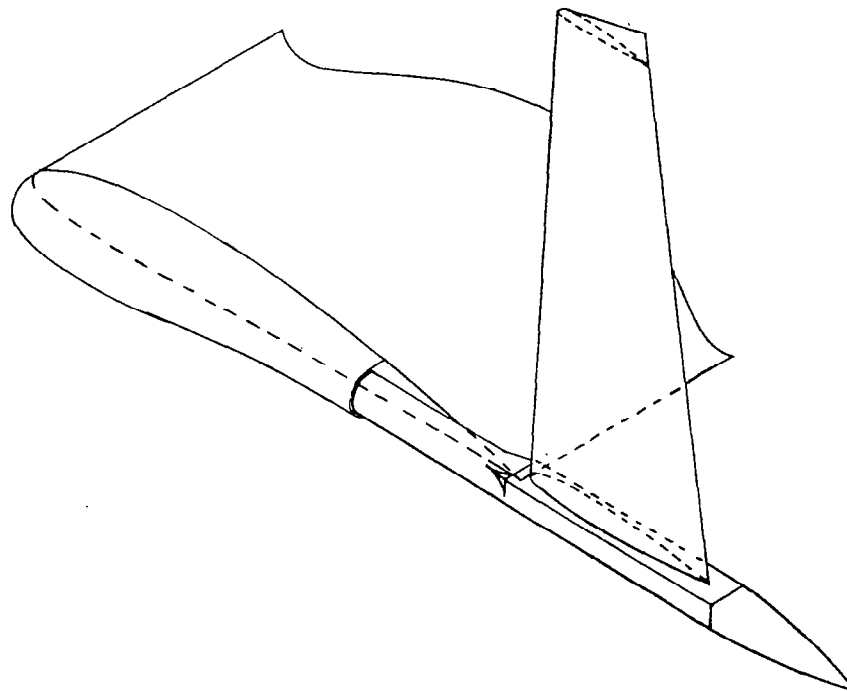
Right wing tip sail

Lockheed vortex diffuser vane

Figure 9. - Wingtip sails and tip vortex diffusers tested on model. Dimensions are given
in centimeters (inches), model scale.

APPENDIX

(a) $\alpha = 8$ to 16 deg, SR $= 152.4$ cm (60 in).

Figure A1.-Effect of rotation rate and angle of attack on yawing-moment coefficient for basic configuration. $\delta_e = 0°$, $\delta_a = 0°$, $\delta_r = 0°$, $\beta = 0°$.
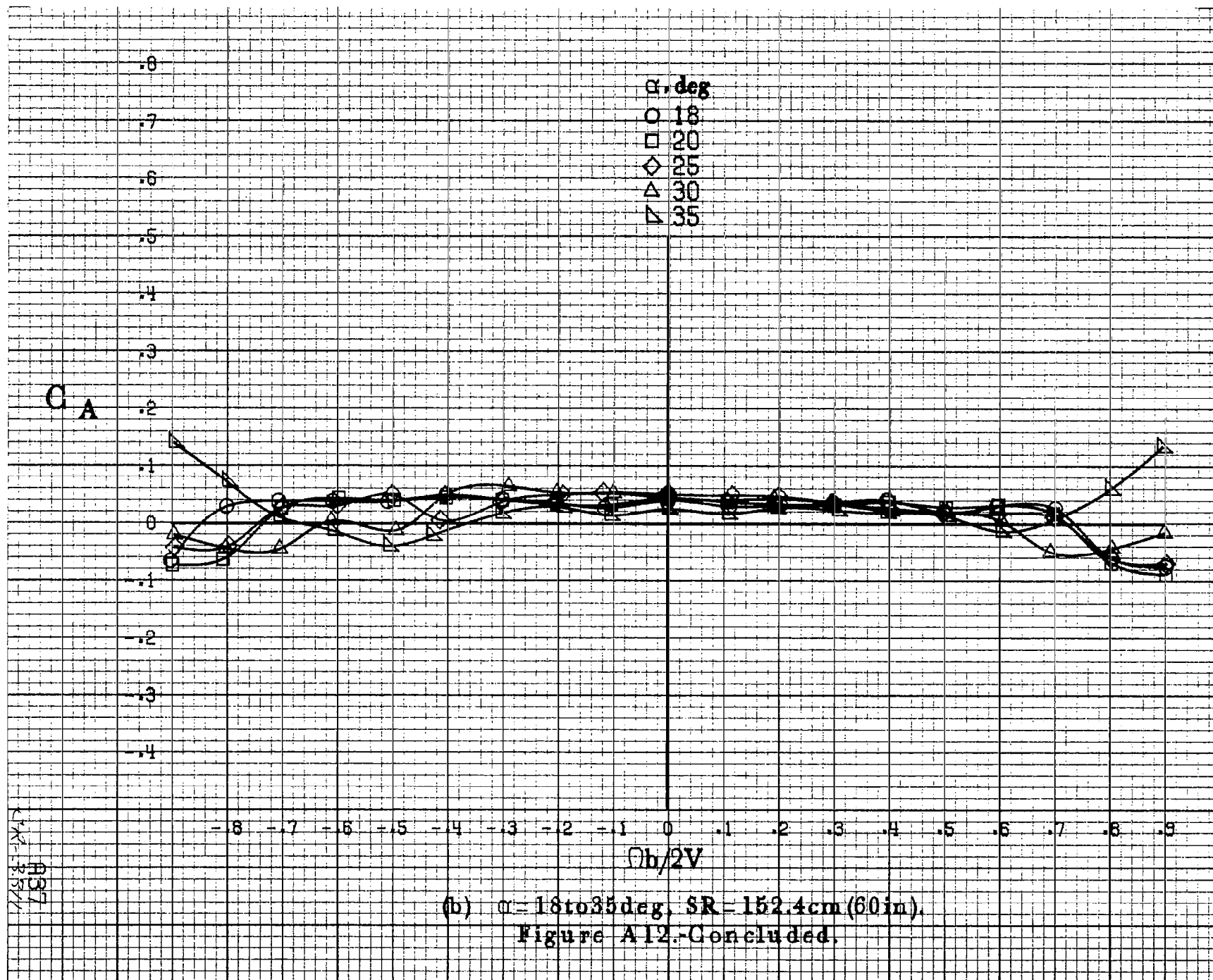
(b) α = 18 to 35 deg, SR = 152.4 cm (60 in).

Figure A1.-Continued.

(c) α = 30 to 50 deg, SR = 0.

Figure A1.-Continued.

(d) α = 55 to 90 deg, SR = 0.

Figure A1. Concluded.
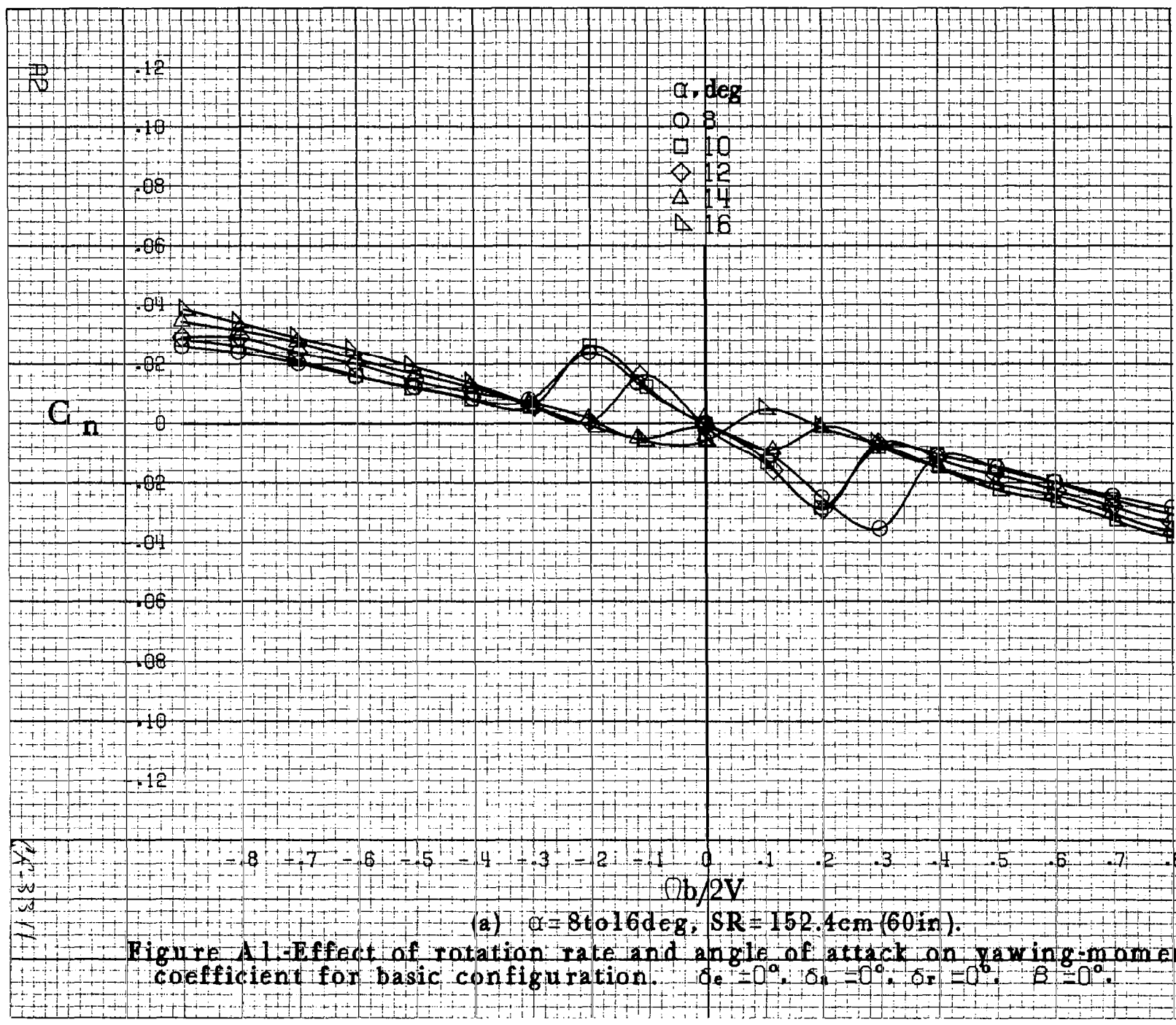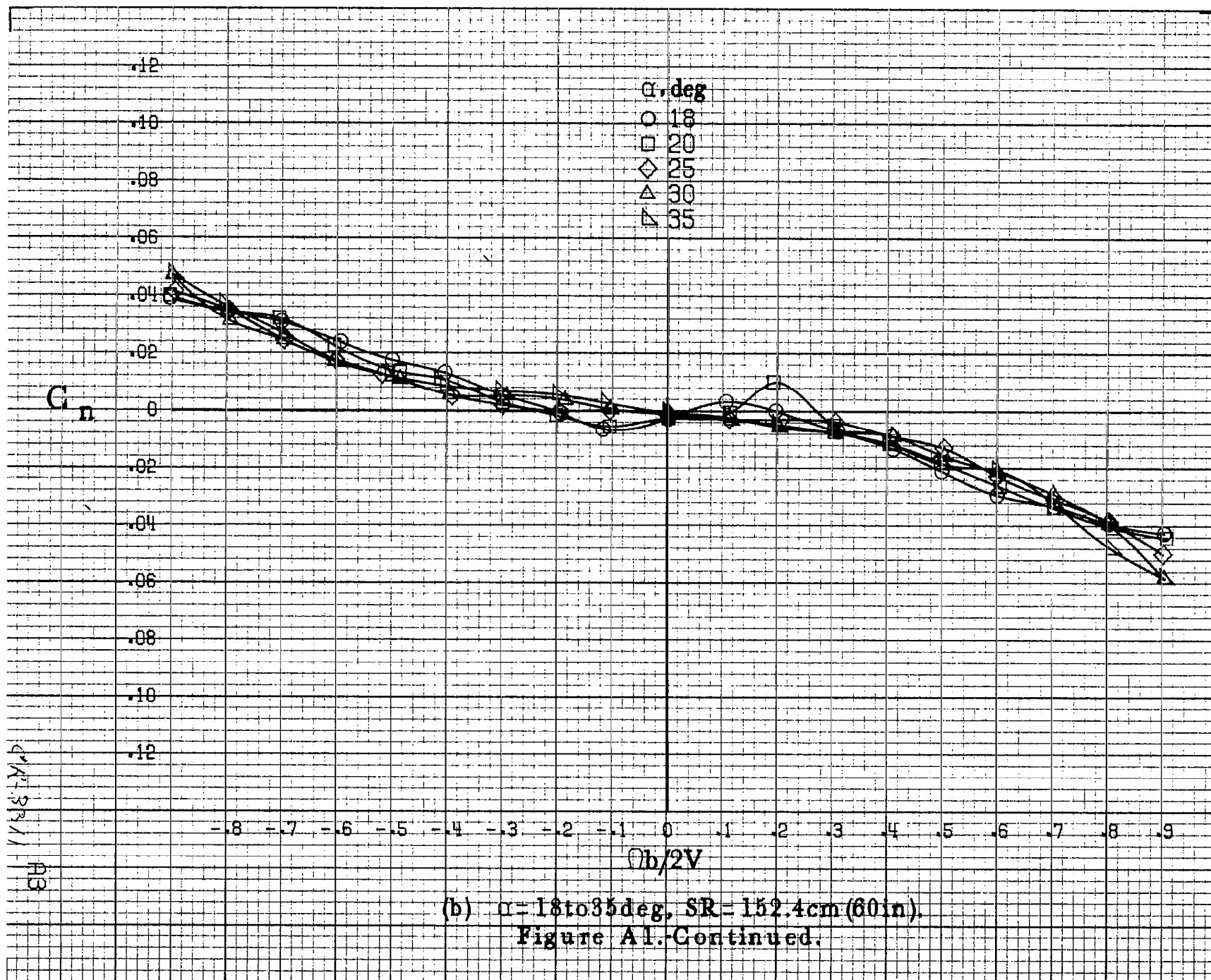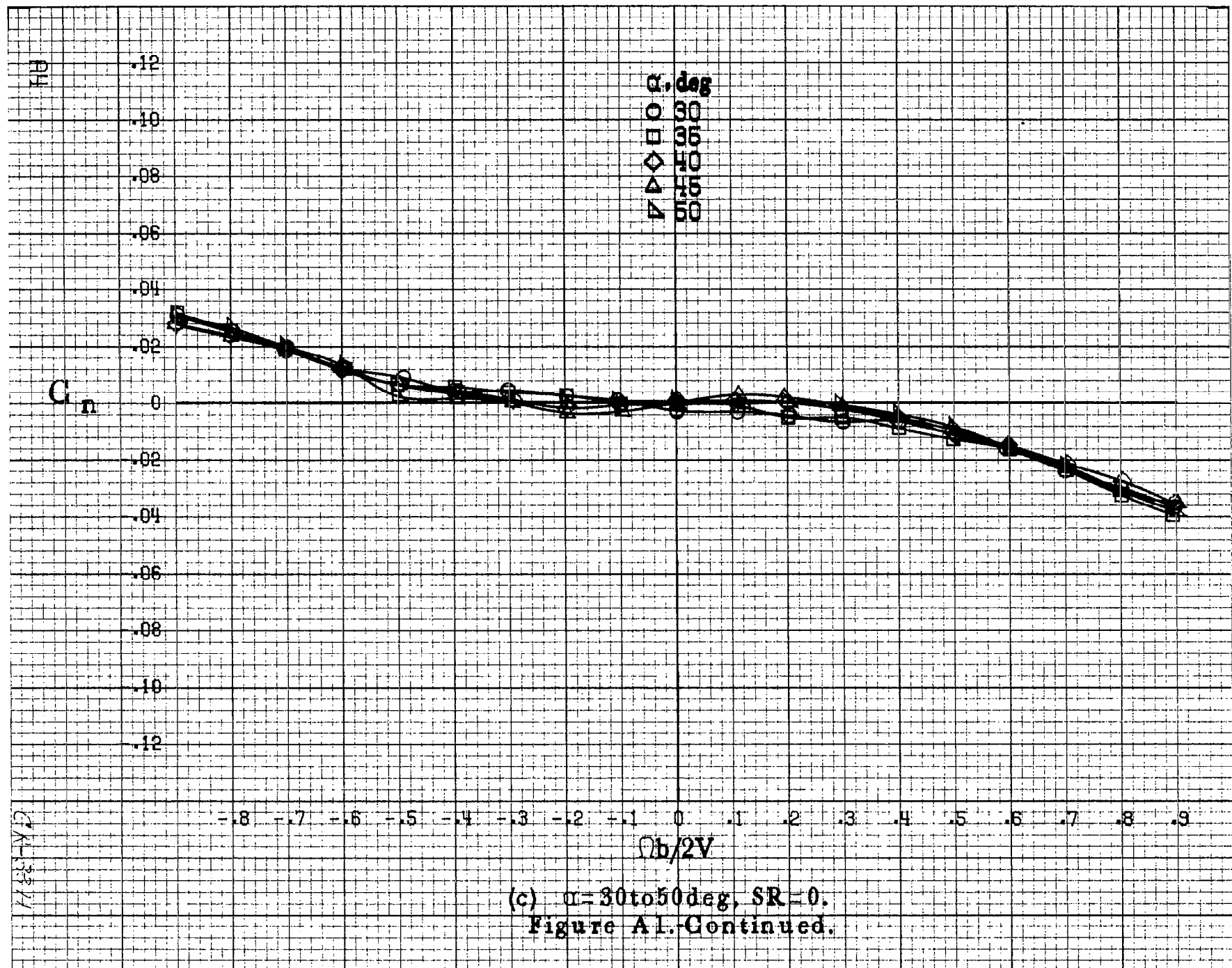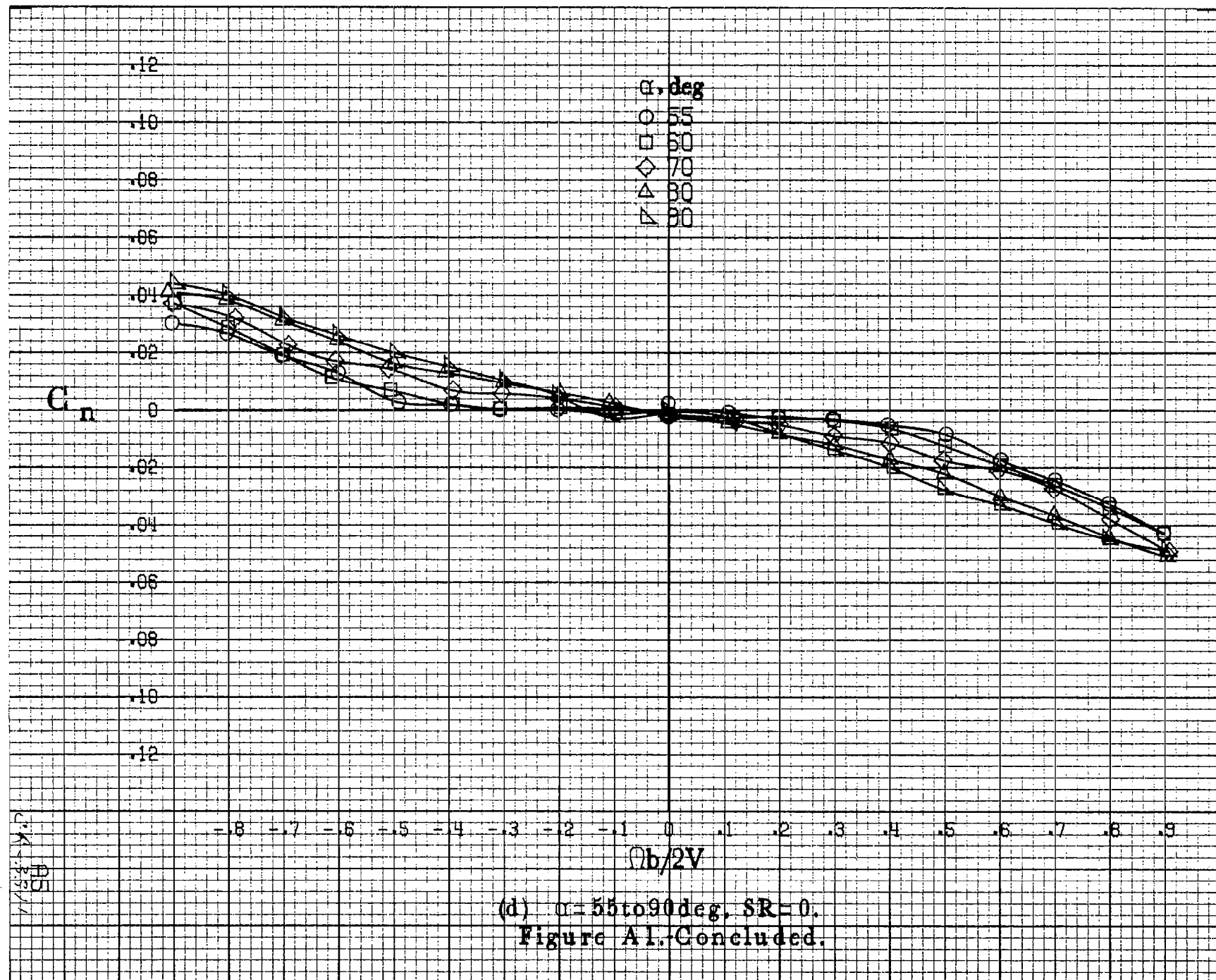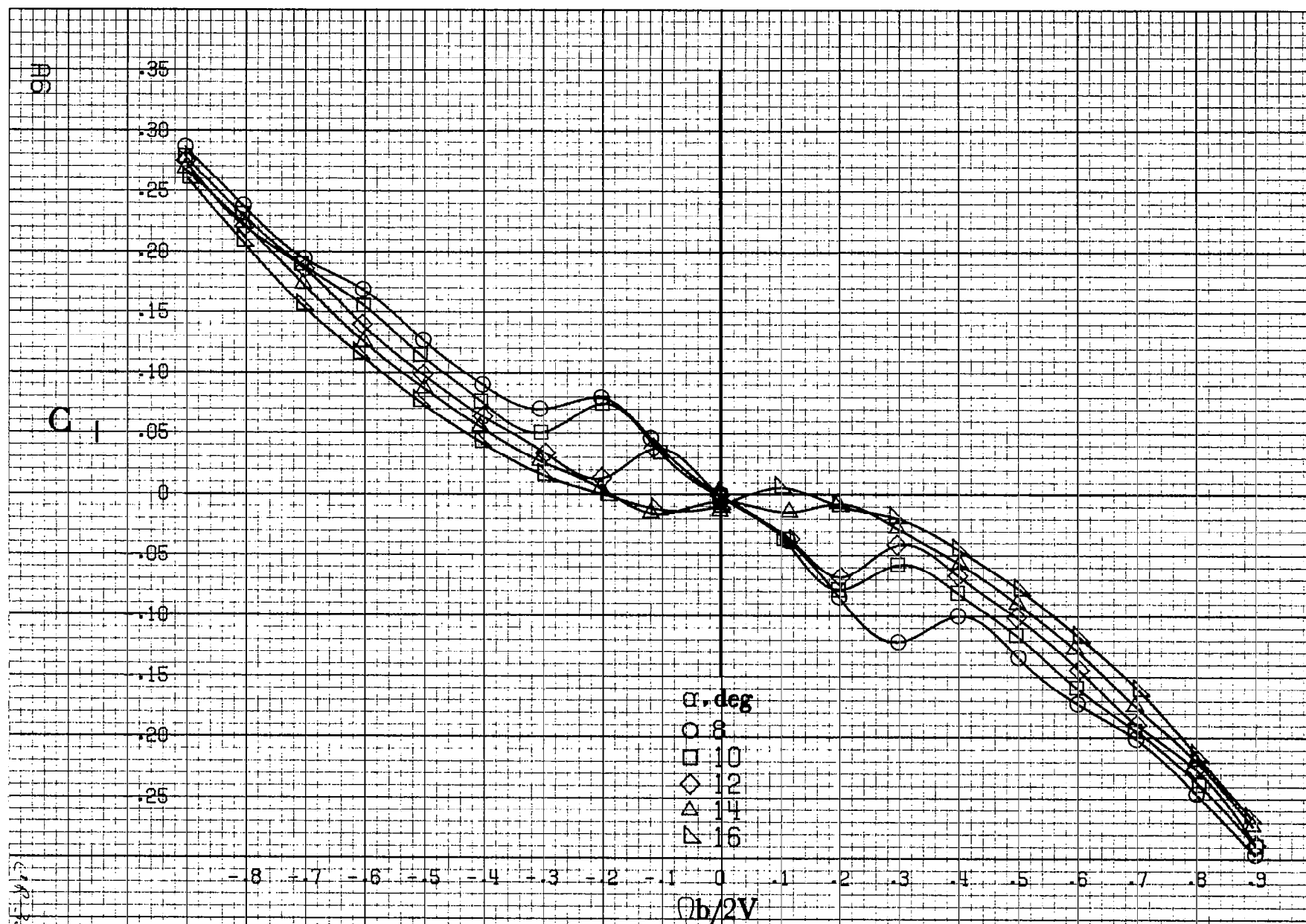
(a) $\alpha = 8$ to 16 deg, SR $= 152.4$ cm $(60$ in $)$.

Figure A2.-Effect of rotation rate and angle of attack on rolling-moment coefficient for basic configuration. $\delta_e = 0°$, $\delta_a = 0°$, $\delta_r = 0°$, $\beta = 0°$.
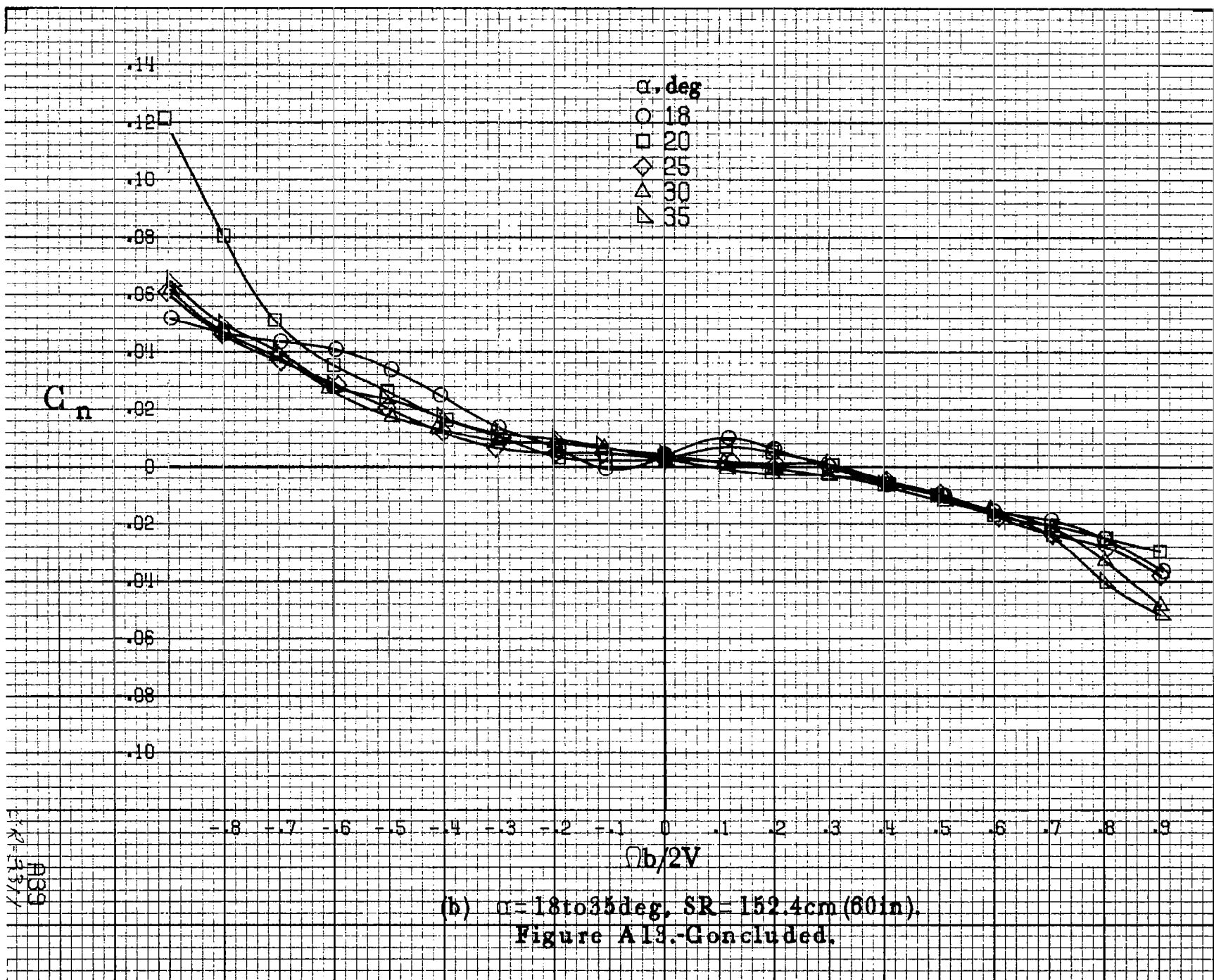
(b) α = 18 to 35 deg, SR = 152.4 cm (60 in).

Figure A2.-Continued.

(c) α=30to50deg, SR=0.

Figure A2. Continued.

(d) α = 55 to 90 deg, SR = 0.

Figure A2.- Concluded.
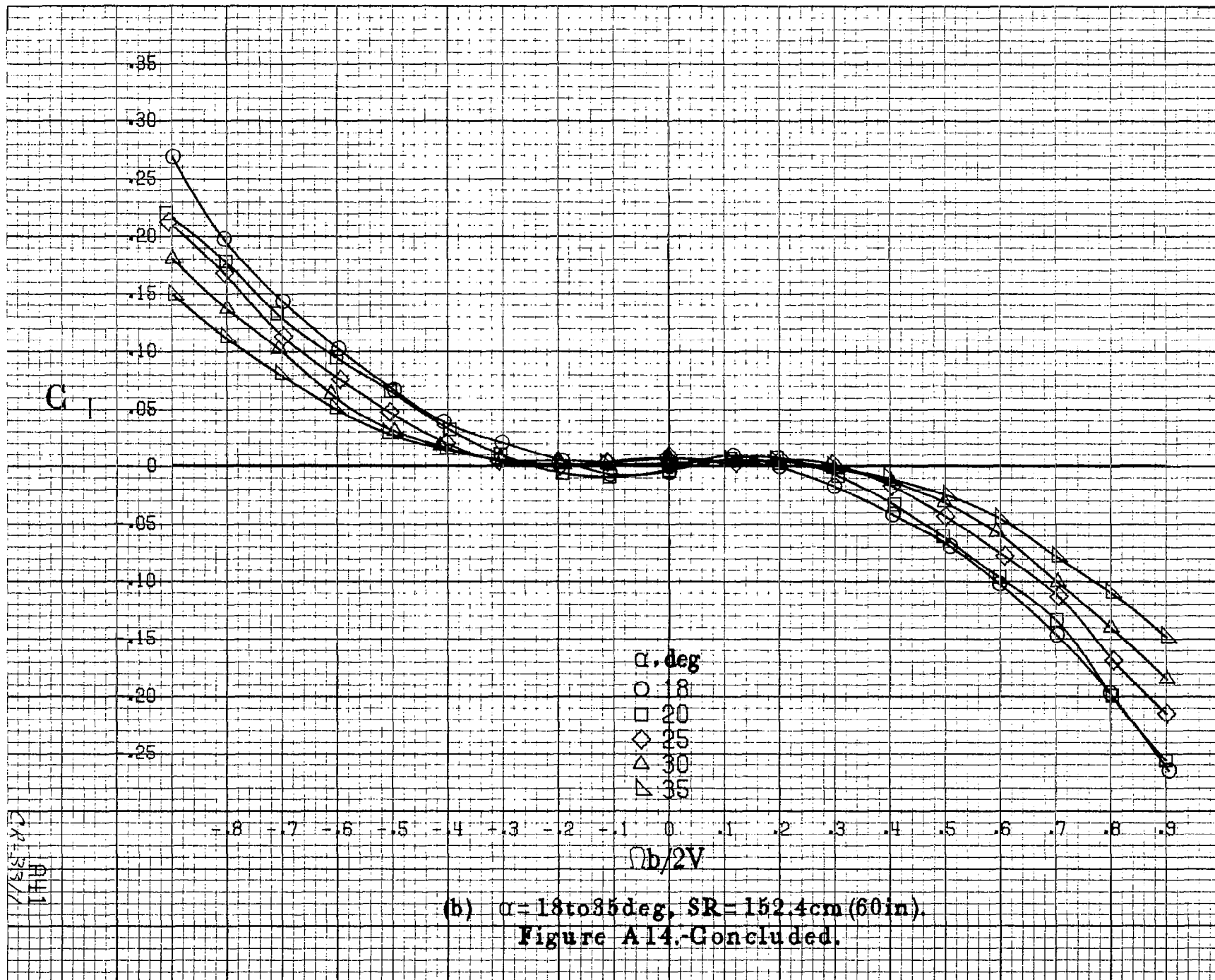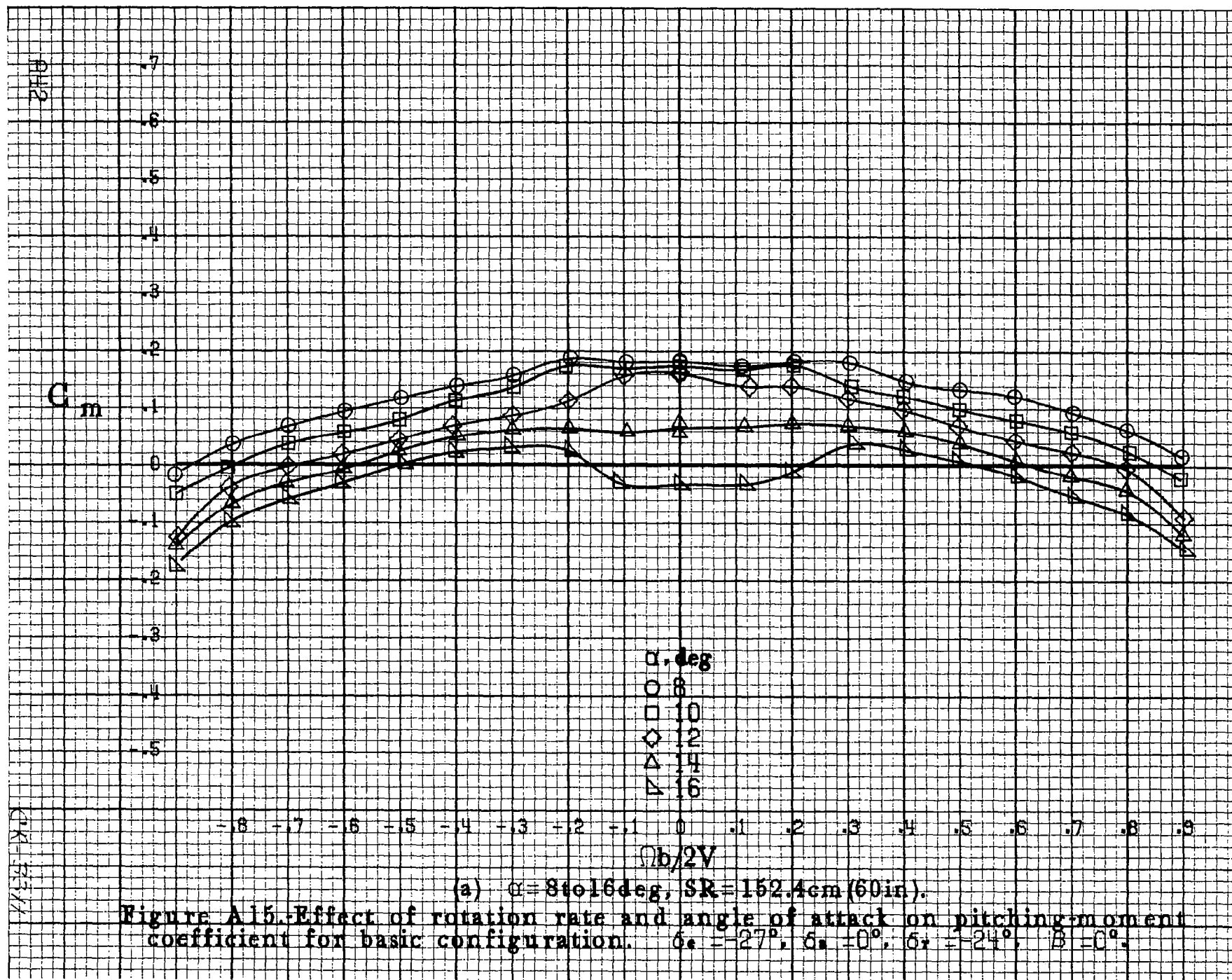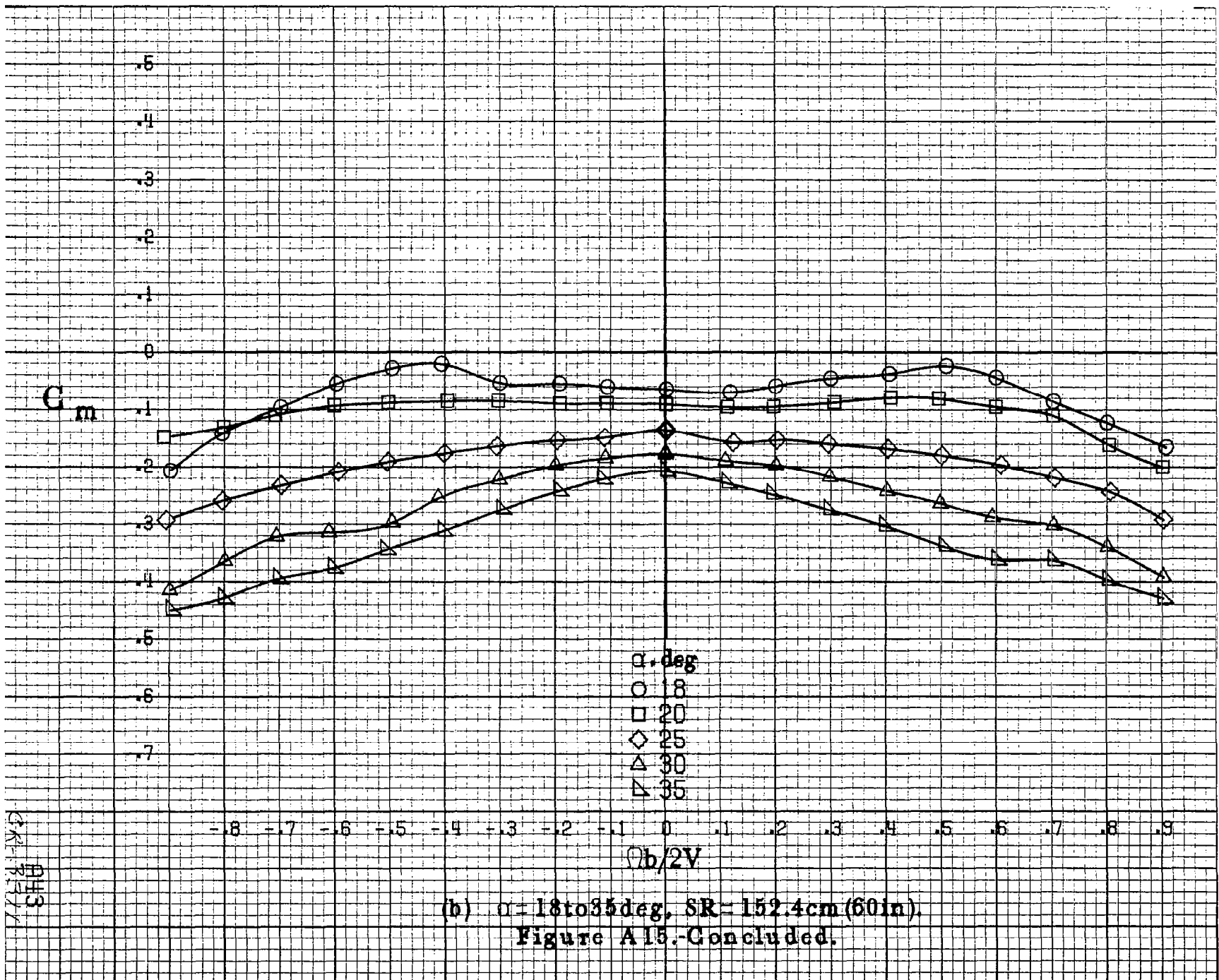
(a) α = 8 to 16 deg, SR = 152.4 cm (60 in).

Figure A3.-Effect of rotation rate and angle of attack on pitching-moment coefficient for basic configuration. $\delta_e = 0°$, $\delta_a = 0°$, $\delta_r = 0°$, $\beta = 0°$.
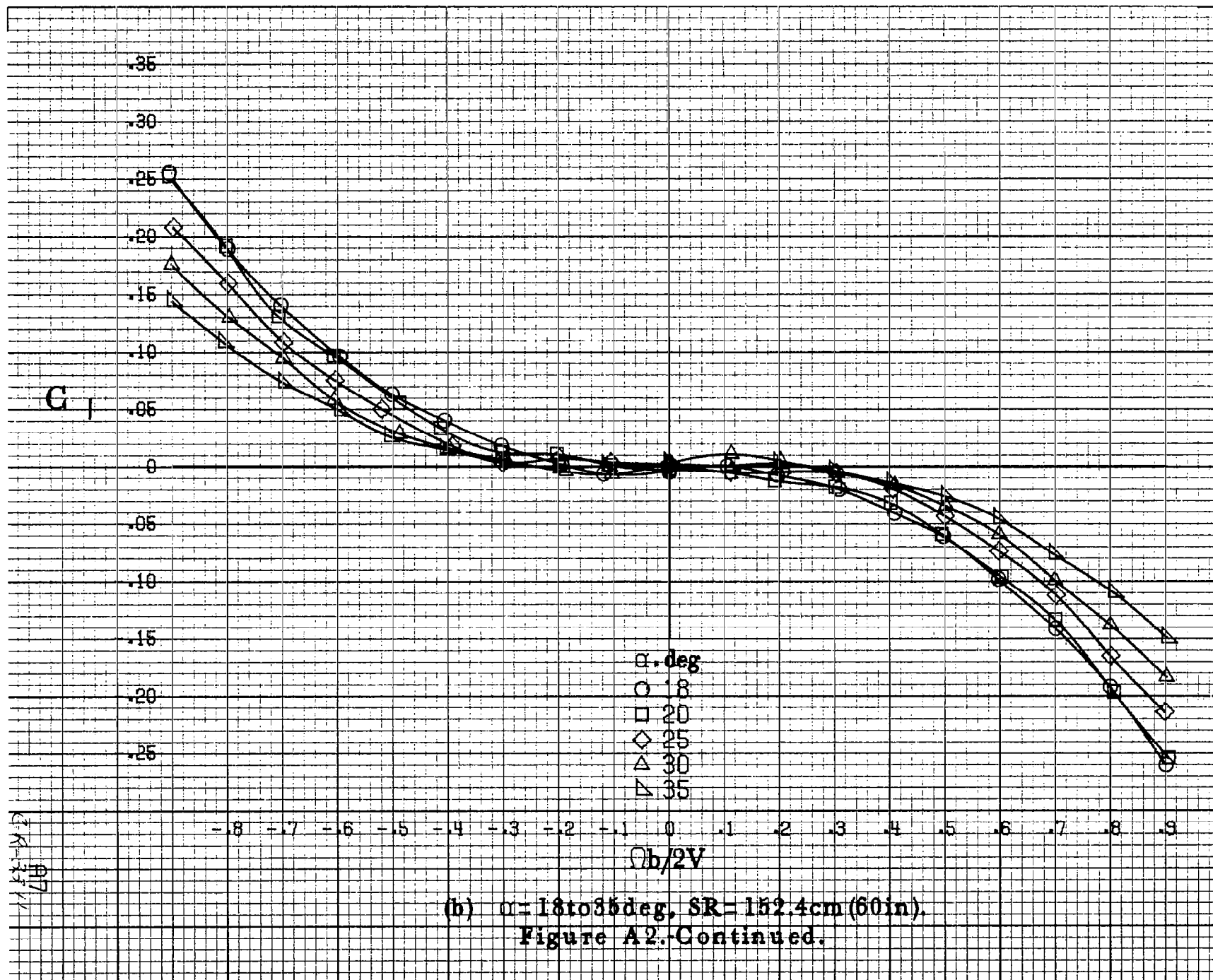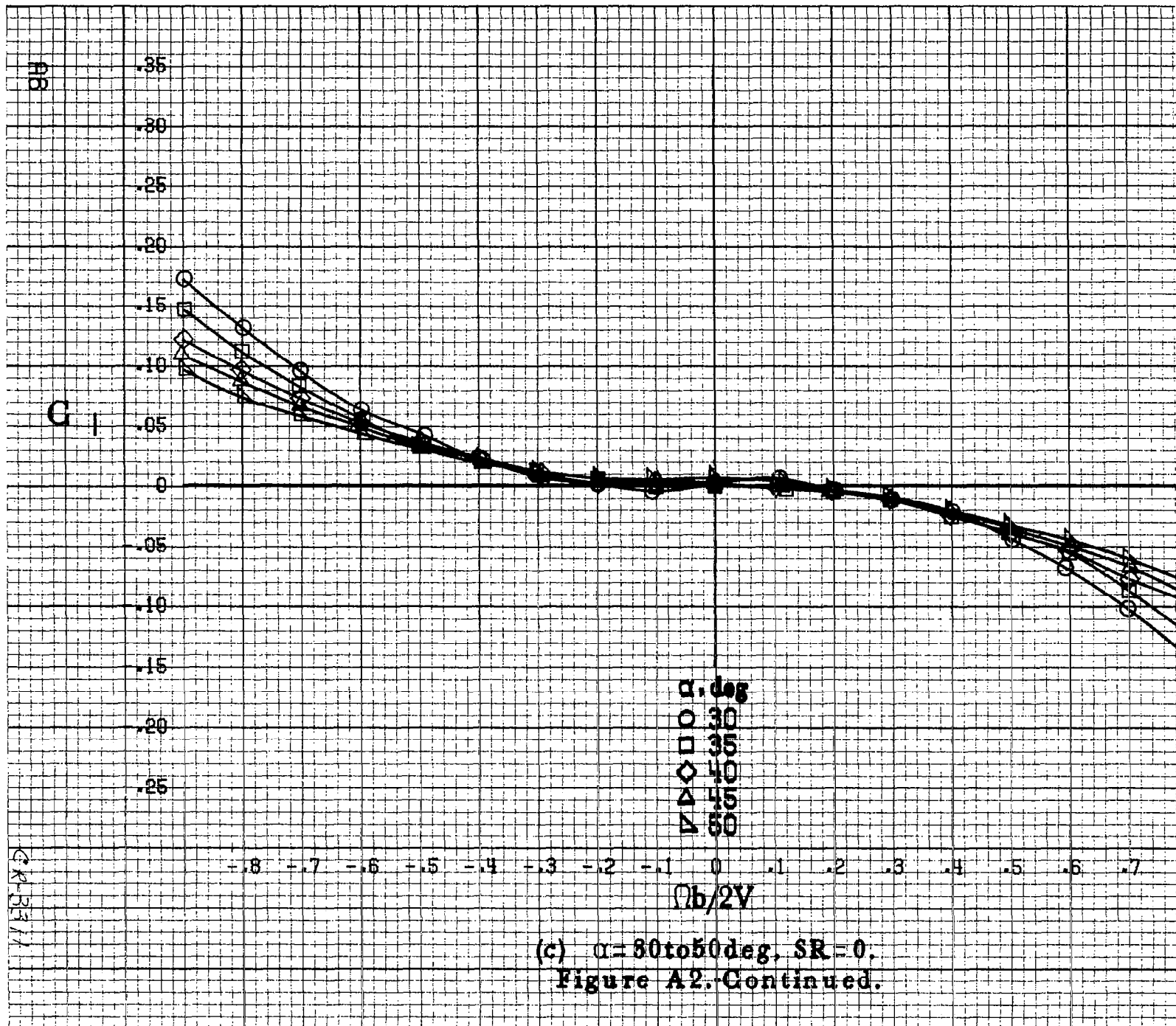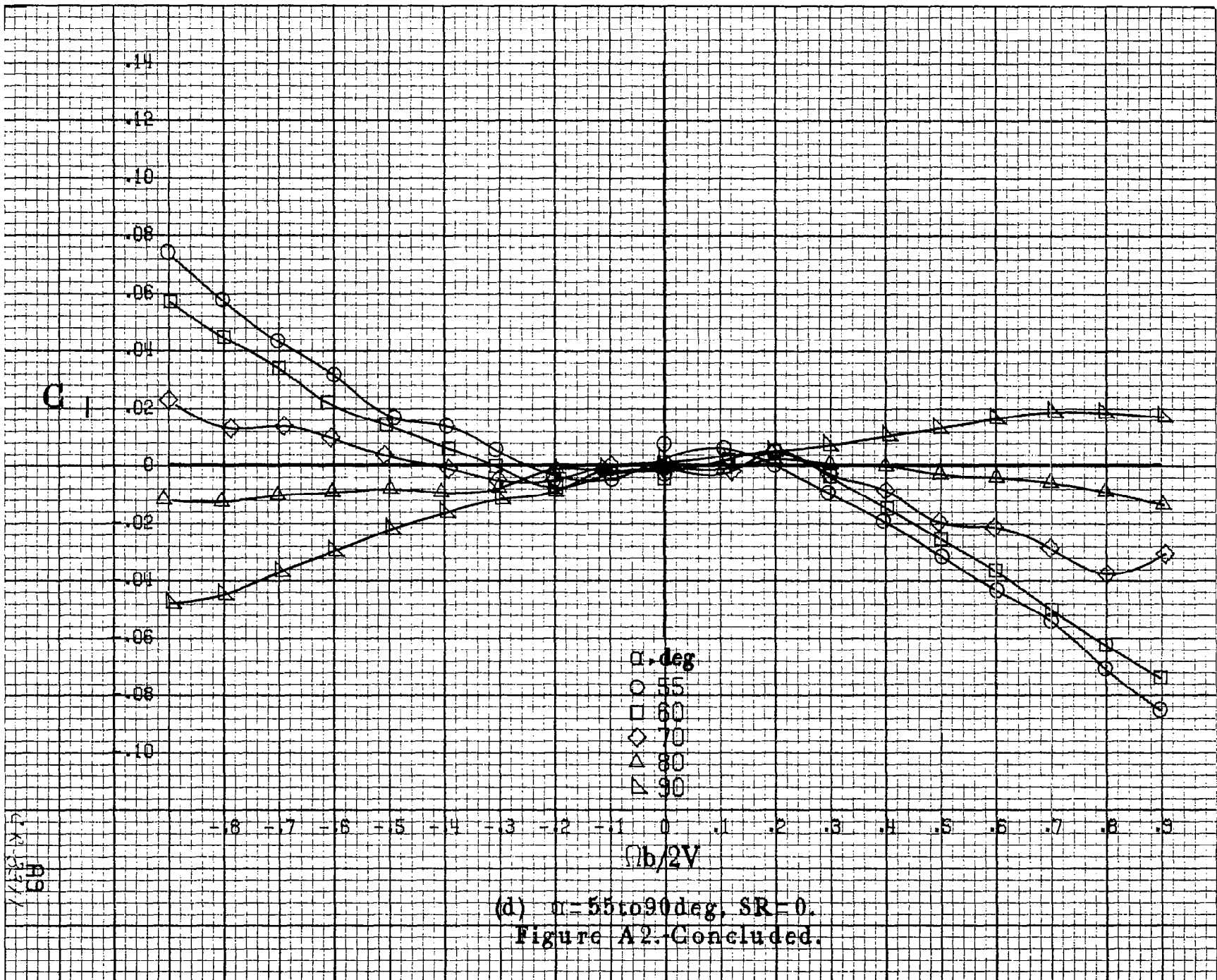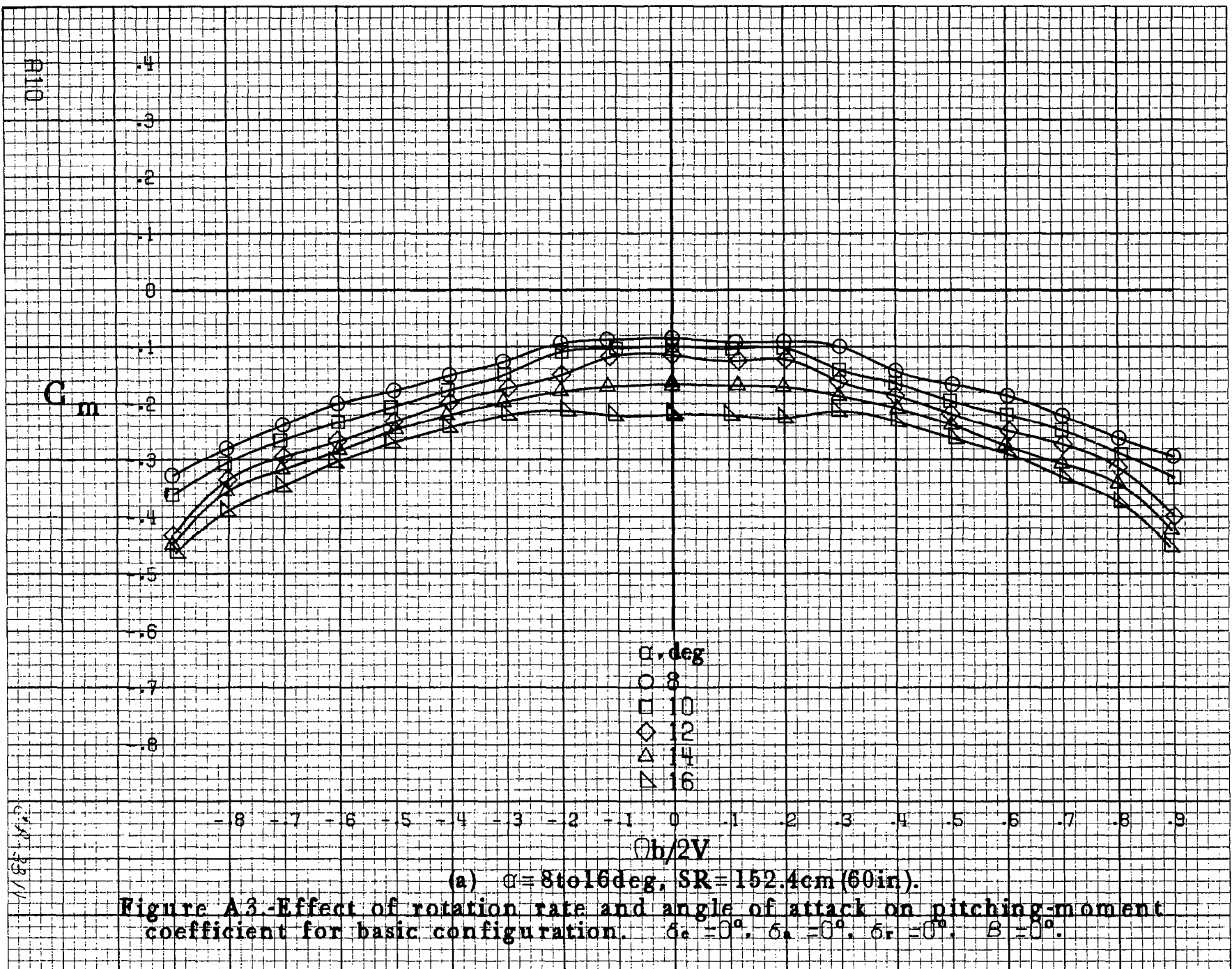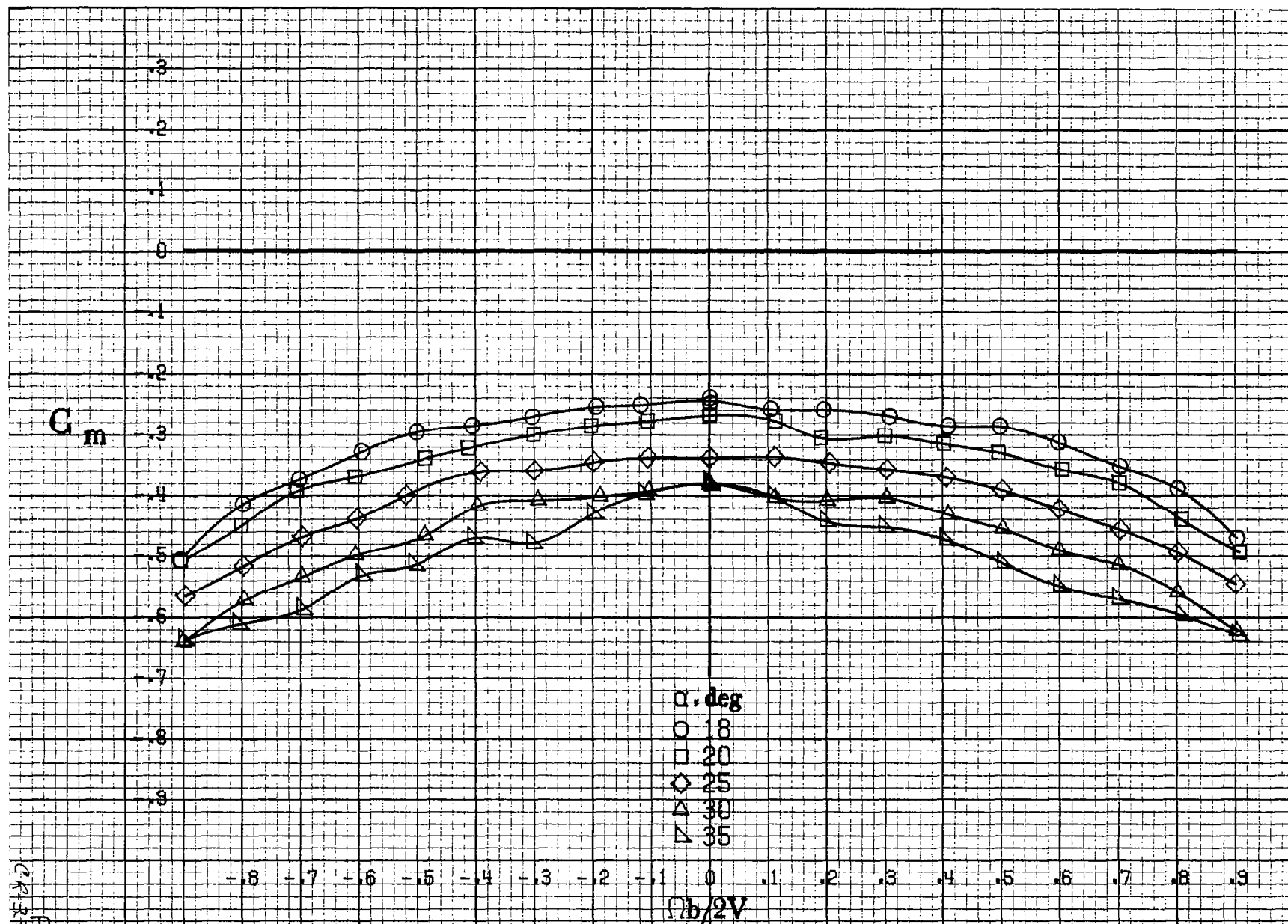
(b) $\alpha = 18$ to 35 deg, $SR = 152.4$ cm (60 in).

Figure A8. Continued.

(c) $\alpha = 30$ to 50 deg, $SR = 0$.

Figure A 3. Continued.

(d) α = 55 to 90 deg, SR = 0.

Figure A3. Concluded.
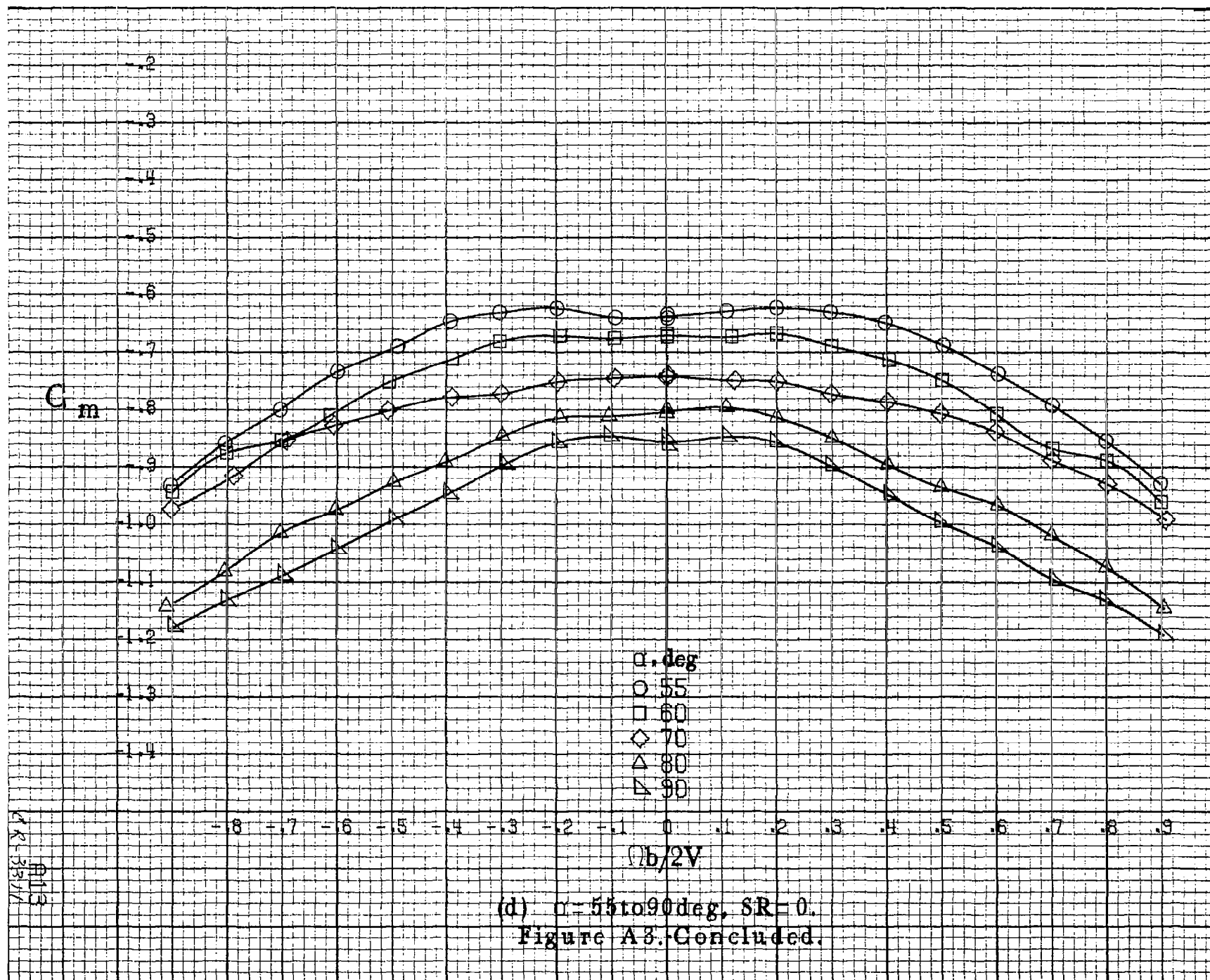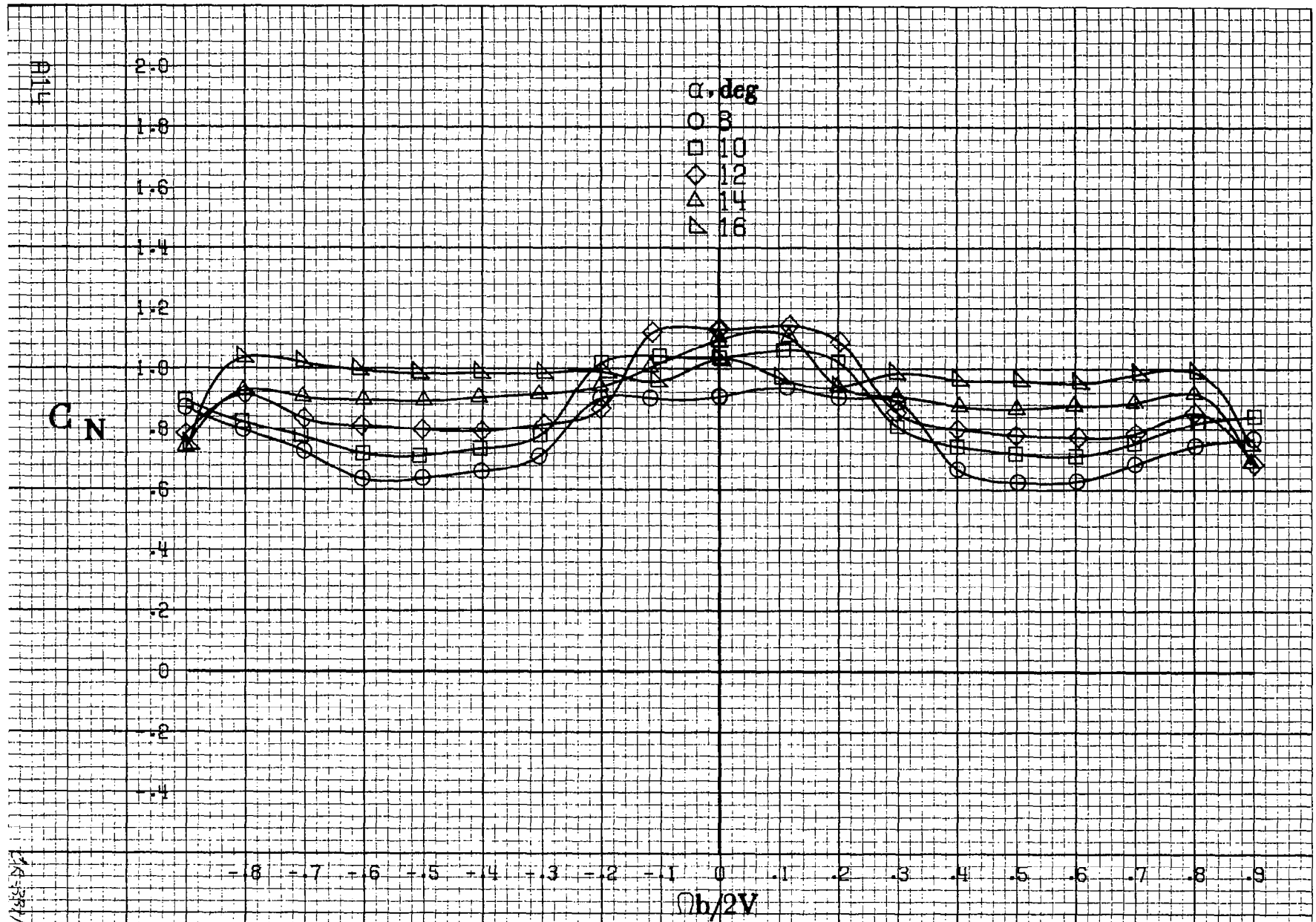
(a) $\alpha = 8$ to 16 deg, $SR = 152.4$ cm (60 in).

Figure A4.-Effect of rotation rate and angle of attack on normal-force coefficient for basic configuration. $\delta_e = 0°$, $\delta_a = 0°$, $\delta_r = 0°$, $\beta = 0°$.
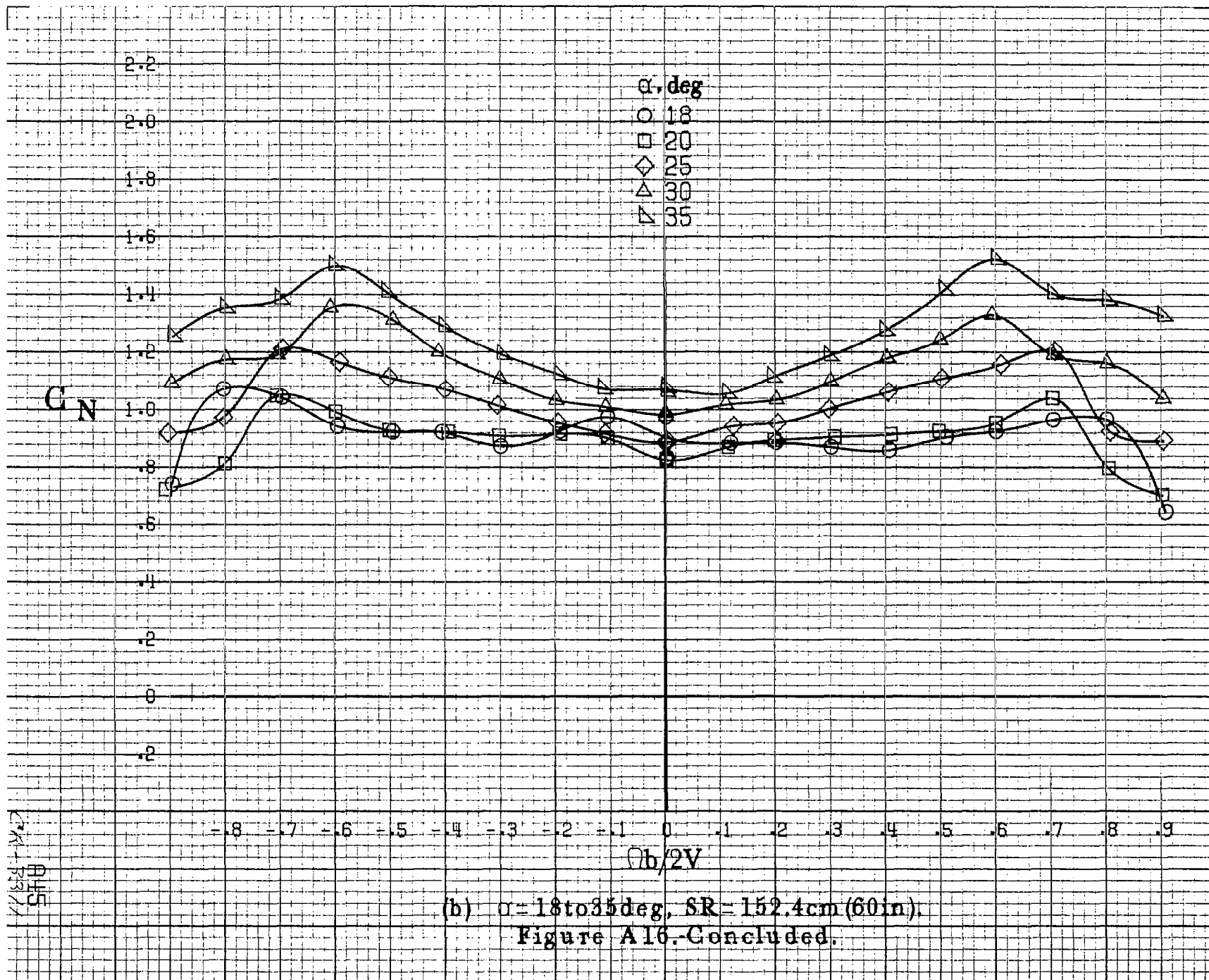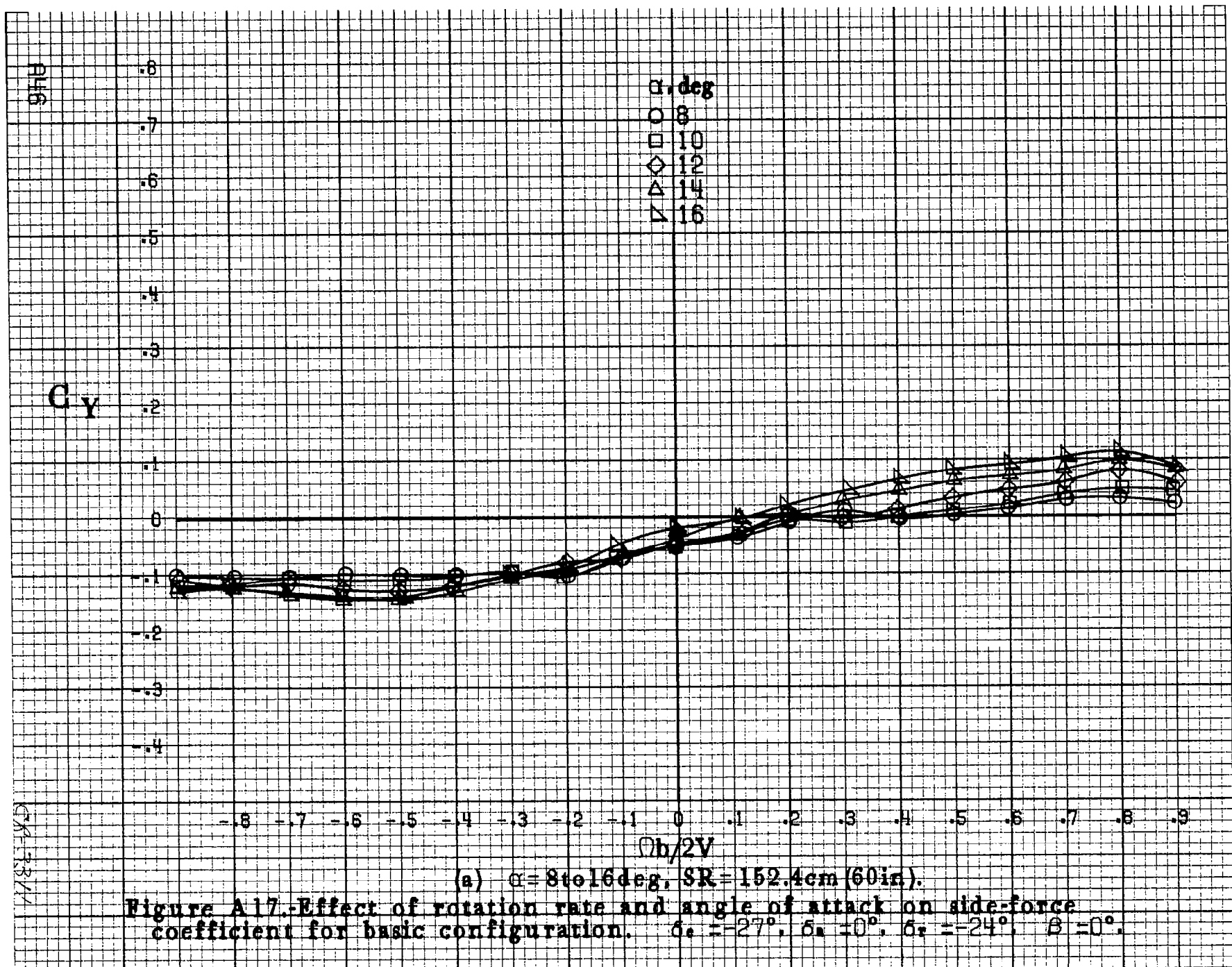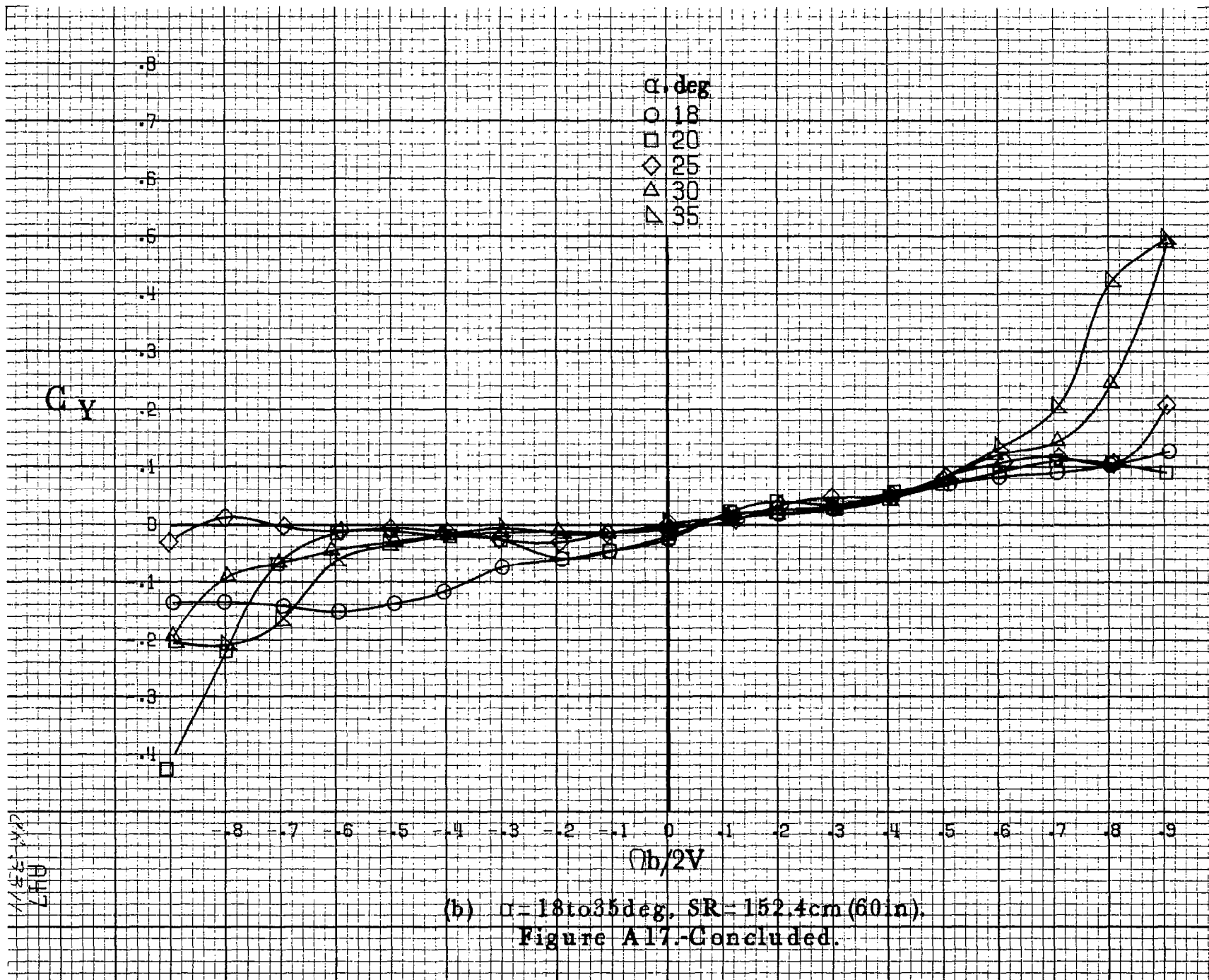
(b) $\alpha = 18$ to 35 deg, $SR = 152.4$ cm $(60$ in$)$.

Figure A 4.- Continued.

(c) α = 30 to 50 deg, SR = 0.
Figure A4. Continued.

(d) α=55 to 90 deg, SR=0.

Figure A4.-Concluded.
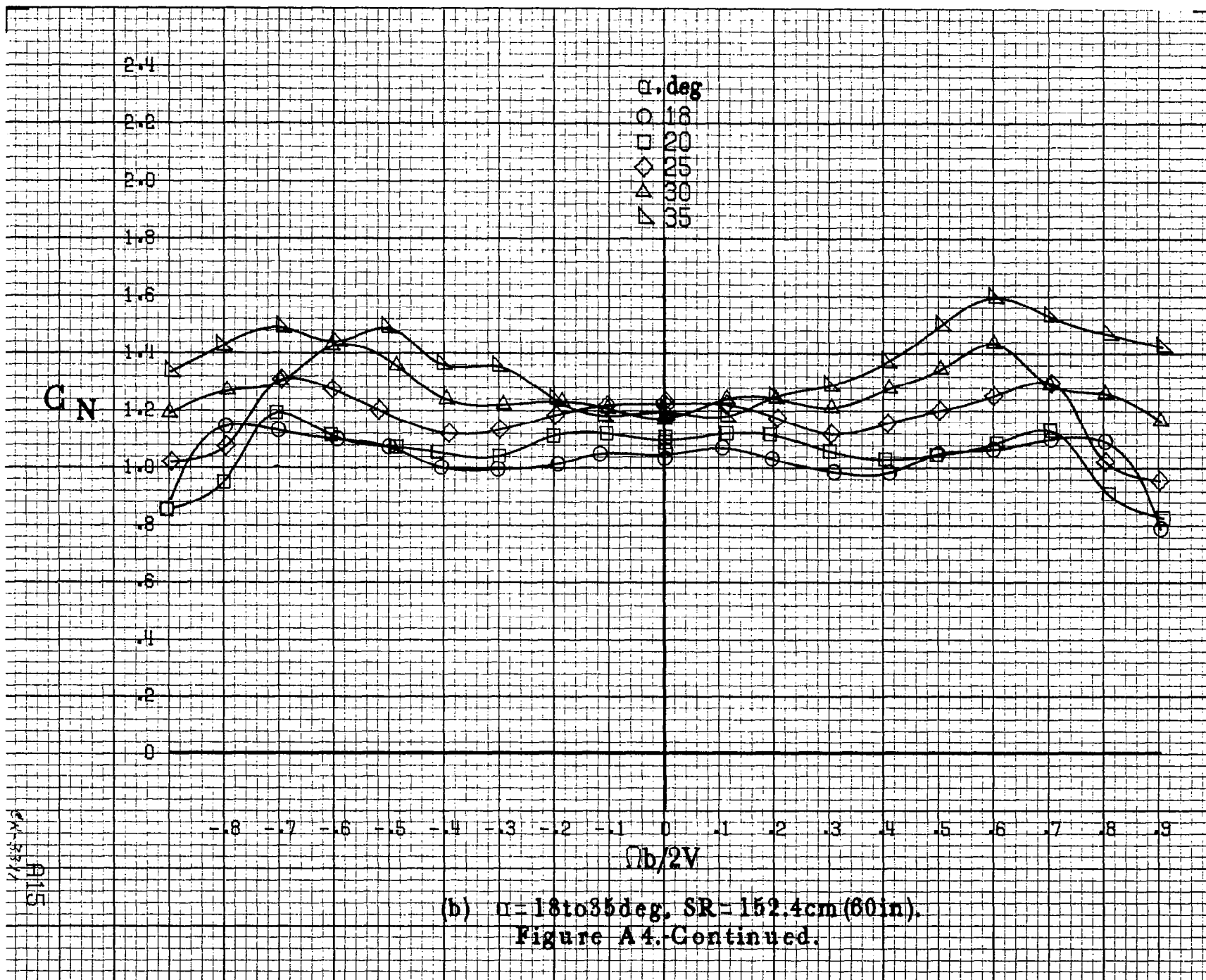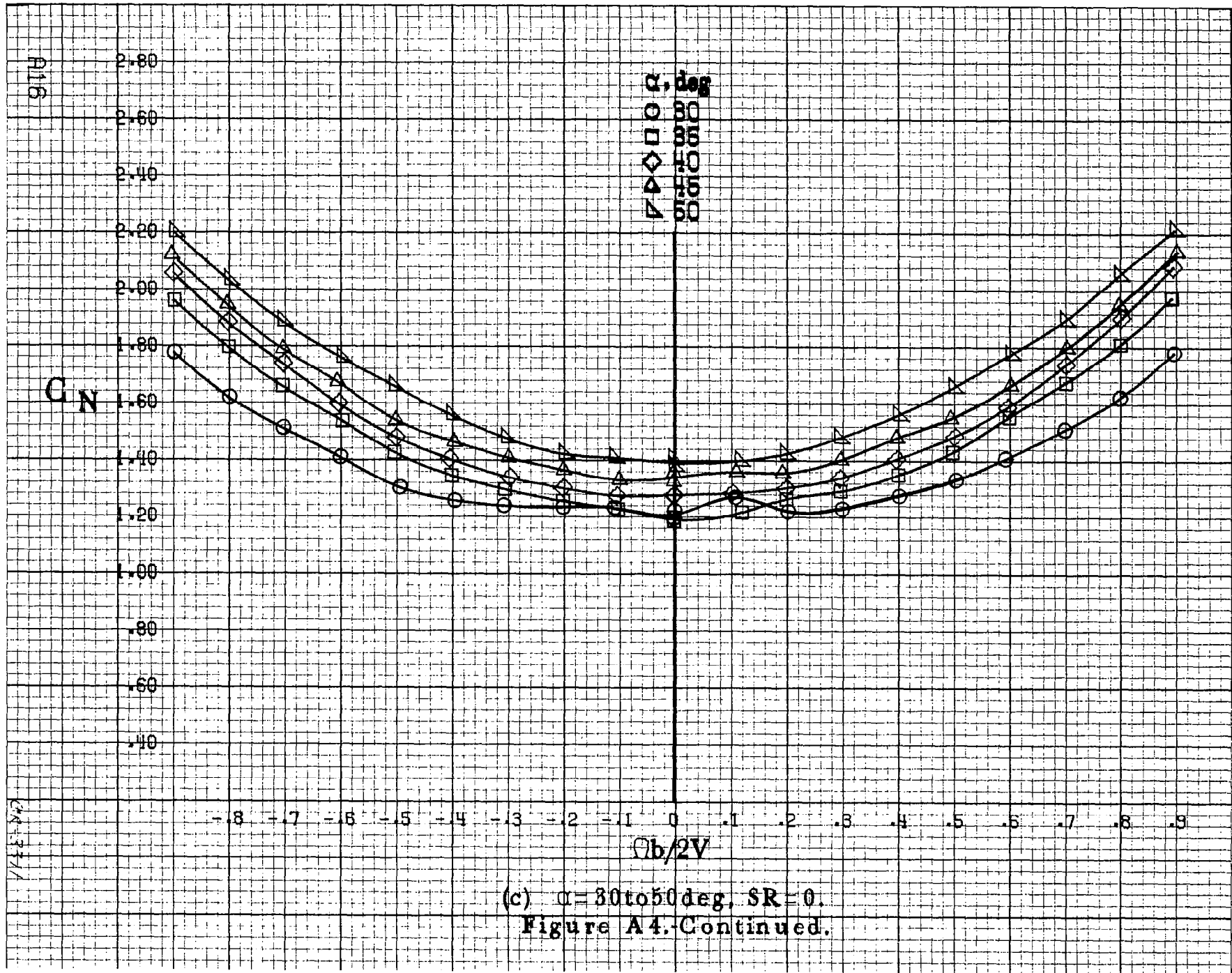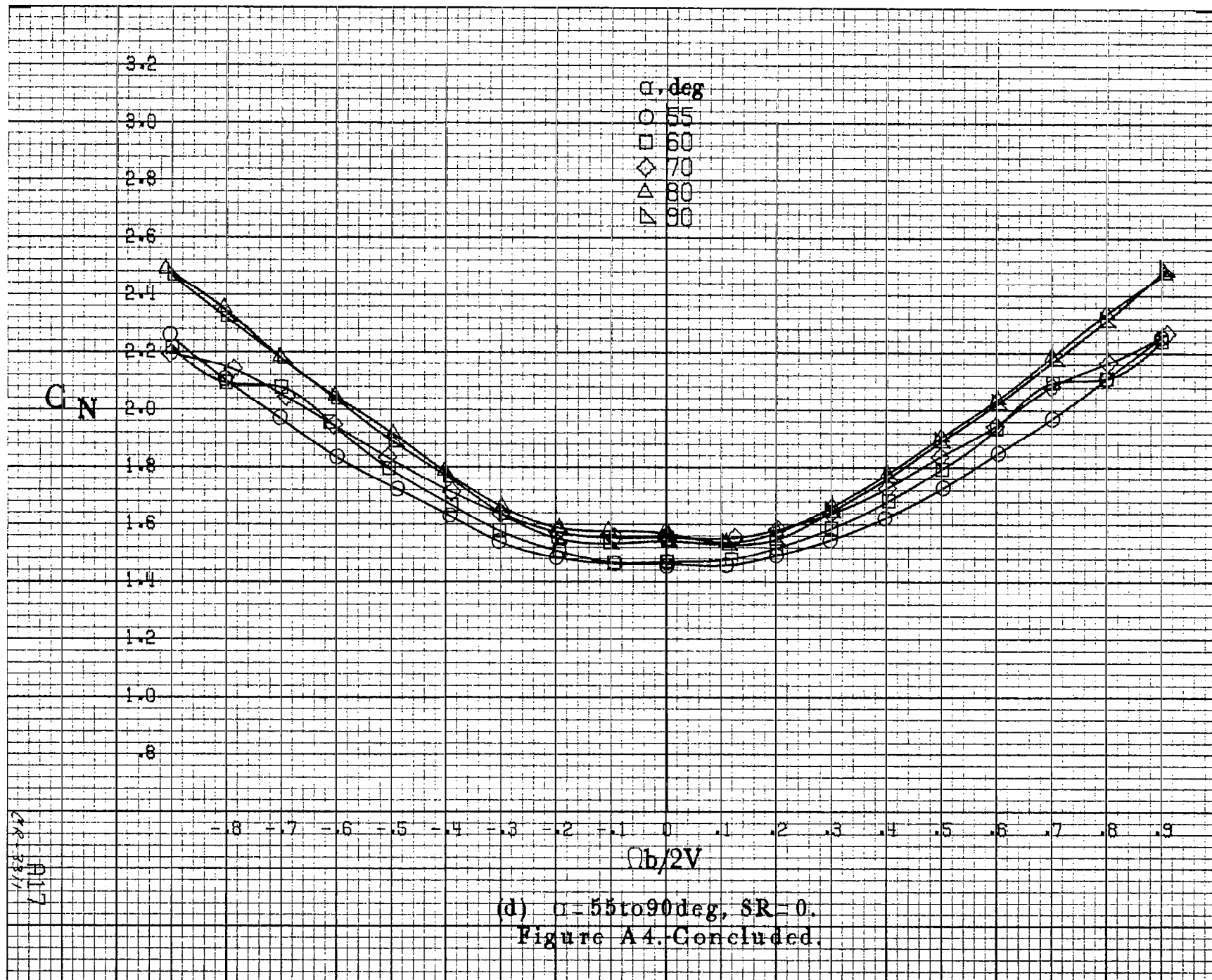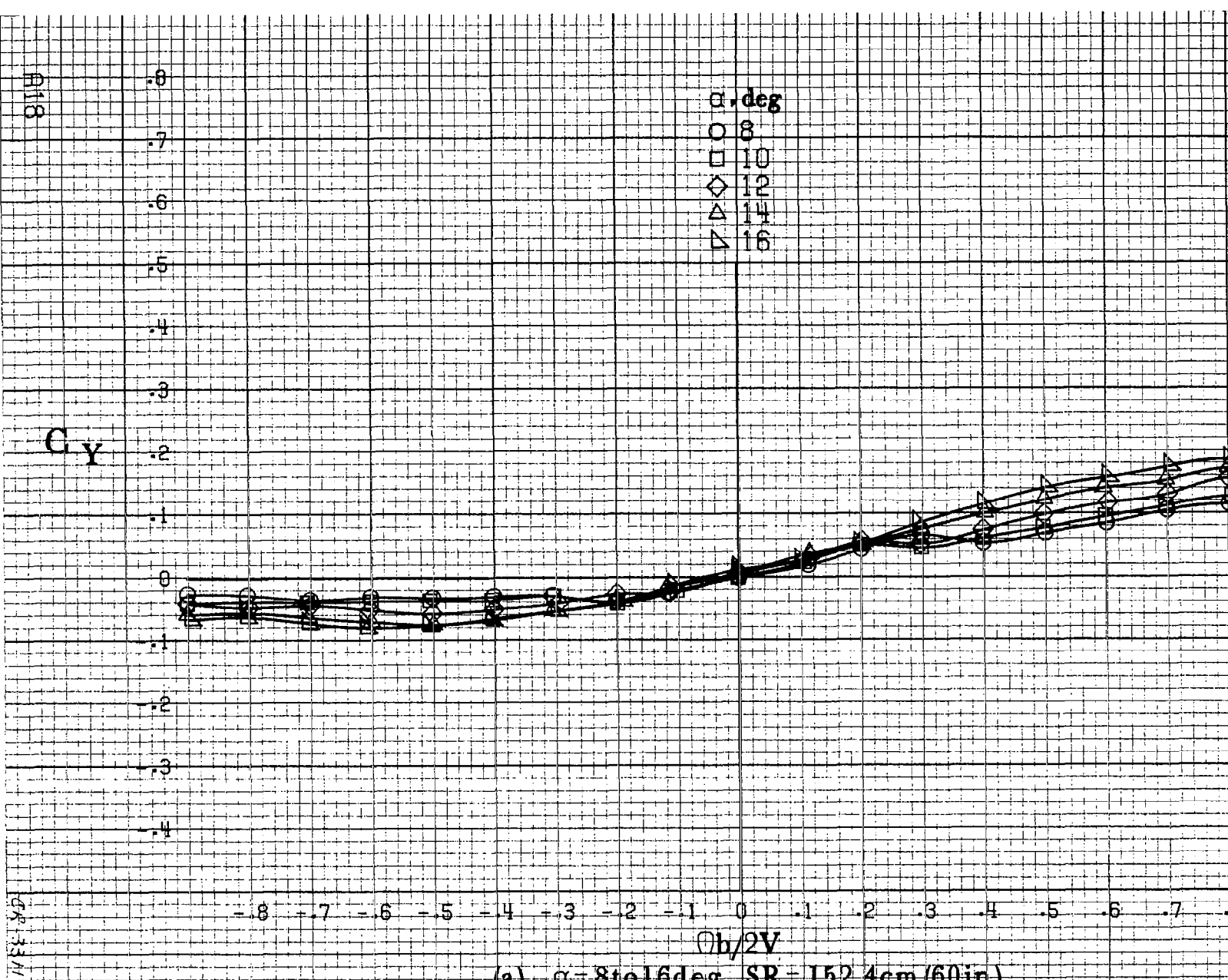
(a) $\alpha = 8 \text{ to } 16 \text{ deg}$, SR = 152.4 cm (60 in).

Figure A5.-Effect of rotation rate and angle of attack on side-force coefficient for basic configuration. $\delta_e = 0°$, $\delta_a = 0°$, $\delta_r = 0°$, $\beta = 0°$.

(b) $\alpha = 18$ to 35 deg, $SR = 152.4$ cm (60 in).

Figure A5.-Continued.

(c) α=30to50deg, SR=0.

Figure A5.-Continued.

C_Y

α, deg
○ 55
□ 60
◇ 70
△ 80
◁ 90

$\Omega b/2V$
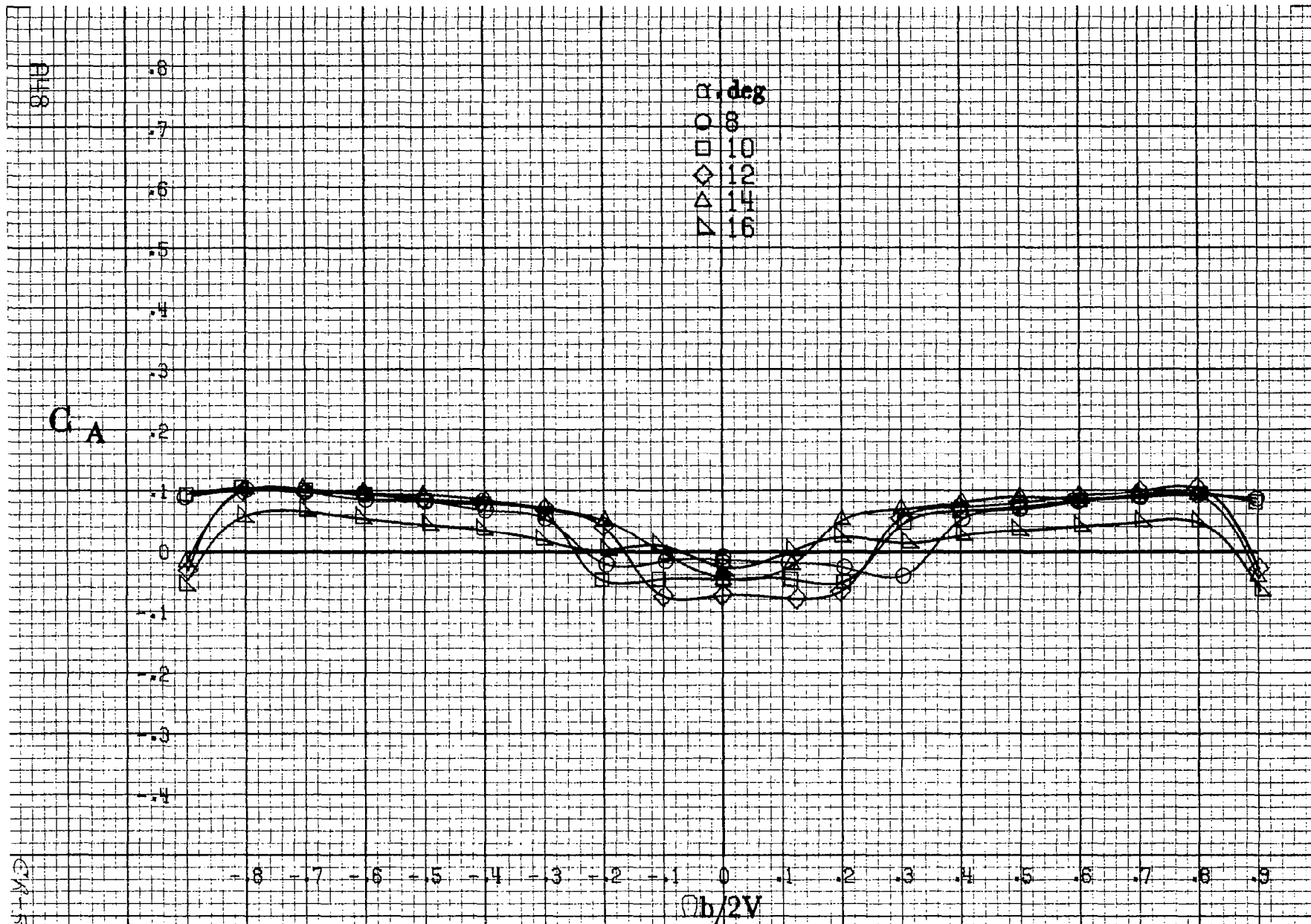
(d) $\alpha = 55$ to 90 deg, $SR = 0$.

Figure A5. Concluded.
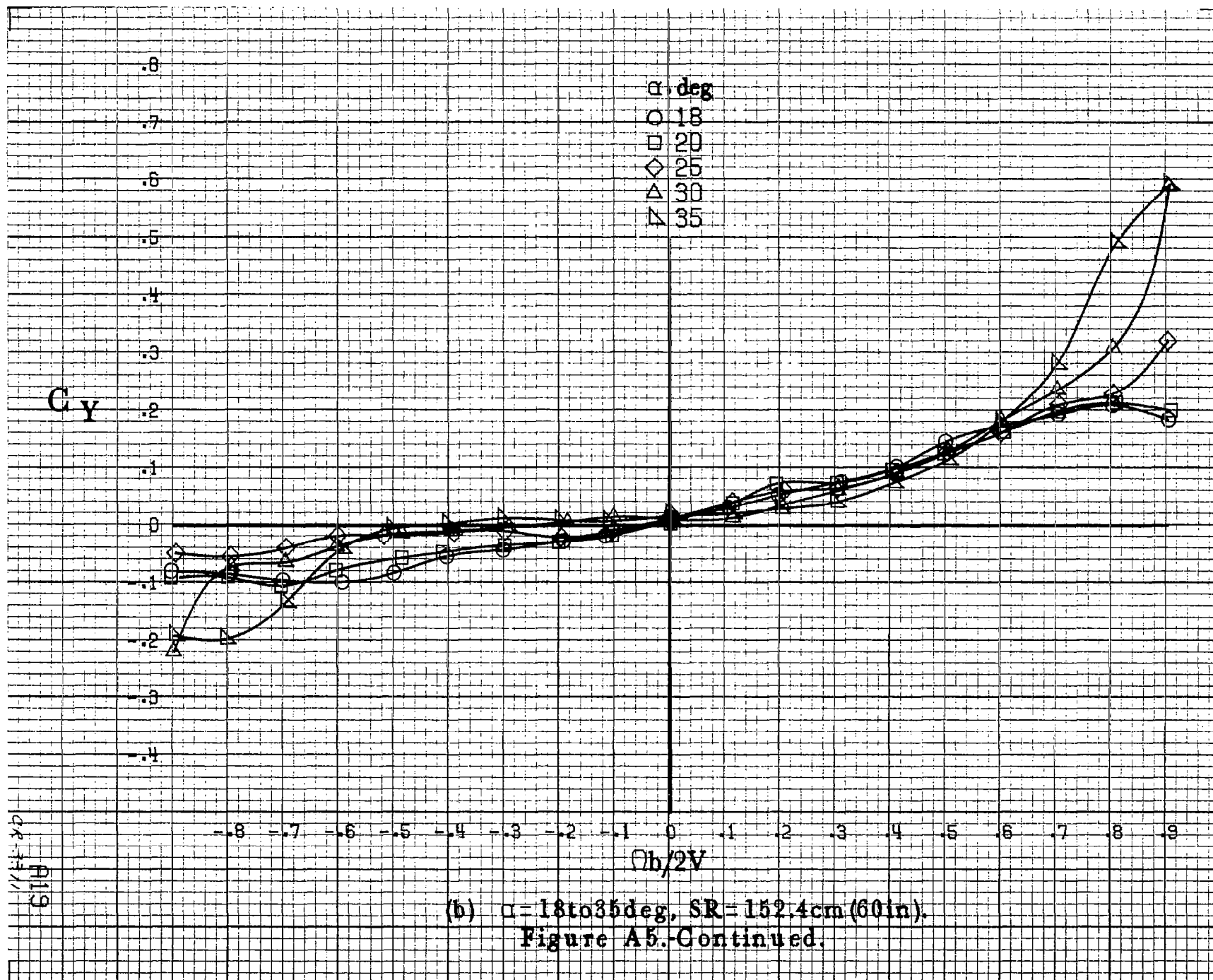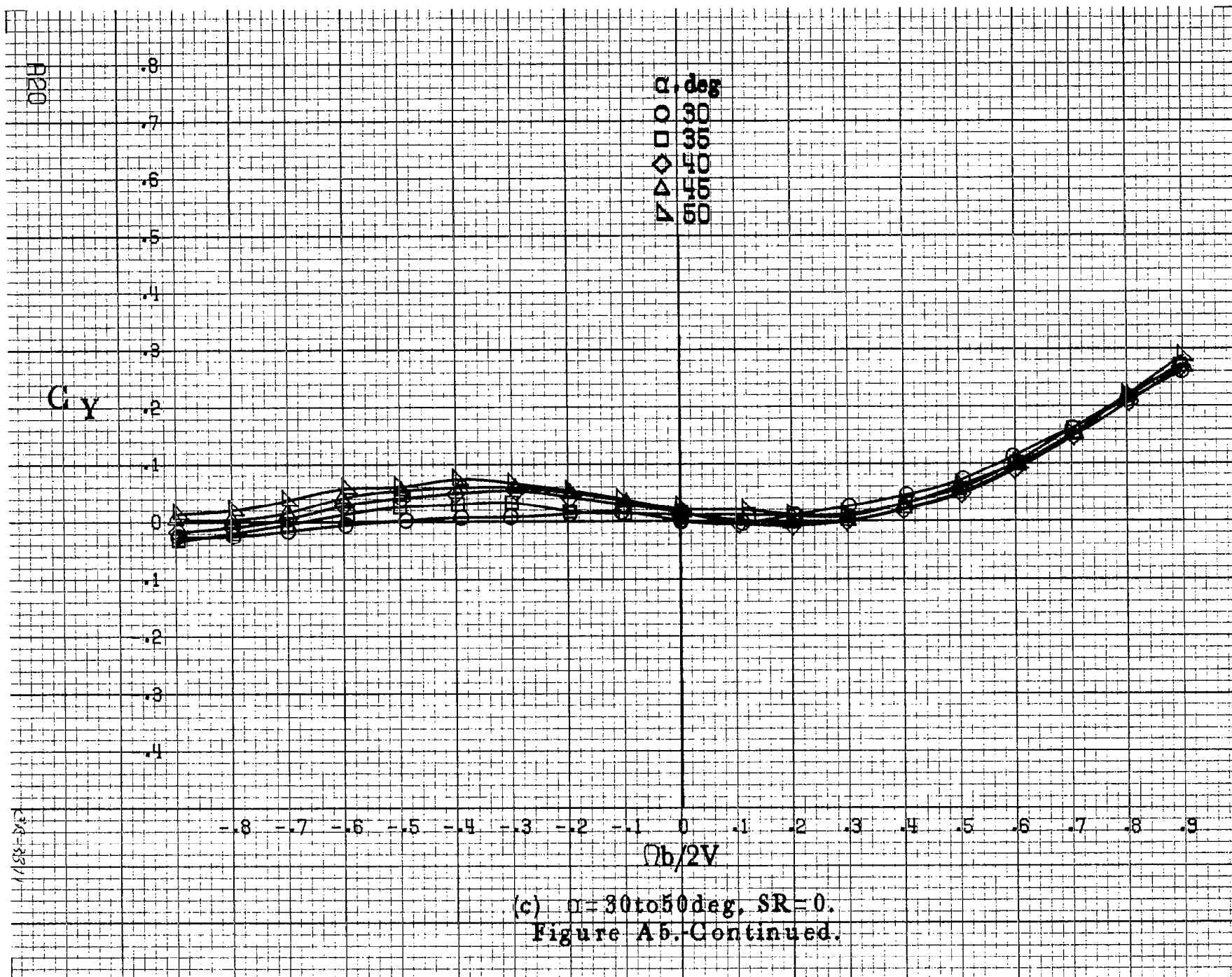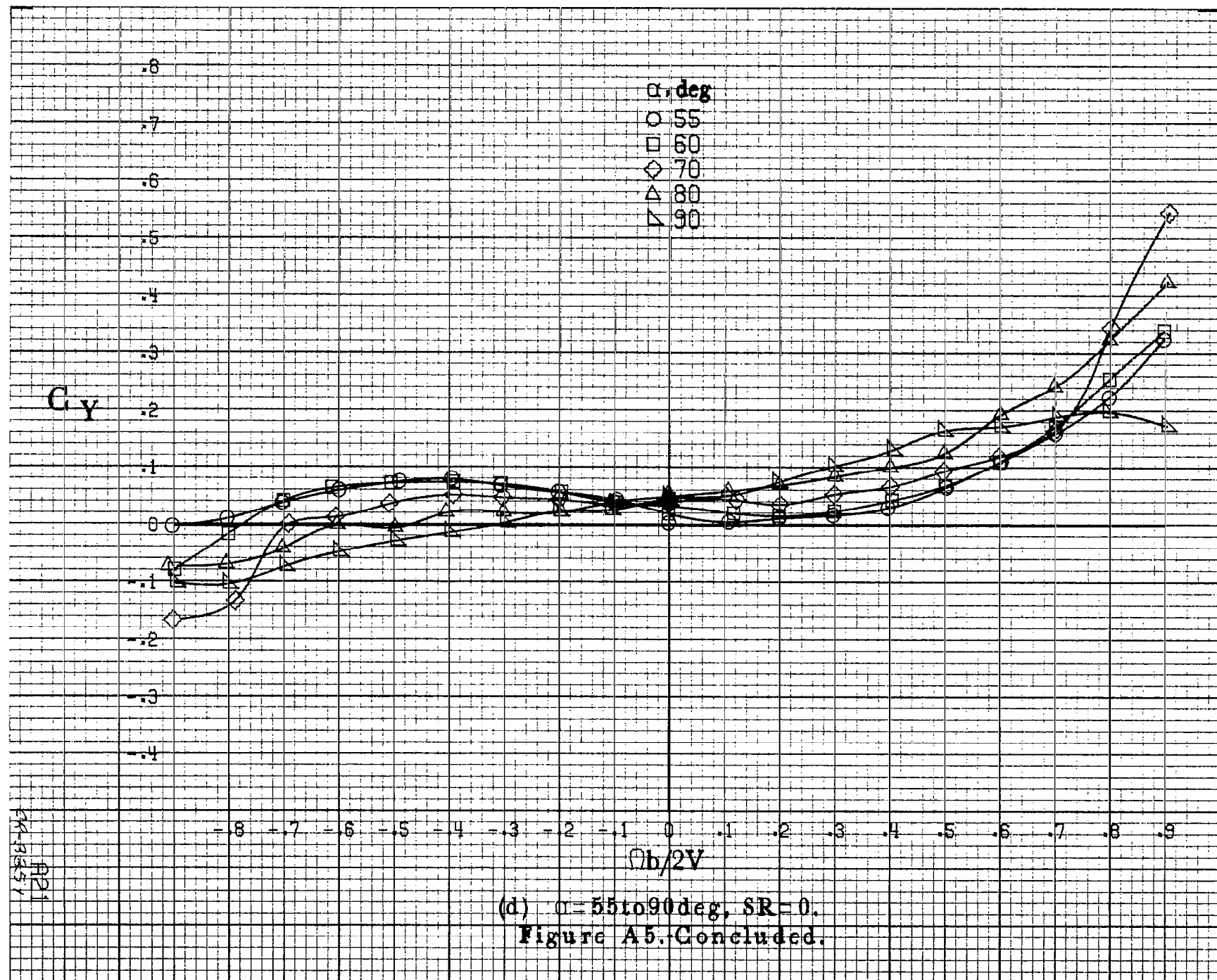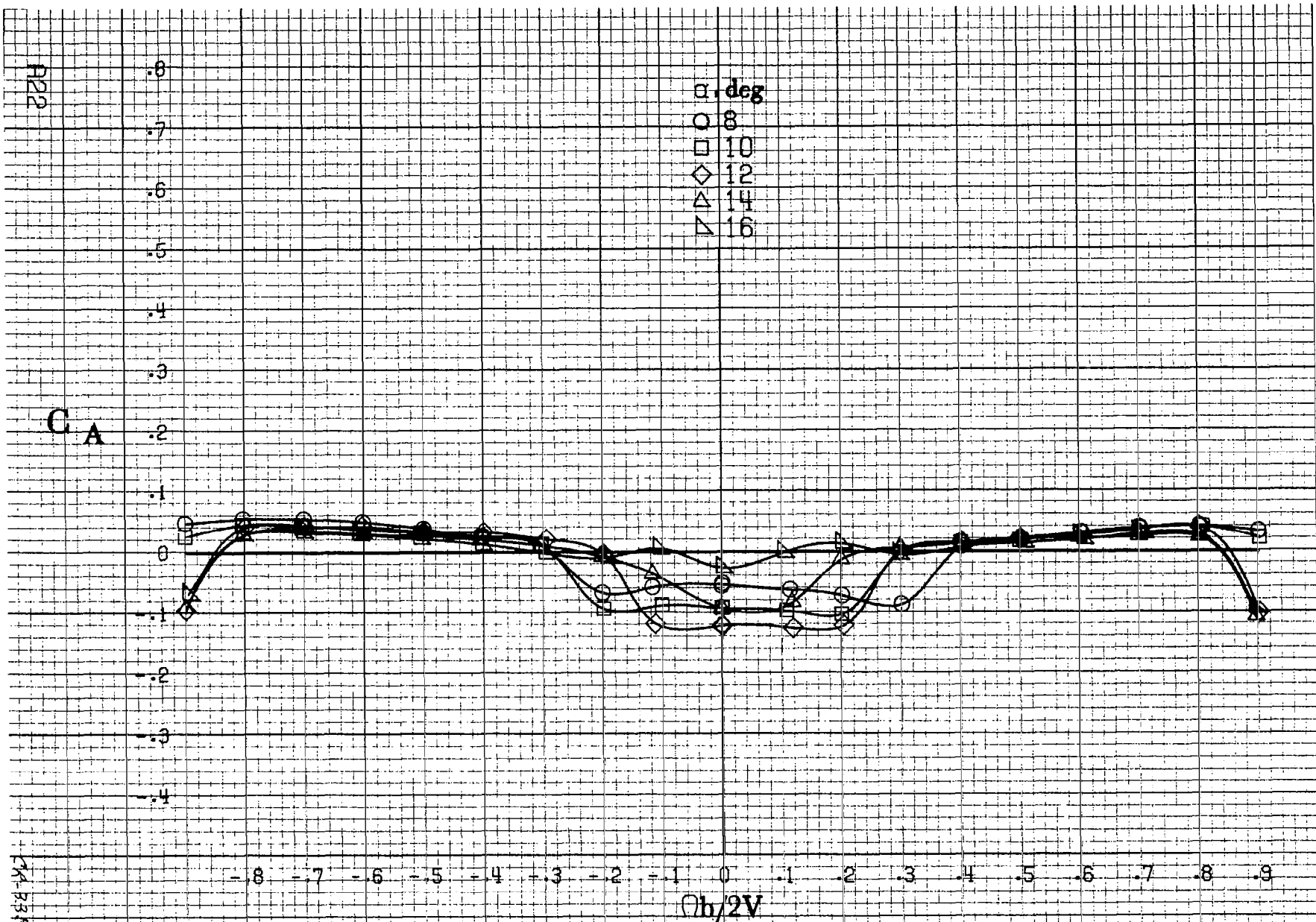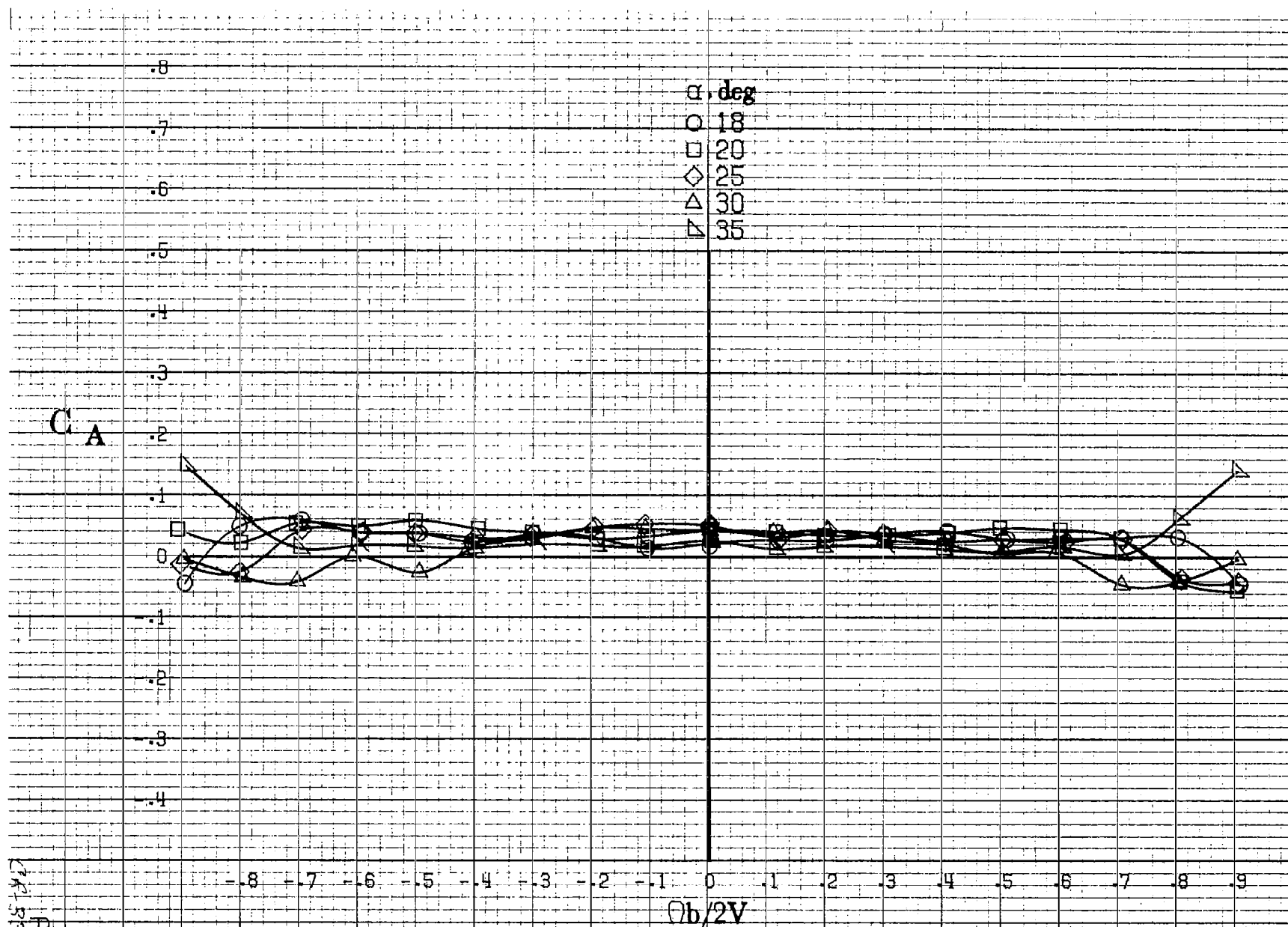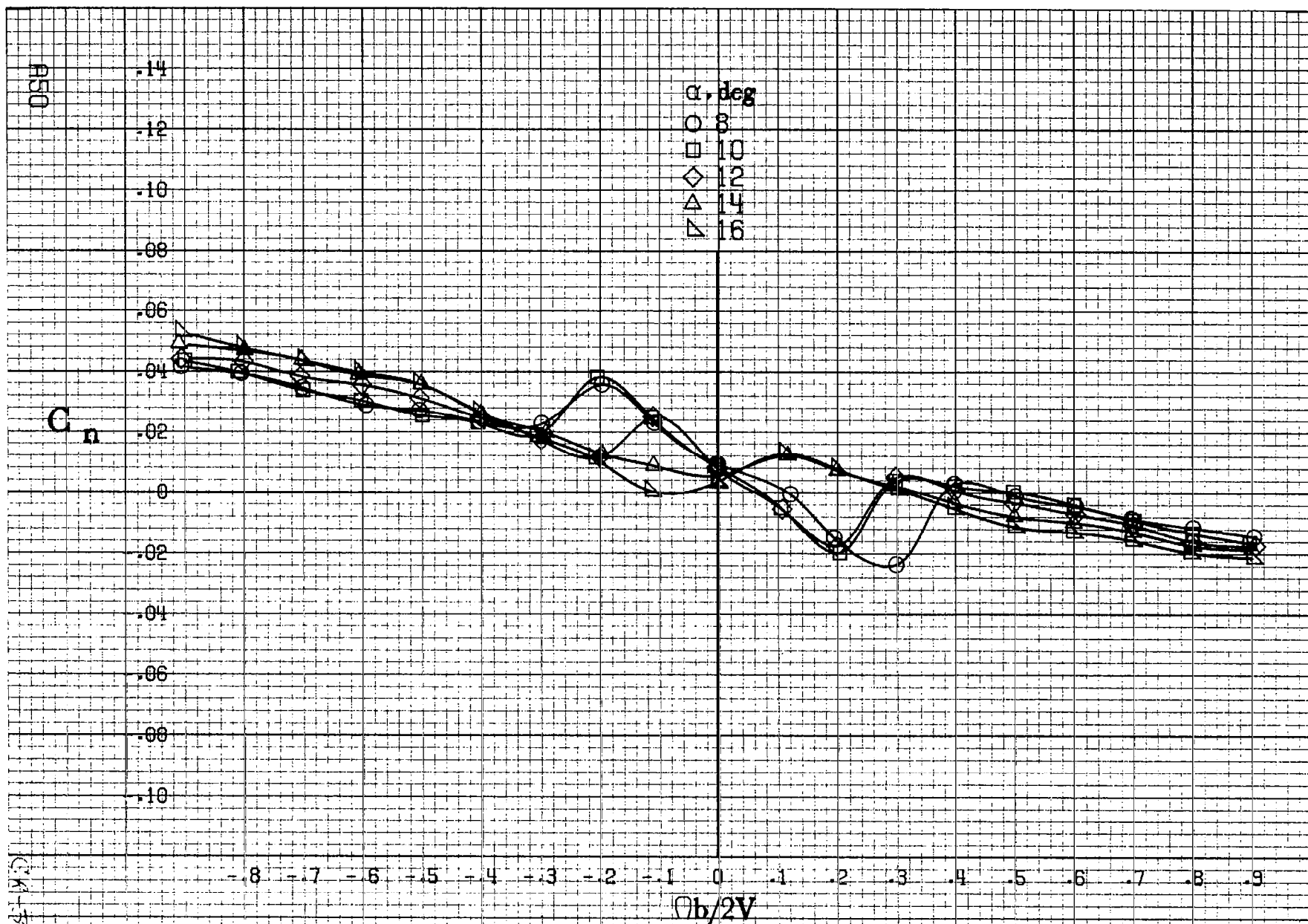
(a) α = 8 to 16 deg, SR = 152.4 cm (60 in).

Figure A6.-Effect of rotation rate and angle of attack on axial-force coefficient for basic configuration. $\delta_e = 0°$, $\delta_a = 0°$, $\delta_r = 0°$, $\beta = 0°$.
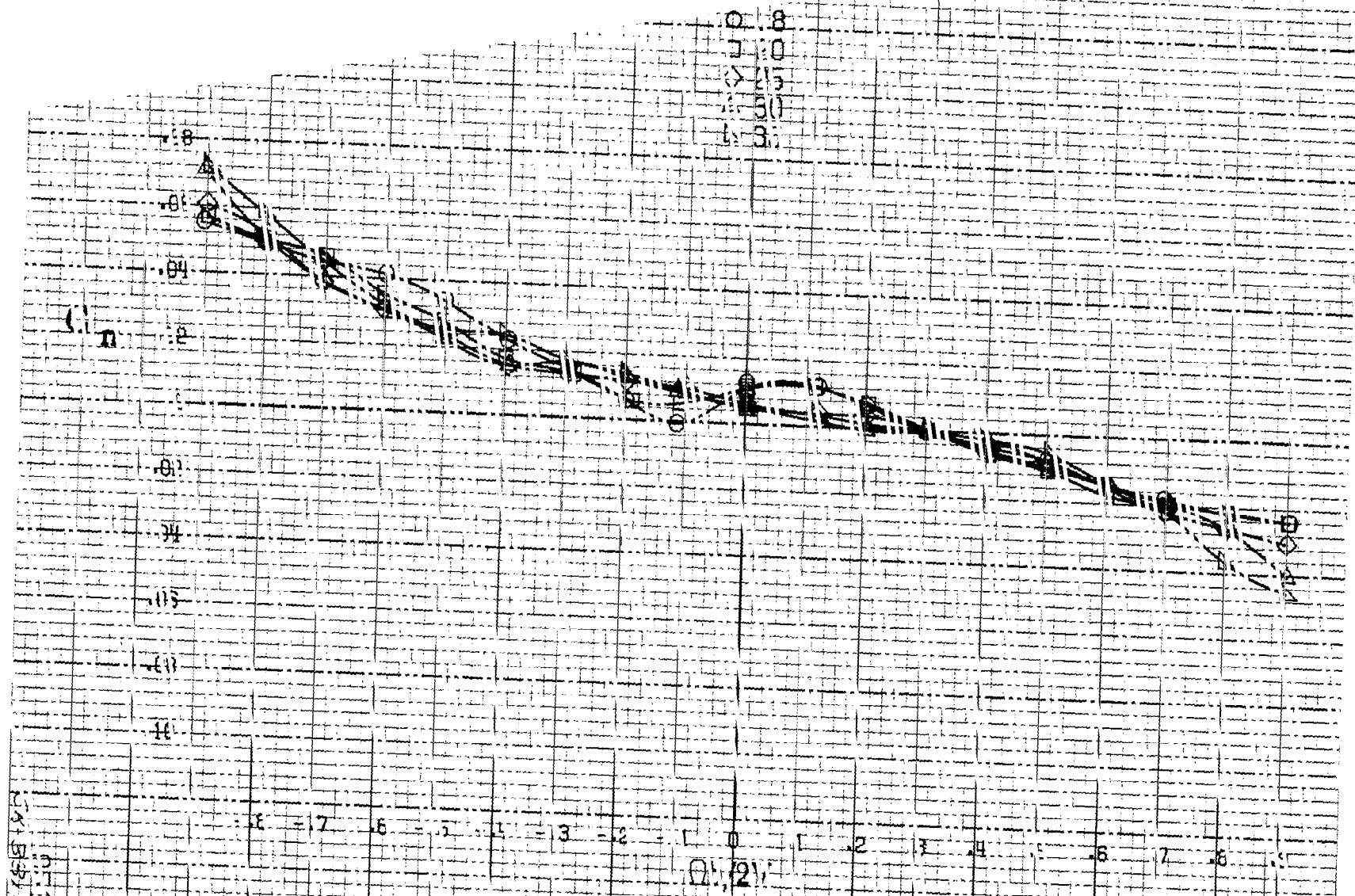
(b) α = 18 to 35 deg, SR = 152.4 cm (60 in).

Figure A6.-Continued.

(c) α = 30 to 50 deg, SR = 0.

Figure A6.- Continued.
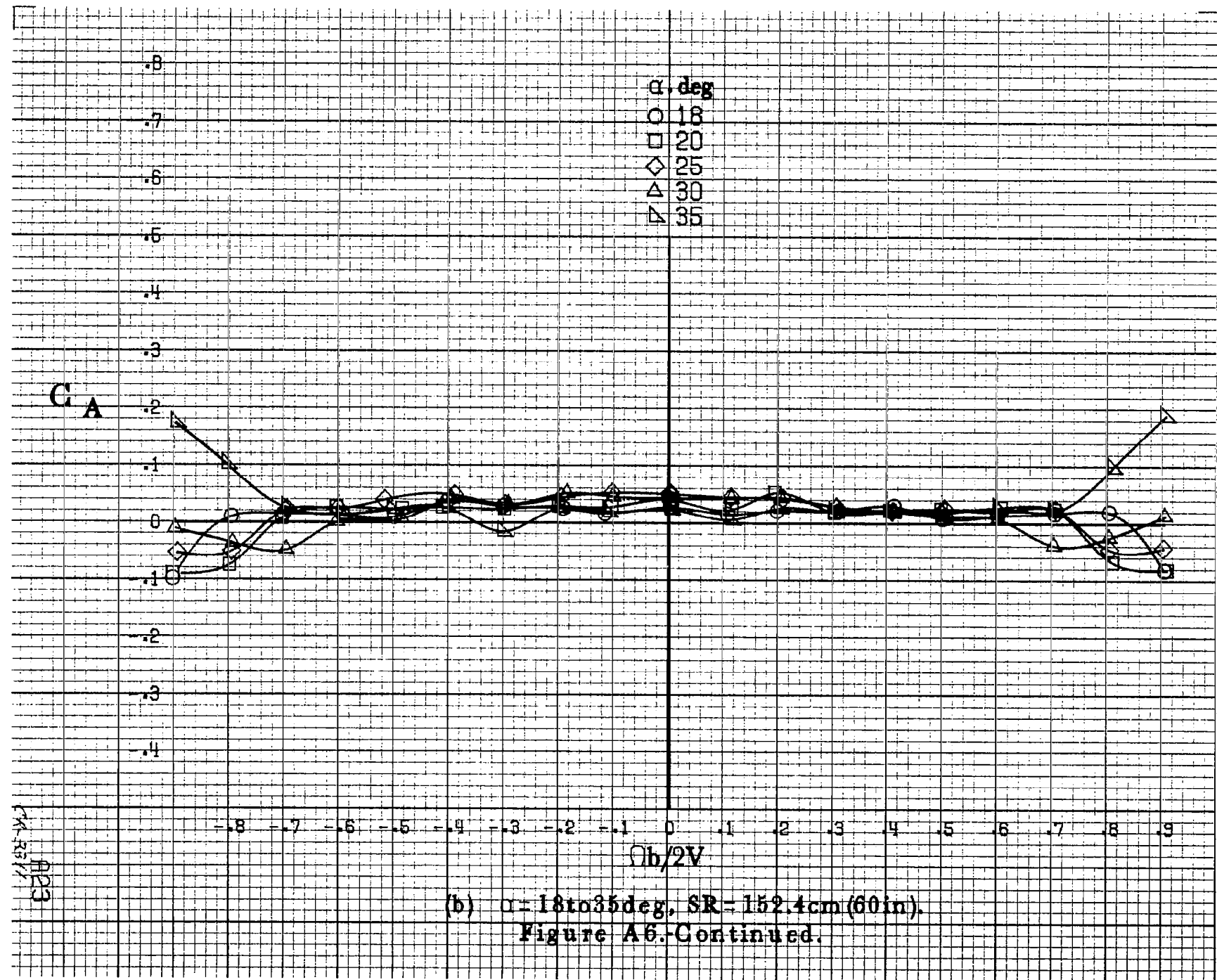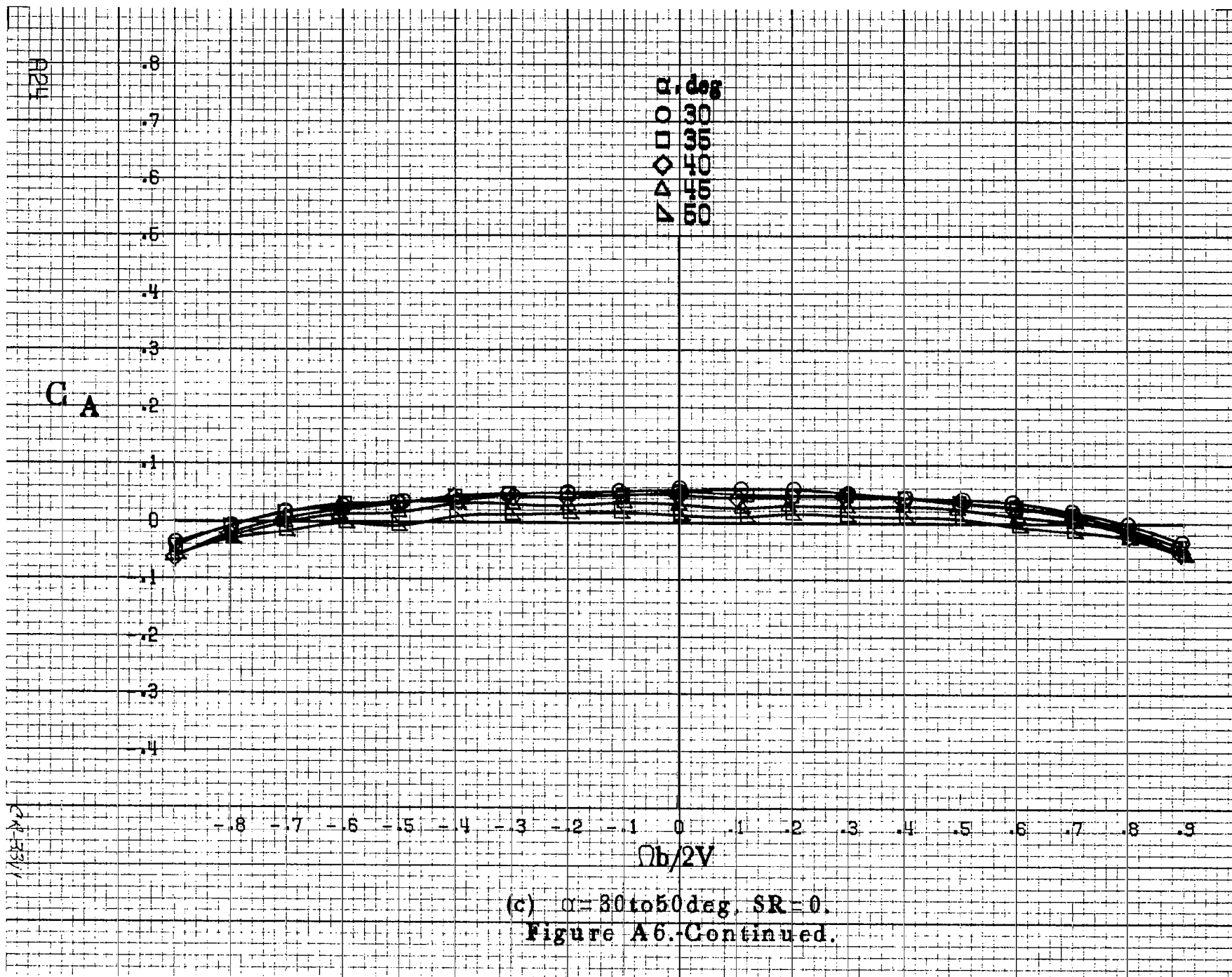
(d) α = 55 to 90 deg, SR = 0.

Figure A6. Concluded.
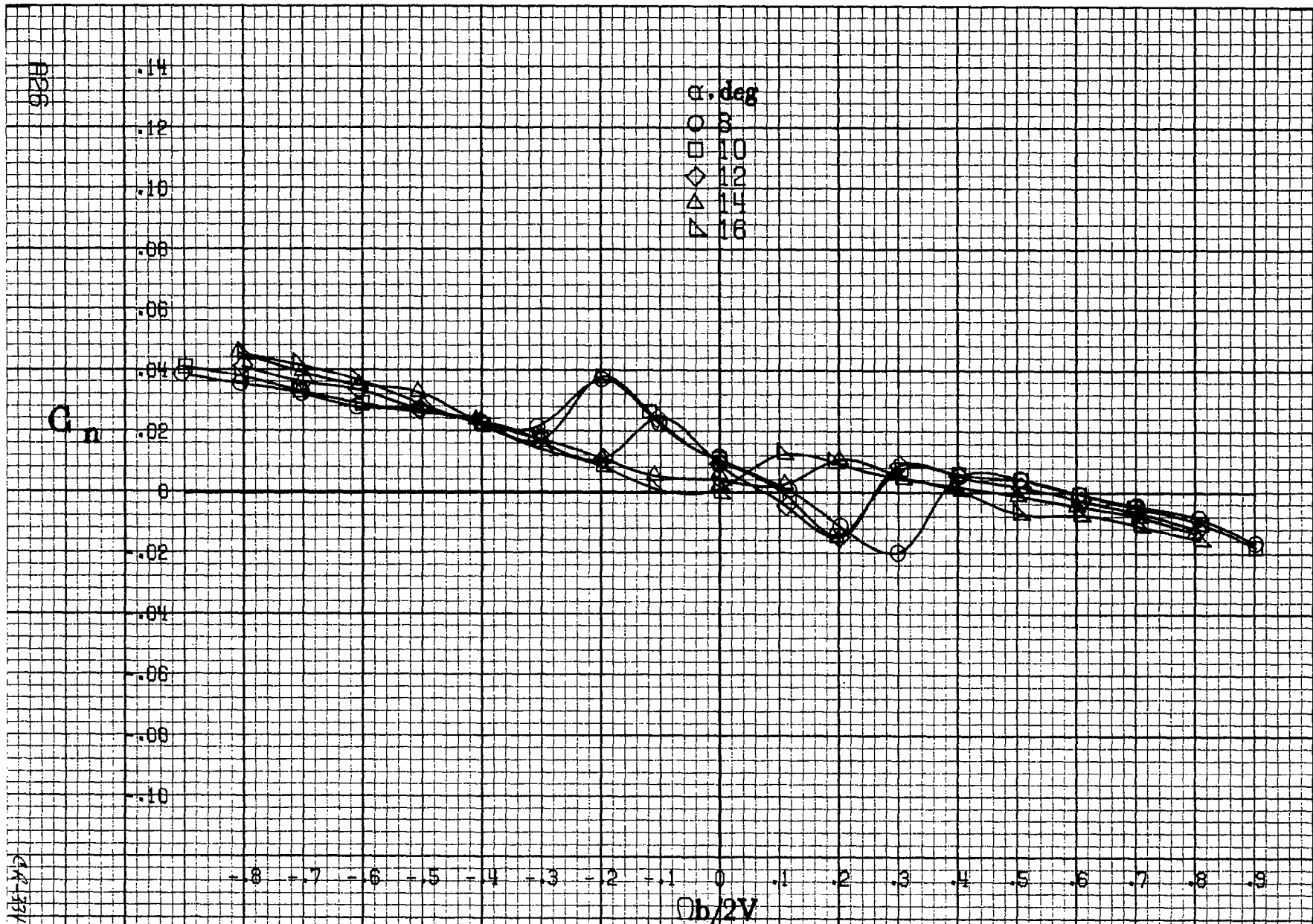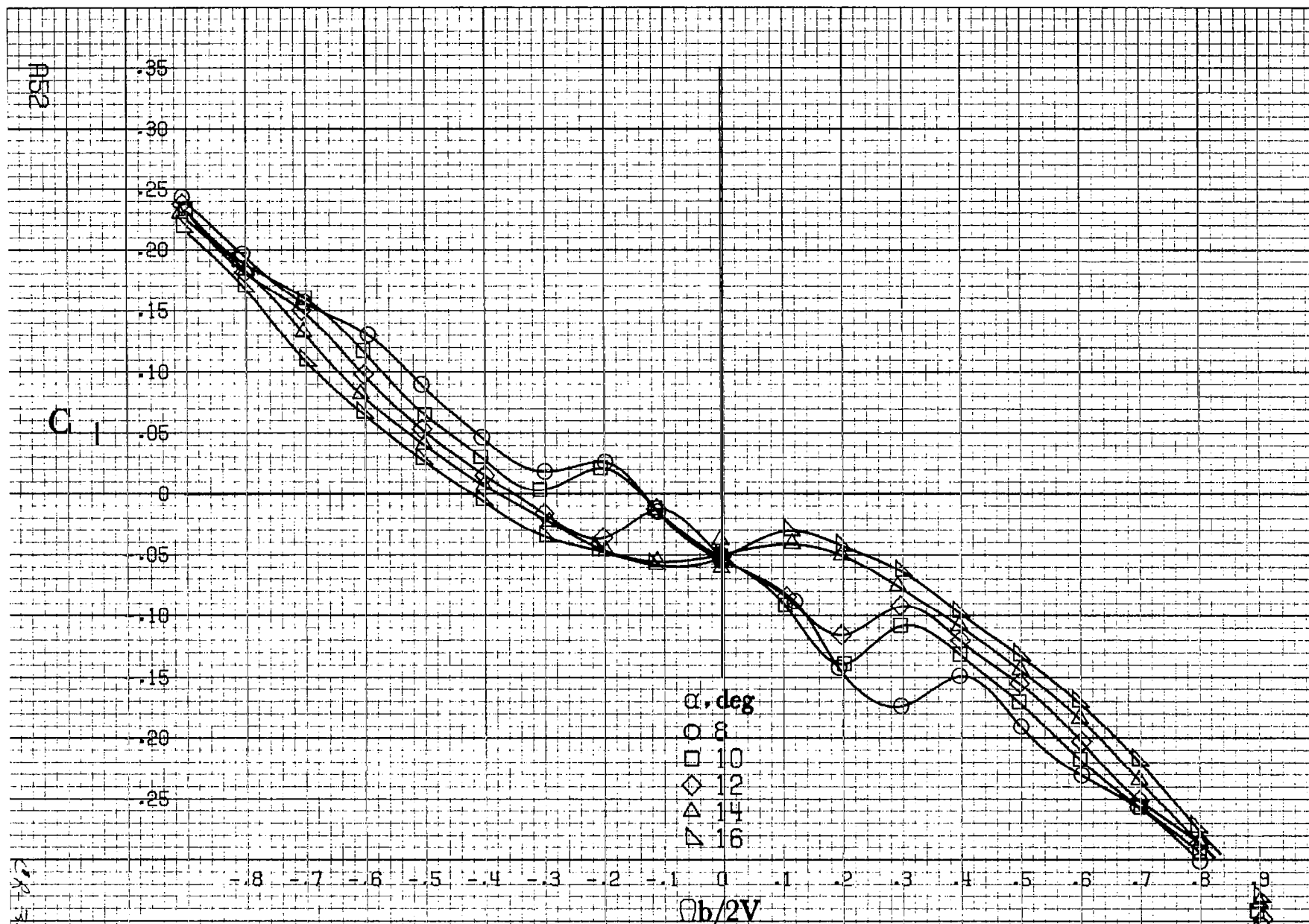
(a) α = 8 to 16 deg, SR = 152.4 cm (60 in).

Figure A7.-Effect of rotation rate and angle of attack on yawing-moment coefficient for basic configuration. δe = 17°, δa = 0°, δr = -24°, β = 0°.
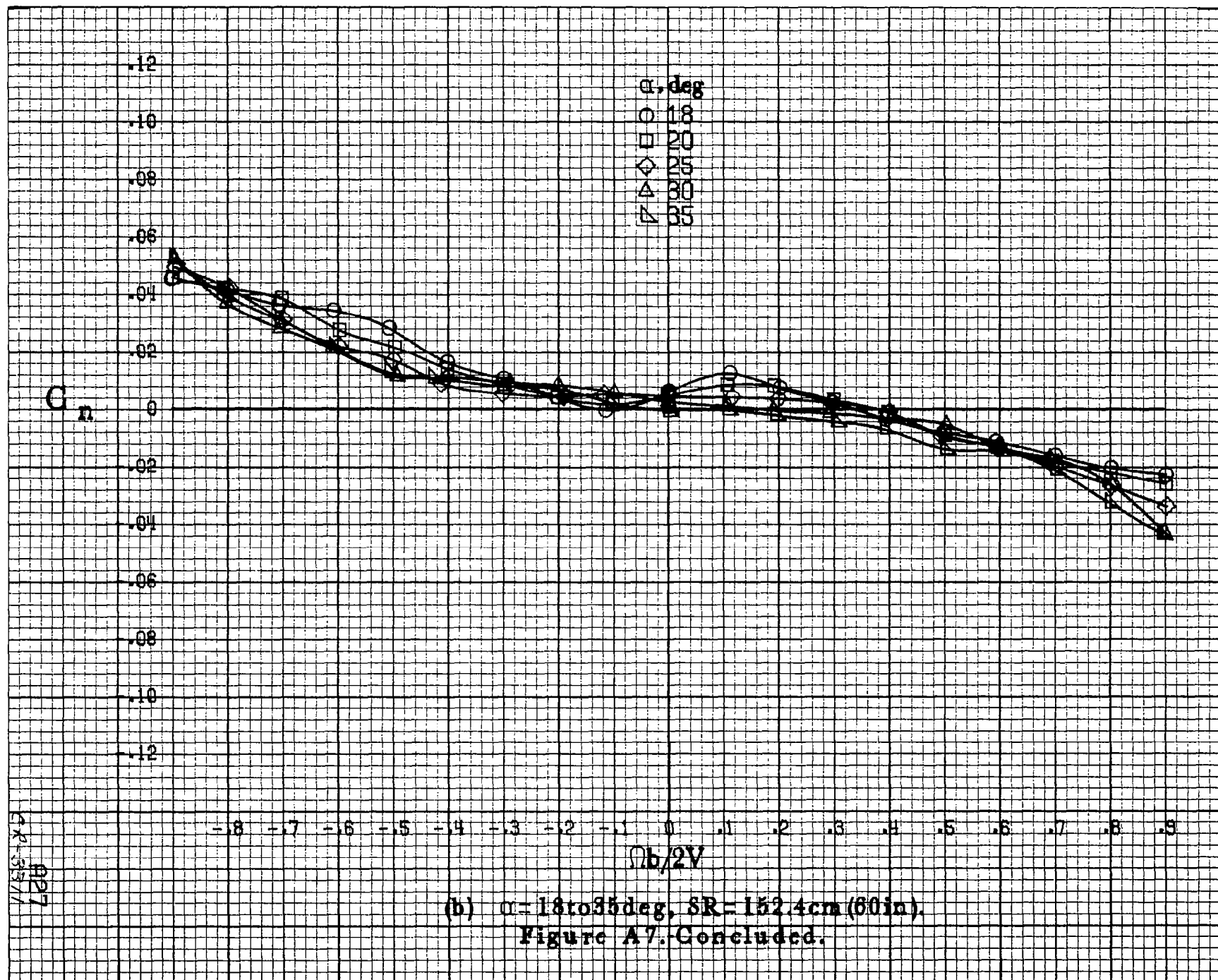
(b) $\alpha = 18$ to 35 deg, $SR = 152.4$ cm (60 in).

Figure A7. Concluded.

(a) $\alpha = 8$ to 16 deg, $SR = 152.4$ cm (60 in).

Figure A8.-Effect of rotation rate and angle of attack on rolling-moment coefficient for basic configuration. $\delta_e = 17°$, $\delta_a = 0°$, $\delta_r = -24°$, $\beta = 0°$.
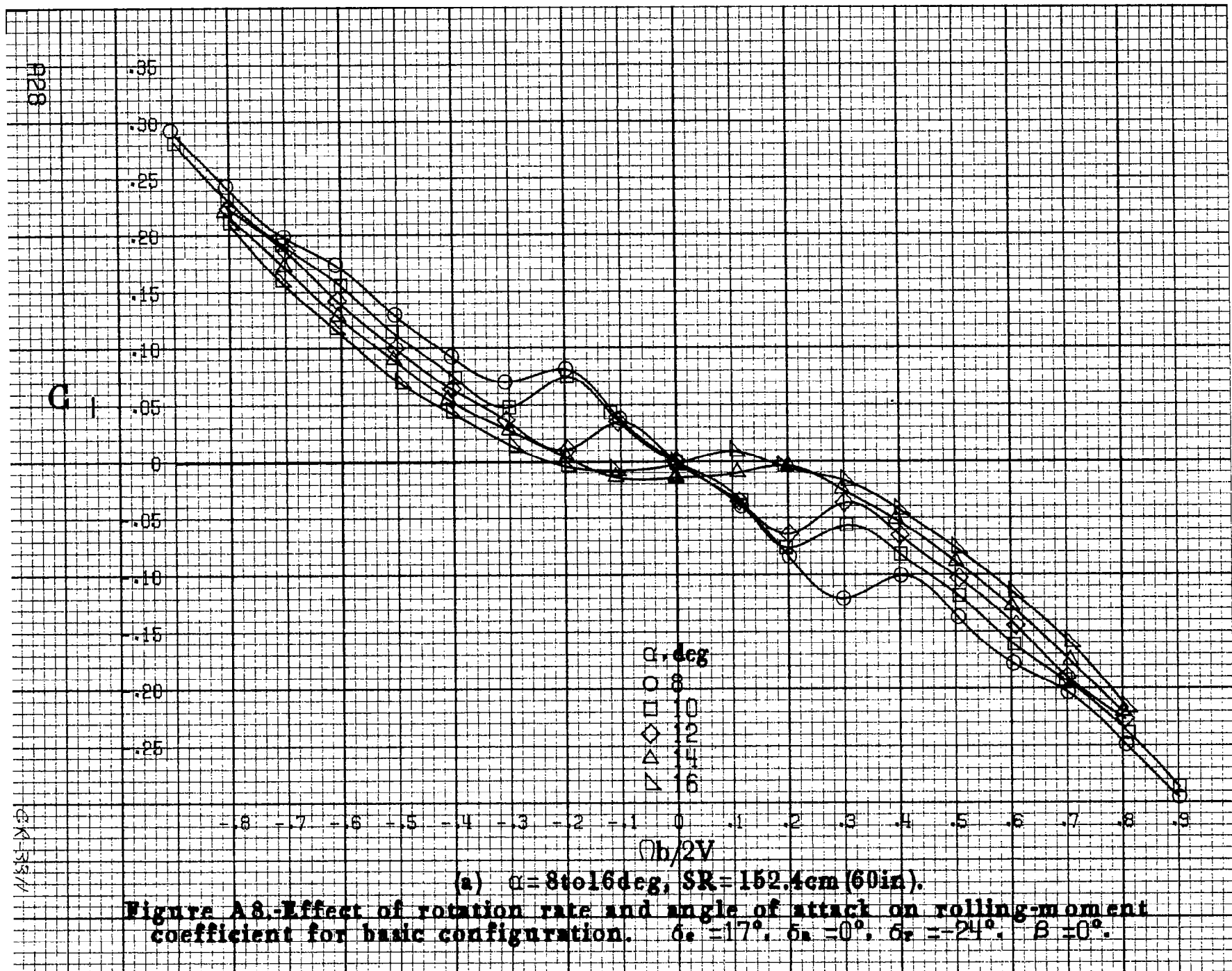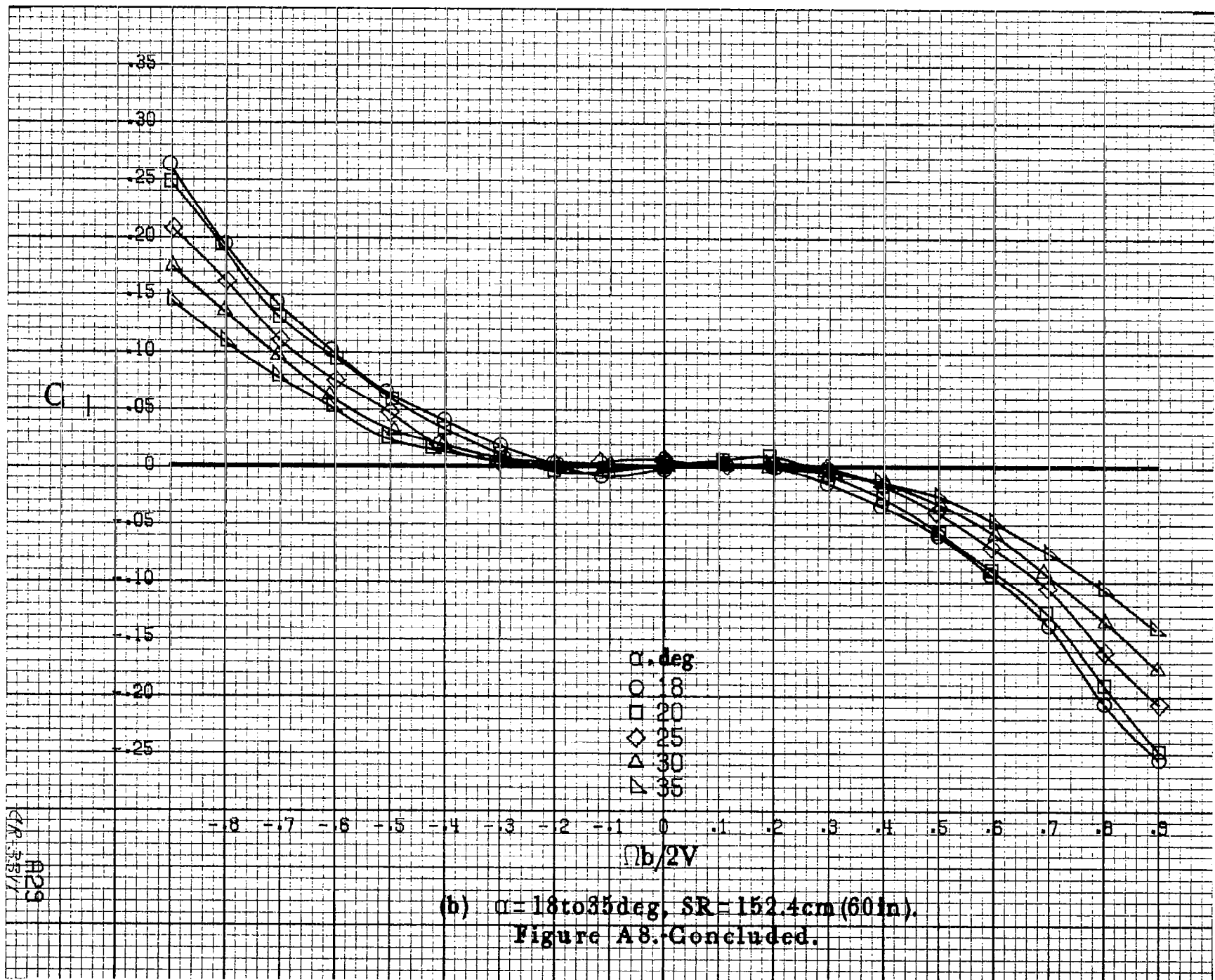
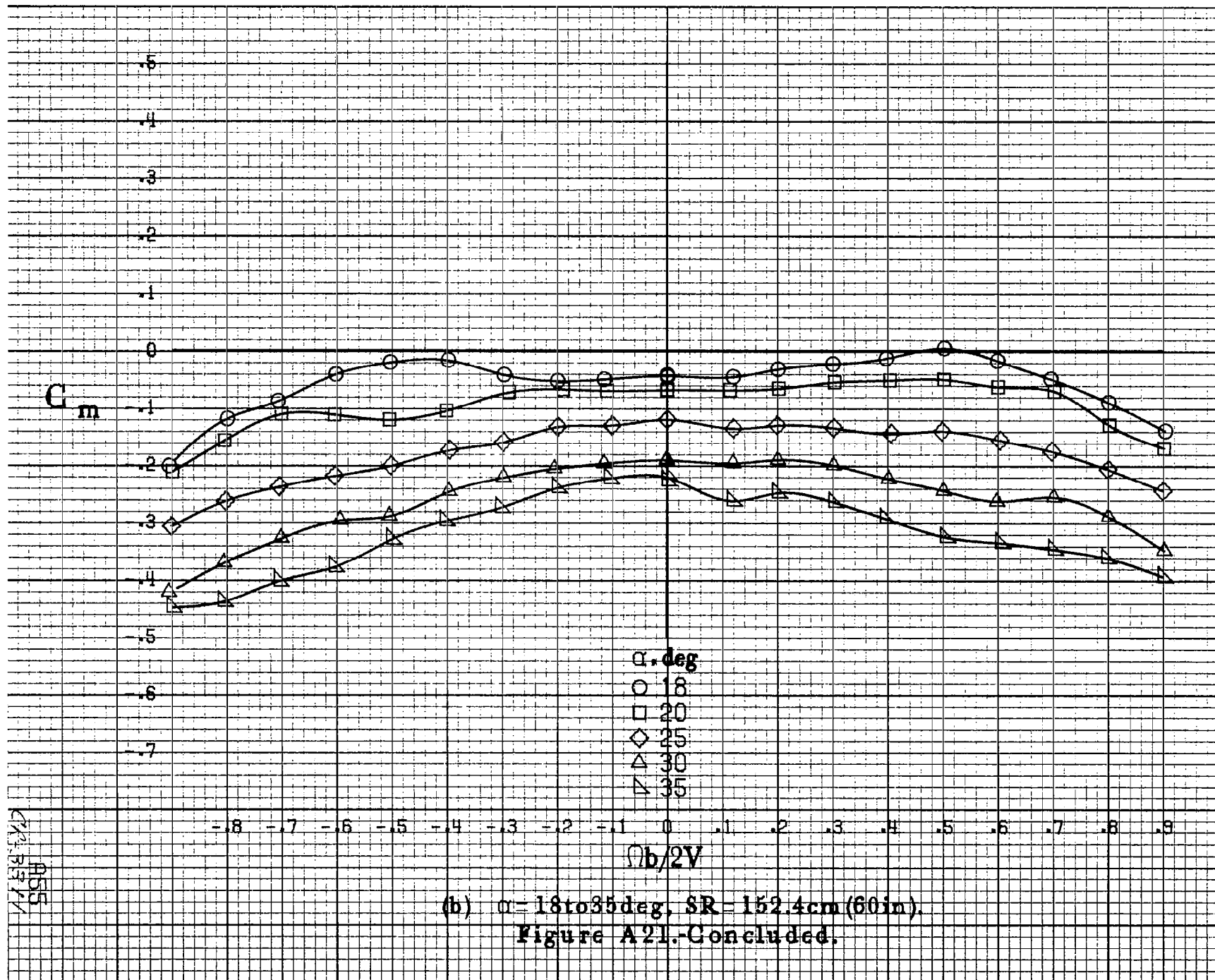(b) α = 18 to 35 deg, SR = 152.4 cm (60 in).

Figure A 8. Concluded.

(a) α = 8 to 16 deg, SR = 152.4 cm (60 in).

Figure A9.-Effect of rotation rate and angle of attack on pitching-moment
coefficient for basic configuration. δe =-17°, δa =0°, δr =-24°, β =0°.
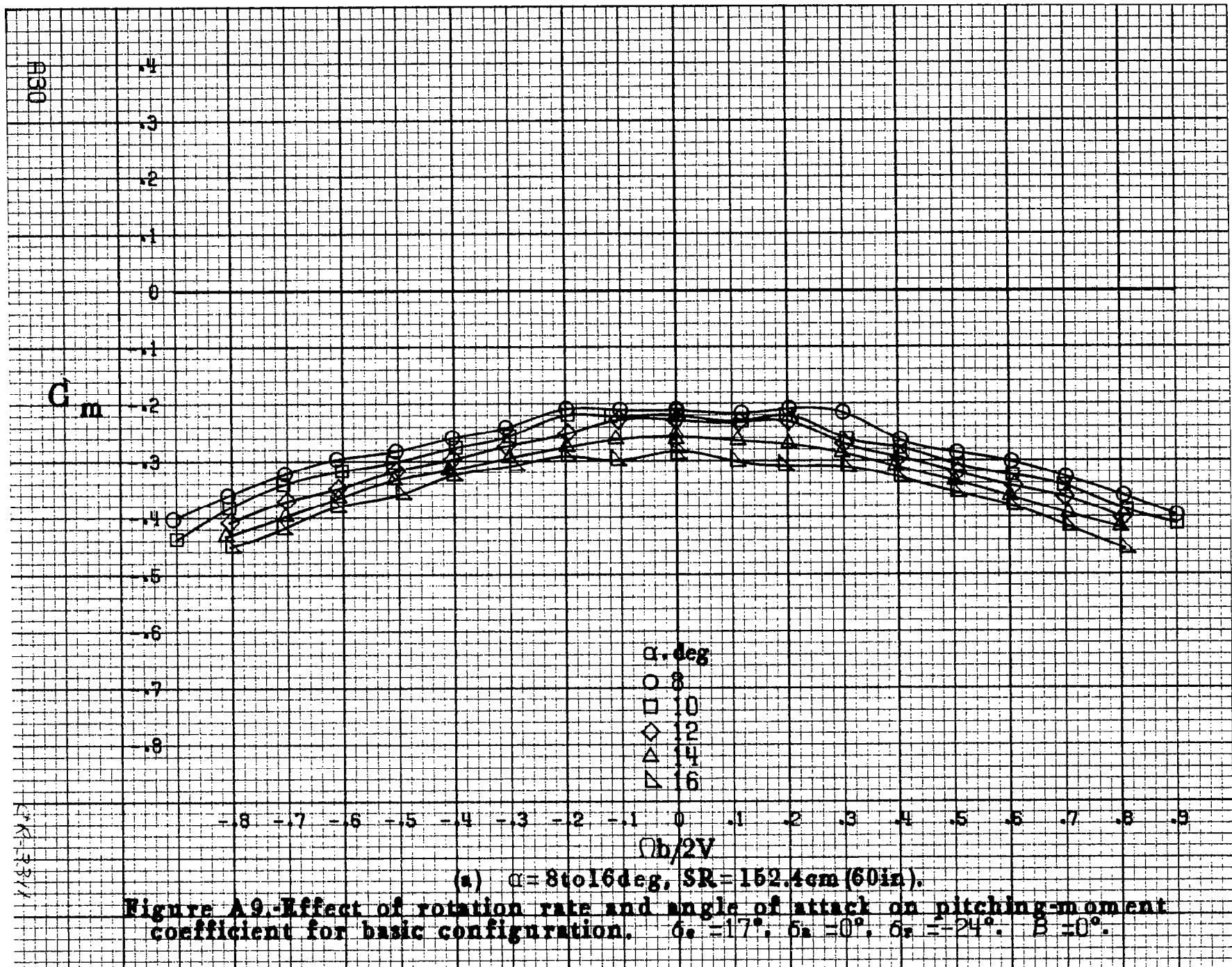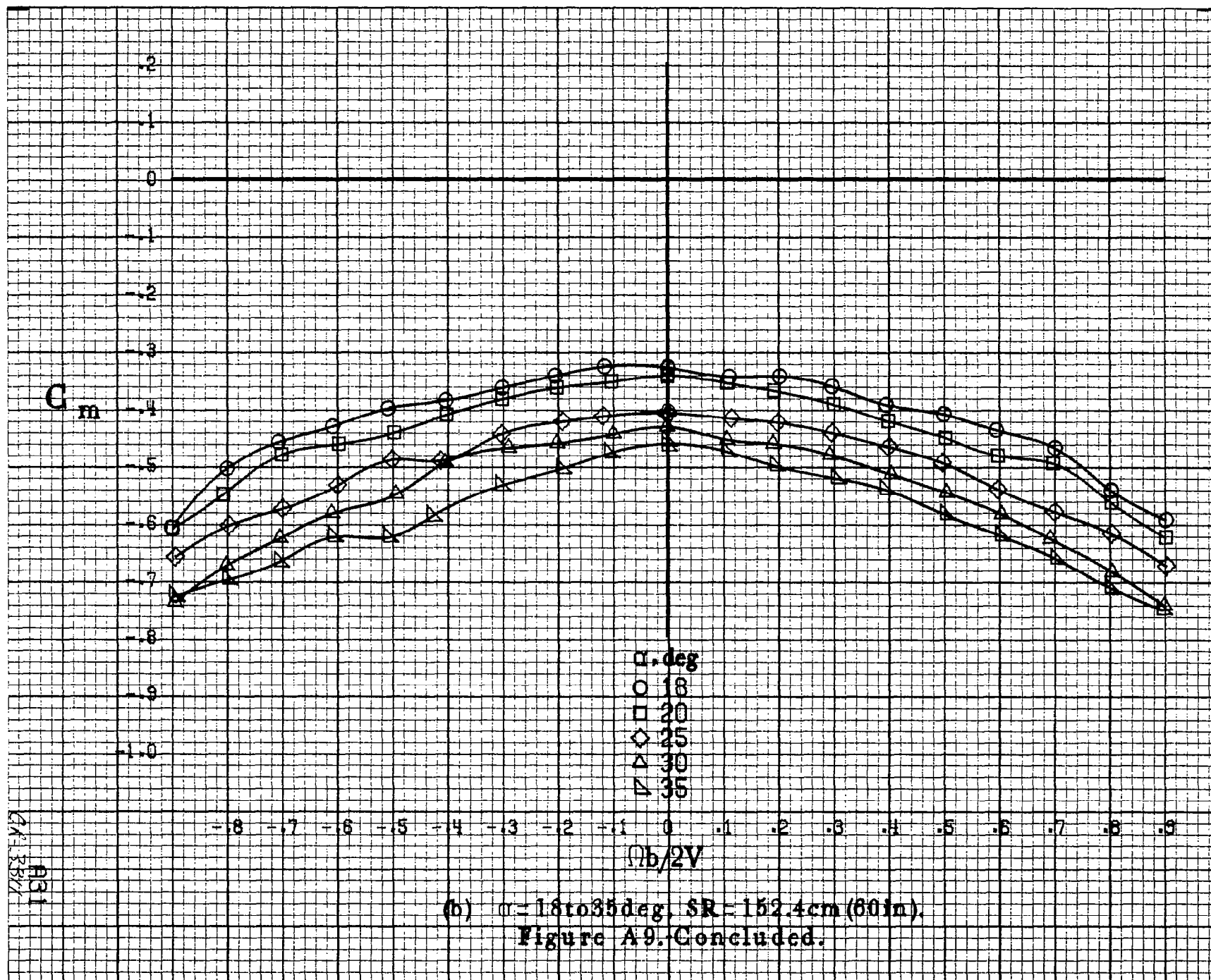
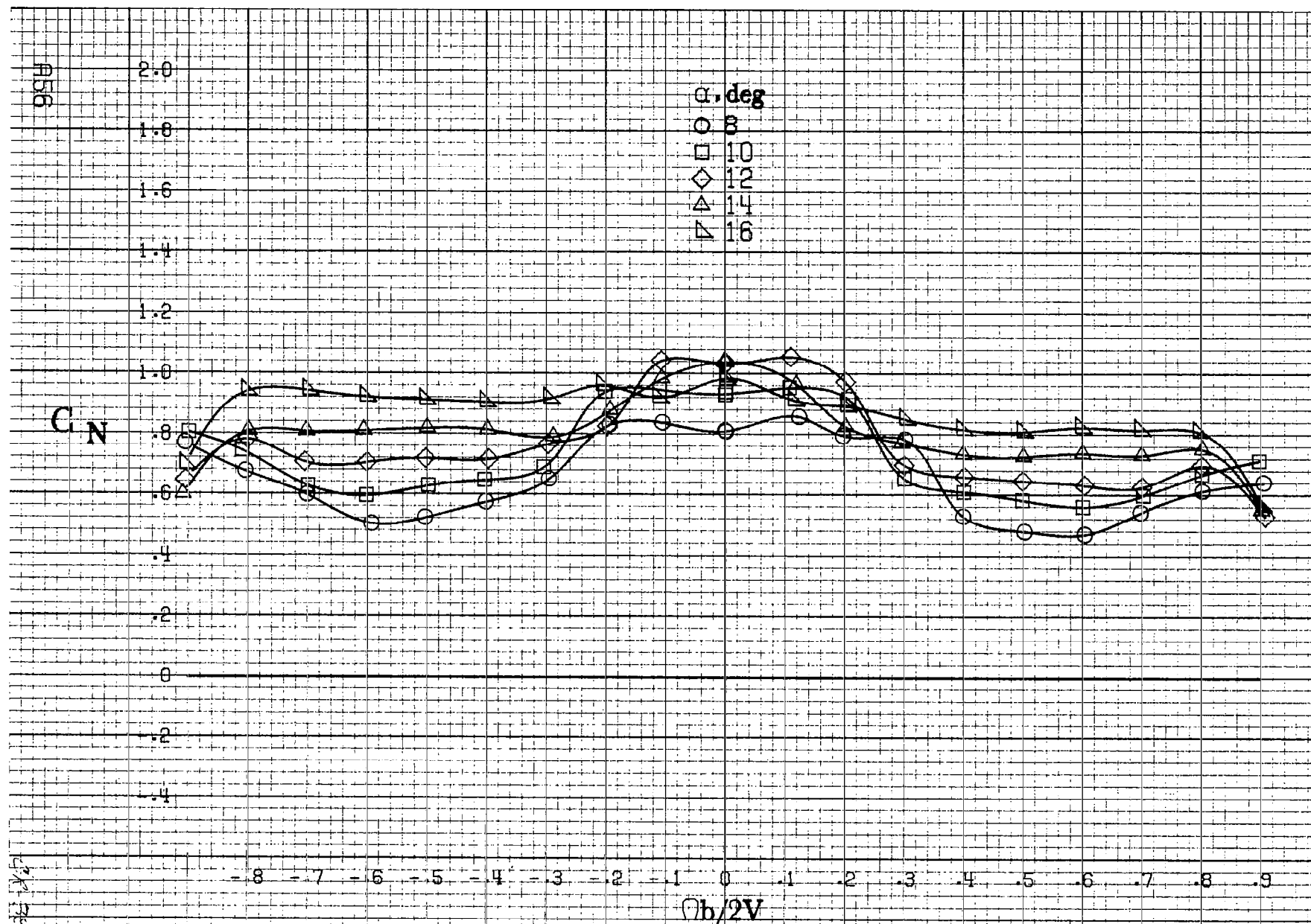(b) α = 18 to 35 deg, SR = 152.4 cm (60 in).

Figure A9. Concluded.
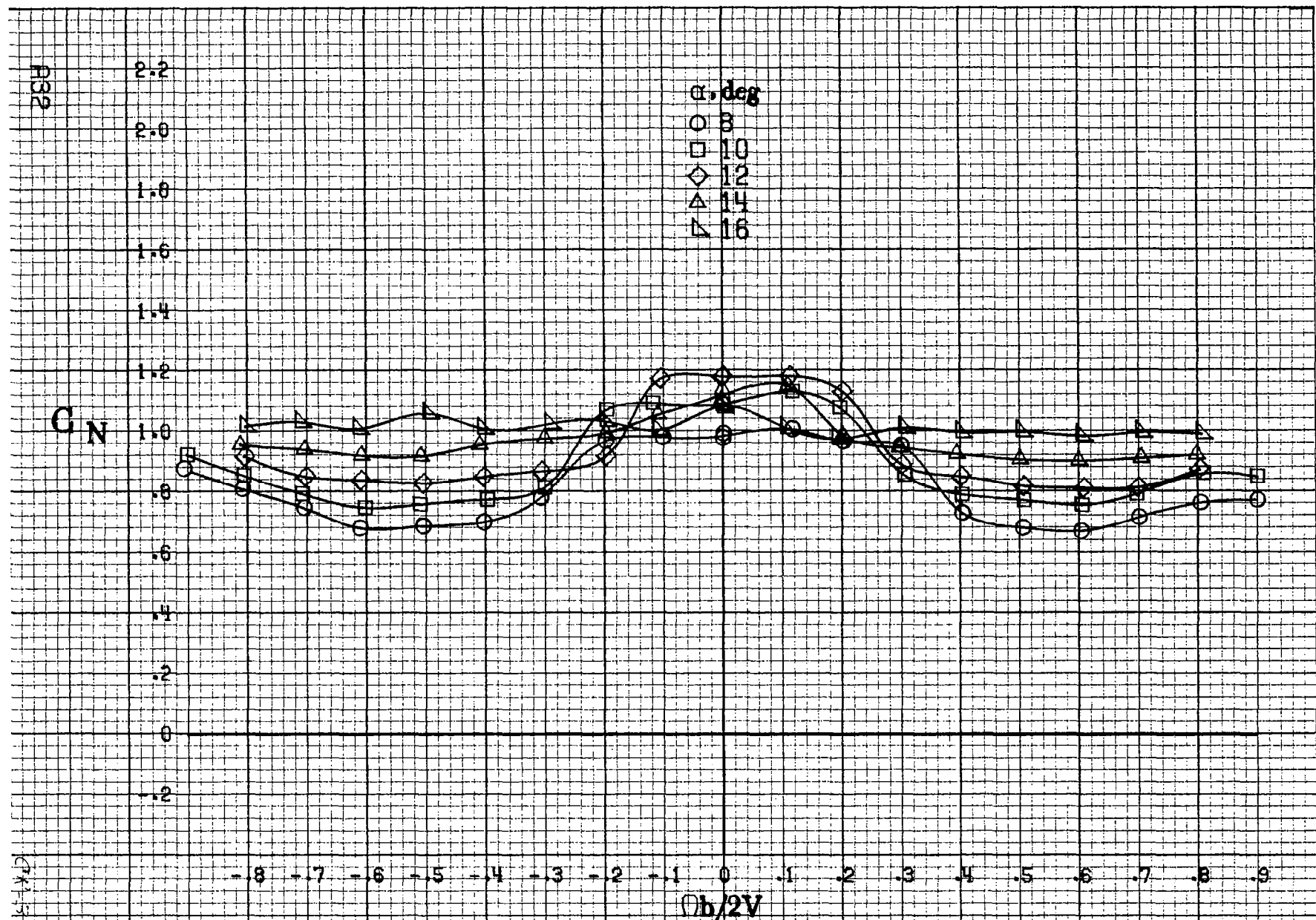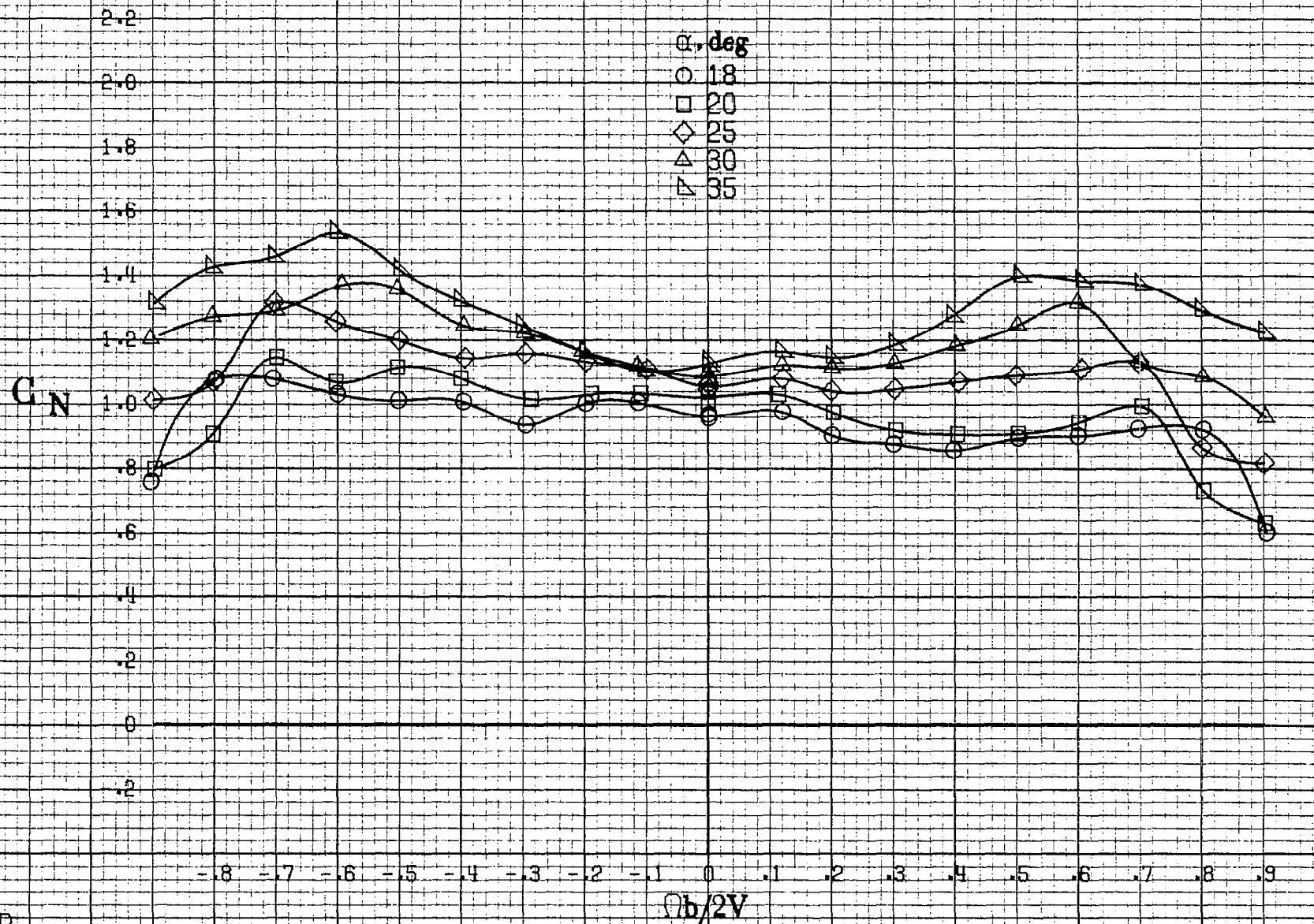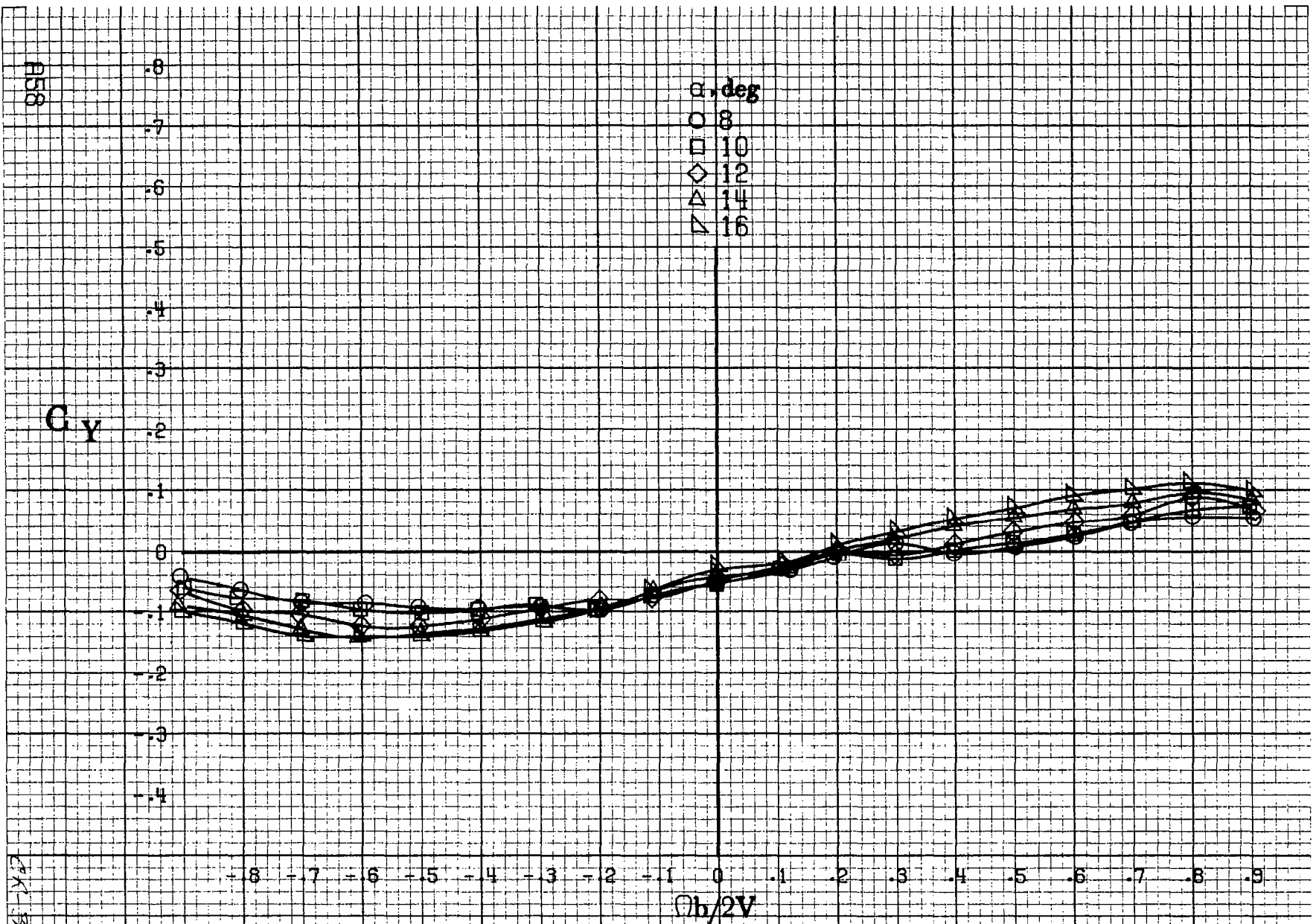
(a) $\alpha = 8$ to 16 deg, $SR = 152.4$ cm (60 in).

Figure A10.- Effect of rotation rate and angle of attack on normal-force coefficient for basic configuration. $\delta_e = -17°$, $\delta_a = 0°$, $\delta_r = -24°$, $\beta = 0°$.
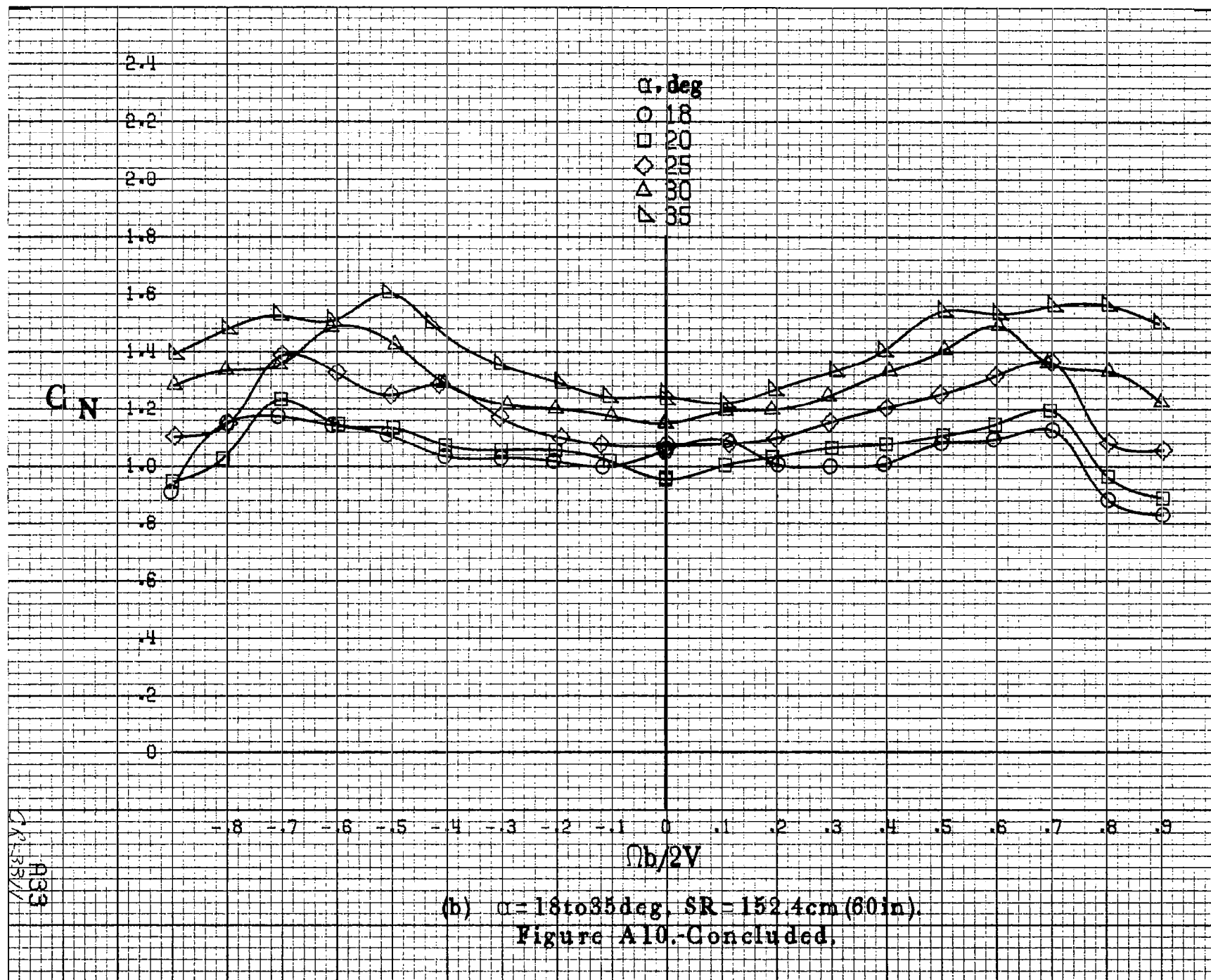
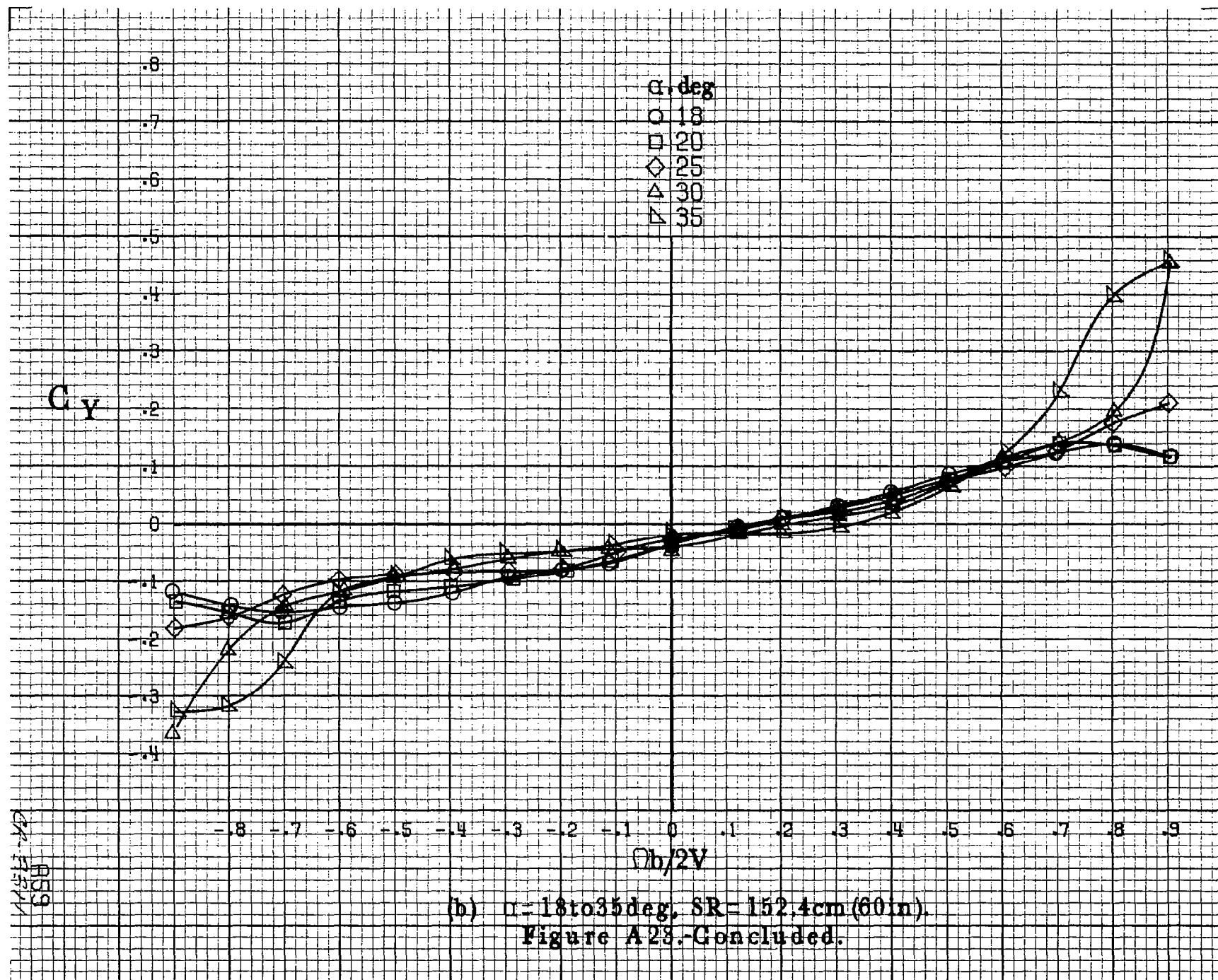(b) α = 18 to 35 deg, SR = 152.4 cm (60 in).

Figure A10.-Concluded.
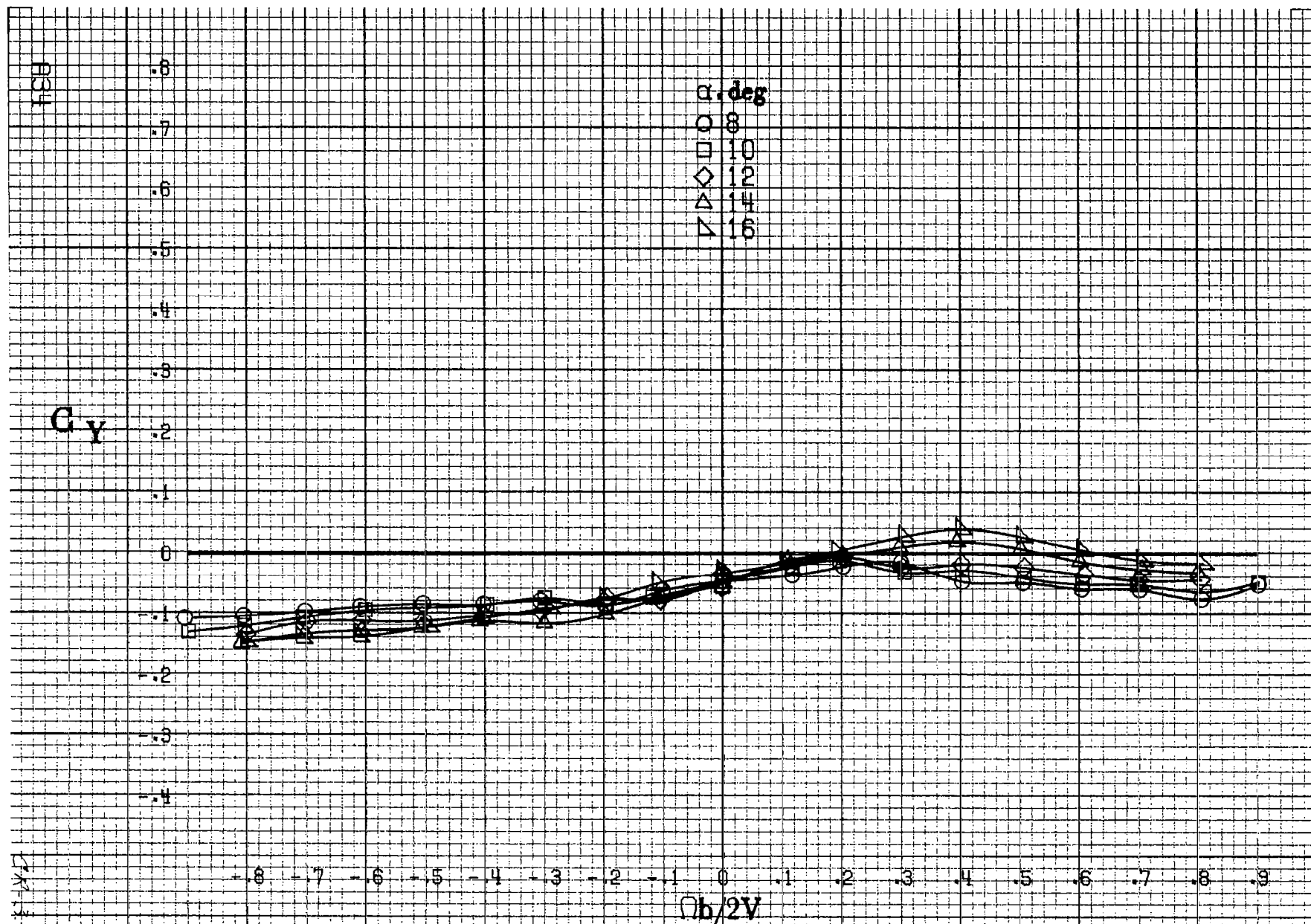
(a) α = 8 to 16 deg, SR = 152.4 cm (60 in).

Figure A11 -Effect of rotation rate and angle of attack on side-force coefficient for basic configuration. δe = 17°, δa = 0°, δr = -24°, β = 0°.

C_Y

α, deg
○ 18
□ 20
◇ 25
△ 30
◁ 35

$\Omega b/2V$

(b) $\alpha = 18$ to 35 deg, $SR = 152.4$ cm $(60$ in$)$.

Figure A11.-Concluded.
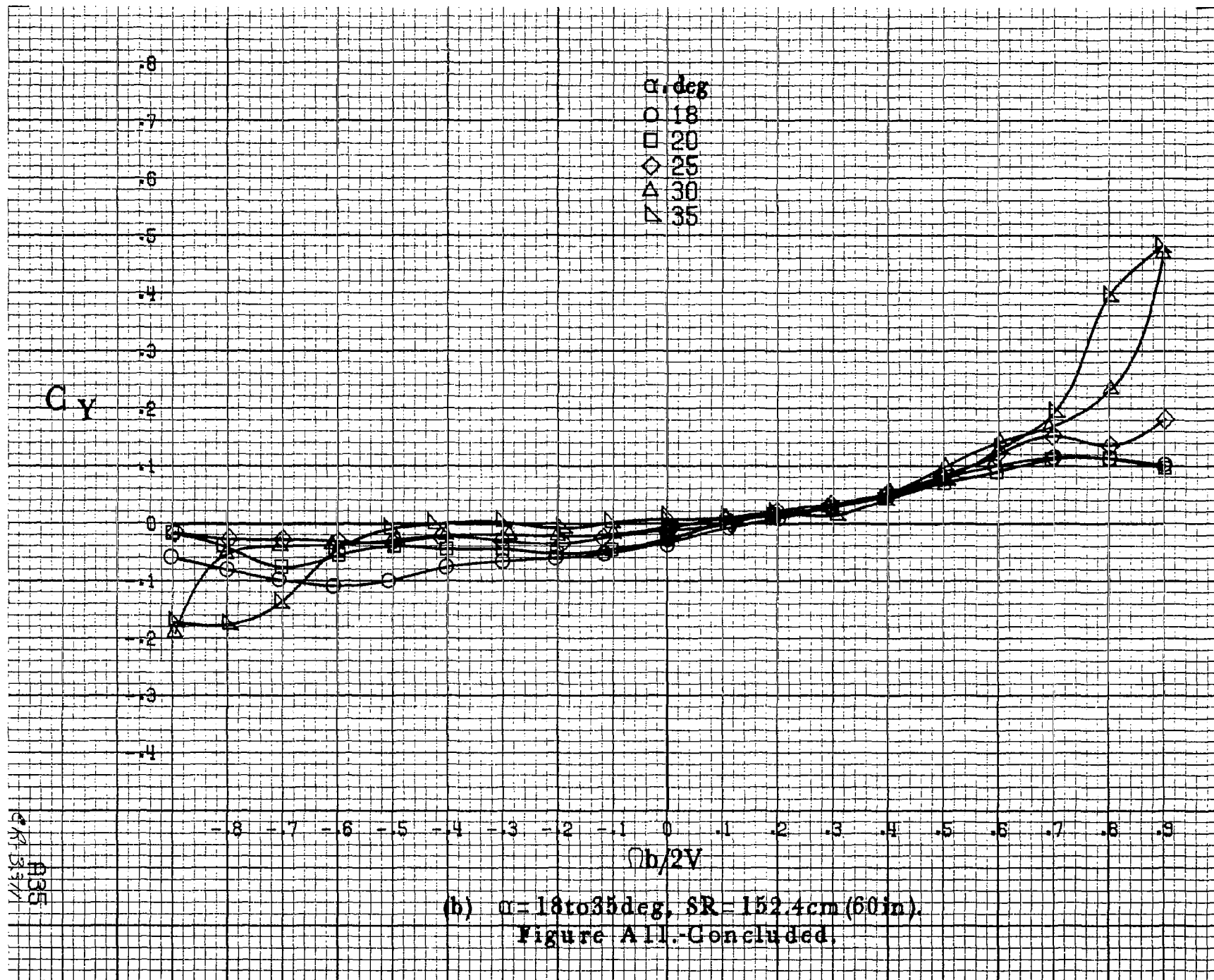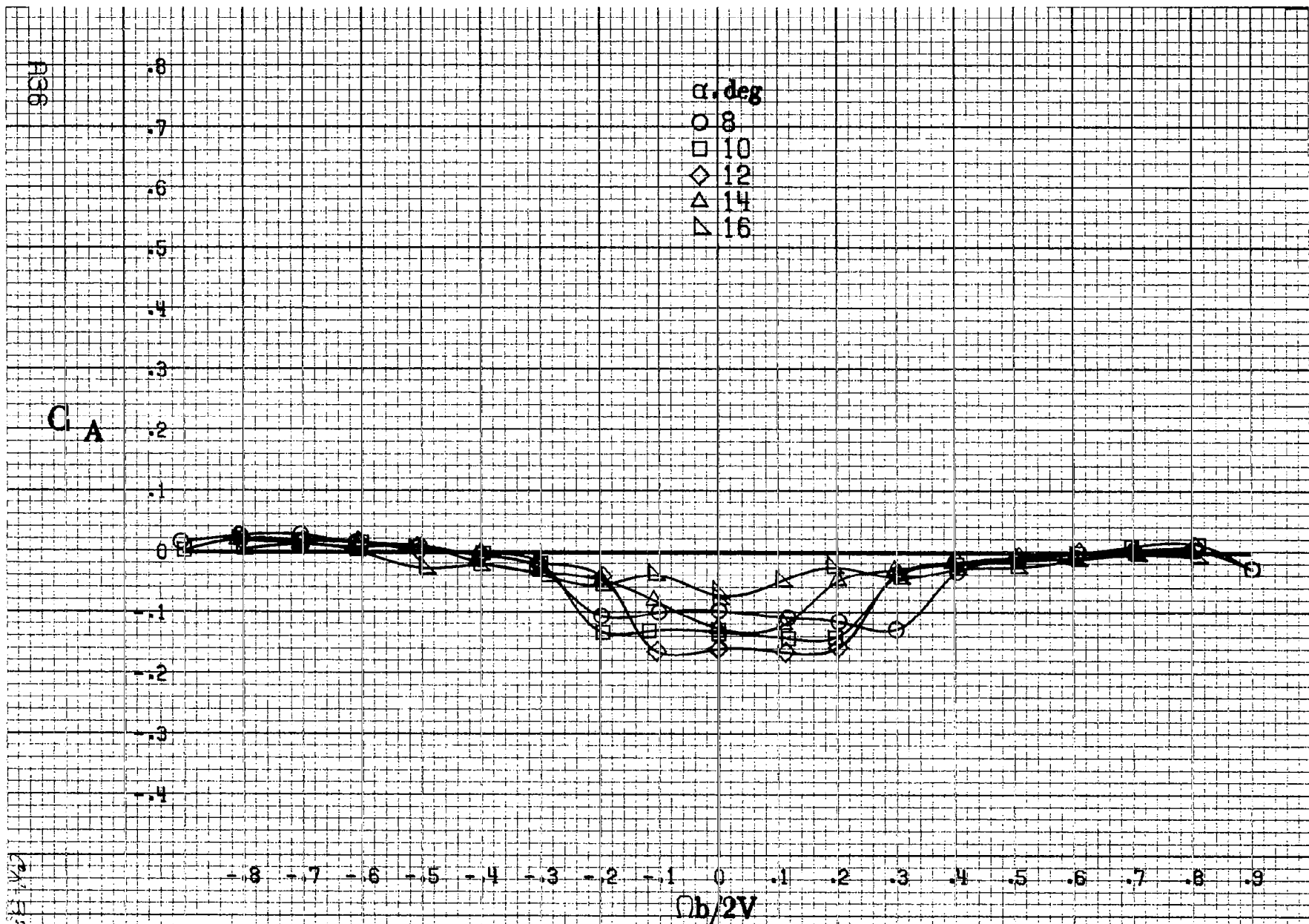
(a) α = 8 to 16 deg, SR = 152.4 cm (60 in).

Figure A12. Effect of rotation rate and angle of attack on axial-force coefficient for basic configuration. $\delta_e = 17°$, $\delta_a = 0°$, $\delta_r = -24°$, $\beta = 0°$.
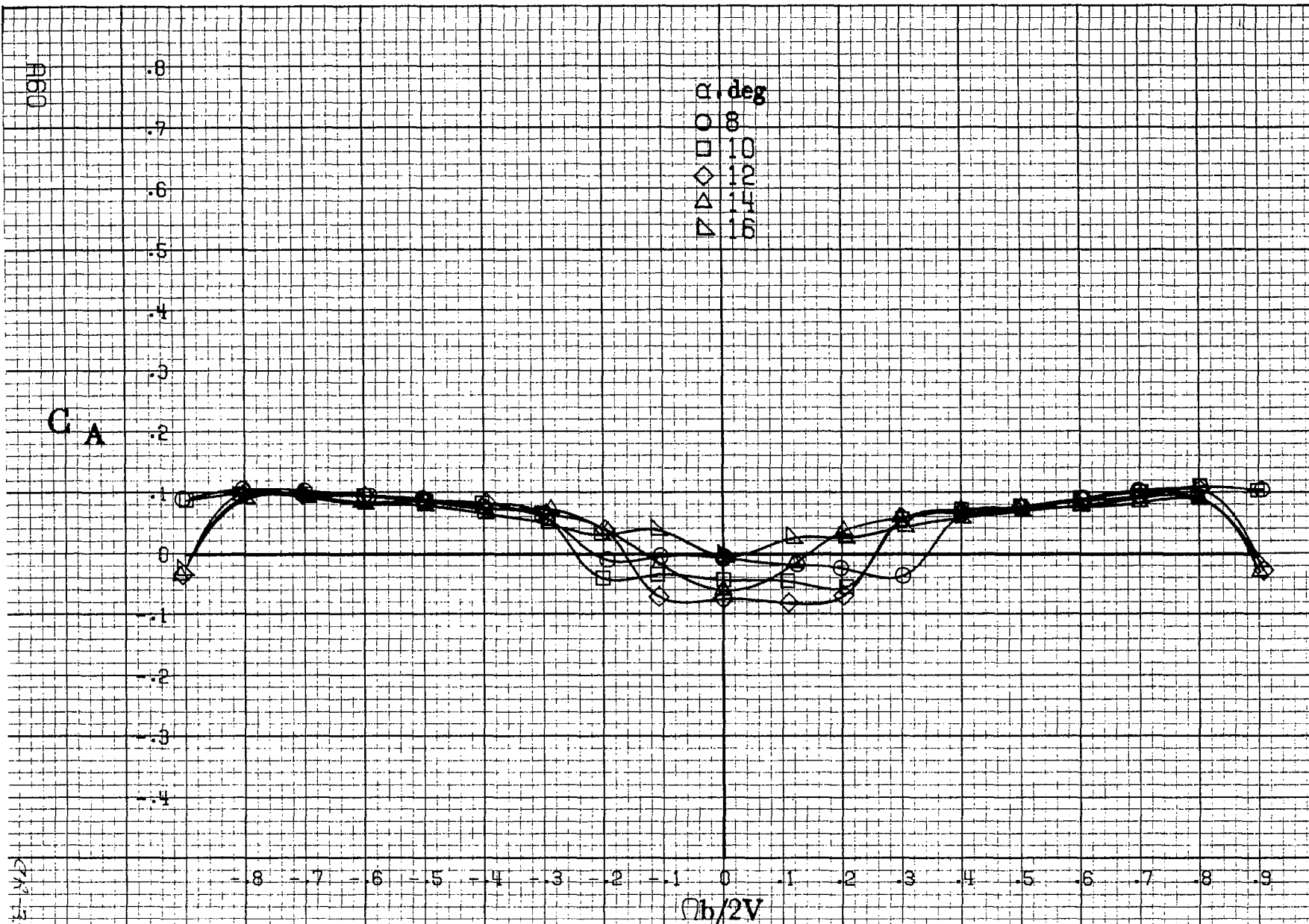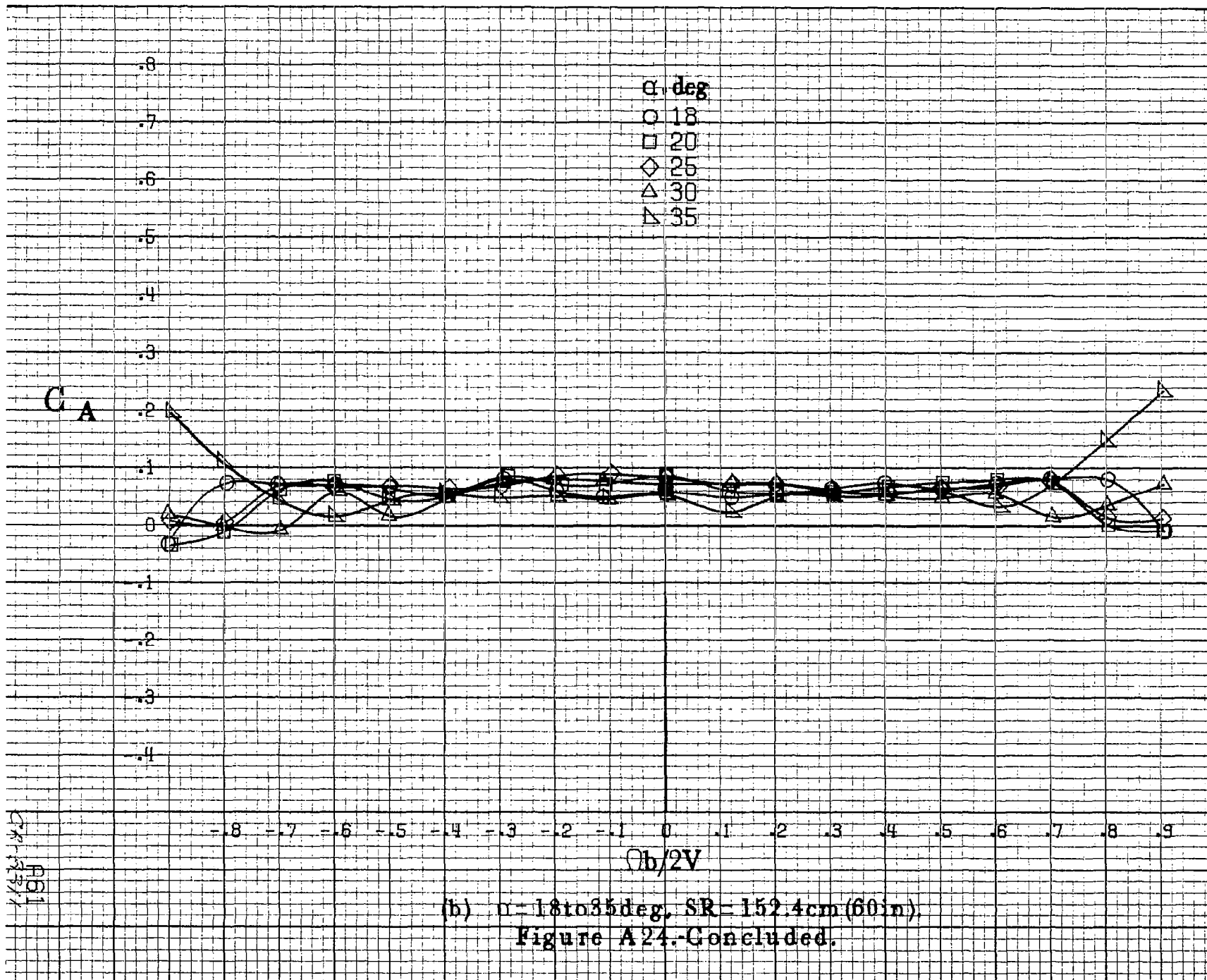
(b) $\alpha = 18$ to 35 deg, $SR = 152.4$ cm $(60$ in).

Figure A12.-Concluded.
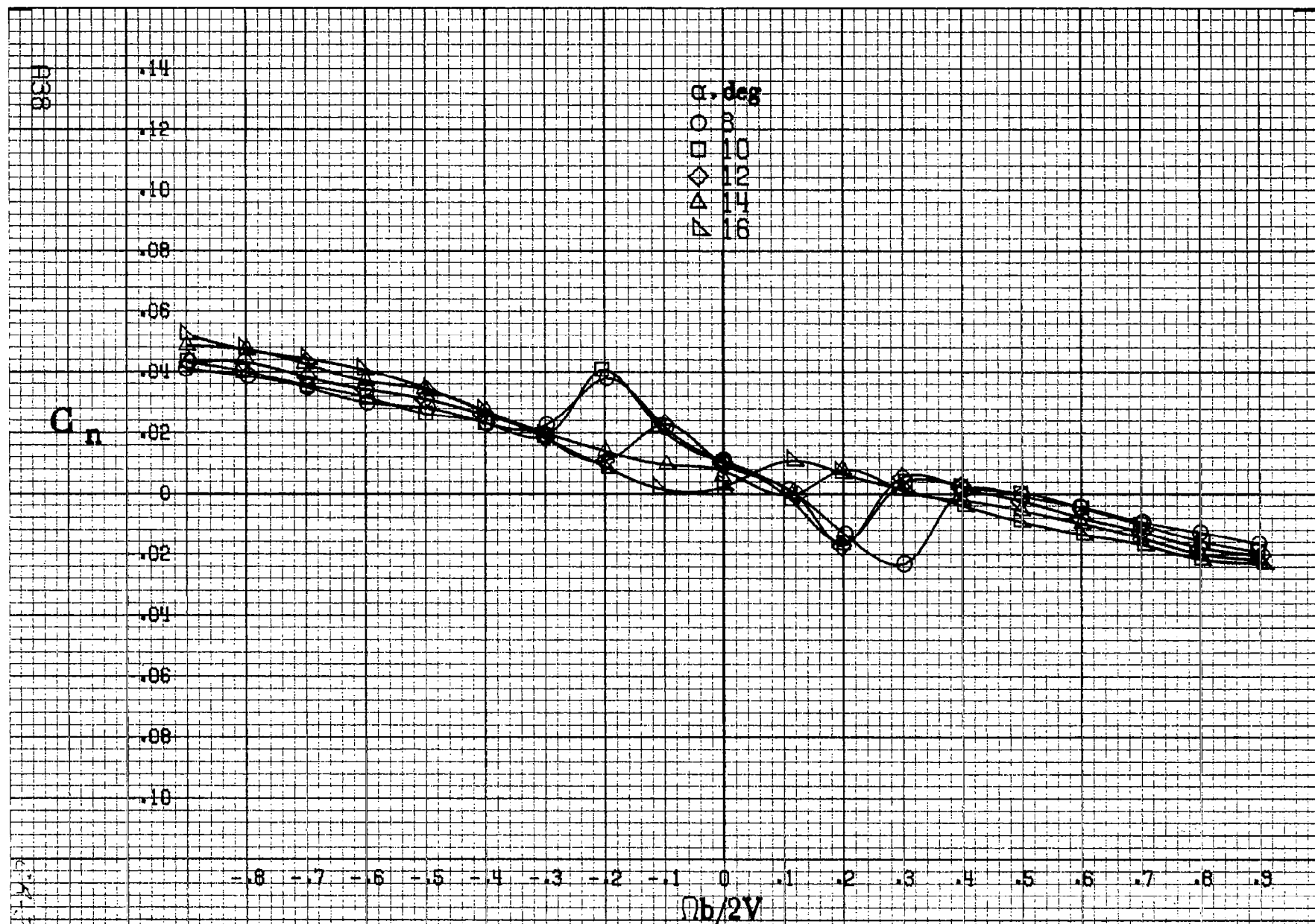
(a) α = 8 to 16 deg; SR = 152.4 cm (60 in).

Figure A13.-Effect of rotation rate and angle of attack on yawing-moment coefficient for basic configuration.   δe = -27°, δa = 0°, δr = -24°, β = 0°.

α, deg
○ 18
□ 20
◇ 25
△ 30
▷ 35

C_n

$\Omega b/2V$

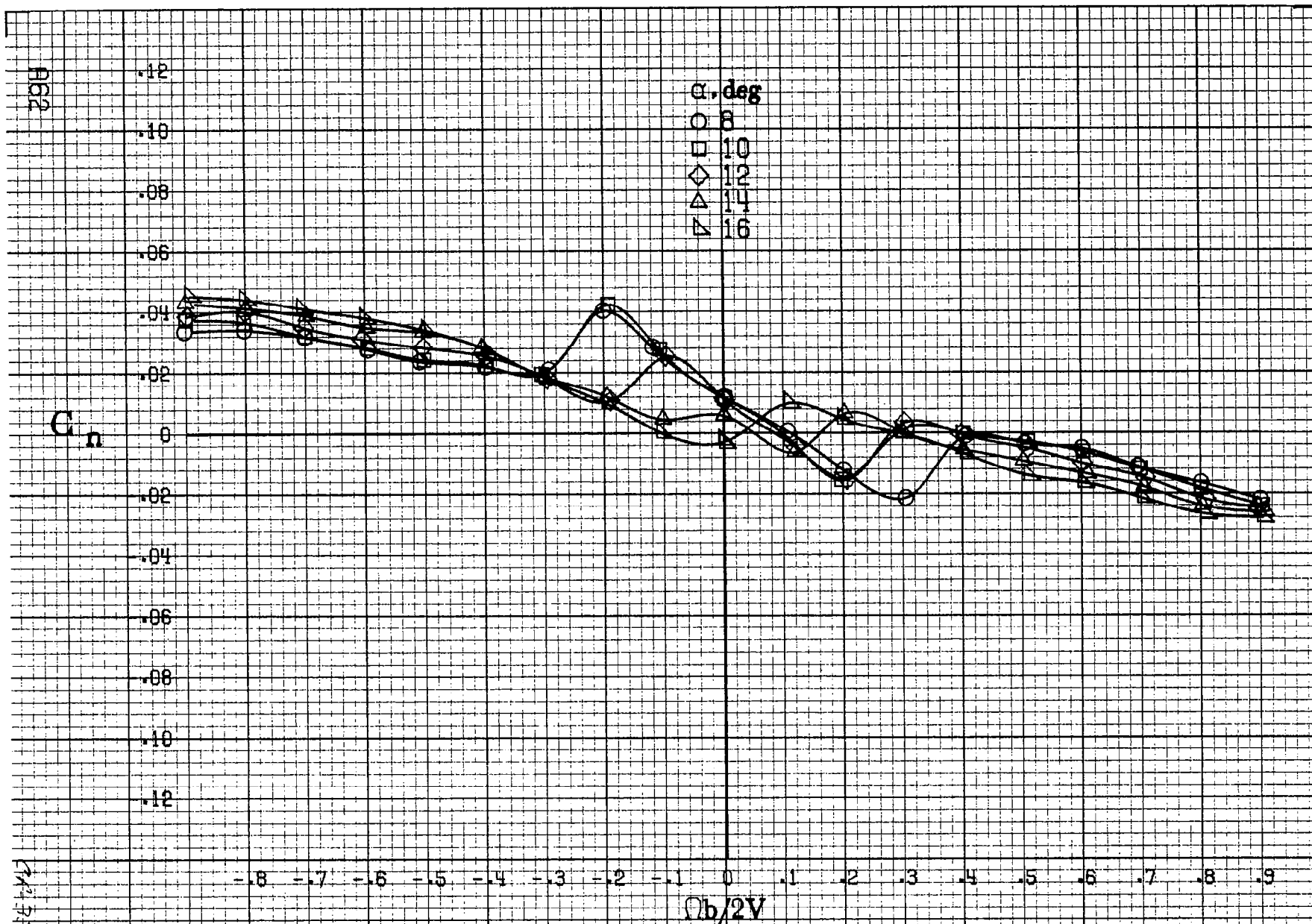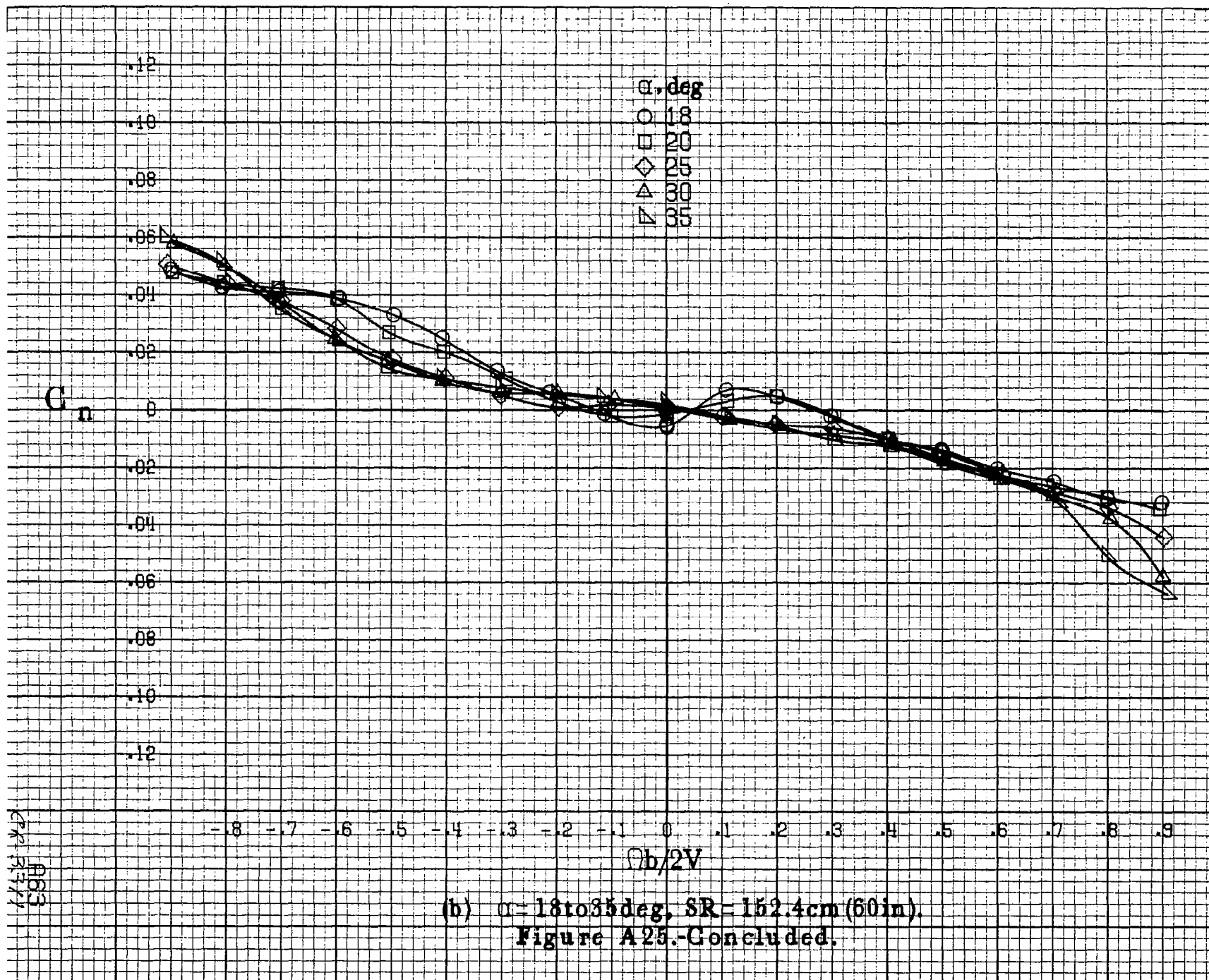(b) α = 18 to 35 deg, SR = 152.4 cm (60 in).

Figure A13.- Concluded.

(a) α = 8 to 16 deg, SR = 152.4 cm (60 in).

Figure A14.- Effect of rotation rate and angle of attack on rolling-moment coefficient for basic configuration. δe = -27°, δa = 0°, δr = -24°, β = 0°.

(b) $\alpha = 18$ to 35 deg, $SR = 152.4$ cm (60 in)

Figure A14.-Concluded.

C_m

α, deg
○ 8
□ 10
◇ 12
△ 14
◁ 16

-.8 -.7 -.6 -.5 -.4 -.3 -.2 -.1 0 .1 .2 .3 .4 .5 .6 .7 .8 .9

Ωb/2V

(a) α = 8 to 16 deg, SR = 152.4 cm (60 in).

Figure A15. Effect of rotation rate and angle of attack on pitching-moment coefficient for basic configuration. δe = -27°, δa = 0°, δr = -24°, β = 0°.
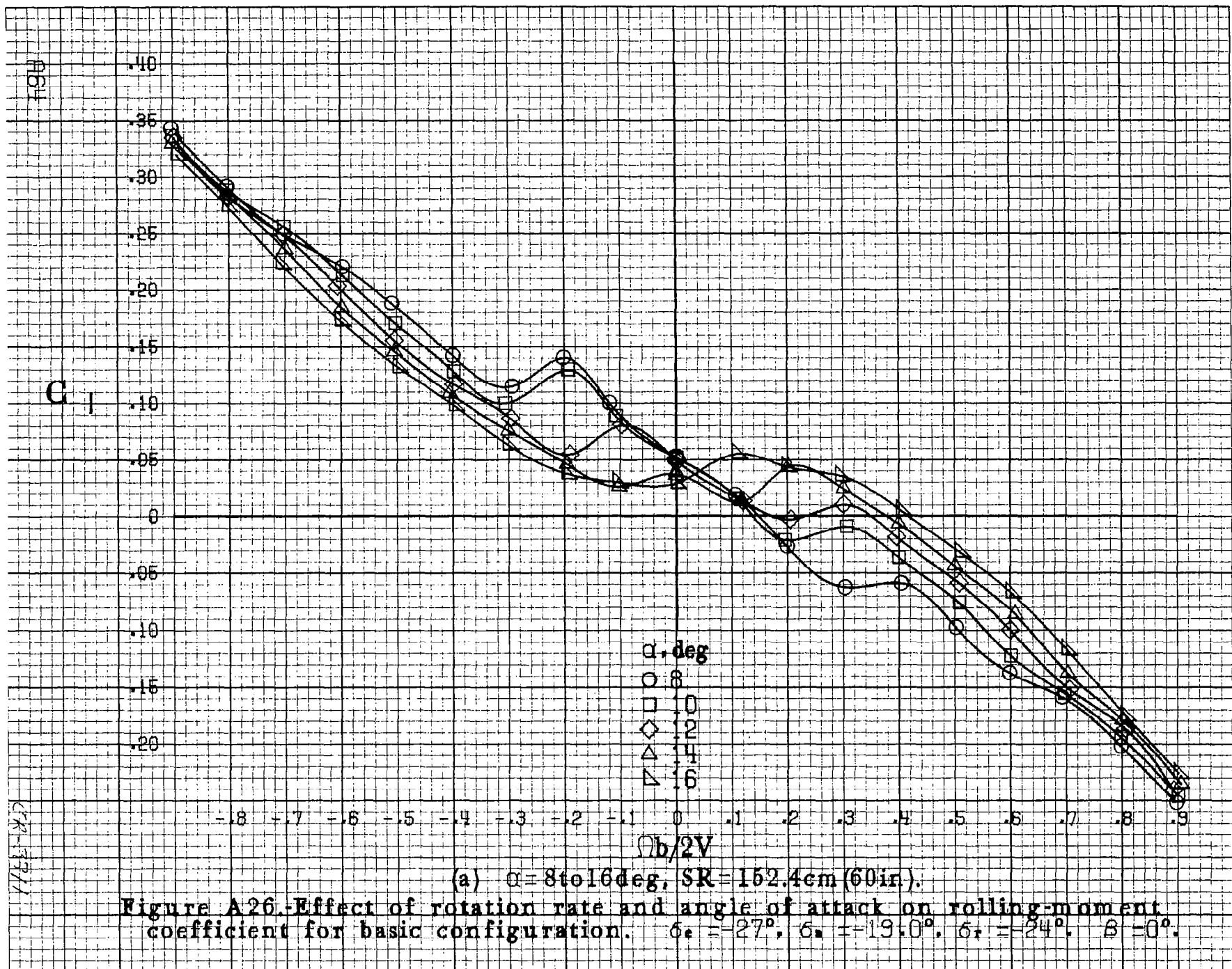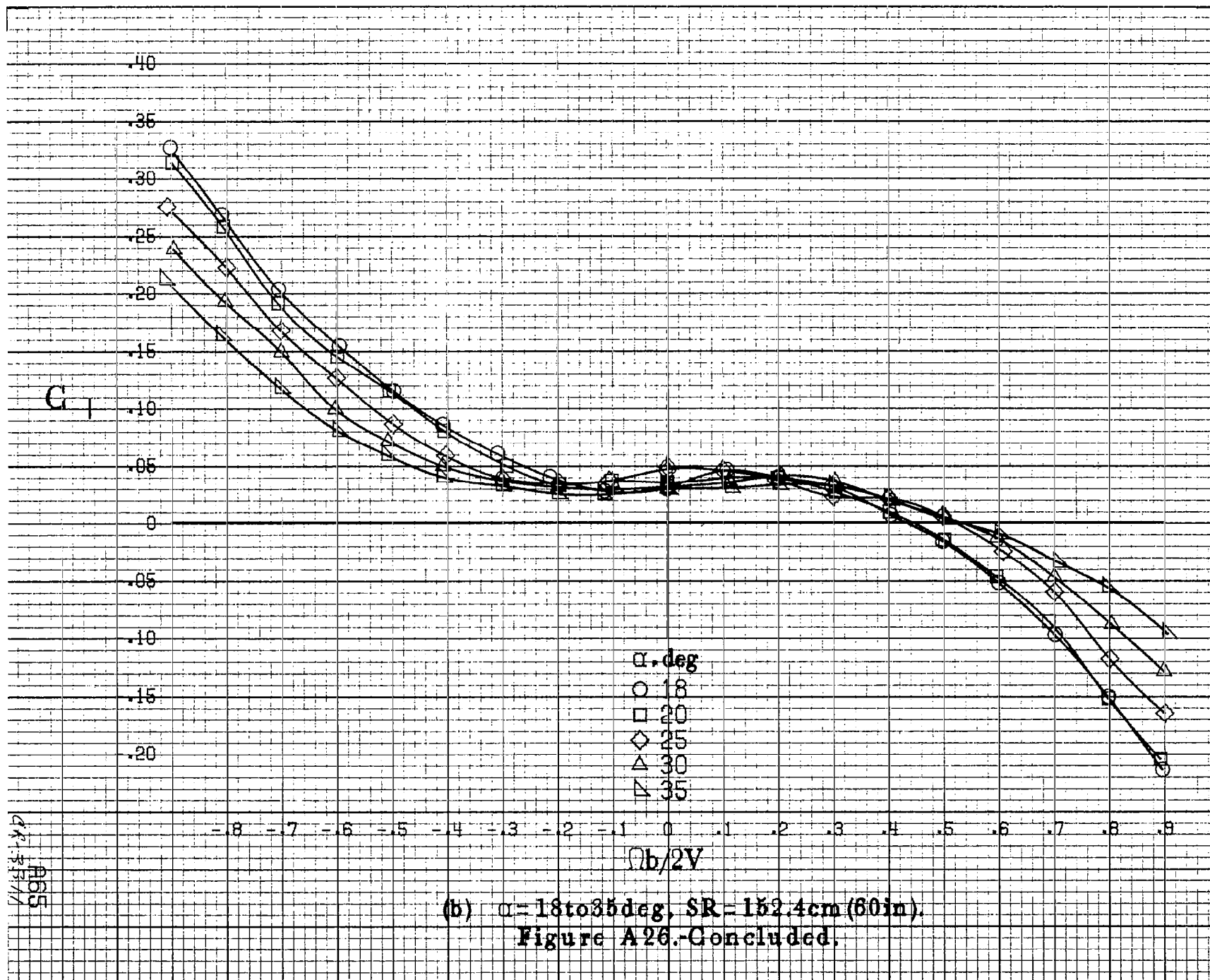
(b) $\alpha = 18$ to 35 deg, $SR = 152.4$ cm (60 in).
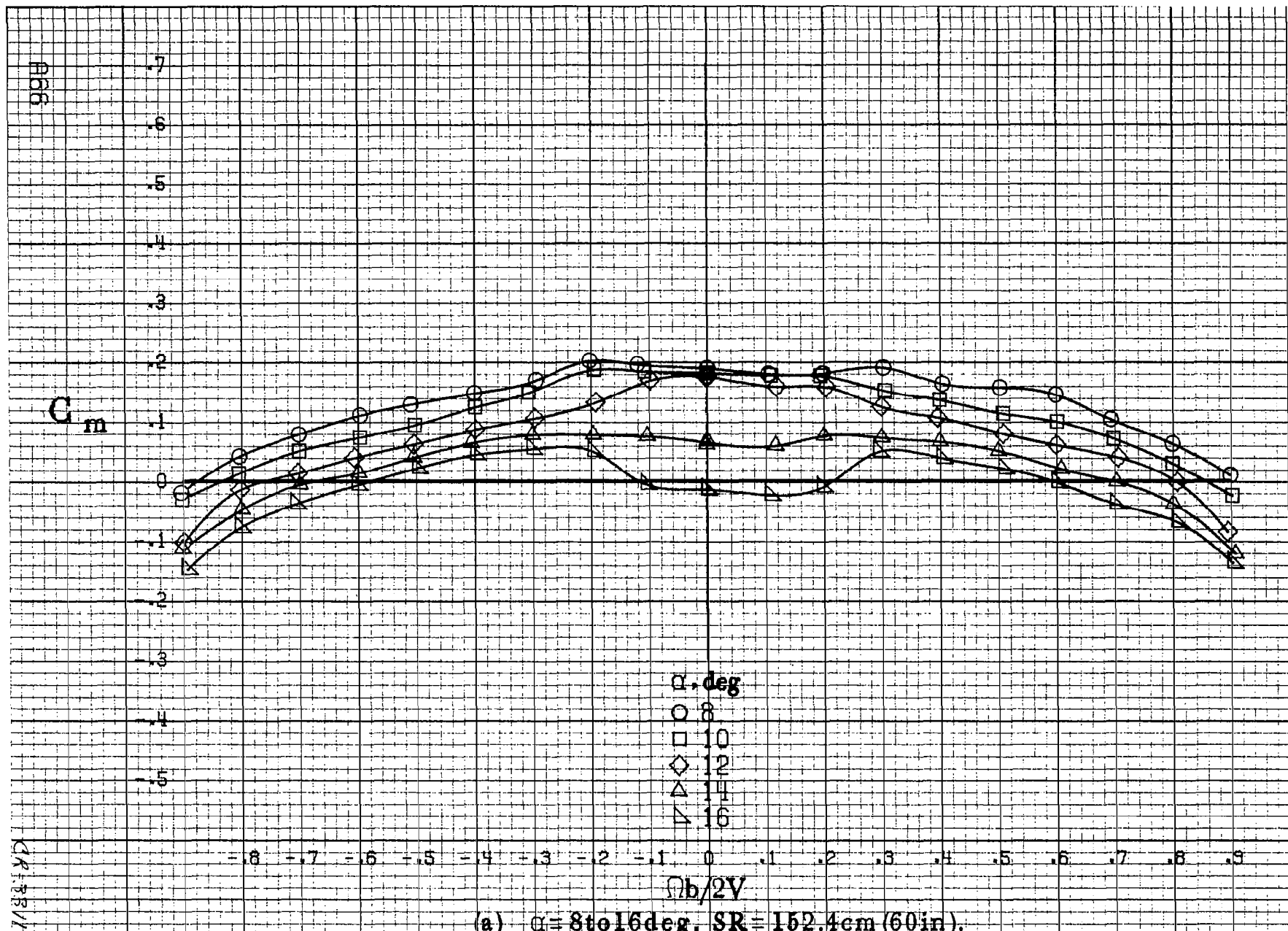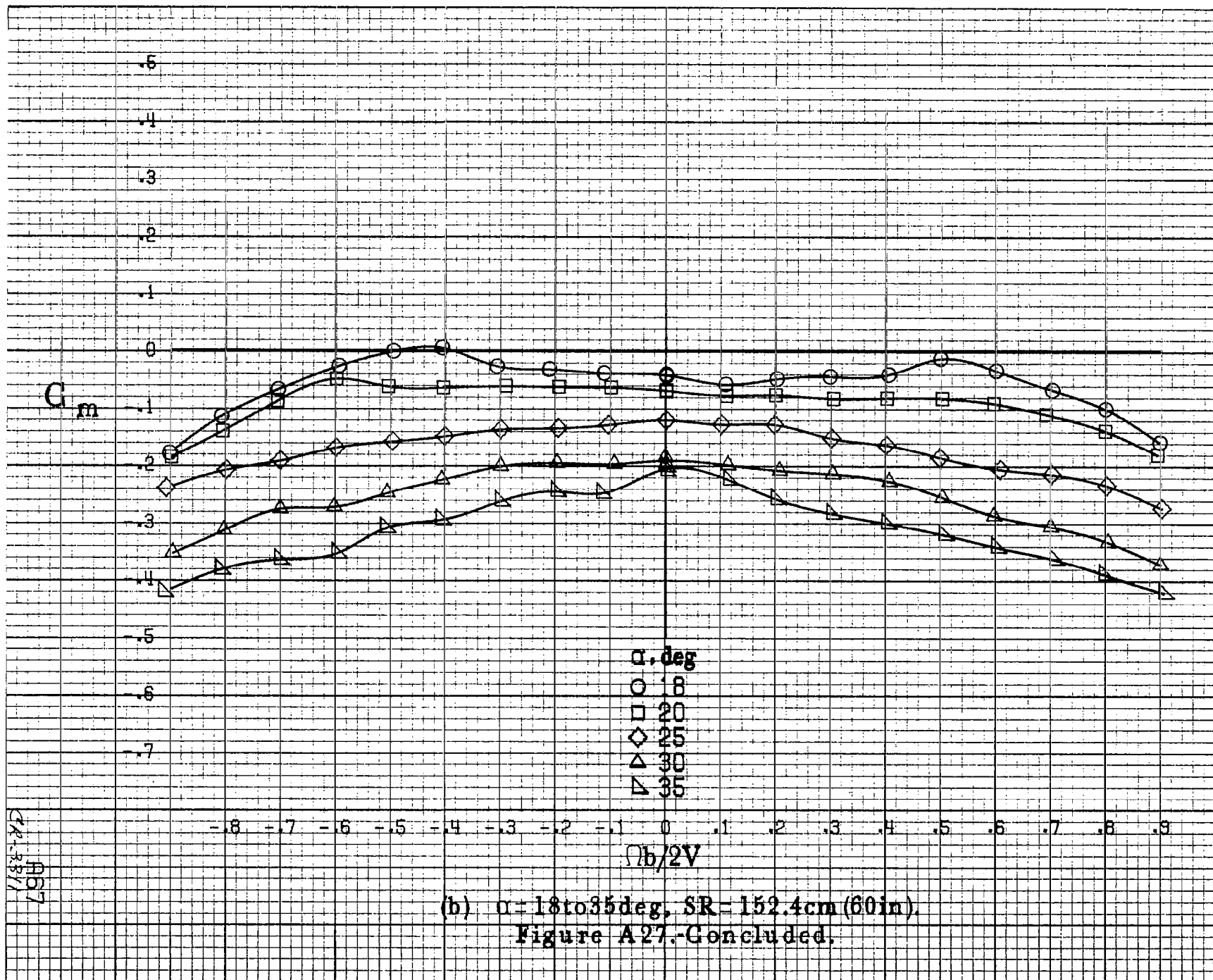
Figure A15.-Concluded.

(a) $\alpha = 8$ to 16 deg, $SR = 152.4$ cm (60 in.).

Figure A16.-Effect of rotation rate and angle of attack on normal-force coefficient for basic configuration. $\delta_e = -27°$, $\delta_a = 0°$, $\delta_r = -24°$. $\beta = 0°$.

(b) α = 18 to 35 deg, SR = 152.4 cm (60 in).

Figure A16.-Concluded.

(a) α = 8 to 16 deg, SR = 152.4 cm (60 in.).

Figure A17.-Effect of rotation rate and angle of attack on side-force coefficient for basic configuration. $\delta_e = -27°$, $\delta_a = 0°$, $\delta_r = -24°$, $\beta = 0°$.
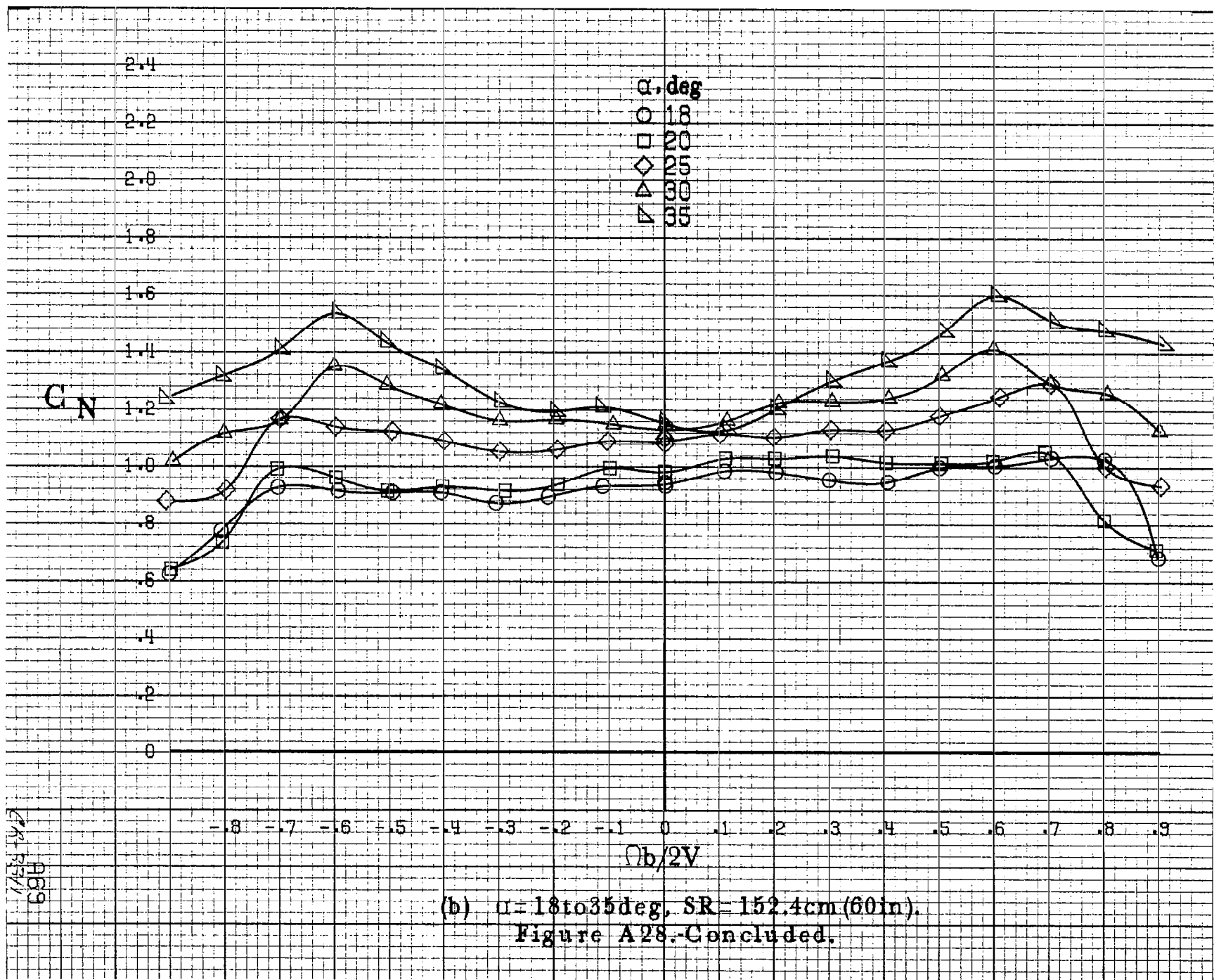
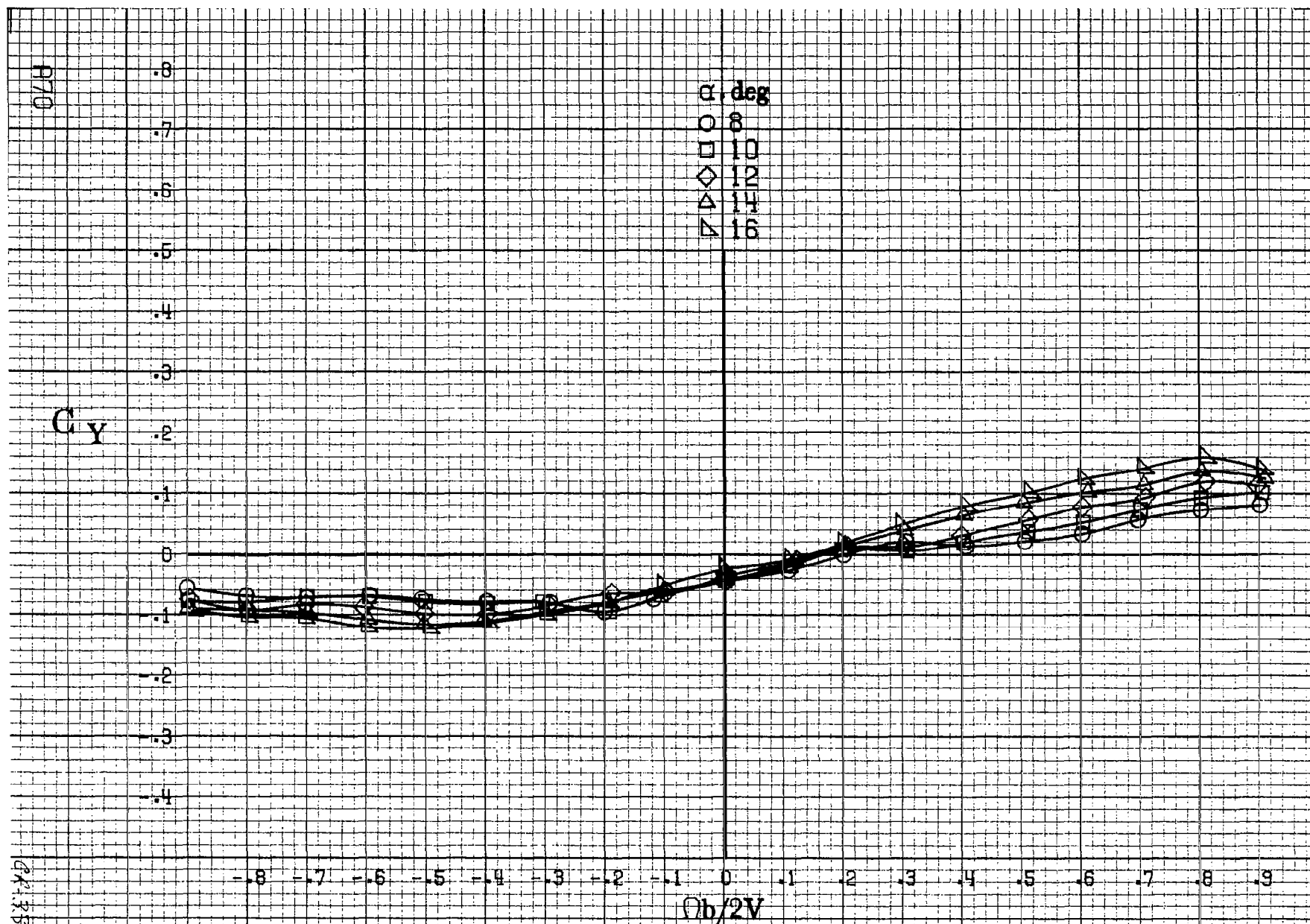(b) α = 18 to 35 deg, SR = 152.4 cm (60 in).
Figure A17.-Concluded.

(a) $\alpha = 8$ to 16 deg, $SR = 152.4$ cm $(60$ in$)$.

Figure A18.-Effect of rotation rate and angle of attack on axial-force coefficient for basic configuration. $\delta_e = -27°$, $\delta_a = 0°$, $\delta_r = -24°$, $\beta = 0°$.

(b) α = 18 to 35 deg, SR = 152.4 cm (60 in).

Figure A18.-Concluded.

(a) $\alpha = 8$ to 16 deg, SR = 152.4 cm (60 in).

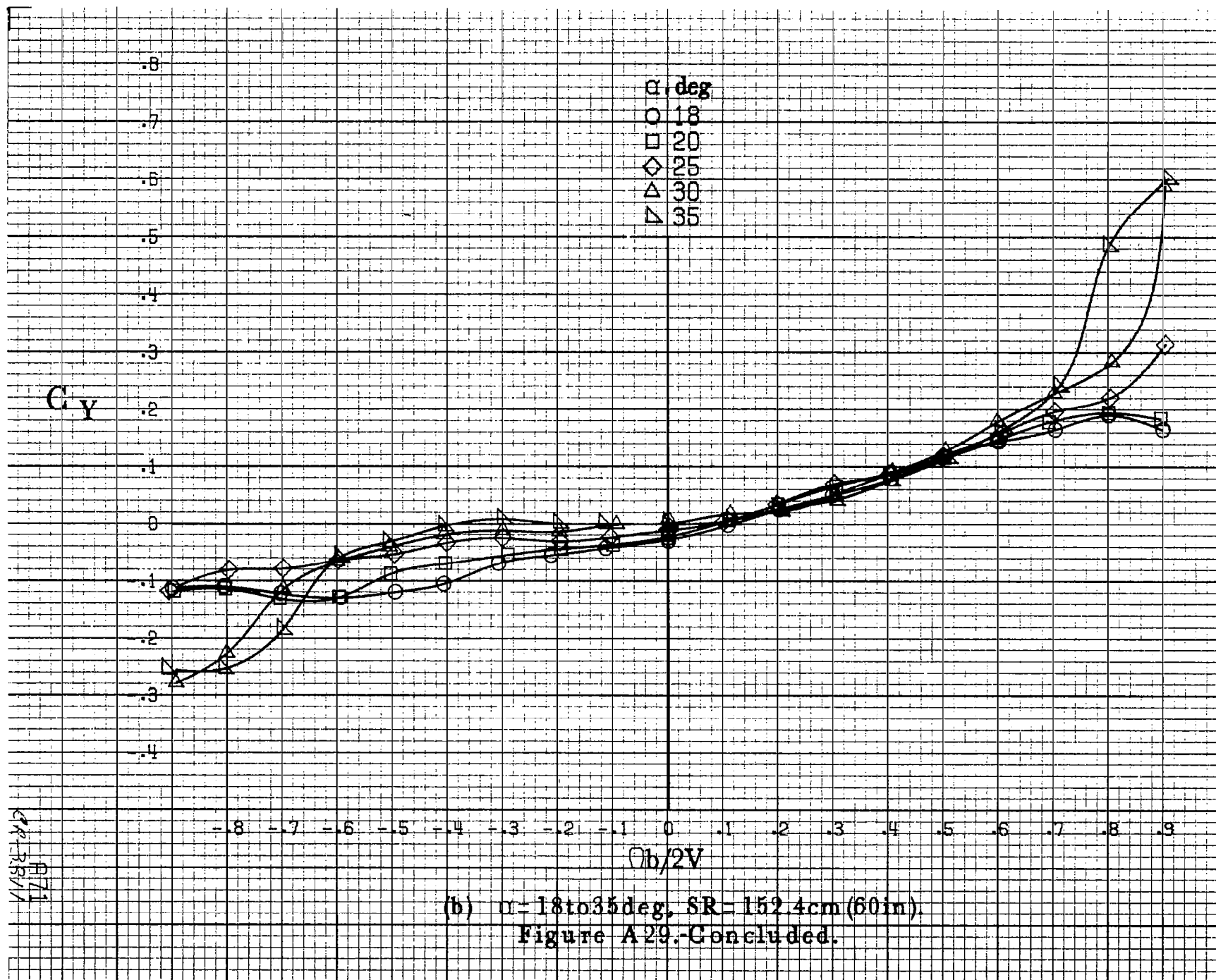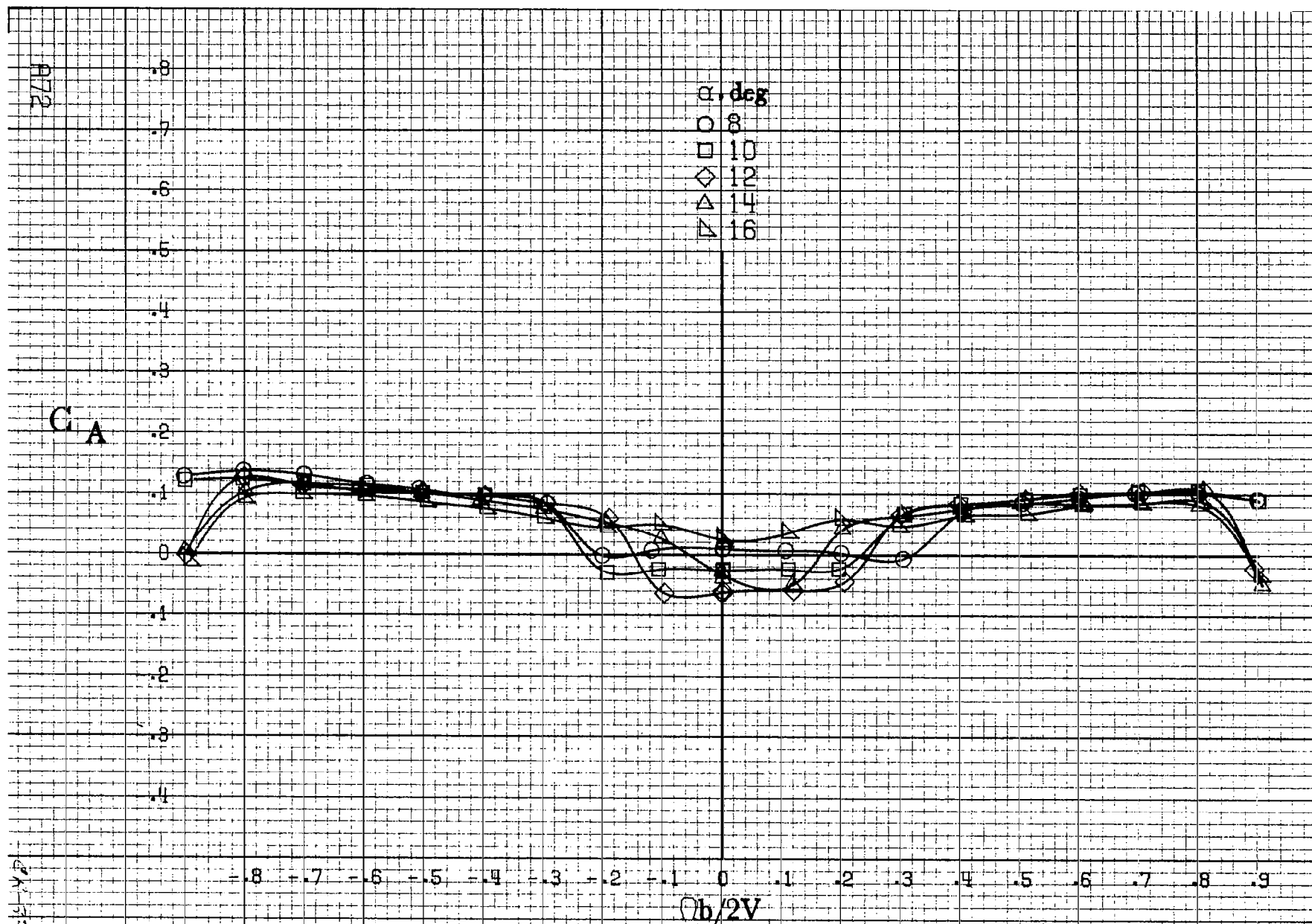Figure A19. Effect of rotation rate and angle of attack on yawing-moment coefficient for basic configuration. $\delta_e = -27°$, $\delta_a = -19.0°$, $\delta_r = -24°$. $\beta = 0°$.

(b) α = 18° iles ; λ = 15.24 m; 60 m

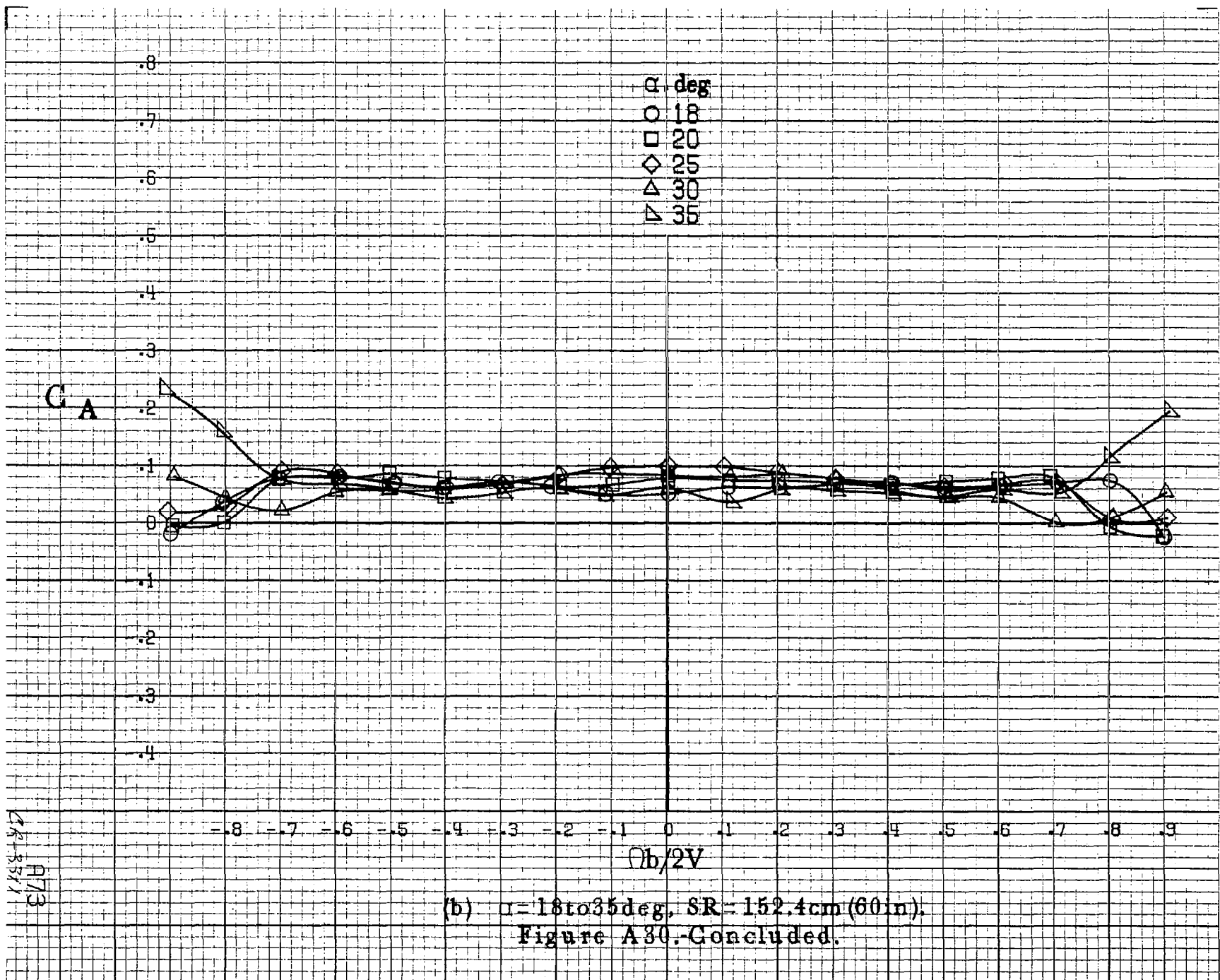Figure 11.- Concluded.

(a) α = 8 to 16 deg, SR = 152.4 cm (60 in).

Figure A20.-Effect of rotation rate and angle of attack on rolling-moment
coefficient for basic configuration. δ_e = -27°, δ_a = 19.0°, δ_r = -24°. β = 0°.

(b) α = 18 to 35 deg, SR = 152.4 cm (60 in).

Figure A20.-Concluded.

C_m

$\Omega b/2V$

α, deg
○ 8
□ 10
◇ 12
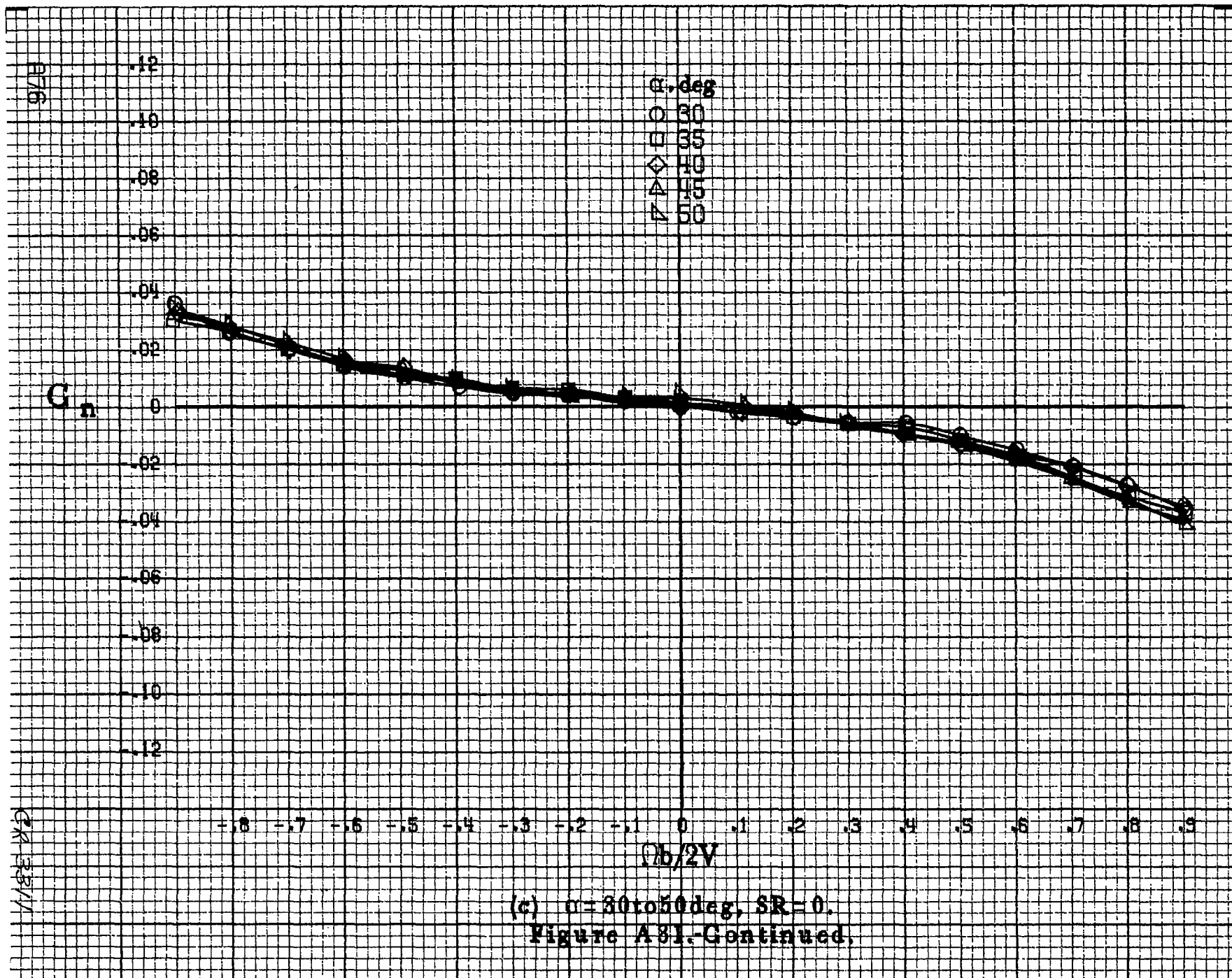△ 14
▷ 16
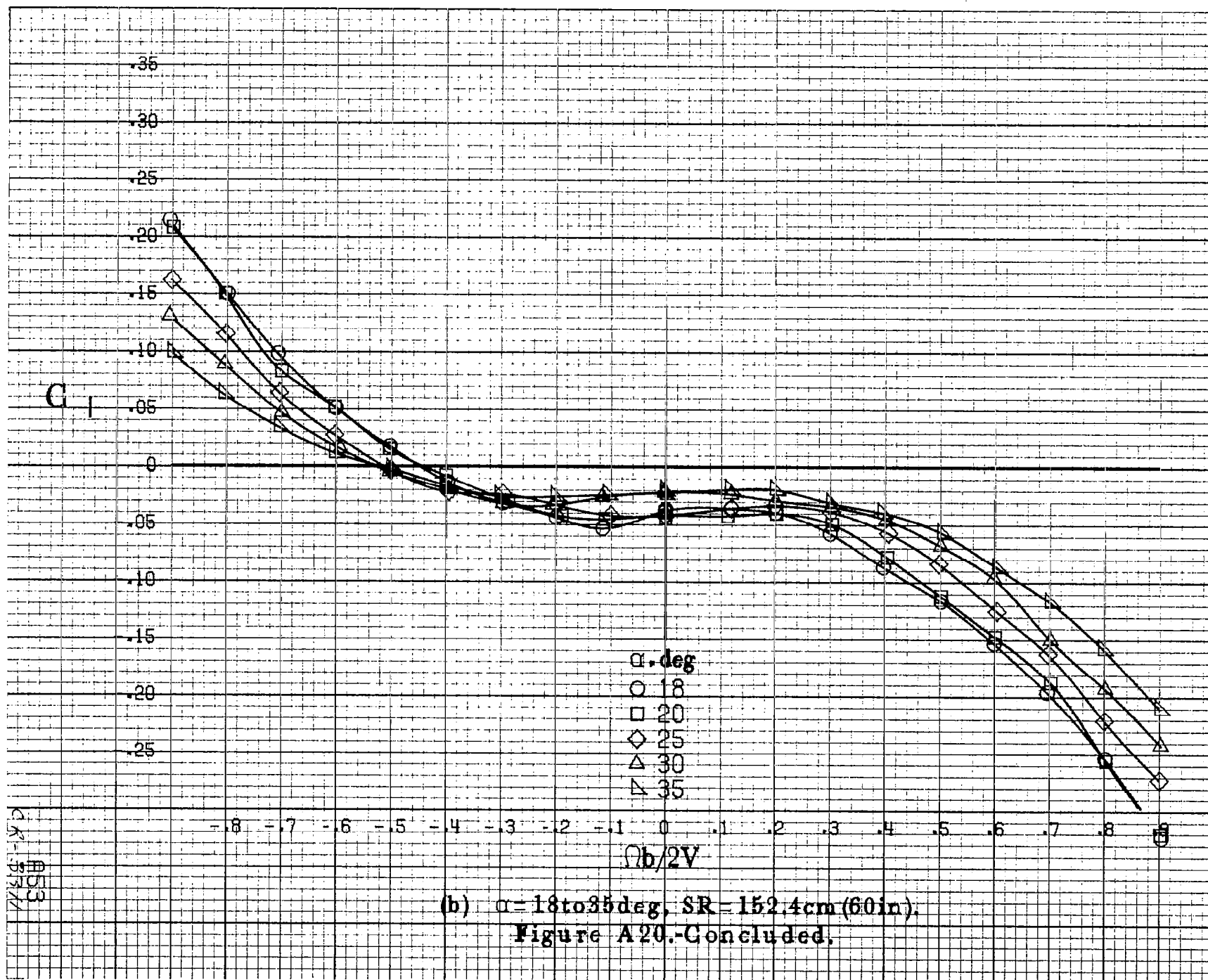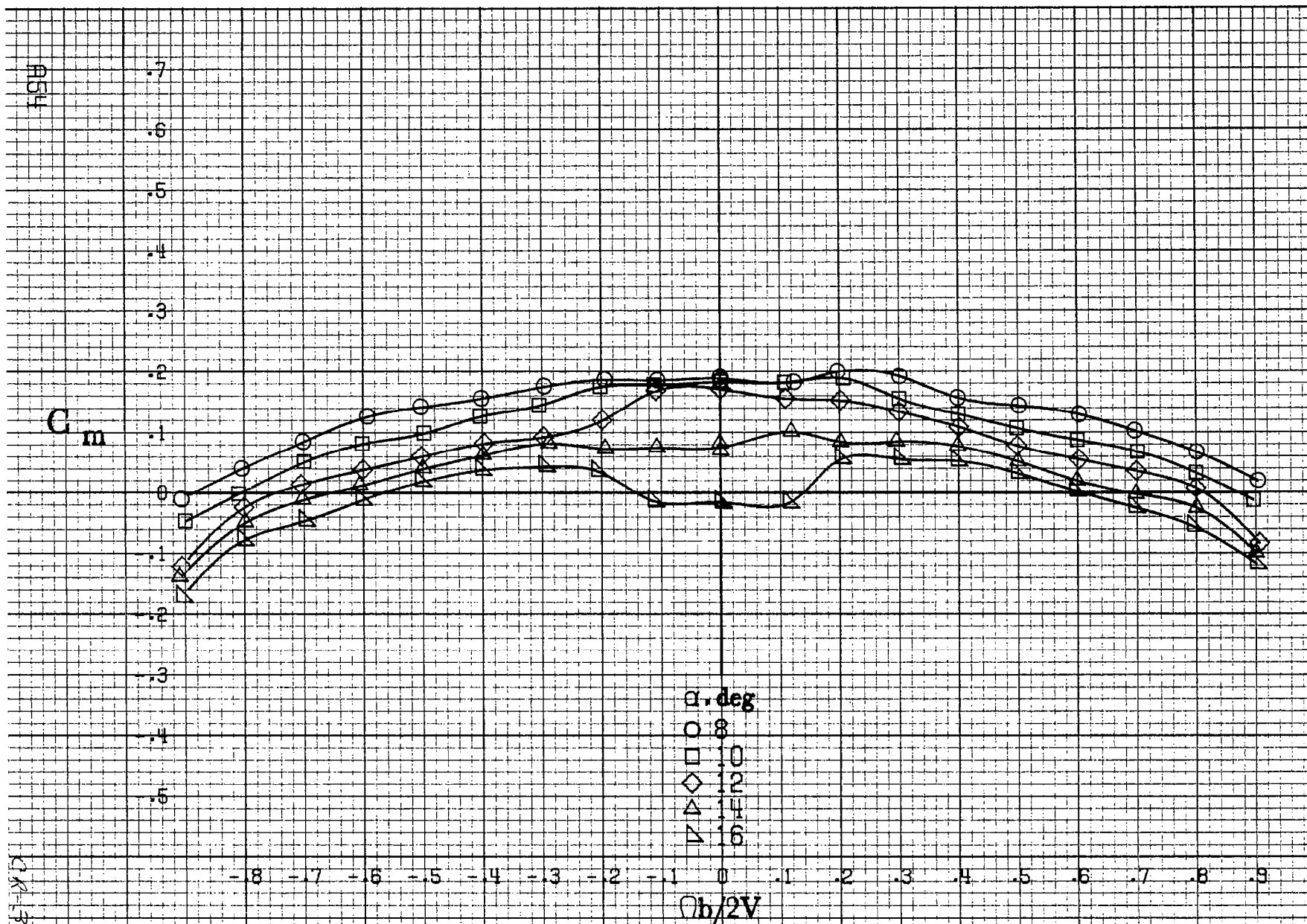
(a)   α = 8 to 16 deg, SR = 152.4 cm (60 in).

Figure A21. Effect of rotation rate and angle of attack on pitching-moment coefficient for basic configuration. $\delta_e = -27°$, $\delta_a = 19.0°$, $\delta_r = -24°$, $\beta = 0°$.

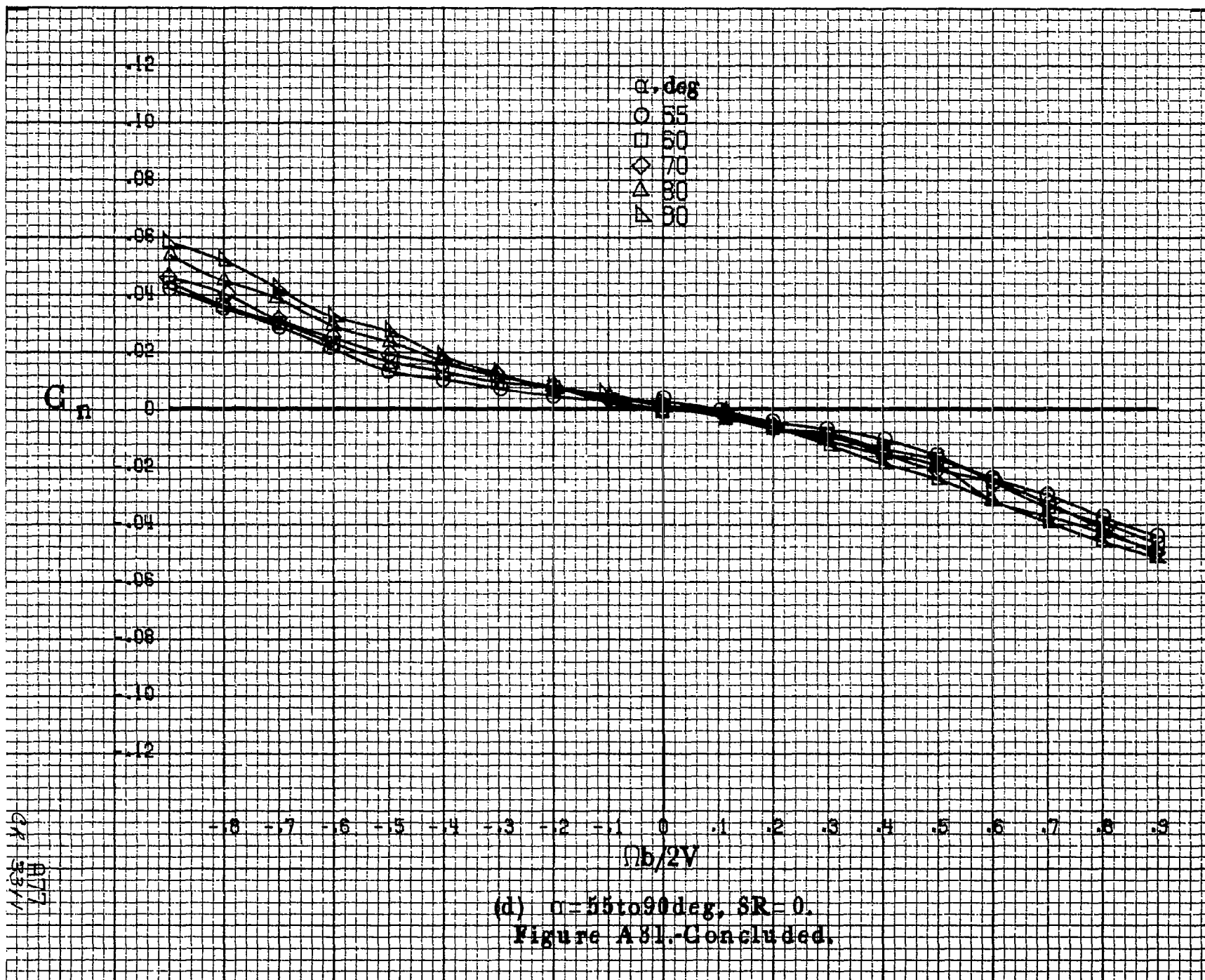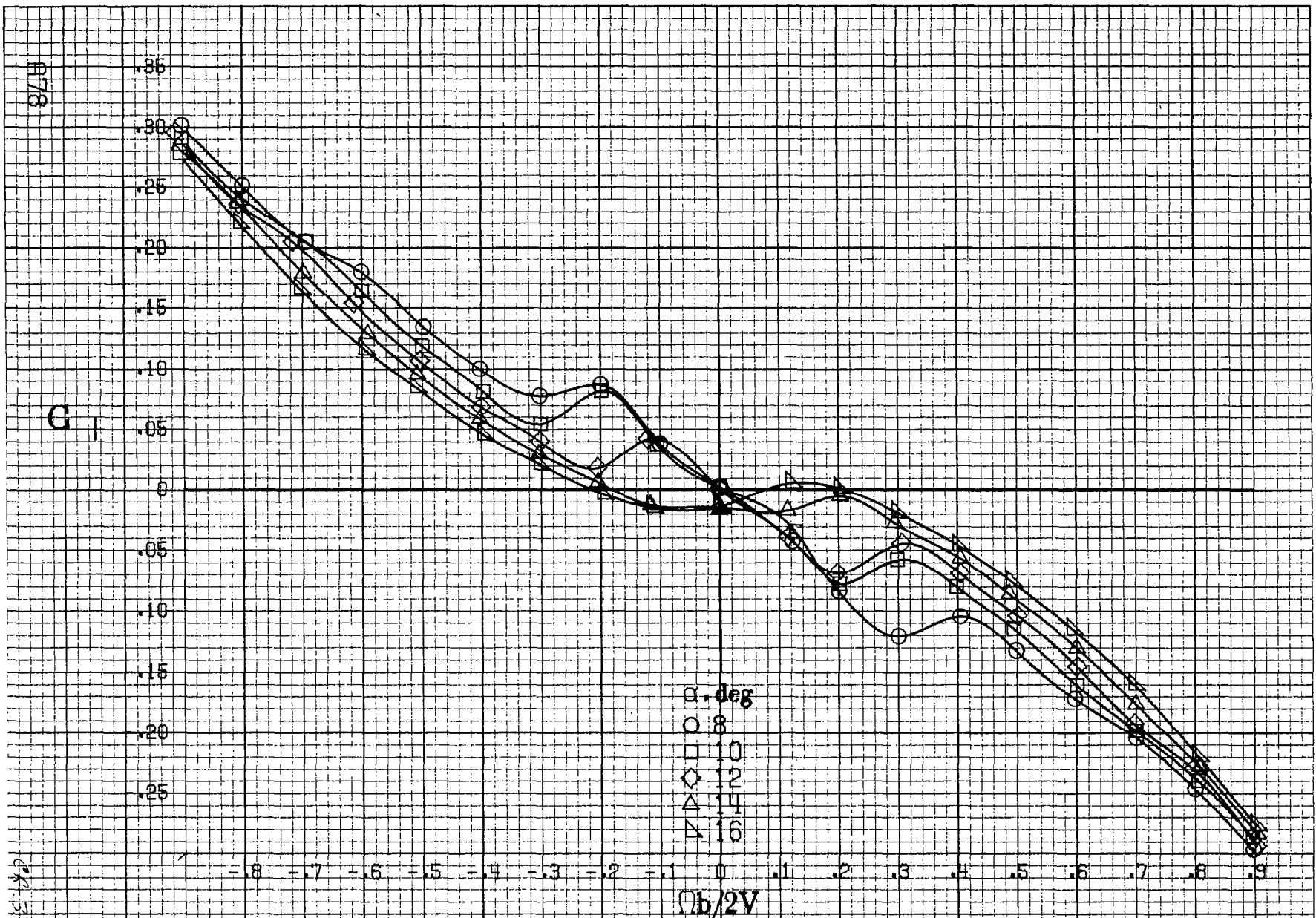(b) α = 18 to 35 deg, SR = 152.4 cm (60 in).

Figure A21.-Concluded.

(a) $\alpha = 8$ to 16 deg, $SR = 152.4$ cm (60 in).

Figure A22.-Effect of rotation rate and angle of attack on normal-force coefficient for basic configuration. $\delta_e = -27°$, $\delta_a = -19.0°$, $\delta_r = 24°$, $\beta = 0°$.

(b)   α = 18 to 35 deg, SR = 152.4 cm (60 in).

Figure A 22.-Concluded.

(a) α = 8 to 16 deg, SR = 152.4 cm (60 in.).

Figure A28.-Effect of rotation rate and angle of attack on side-force coefficient for basic configuration.   δe = -27°, δa = ±19.0°, δr = -24°.   β = 0°.

(b) α=18 to 35 deg, SR=152.4 cm (60 in).

Figure A 23.-Concluded.

(a) α = 8 to 16 deg, SR = 152.4 cm (60 in).

Figure A24.-Effect of rotation rate and angle of attack on axial-force coefficient for basic configuration. $\delta_e = 27°$, $\delta_a = 19.0°$, $\delta_r = 24°$, $\beta = 0°$.

(b) α = 18 to 35 deg, SR = 152.4 cm (60 in)

Figure A 24.-Concluded.

(a)   α = 8 to 16 deg,   SR = 152.4 cm (60 in).

Figure A25.-Effect of rotation rate and angle of attack on yawing-moment coefficient for basic configuration.   δe = -27°, δa = -19.0°, δr = -24°.   β = 0°.

(b) α = 18 to 35 deg, SR = 152.4 cm (60 in).

Figure A 25.-Concluded.

(a) α = 8 to 16 deg, SR = 152.4 cm (60 in).

Figure A26.-Effect of rotation rate and angle of attack on rolling-moment coefficient for basic configuration. δe = -27°, δa = -19.0°, δr = -24°, β = 0°.

(b) $\alpha = 18$ to 35 deg, SR $= 152.4$ cm (60 in).

Figure A26.-Concluded.
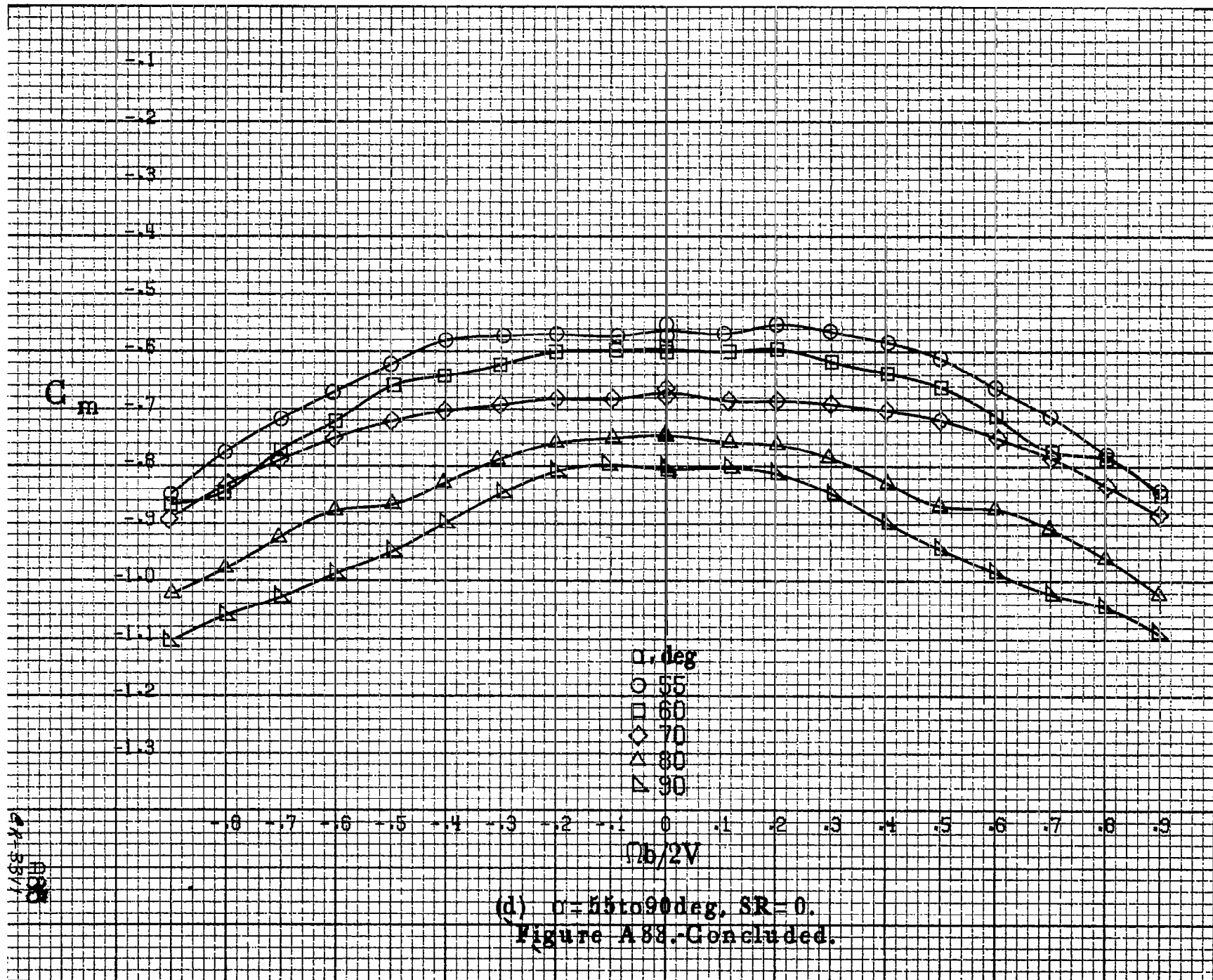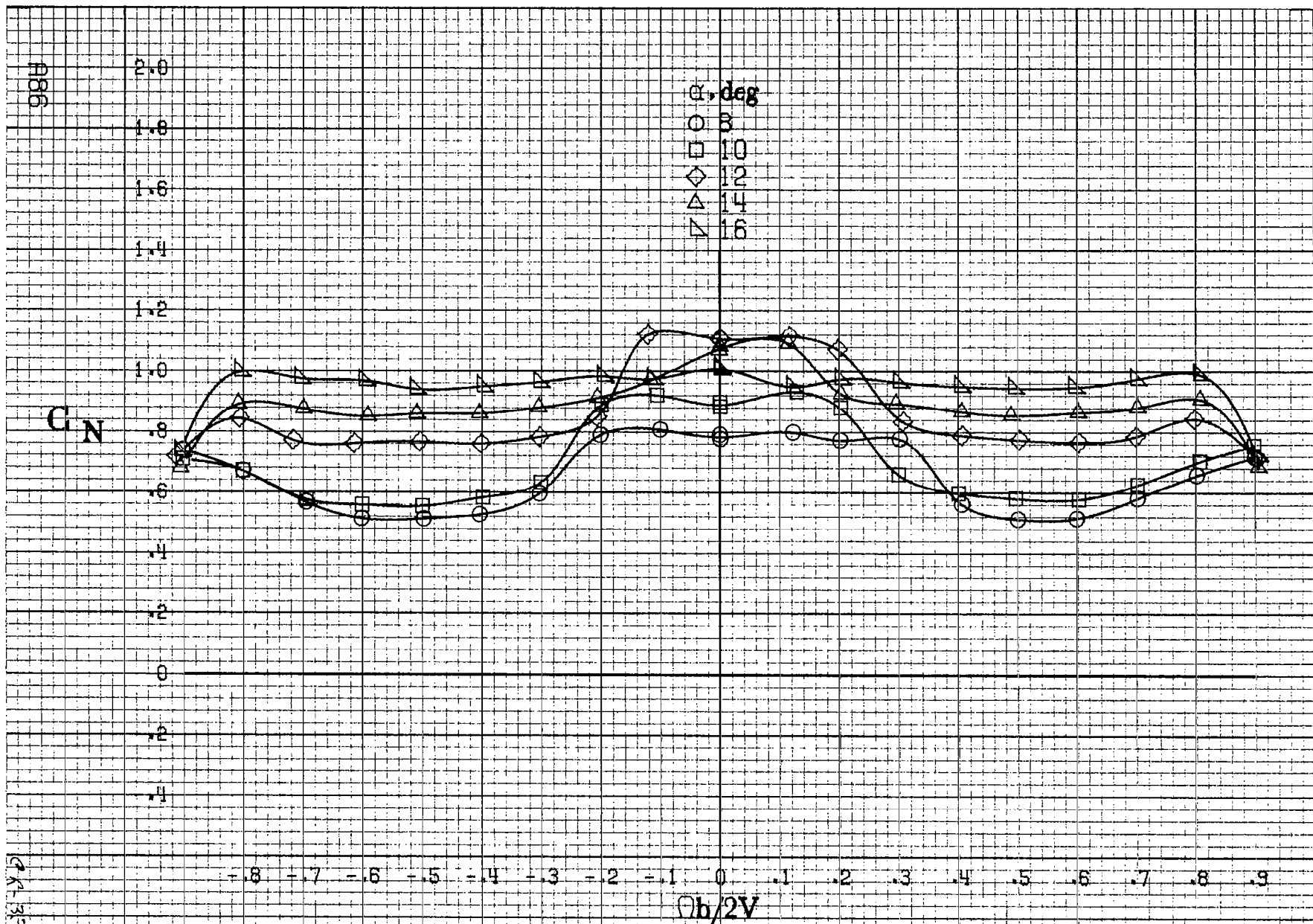
(a) α = 8 to 16 deg, SR = 152.4 cm (60 in).

Figure A27.- Effect of rotation rate and angle of attack on pitching-moment coefficient for basic configuration. $\delta_e = -27°$, $\delta_a = -19.0°$, $\delta_r = -24°$, $\beta = 0°$.

(b) α = 18 to 35 deg, SR = 152.4 cm (60 in).

Figure A27.- Concluded.
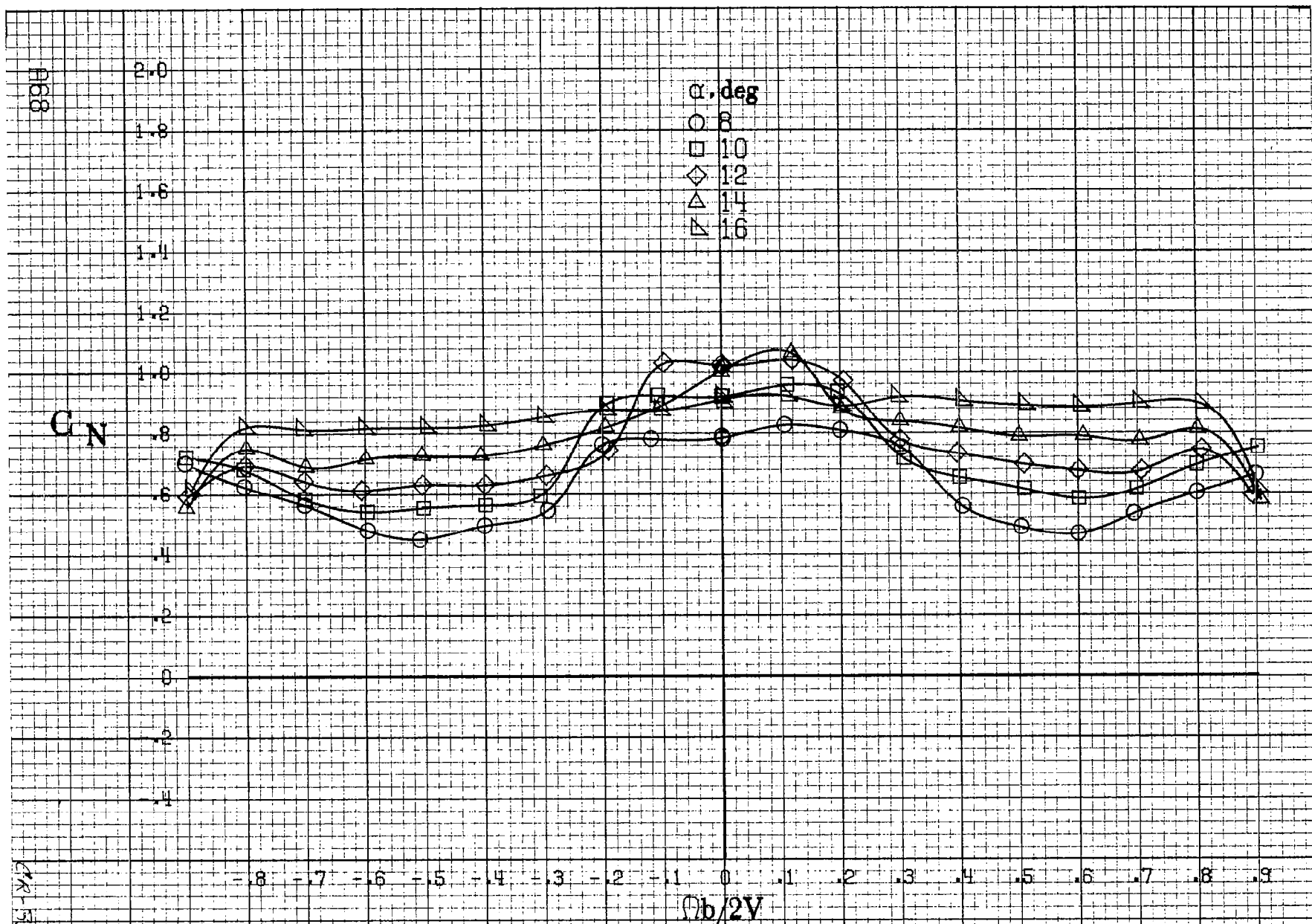
(a) α = 8 to 16 deg, SR = 152.4 cm (60 in).
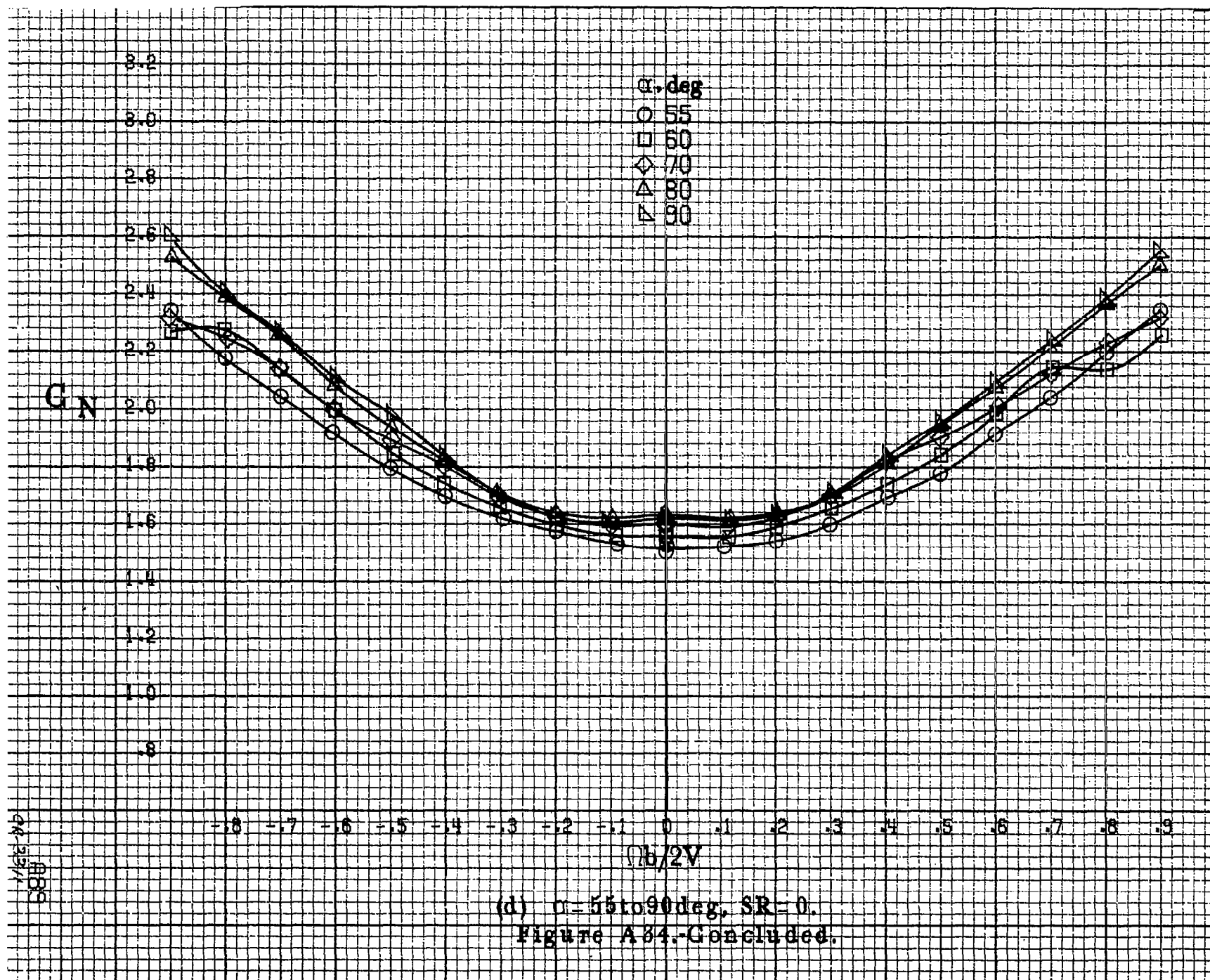
Figure A28.- Effect of rotation rate and angle of attack on normal-force coefficient for basic configuration. $\delta_e = -27°$, $\delta_a = -19.0°$, $\delta_r = -24°$, $\beta = 0°$.

(b) $\alpha = 18$ to 35 deg, SR $= 152.4$ cm (60 in).

Figure A 28.-Concluded.

(a) α = 8 to 16 deg, SR = 152.4 cm (60 in).

Figure A29.- Effect of rotation rate and angle of attack on side-force coefficient for basic configuration. $\delta_e = -27°$, $\delta_a = -19.0°$, $\delta_r = -24°$, $\beta = 0°$.
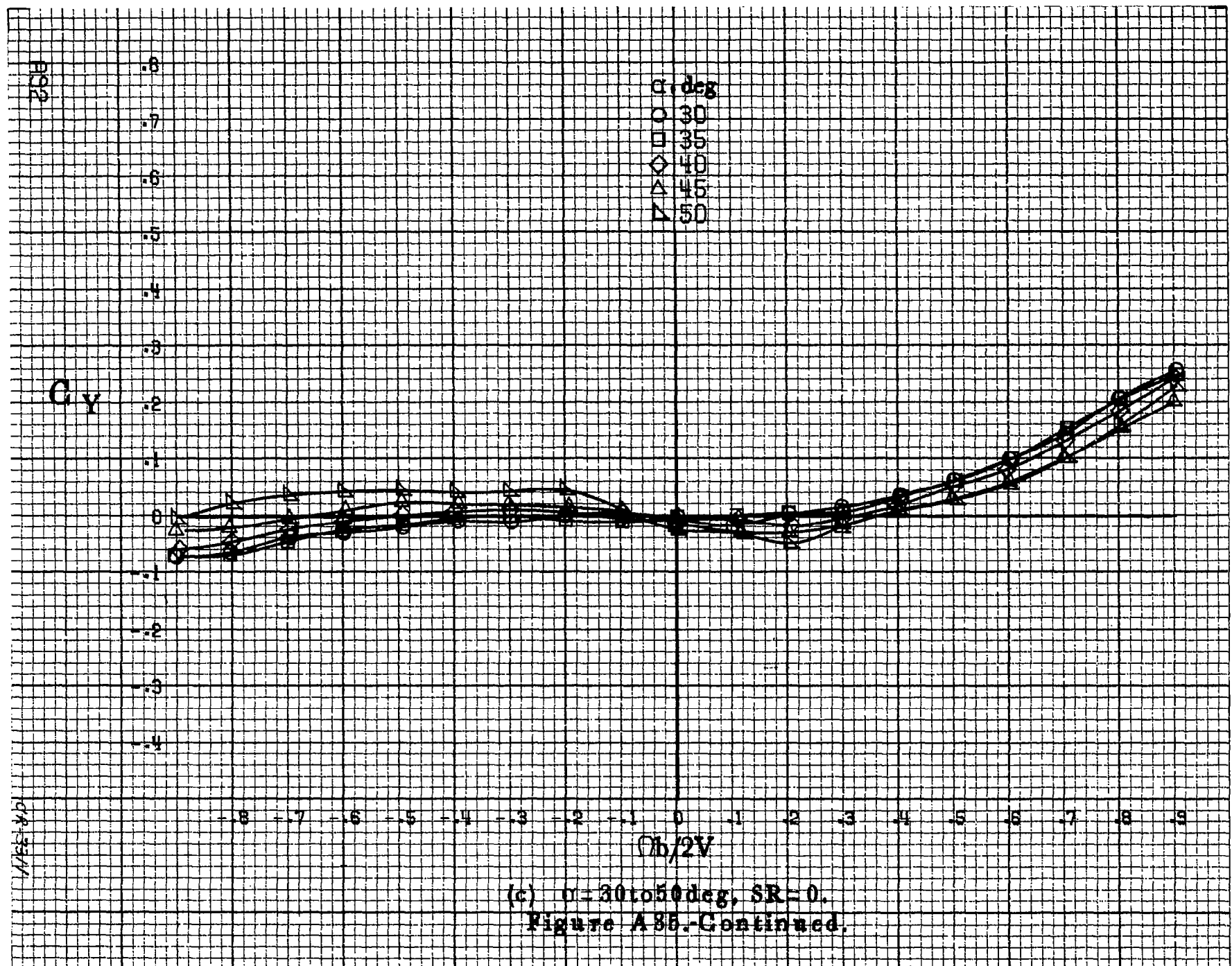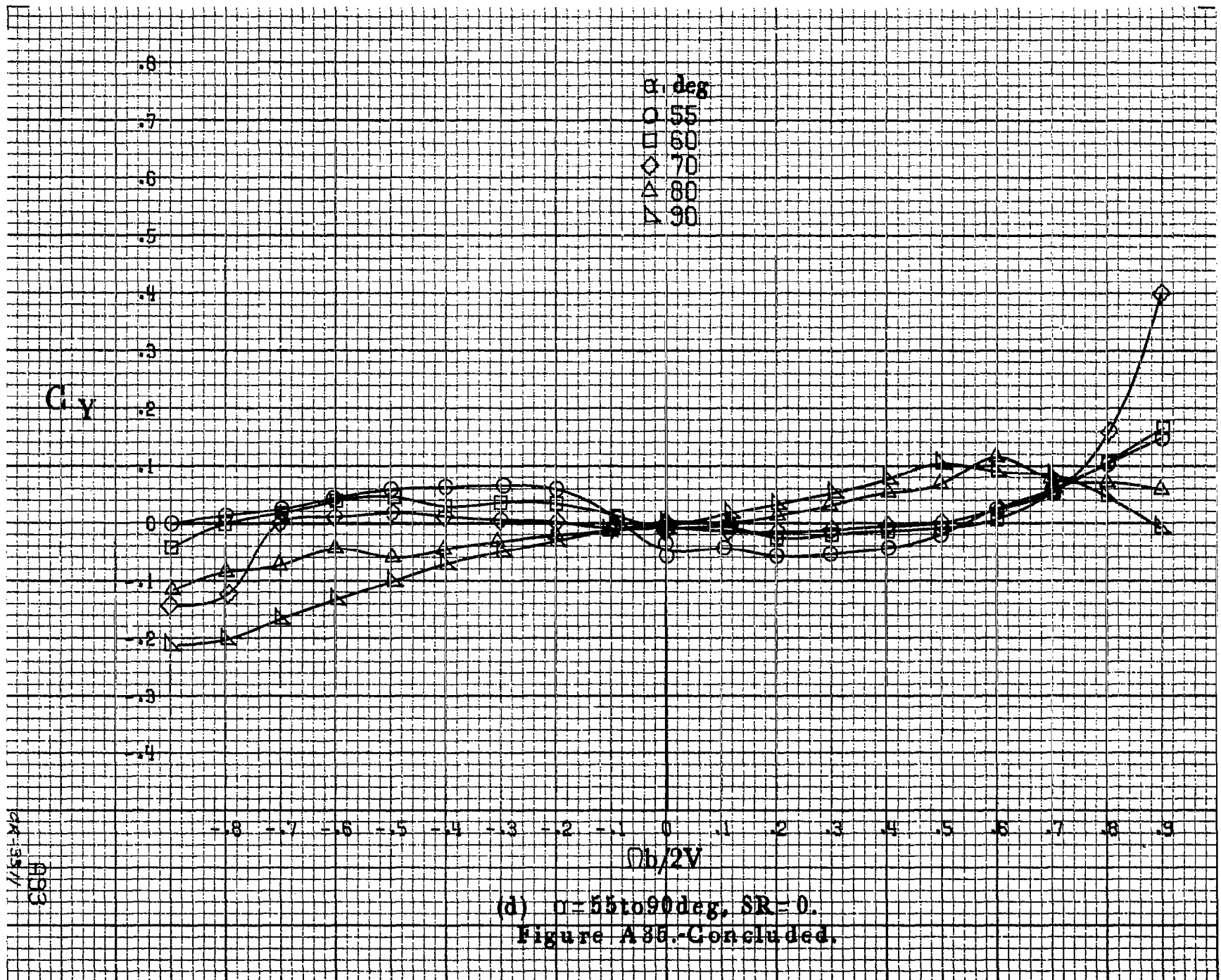
(b) α = 18 to 35 deg, SR = 152.4 cm (60 in).

Figure A29.- Concluded.

(a) α = 8 to 16 deg, SR = 152.4 cm (60 in).

Figure A30.-Effect of rotation rate and angle of attack on axial-force coefficient for basic configuration. δ_e = -27°, δ_a = -19.0°, δ_r = -24°. β = 0°.

(b) $\alpha = 18$ to 35 deg, SR = 152.4 cm (60 in).

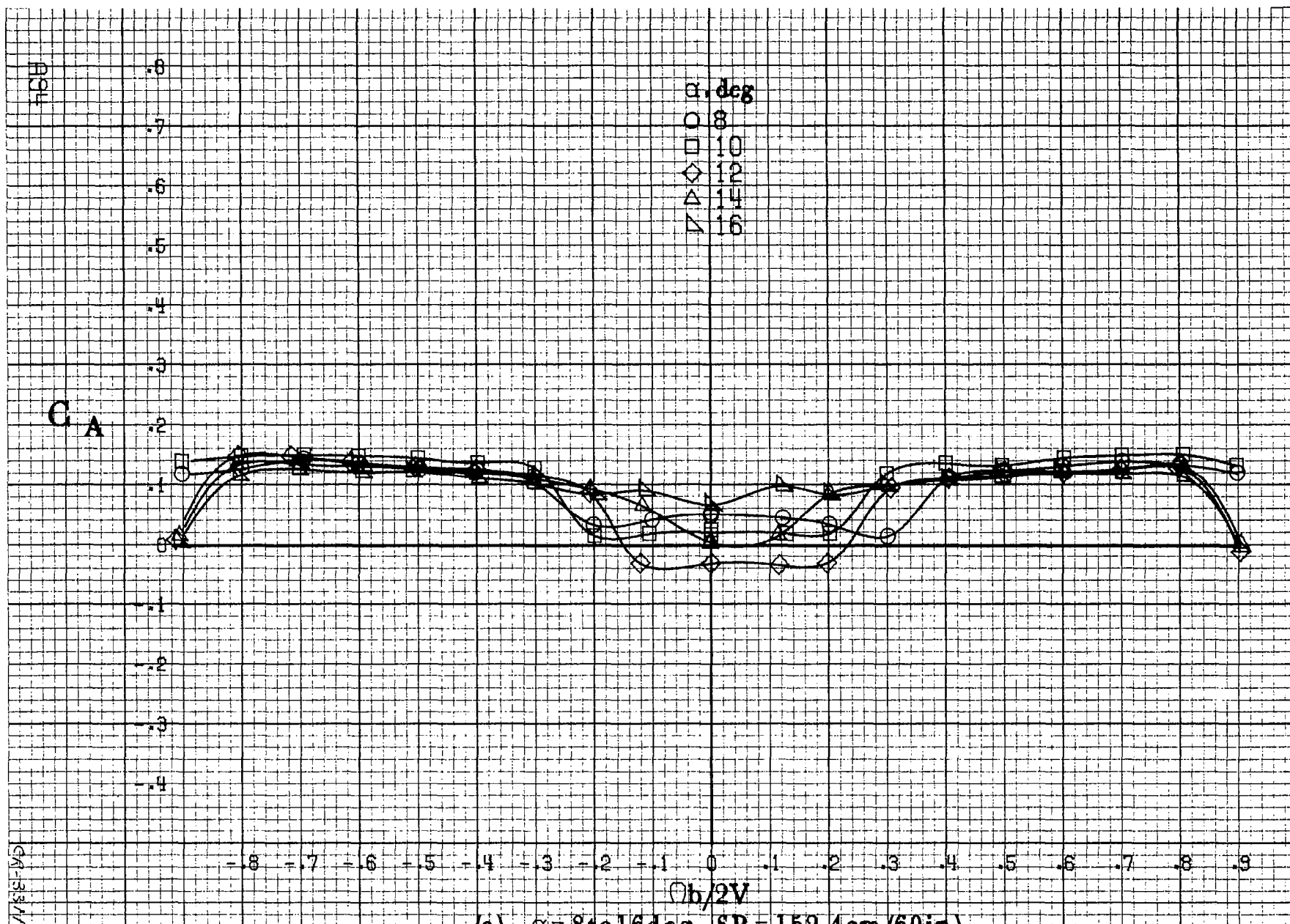Figure A30.-Concluded.
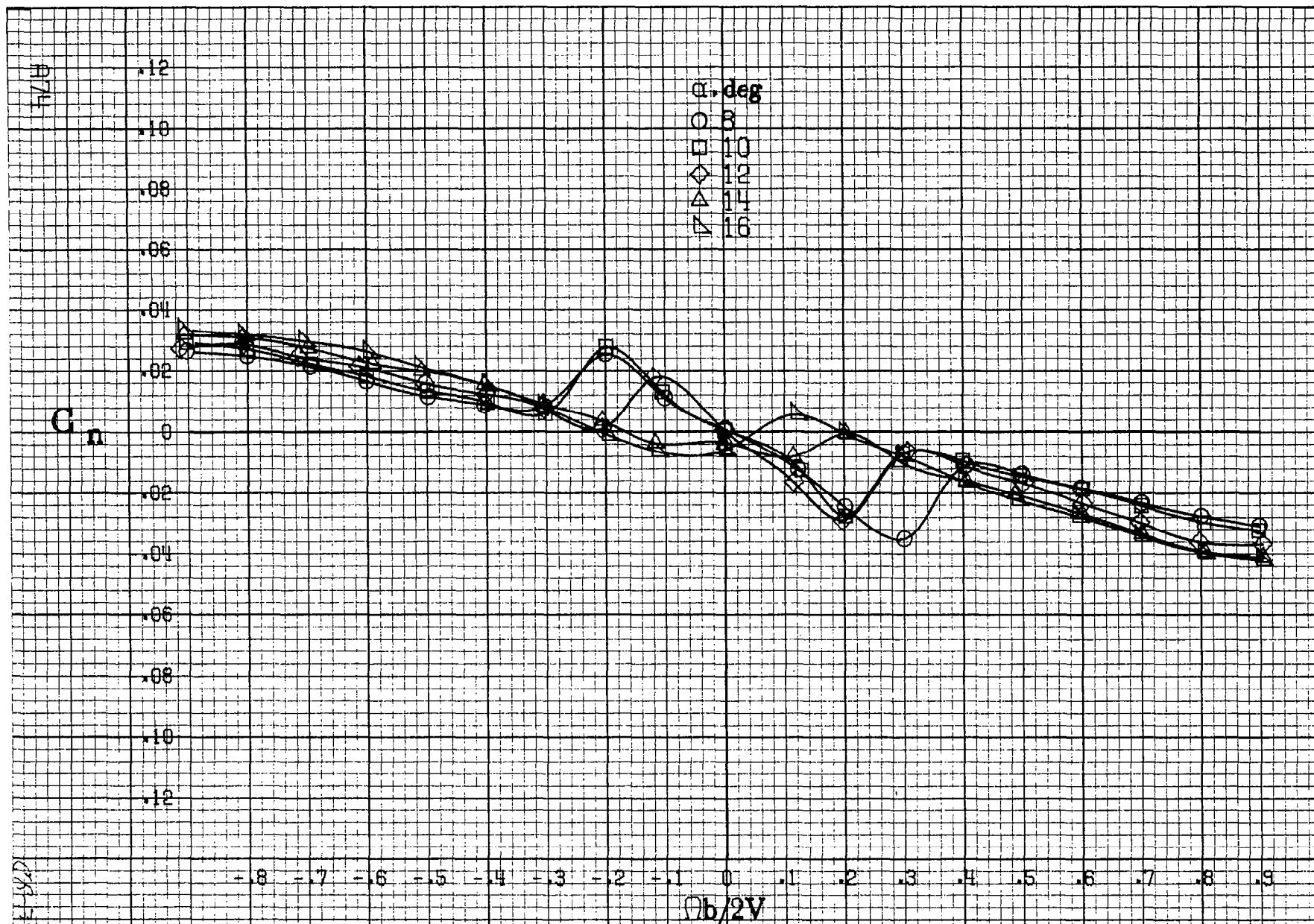
(a) α = 8 to 16 deg, SR = 152.4 cm (60 in).

Figure A31.-Effect of rotation rate and angle of attack on yawing-moment coefficient for turbine nose configuration. $\delta_a = 0°$, $\delta_e = 0°$, $\delta_r = 0°$, $\beta = 0°$.

(b) α = 18 to 35 deg, SR = 152.4 cm (60 in).

Figure A31.-Continued.

(c) α = 30 to 50 deg, SR = 0.

Figure A81.-Continued.

(d) $\alpha = 55$ to 90 deg, $\delta R = 0$.

Figure A81.-Concluded.
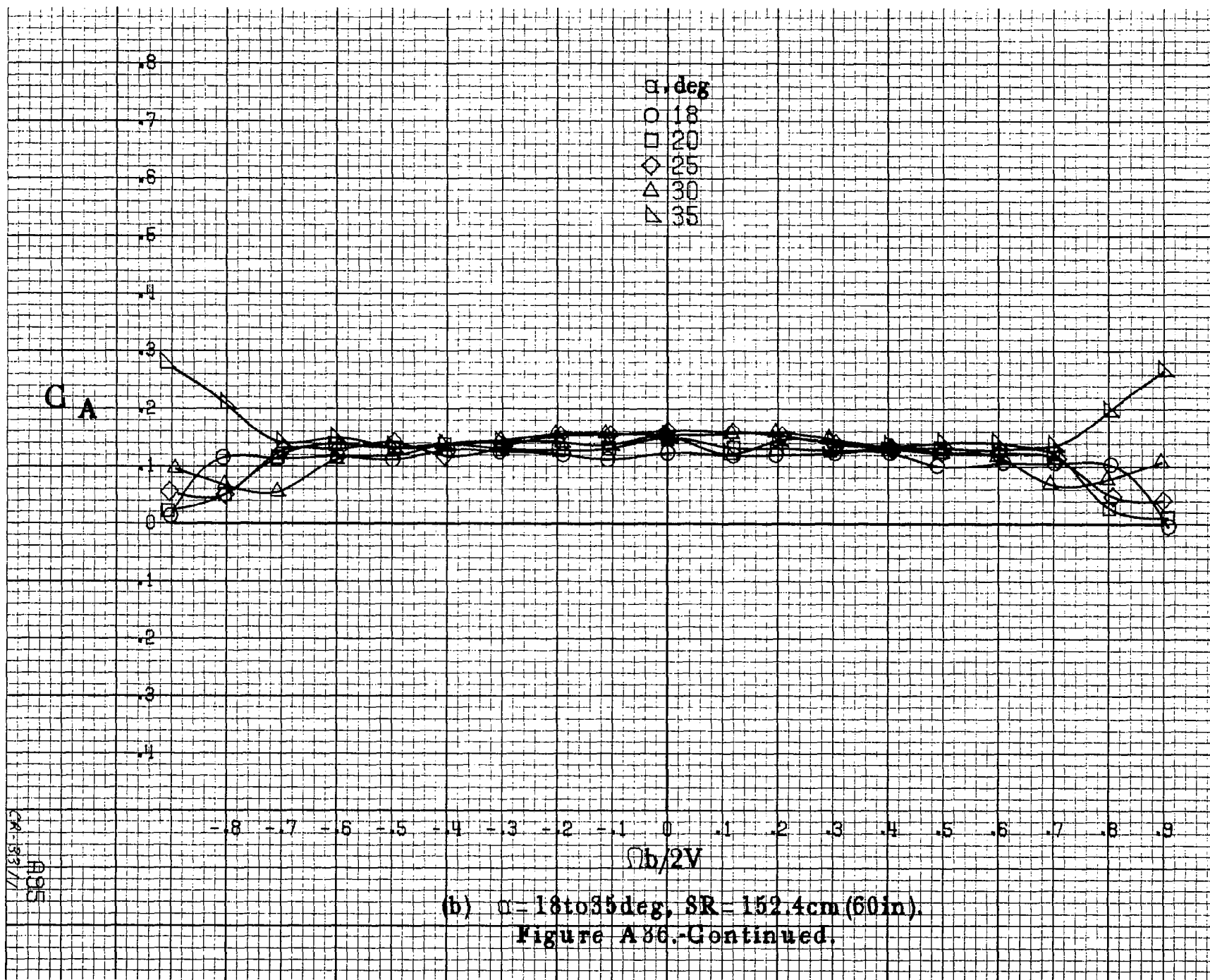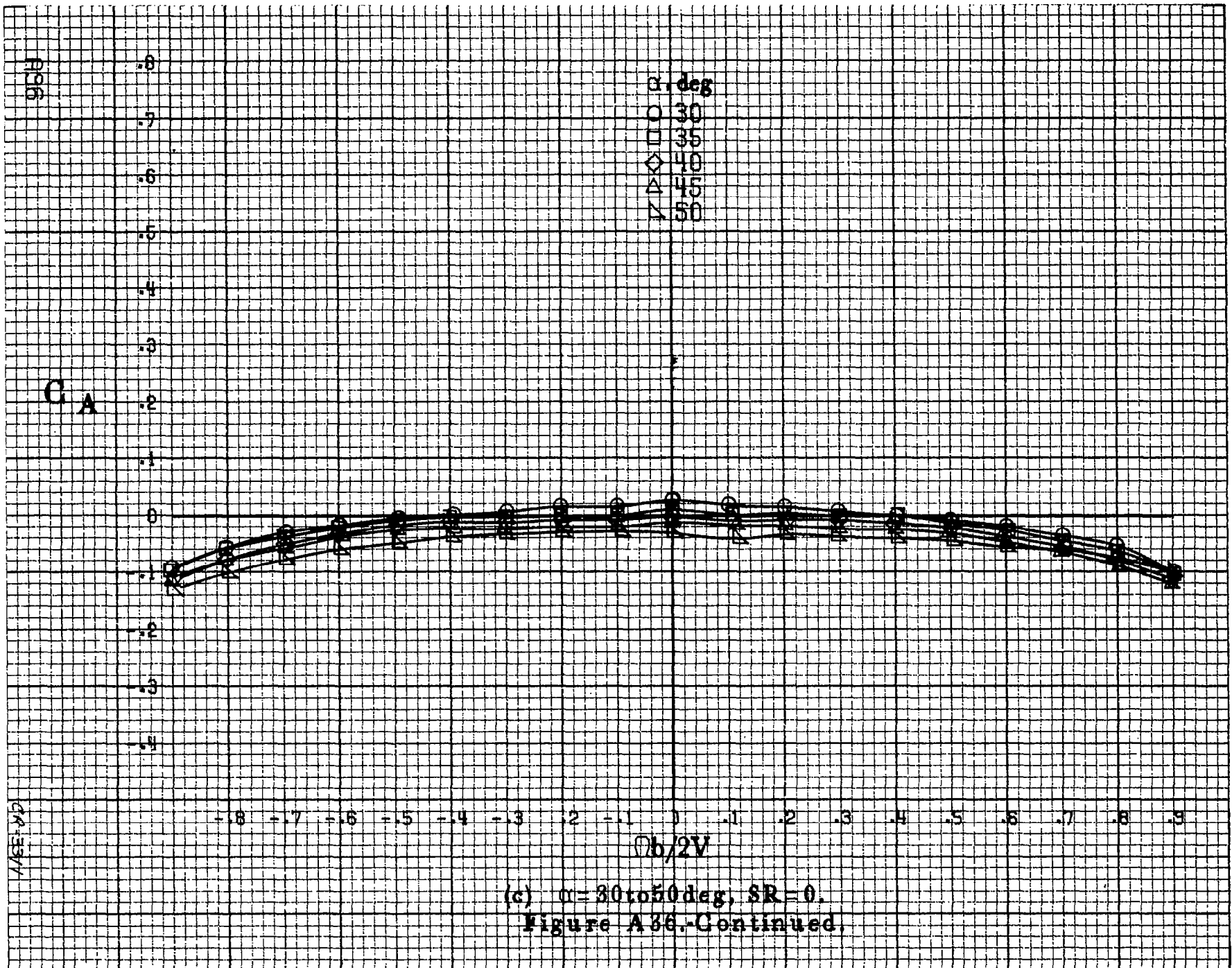
(a) α = 8 to 16 deg, SR = 152.4 cm (60 in).

Figure A32.-Effect of rotation rate and angle of attack on rolling-moment coefficient for turbine nose configuration. δ_e = 0°, δ_a = 0°, δ_r = 0°, β = 0°.

(b)   α = 18 to 35 deg, SR = 152.4 cm (60 in).
Figure A 32.- Continued.

(c) α = 30 to 50 deg, SR = 0.
Figure A82.-Continued.

(d) α = 55 to 90 deg, SR = 0.

Figure A 52.-Concluded.

α, deg
○ 55
□ 60
◇ 70
△ 80
▽ 90

C_l

$\Omega b/2V$
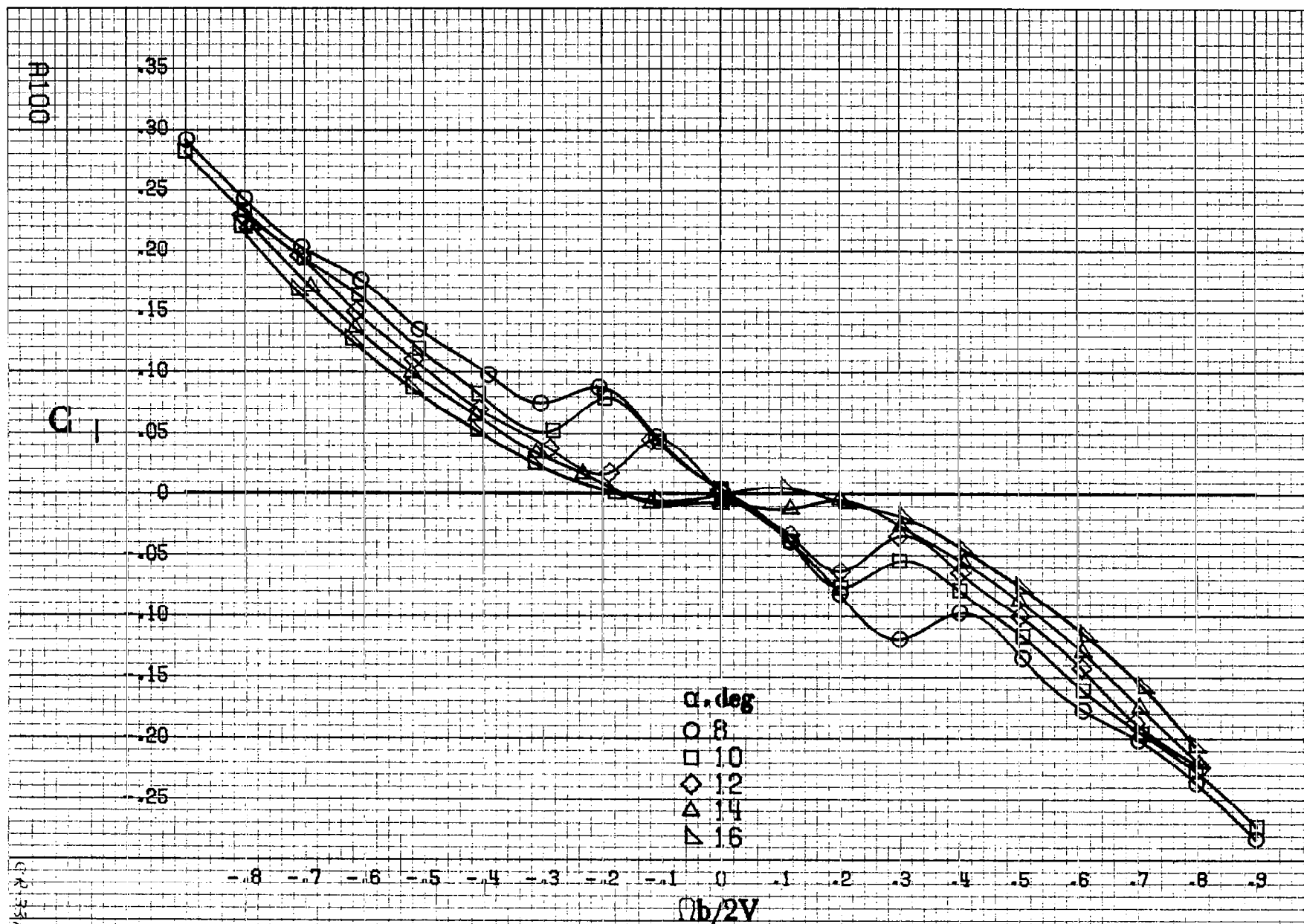
(a) α = 8 to 16 deg, SR = 152.4 cm (60 in).

Figure A38.-Effect of rotation rate and angle of attack on pitching-moment coefficient for turbine nose configuration. δe = 0°, δa = 0°, δr = 0°, β = 0°.

(b) $\alpha = 18$ to 35 deg, $SR = 152.4$cm (60in).

Figure A 33.-Continued.

(c) $\alpha = 30$ to 50 deg, $SR = 0$.

Figure A88.-Continued.

(d) α = 55 to 90 deg, SR = 0.

Figure A88.-Concluded.

α,deg
○ 8
□ 10
◇ 12
△ 14
▽ 16

C_N

Ωb/2V
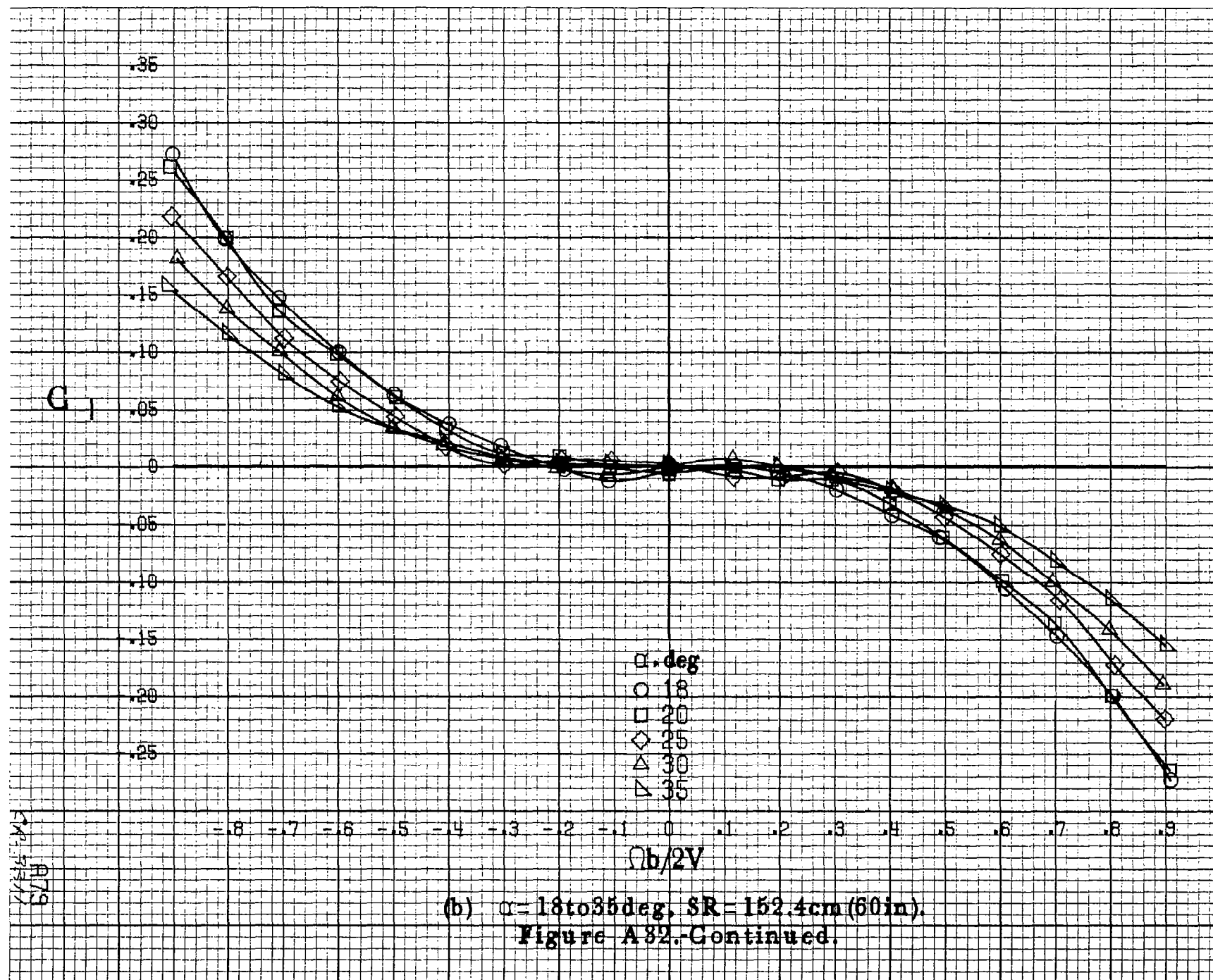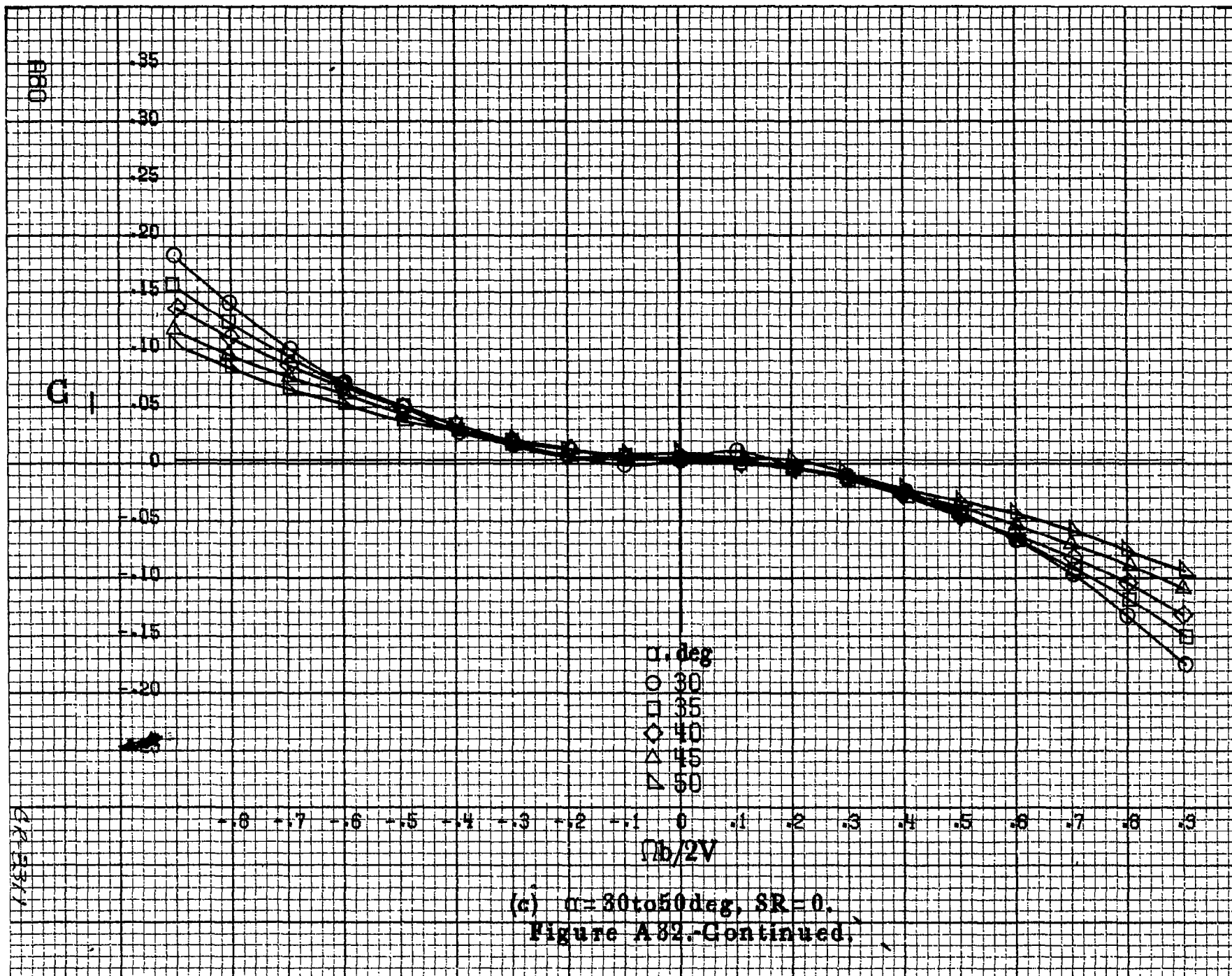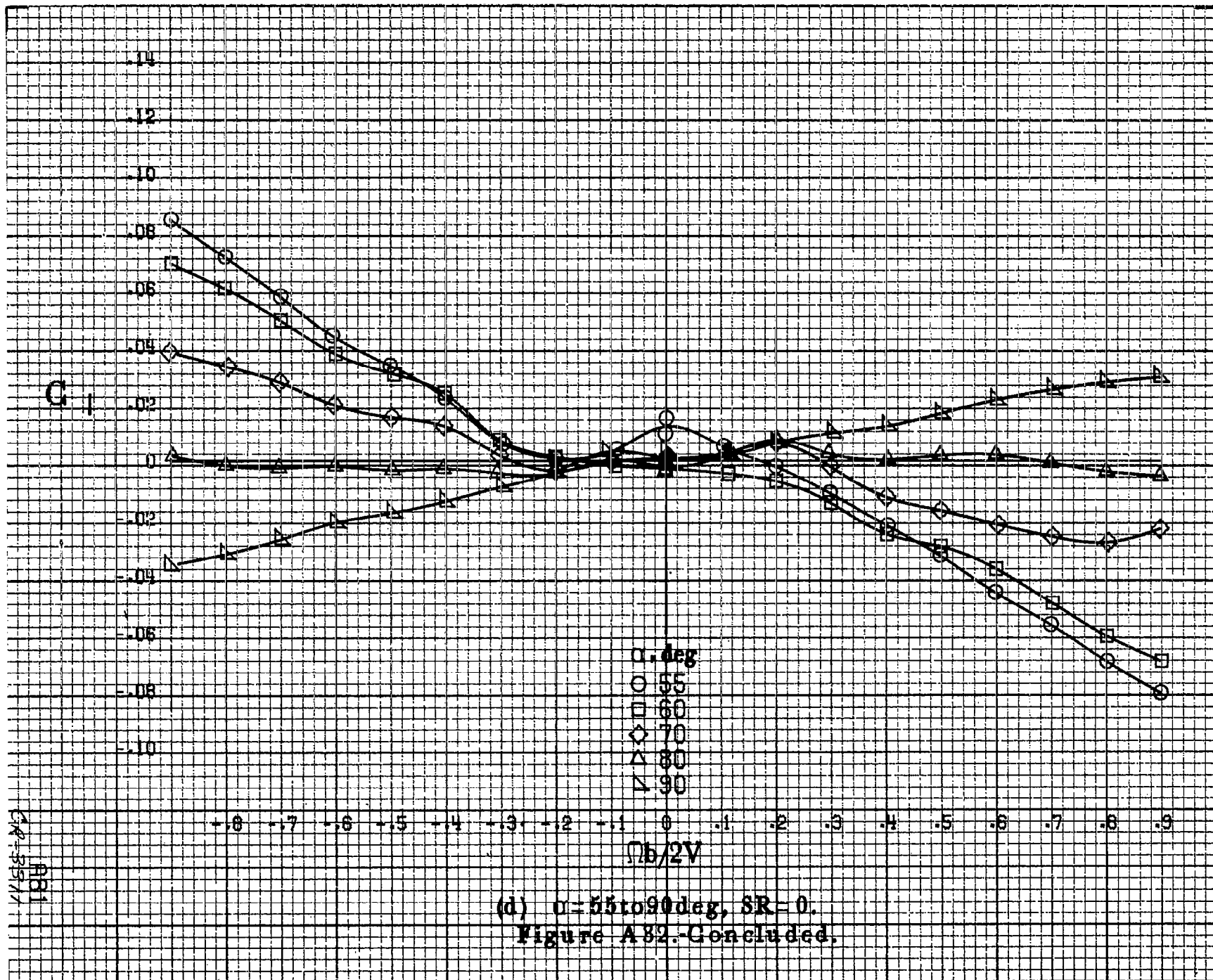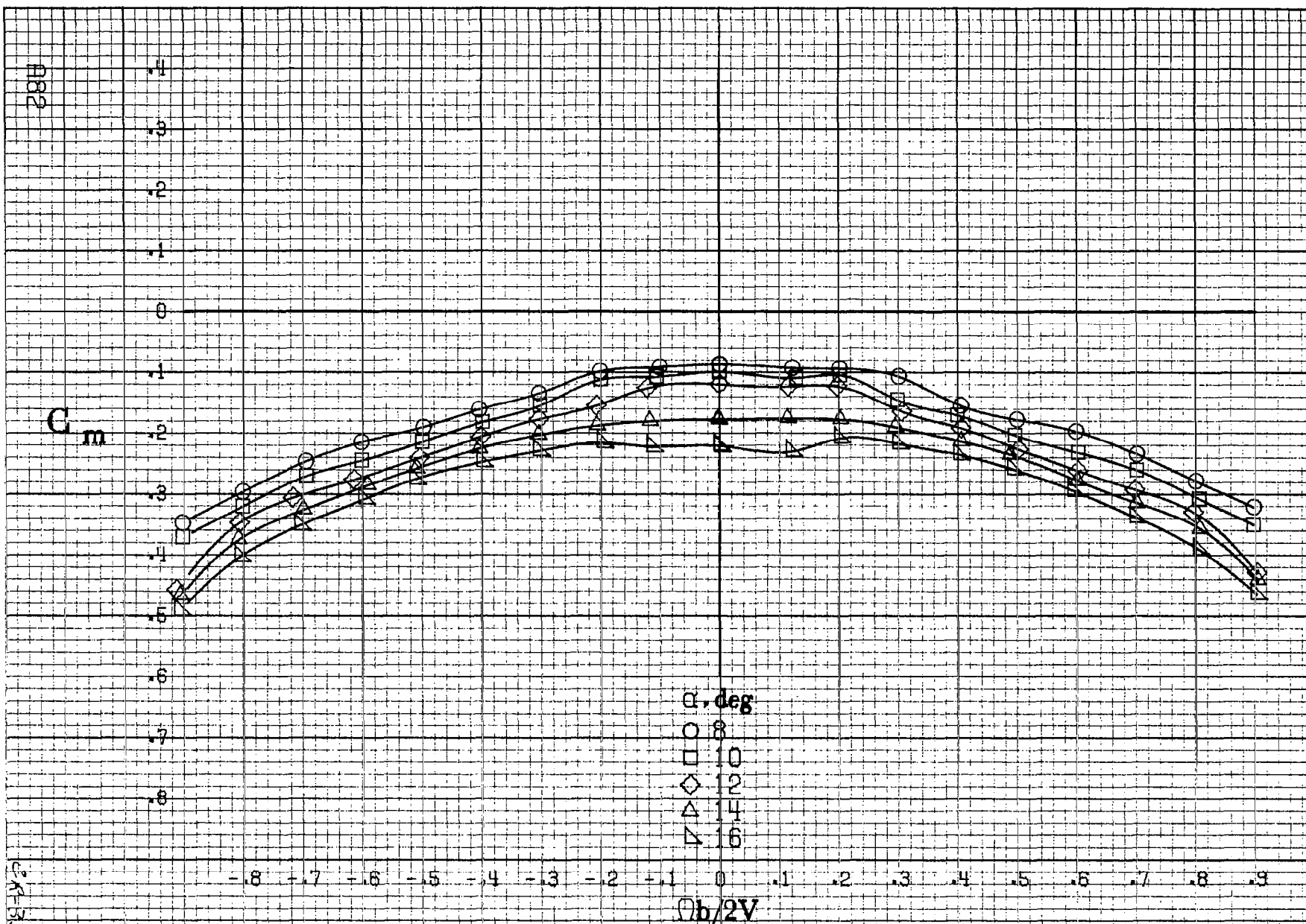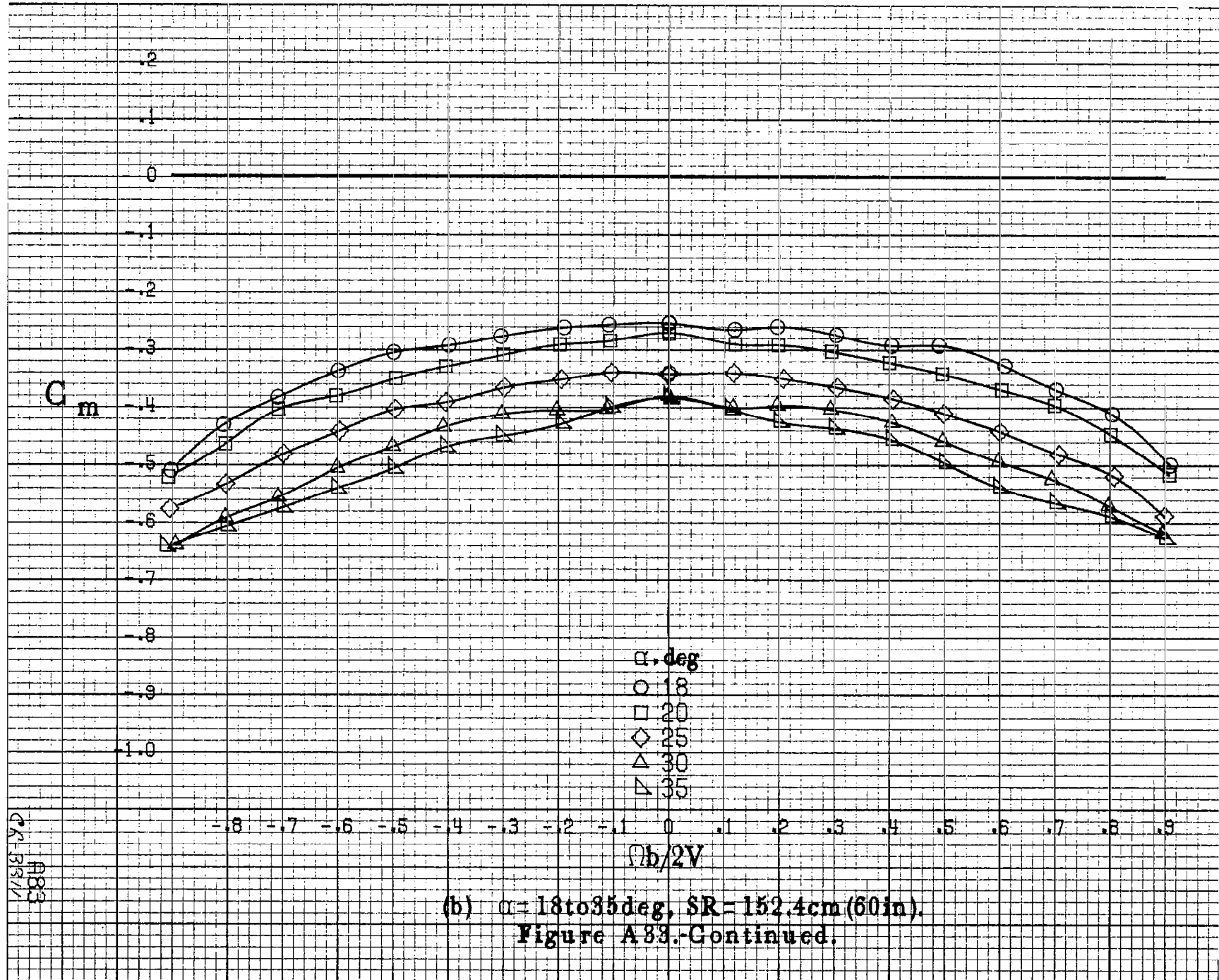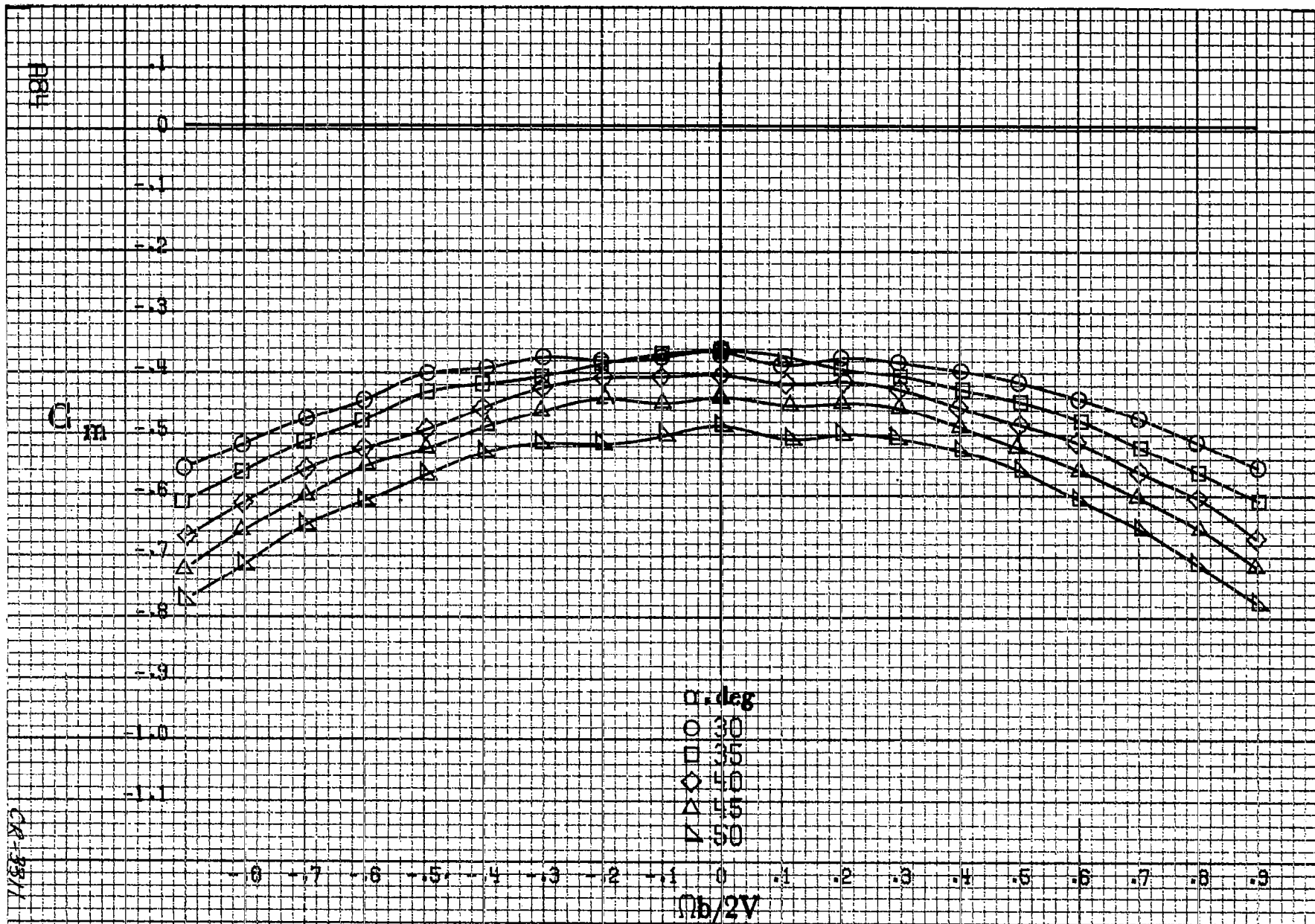
(a) α = 8 to 16 deg, SR = 152.4 cm (60 in.).

Figure A34.-Effect of rotation rate and angle of attack on normal-force coefficient for turbine nose configuration, δ$_e$ =0°, δ$_a$ =0°, δ$_r$ =0°, β =0°.

(b) α=18to35deg, SR=152.4cm(60in).
Figure A34.-Continued.
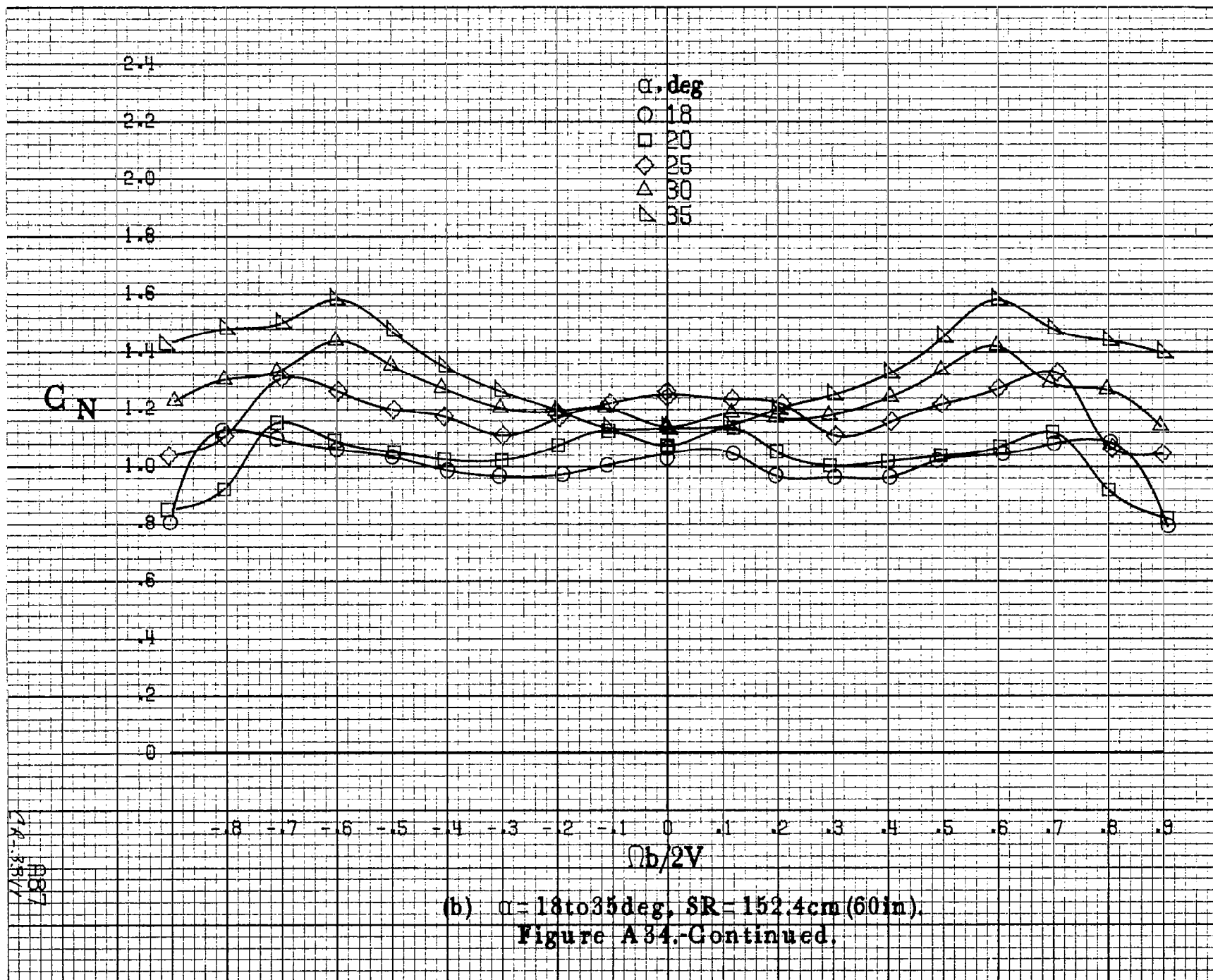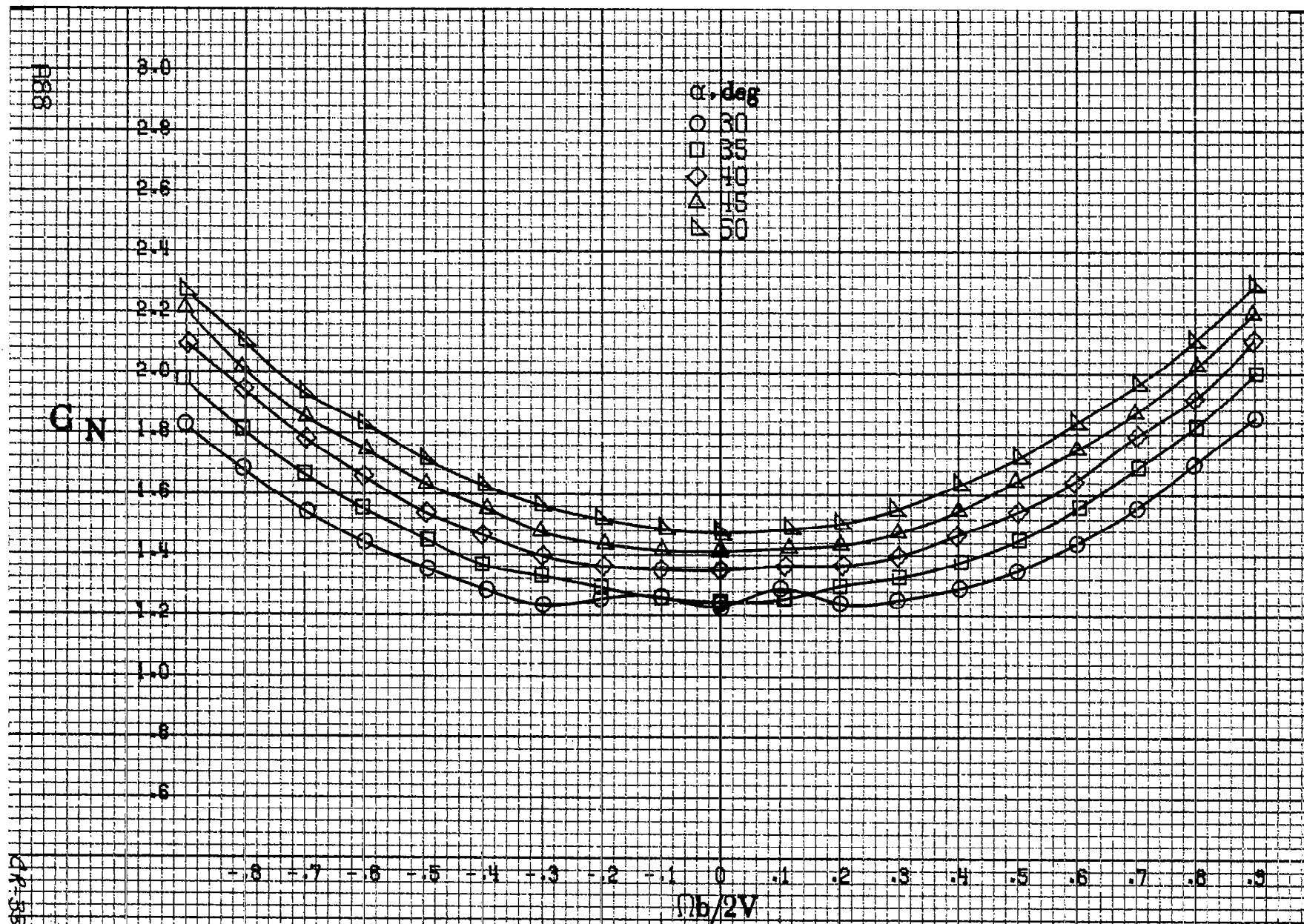
(c) α=30 to 50 deg, SR=0.

Figure A 84.-Continued.

(d) α = 55 to 90 deg, SR = 0.

Figure A 84.-Concluded.
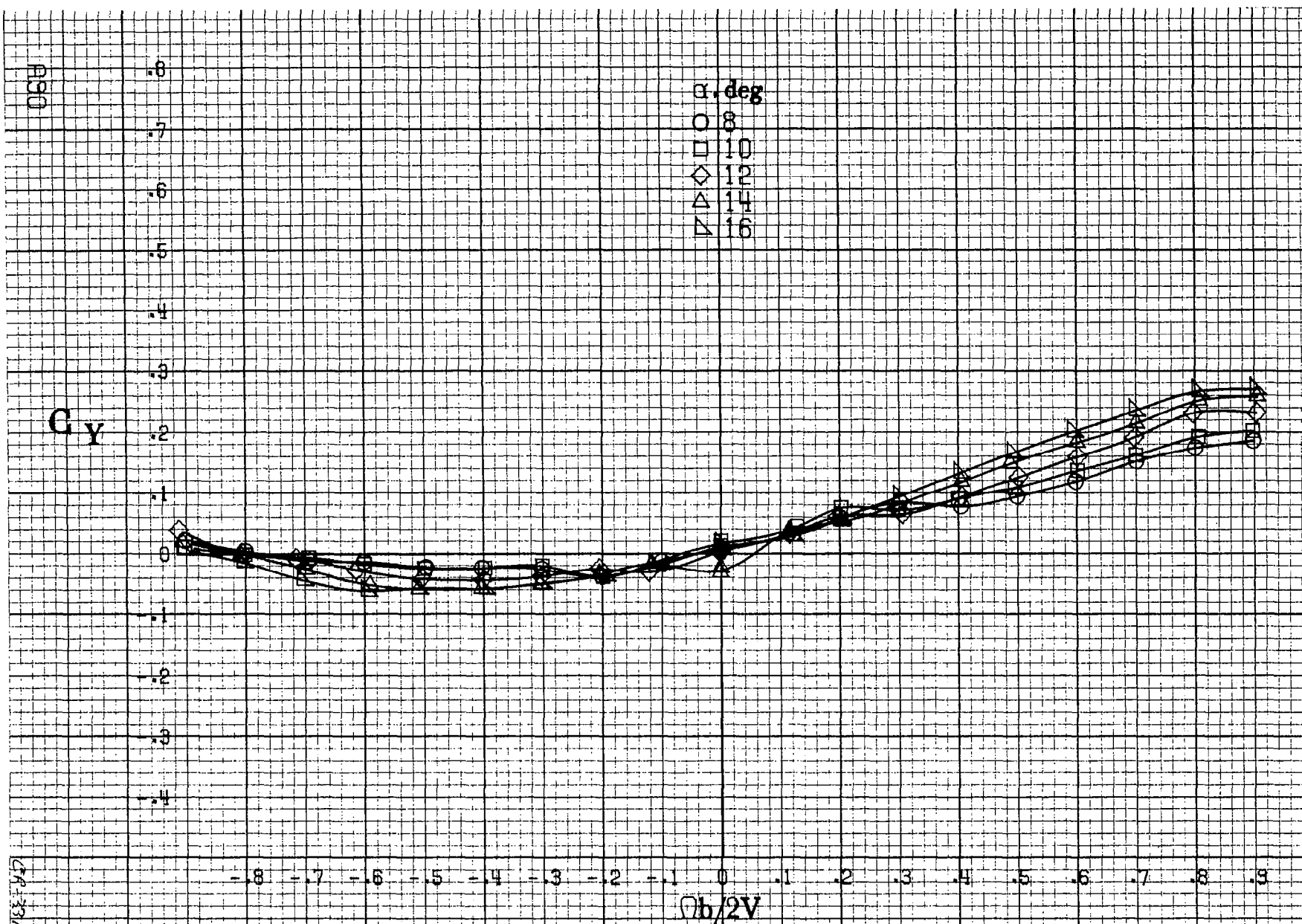
(a) $\alpha = 8$ to 16 deg, $SR = 152.4$ cm (60 in).
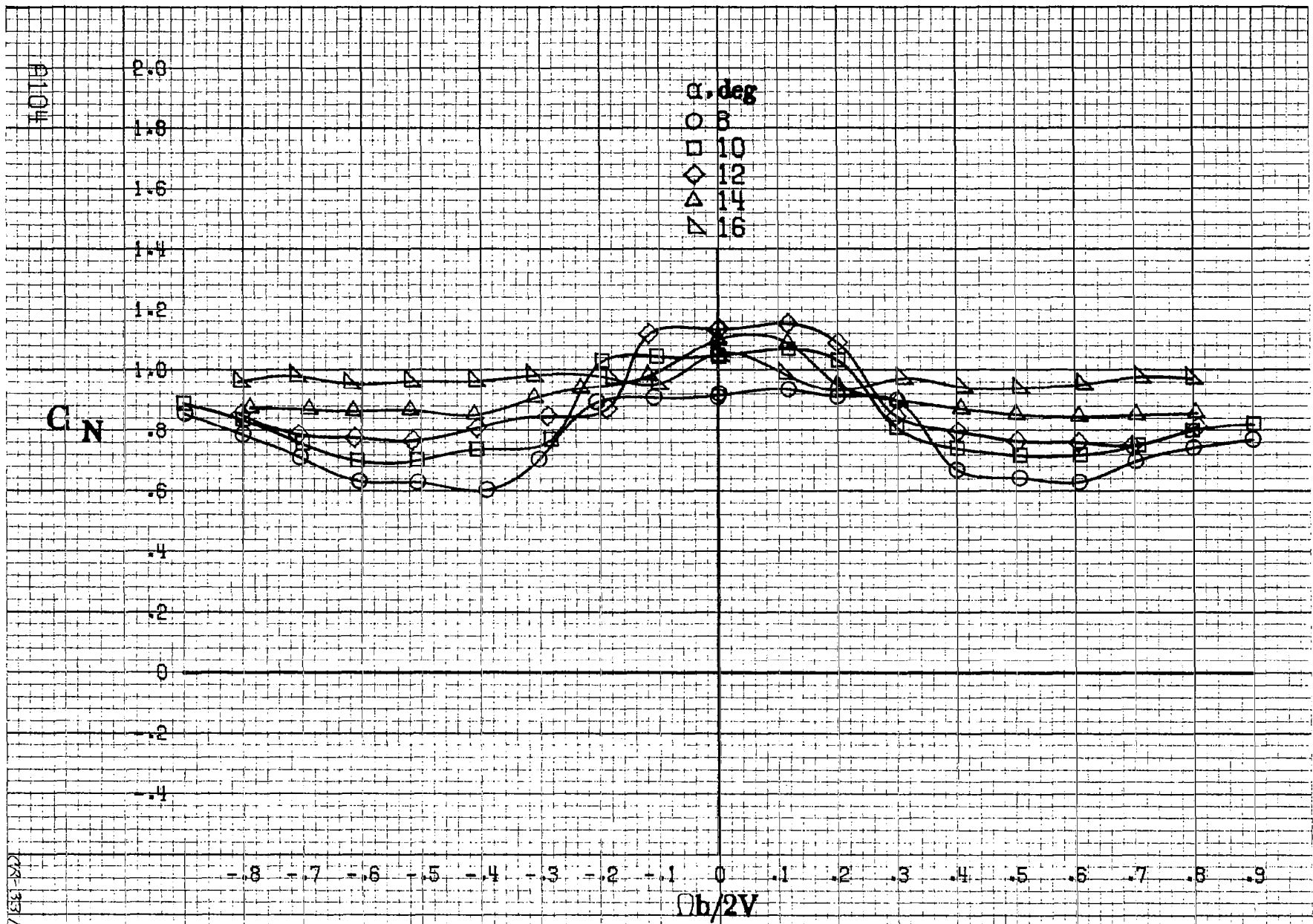
Figure A35.-Effect of rotation rate and angle of attack on side-force coefficient for turbine nose configuration. $\delta_e = 0°$, $\delta_a = 0°$, $\delta_r = 0°$, $\beta = 0°$.

(b) α = 18 to 35 deg, SR = 152.4 cm (60 in).

Figure A35.- Continued.

(c) α = 30 to 50 deg, SR = 0.

Figure A35.-Continued.

(d) α = 55 to 90 deg, SR = 0.

Figure A35.-Concluded.
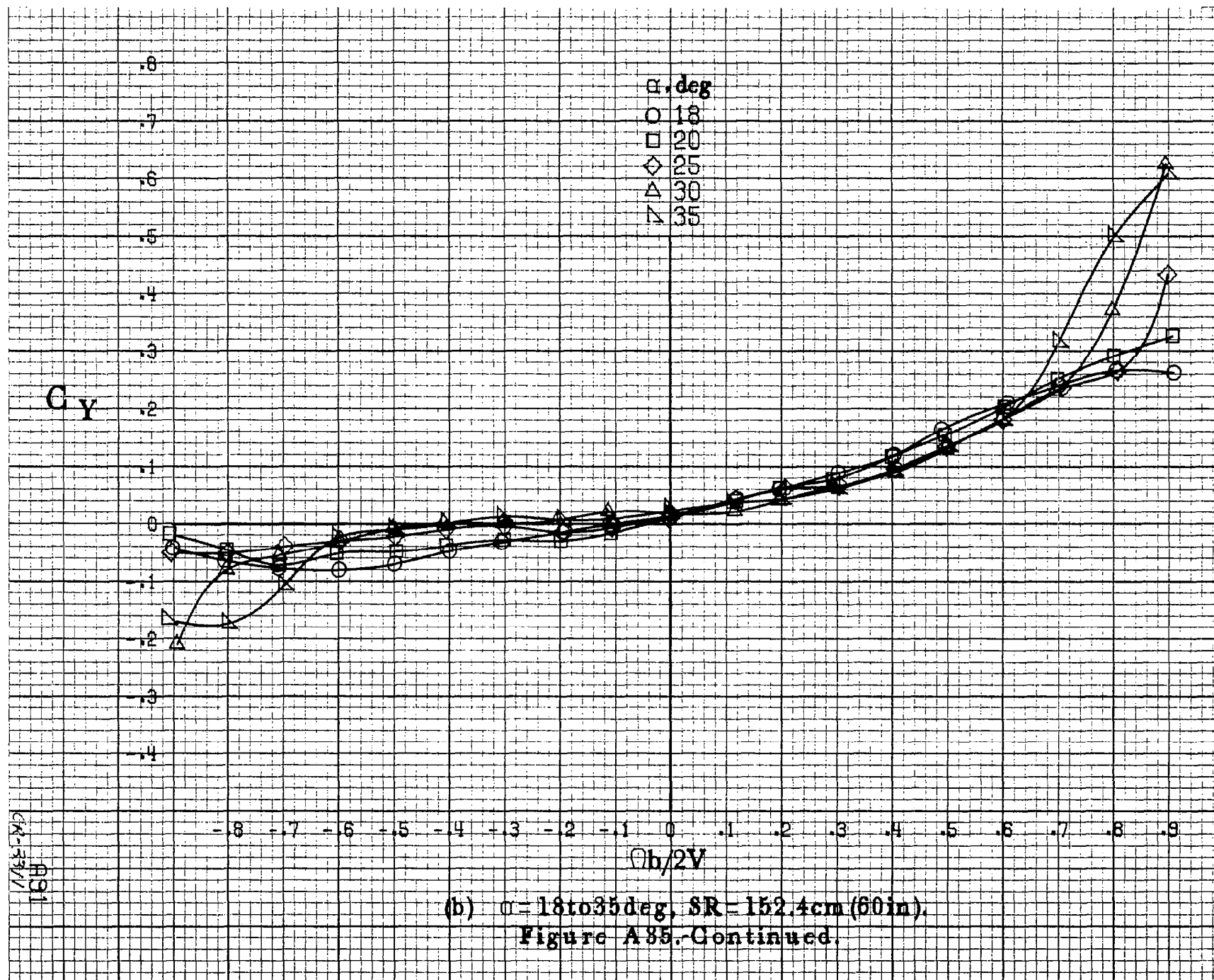
(a) α = 8 to 16 deg, SR = 152.4 cm (60 in).
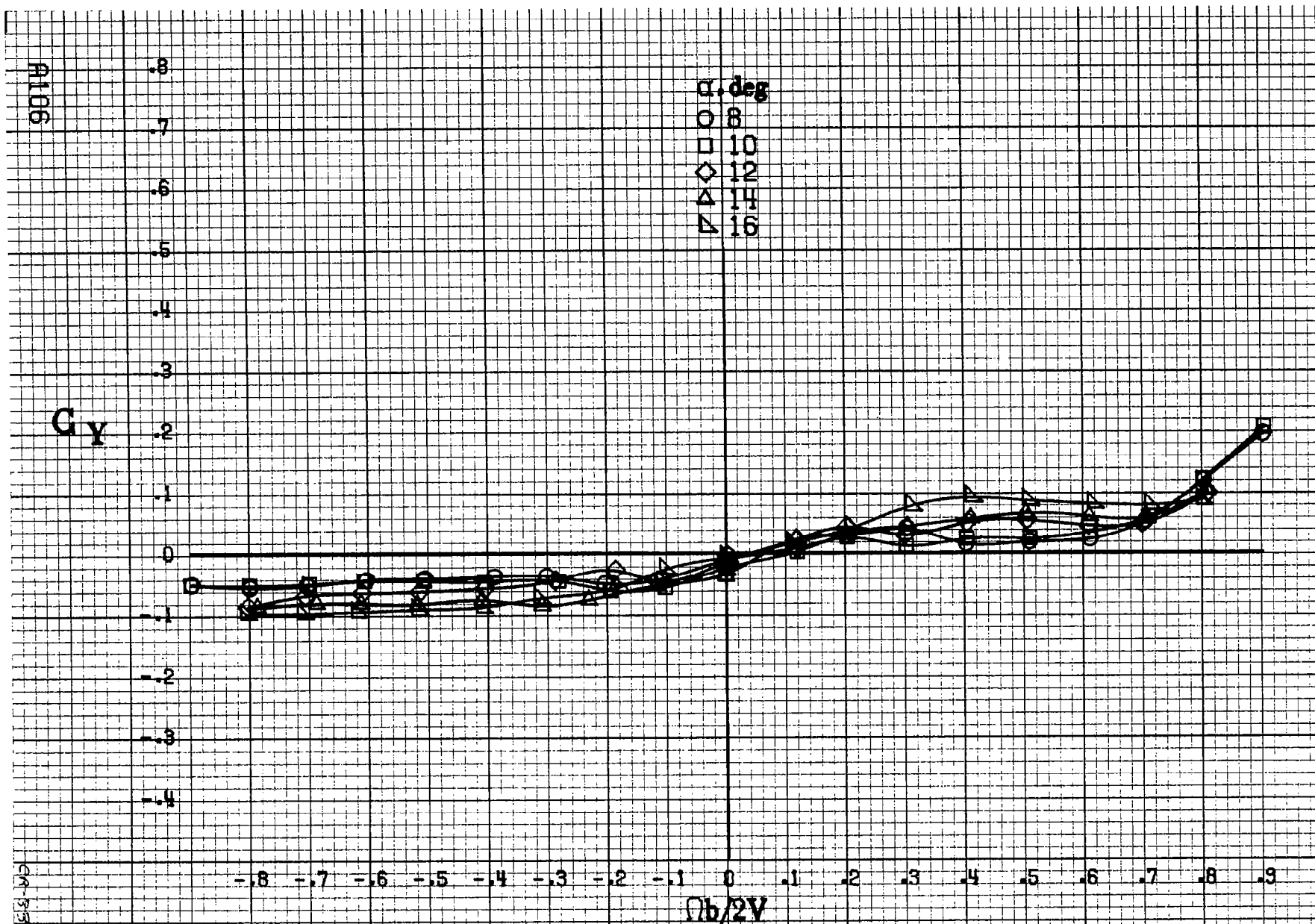
Figure A36.-Effect of rotation rate and angle of attack on axial-force coefficient for turbine nose configuration. $\delta_e = 0°$, $\delta_a = 0°$, $\delta_r = 0°$, $\beta = 0°$.

(b) $\alpha = 18$ to 35 deg, $SR = 152.4$ cm $(60$ in$)$.

Figure A36.-Continued.

(c) α = 30 to 50 deg, SR = 0.

Figure A36.-Continued.

(d) α = 55 to 90 deg, SR = 0.

Figure A36.-Concluded.
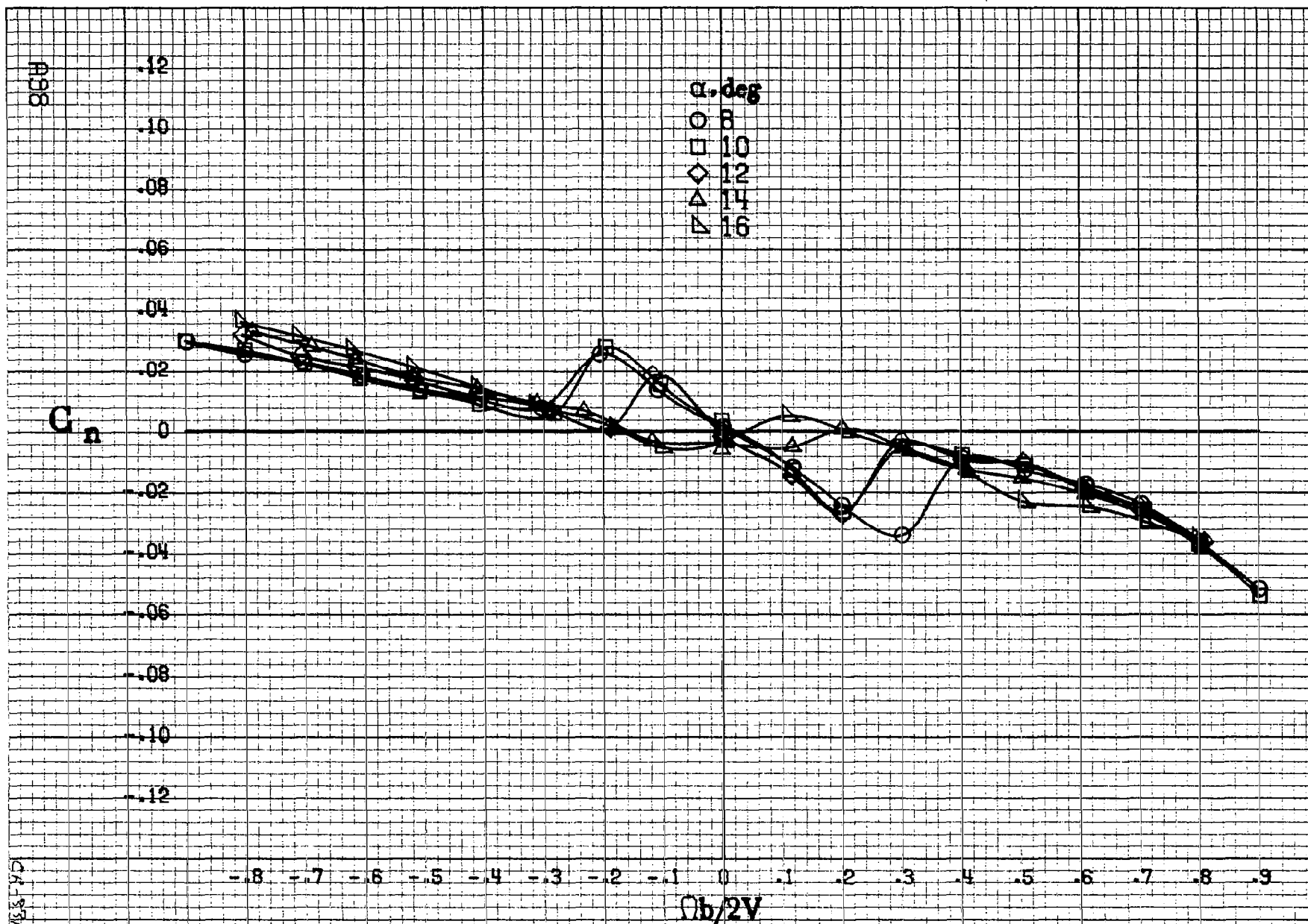
(a) α = 8 to 16 deg, SR = 152.4 cm (60 in).

Figure A37. Effect of rotation rate and angle of attack on yawing-moment coefficient for canopy fairing configuration. δe = 0°. δa = 0°. δr = 0°. β = 0°.

(b) α = 18 to 35 deg, SR = 152.4 cm (60 in).

Figure A37.- Concluded.

(a) α = 8 to 16 deg, SR = 152.4 cm (60 in).

Figure A.38.- Effect of rotation rate and angle of attack on rolling-moment coefficient for canopy fairing configuration. $\delta_e = 0°$, $\delta_a = 0°$, $\delta_r = 0°$, $\beta = 0°$.

(b) α = 18 to 35 deg; SR = 152.4 cm (60 in).

Figure A33.-Concluded.
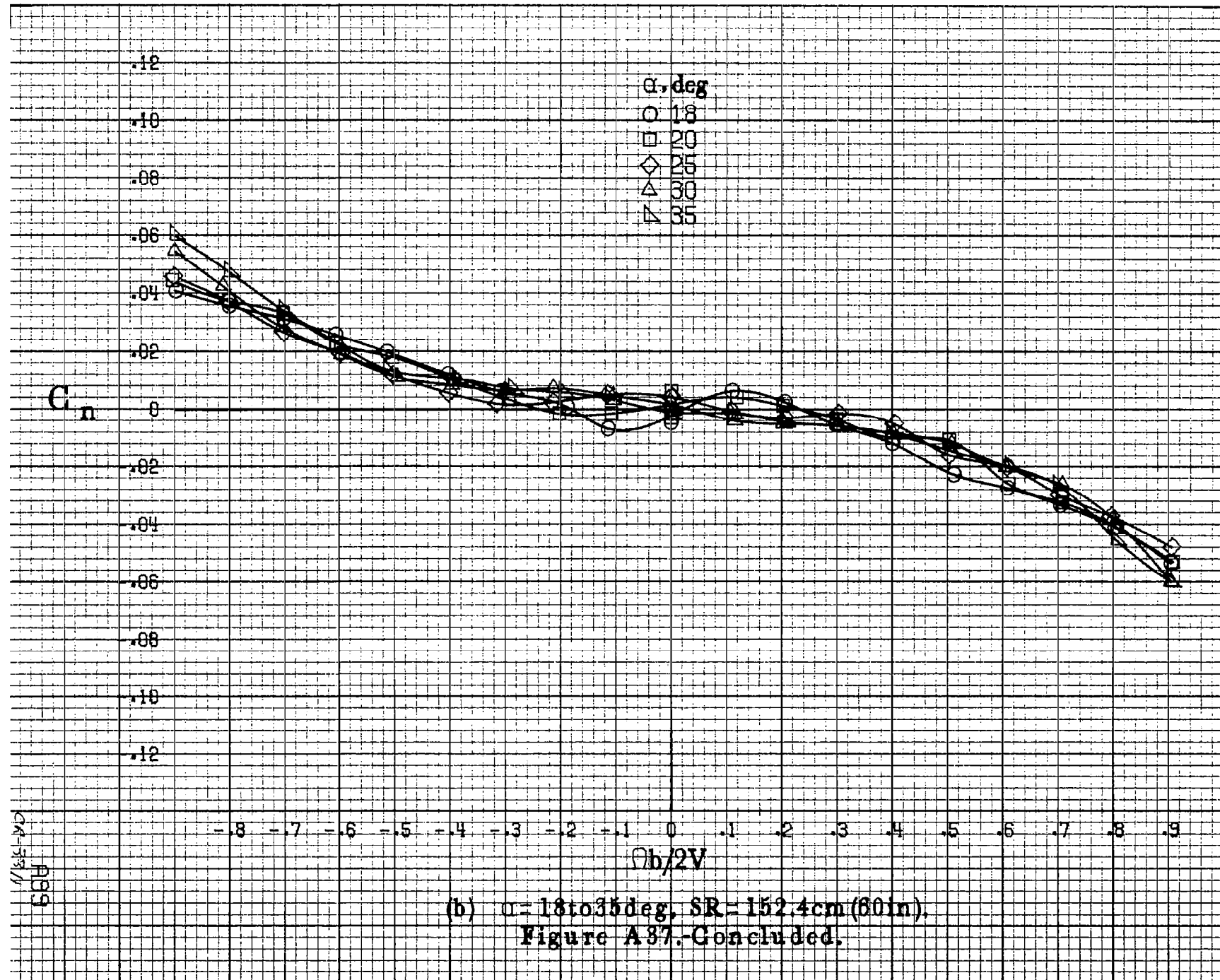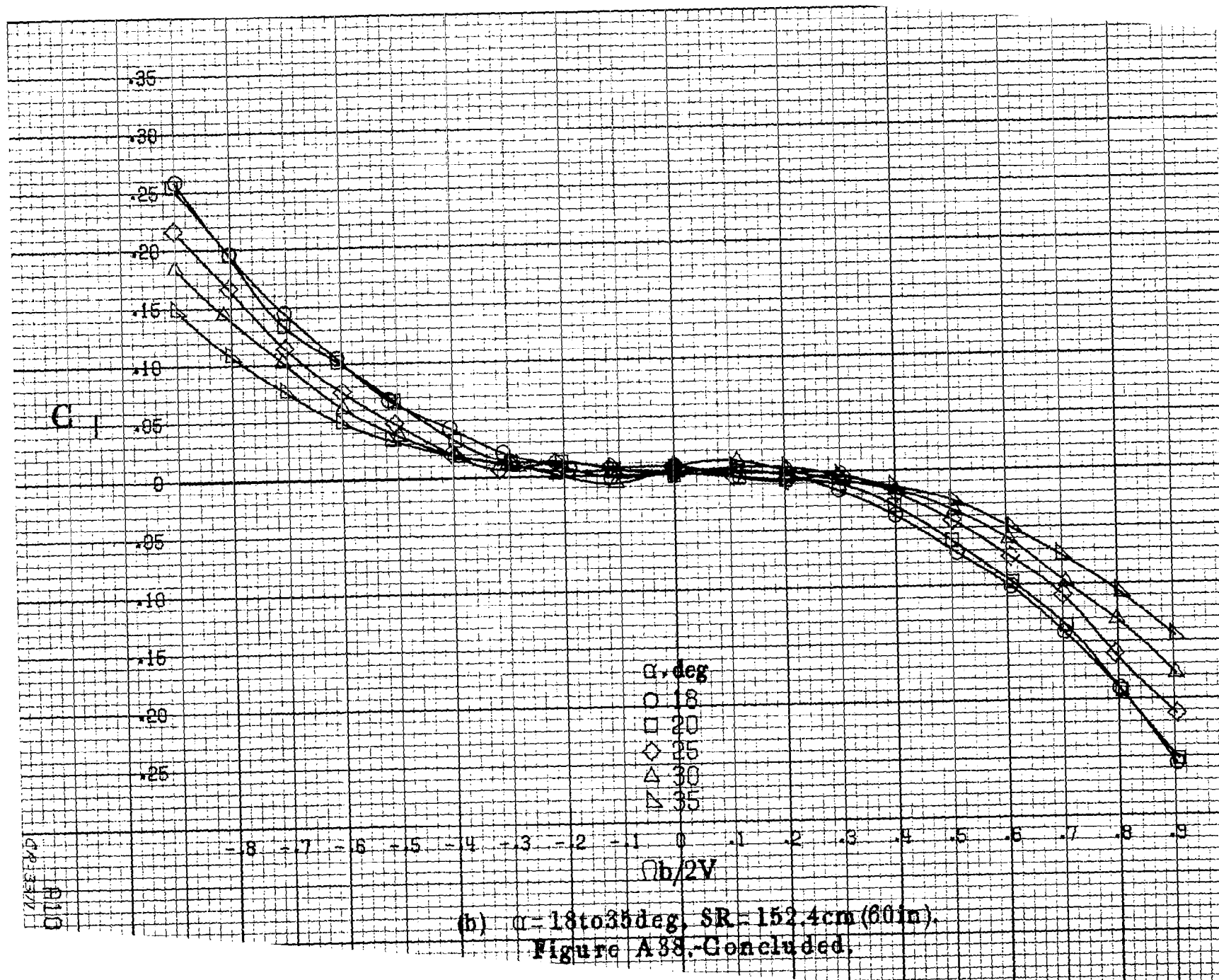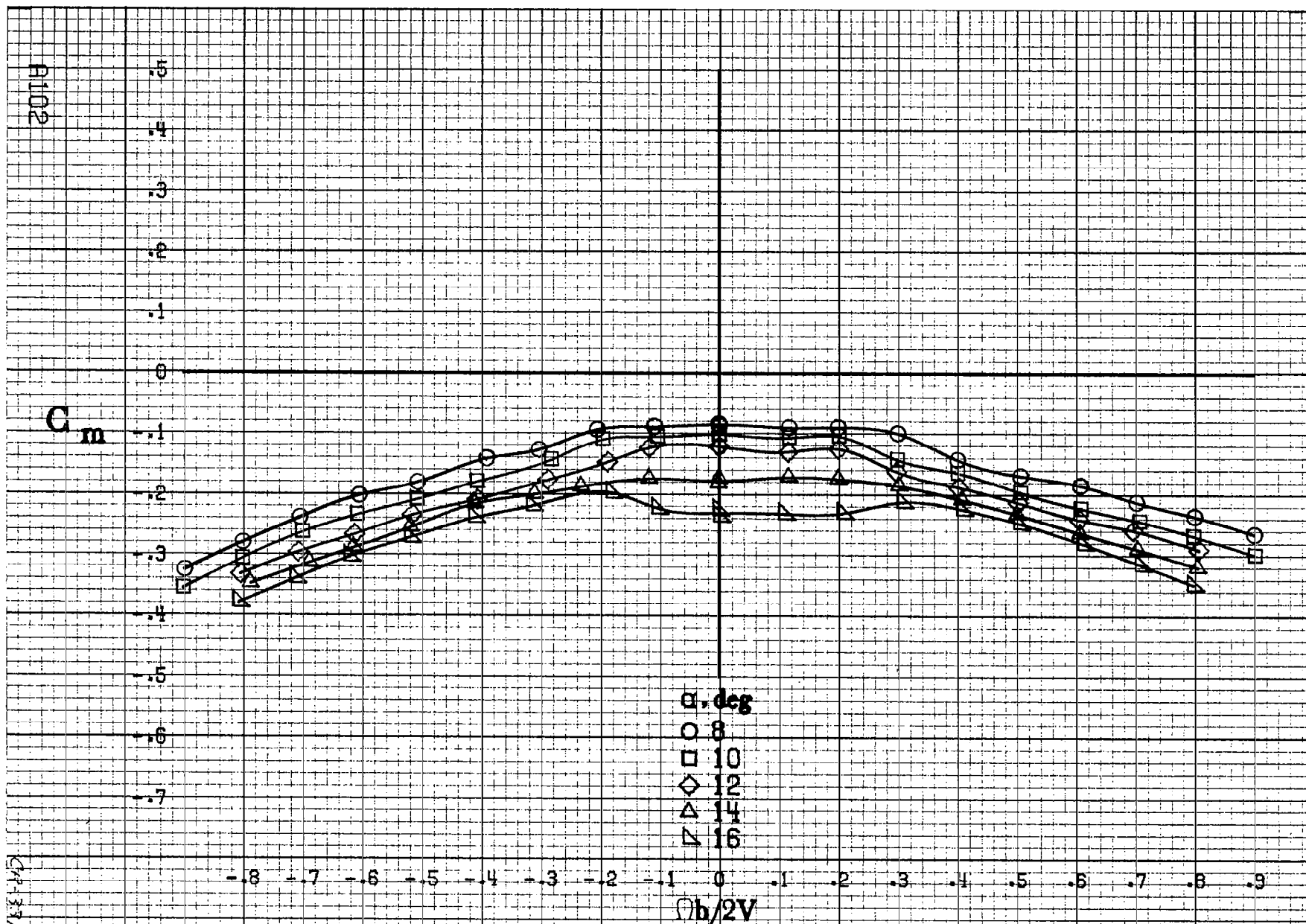
(a) α=8to16deg, SR=152.4cm(60in).

Figure A39.-Effect of rotation rate and angle of attack on pitching-moment coefficient for canopy fairing configuration. δ_e =0°, δ_a =0°, δ_r =0°, β =0°.
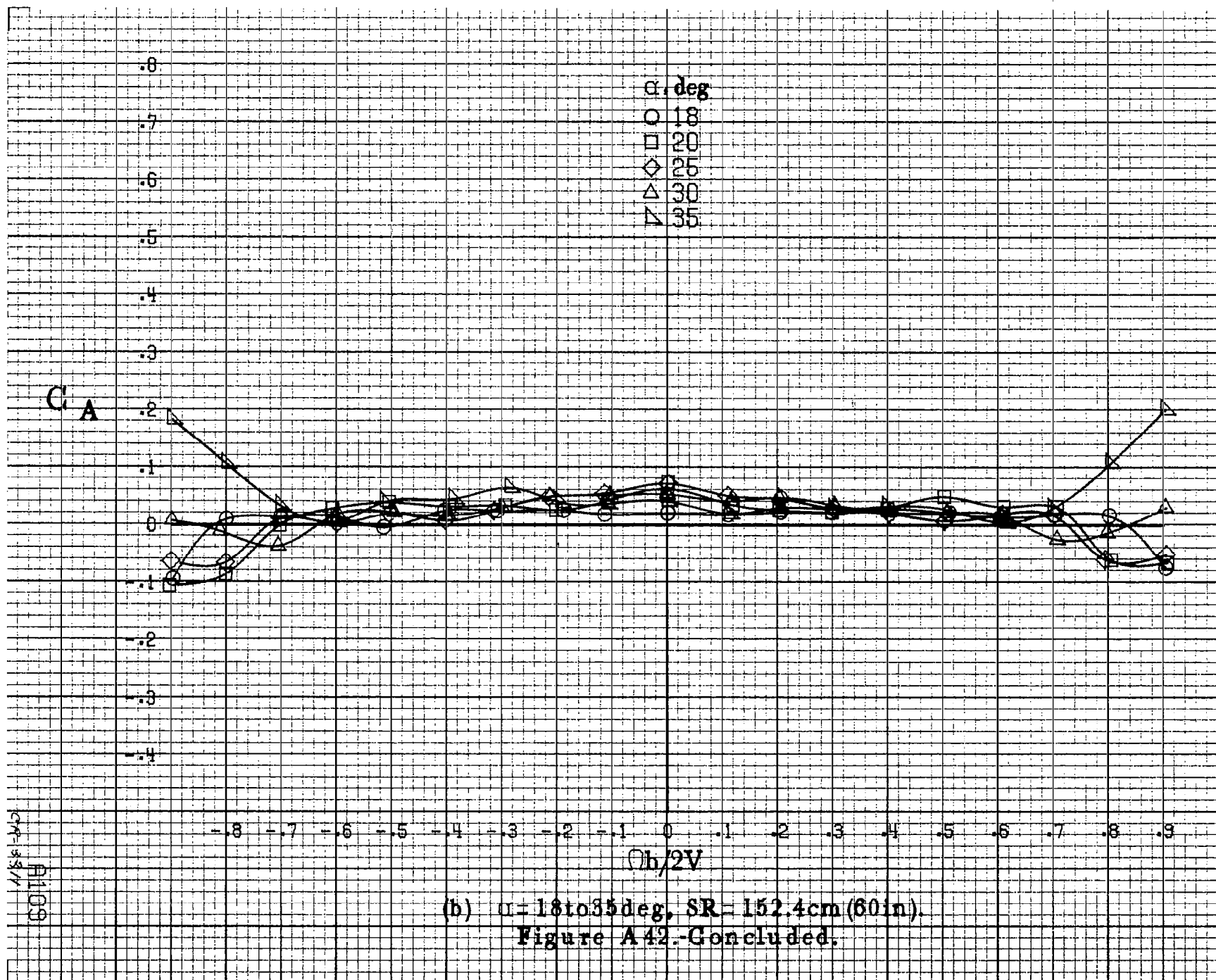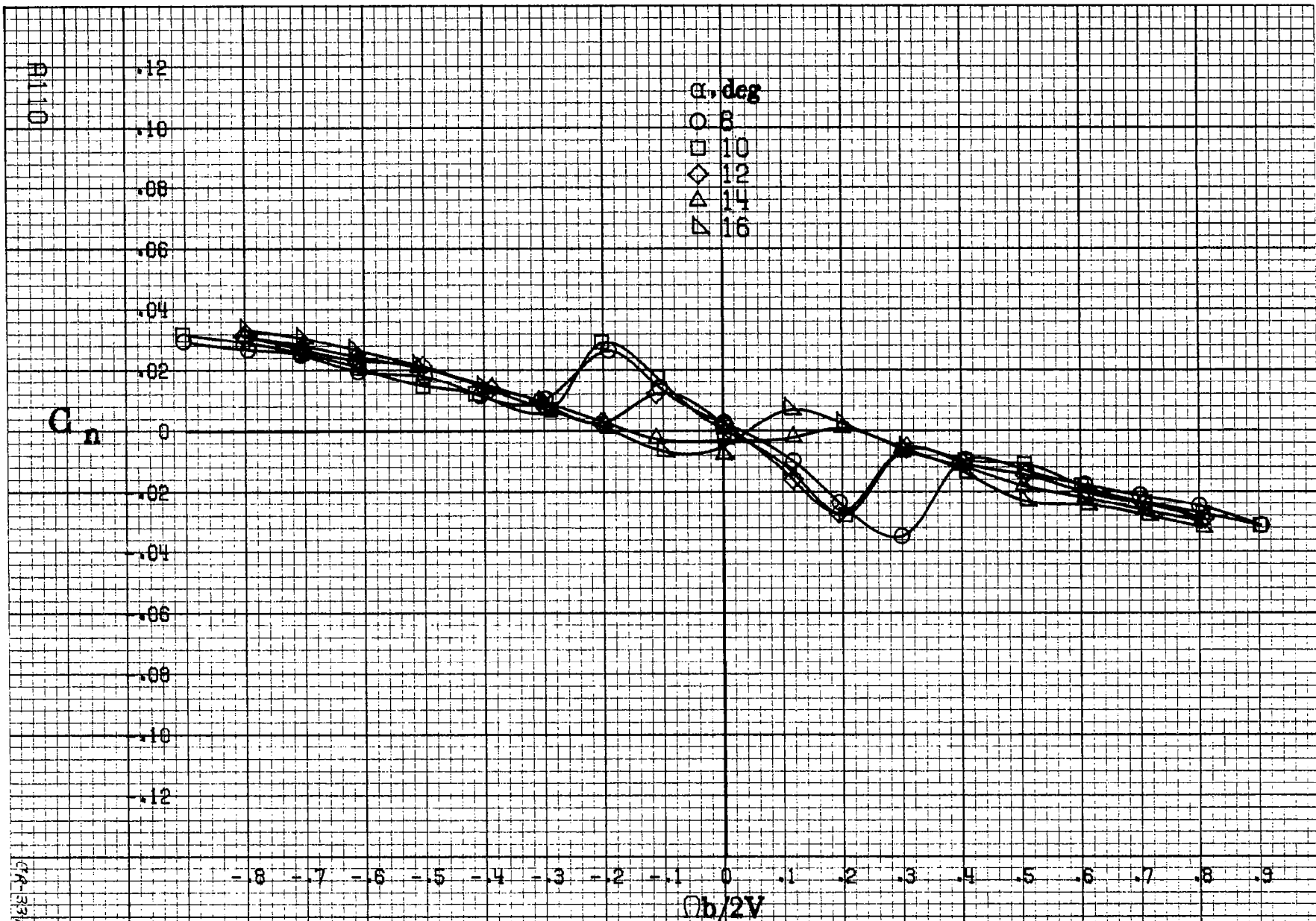
(b) $\alpha = 18$ to 35 deg, $SR = 152.4$ cm $(60$ in$)$.

Figure A39.-Concluded.
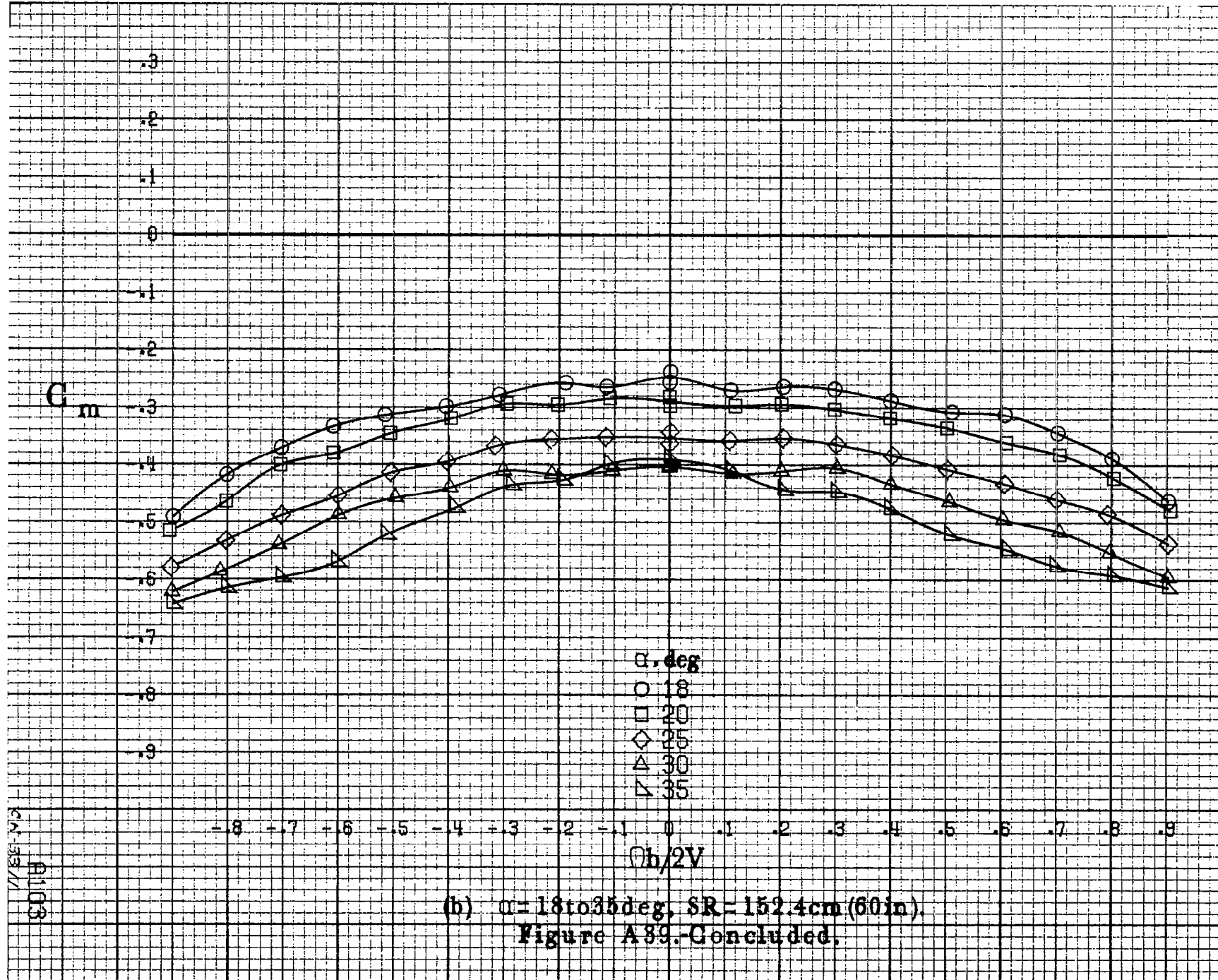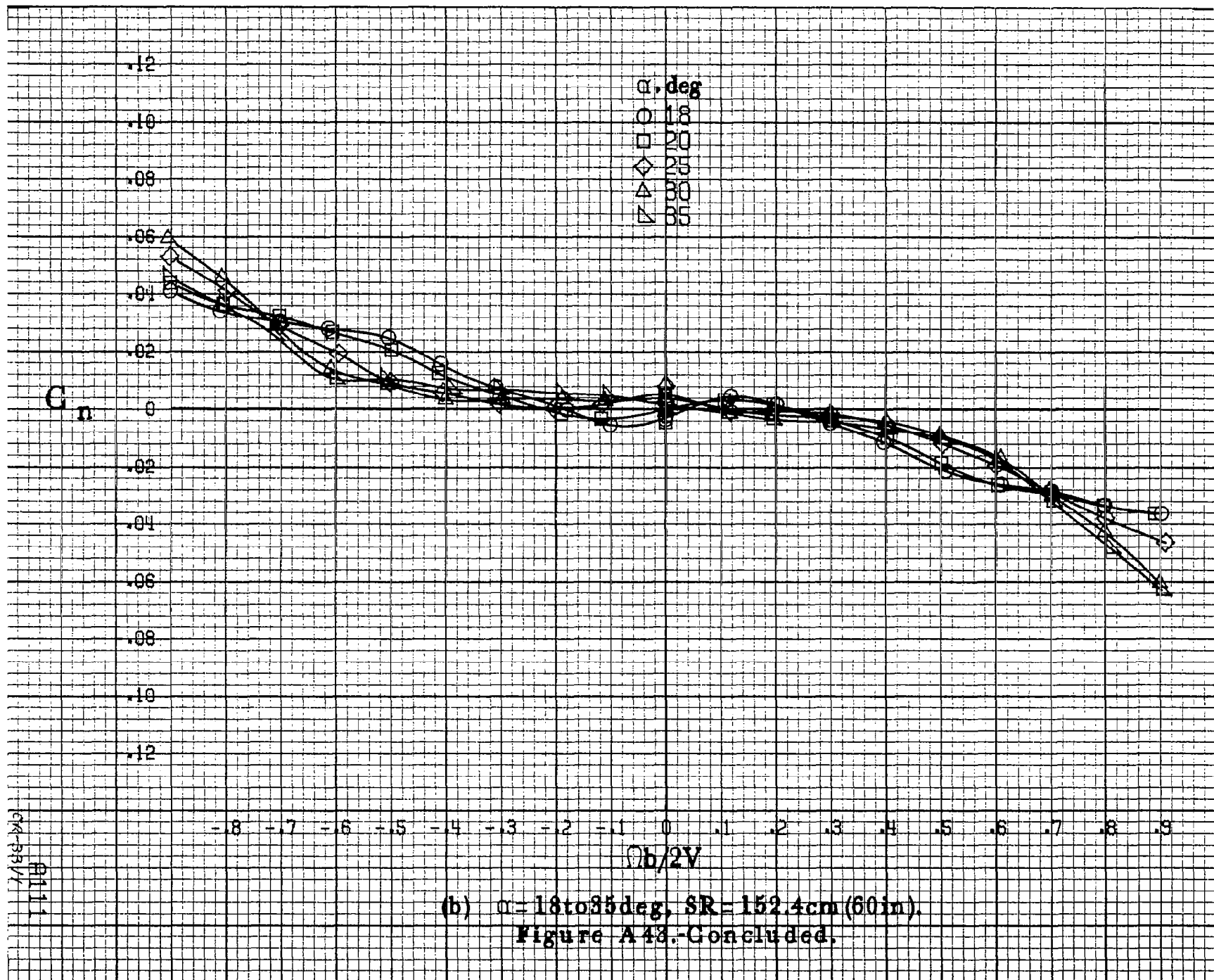
(a) $\alpha = 8$ to 16 deg, $SR = 152.4$ cm (60 in.).

Figure A40.-Effect of rotation rate and angle of attack on normal-force coefficient for canopy fairing configuration. $\delta_e = 0°$, $\delta_a = 0°$, $\delta_r = 0°$, $\beta = 0°$.
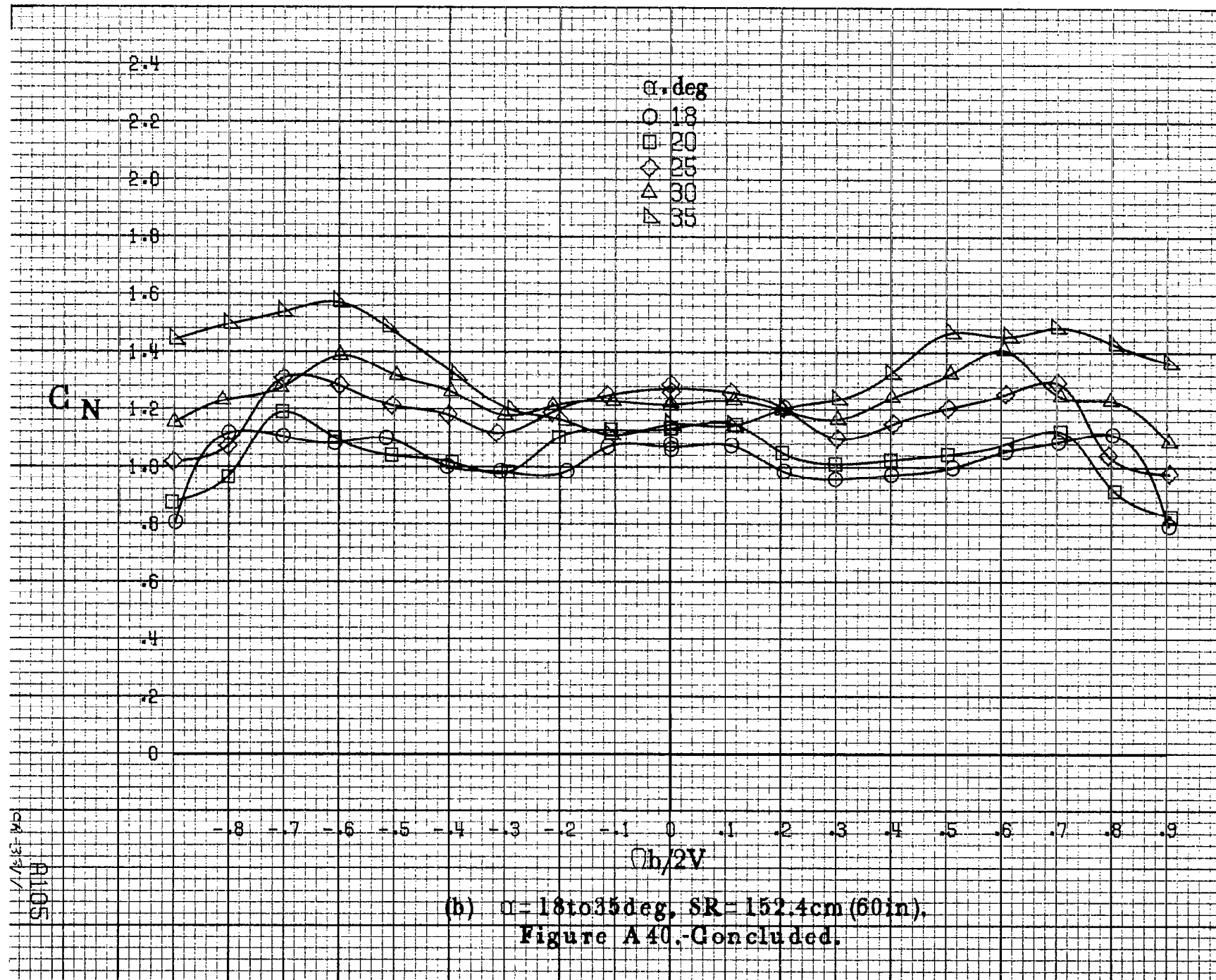
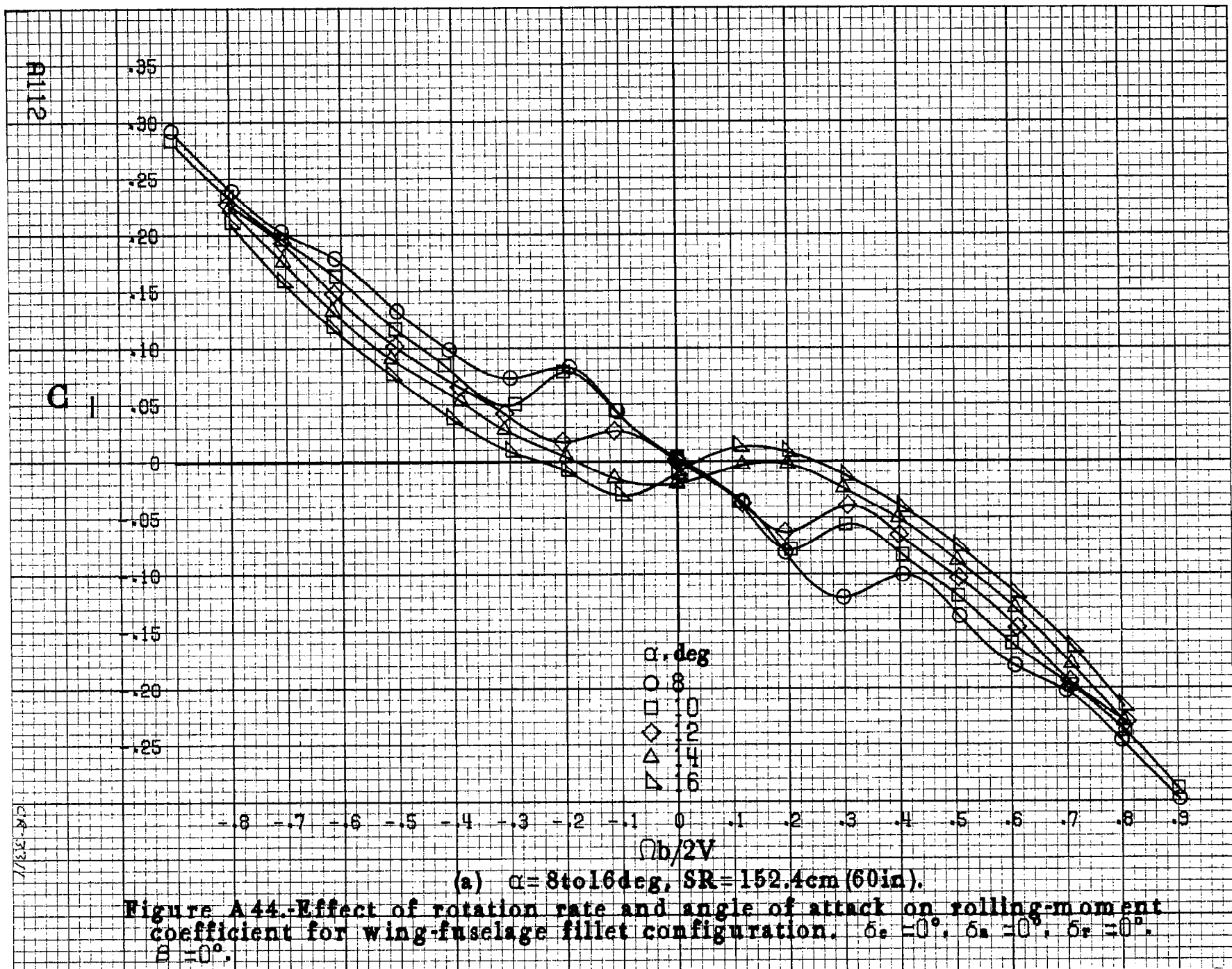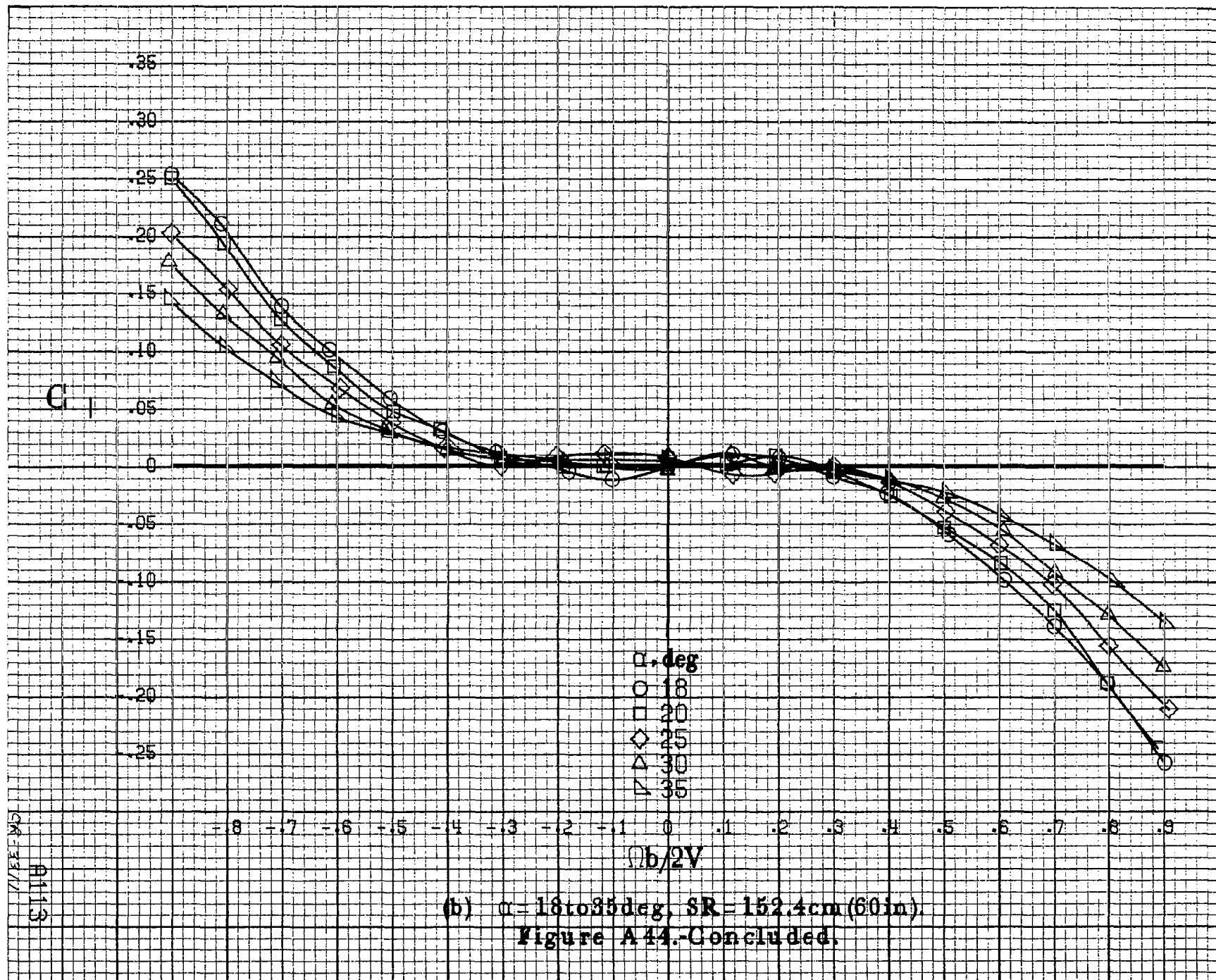(b) α=18 to 35 deg, SR=152.4 cm (60 in).

Figure A40.-Concluded.

(a) α = 8 to 16 deg, SR = 152.4 cm (60 in).
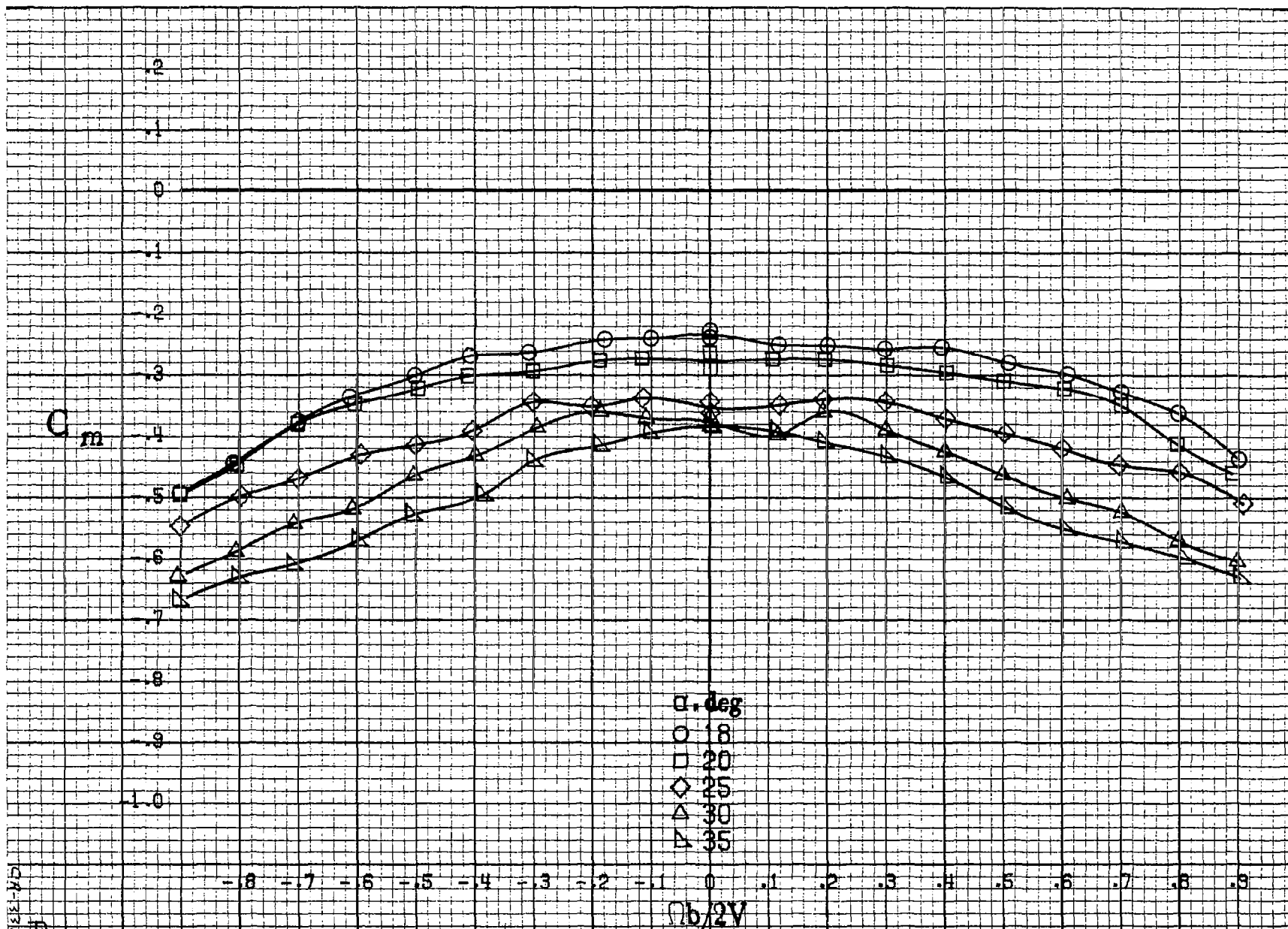
Figure A 41.-Effect of rotation rate and angle of attack on side-force coefficient for canopy fairing configuration. $\delta_e = 0°$, $\delta_a = 0°$, $\delta_r = 0°$. $\beta = 0°$.
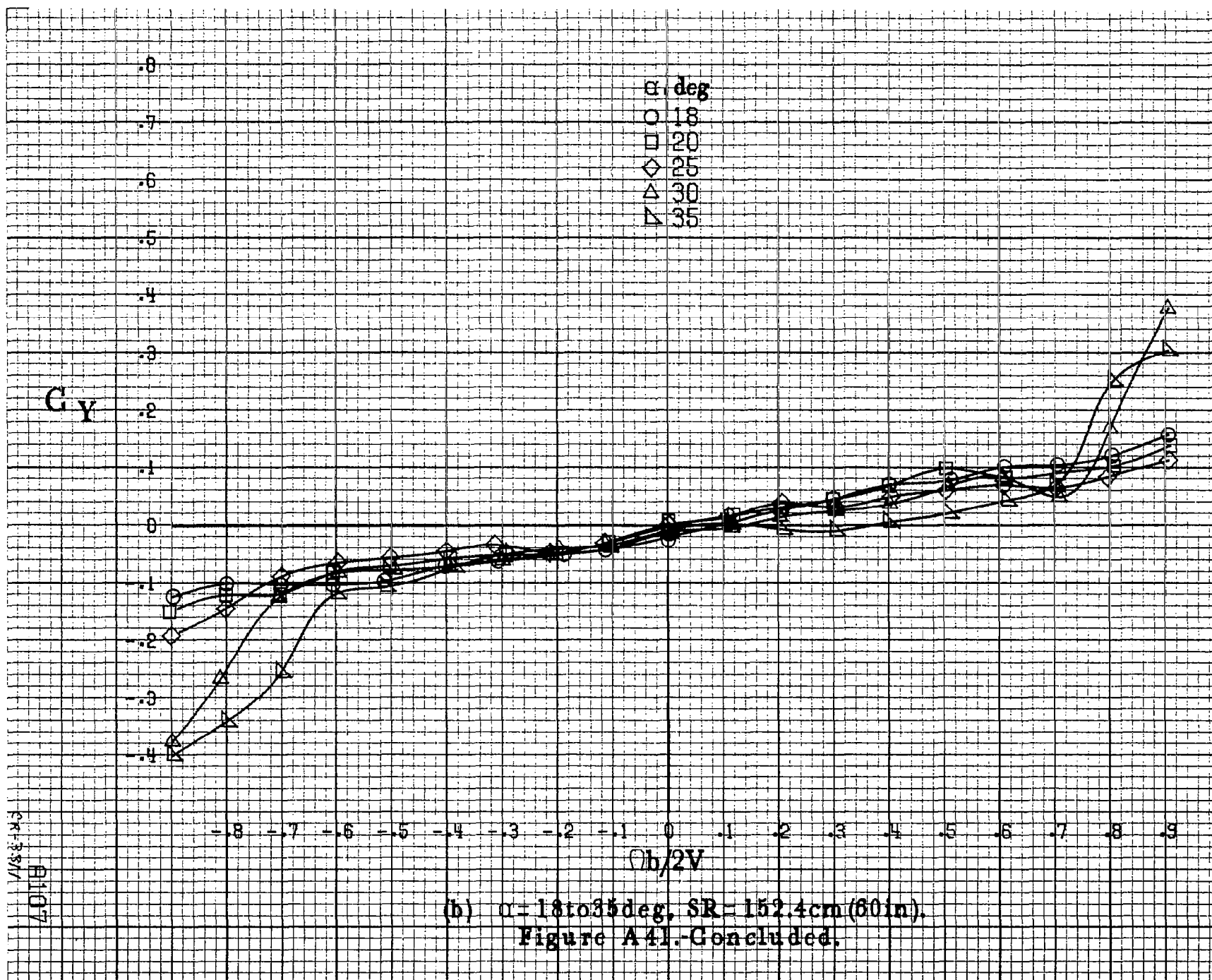
(b) α = 18 to 35 deg, SR = 152.4 cm (60 in).

Figure A41.-Concluded.
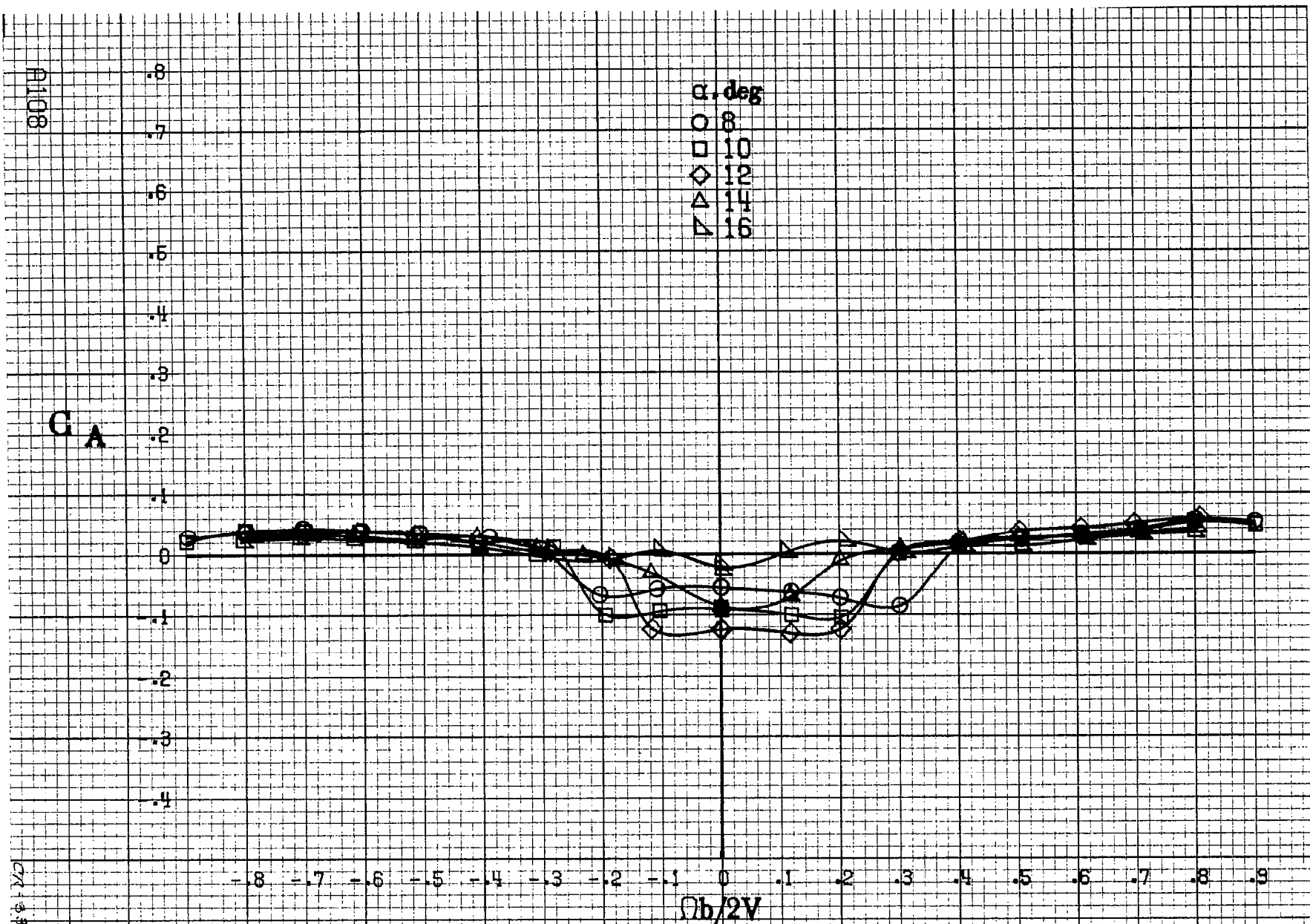
(a) α = 8 to 16 deg, SR = 152.4 cm (60 in).

Figure A 42.-Effect of rotation rate and angle of attack on axial-force coefficient for canopy fairing configuration. $\delta_e = 0°$, $\delta_a = 0°$, $\delta_r = 0°$, $\beta = 0°$.

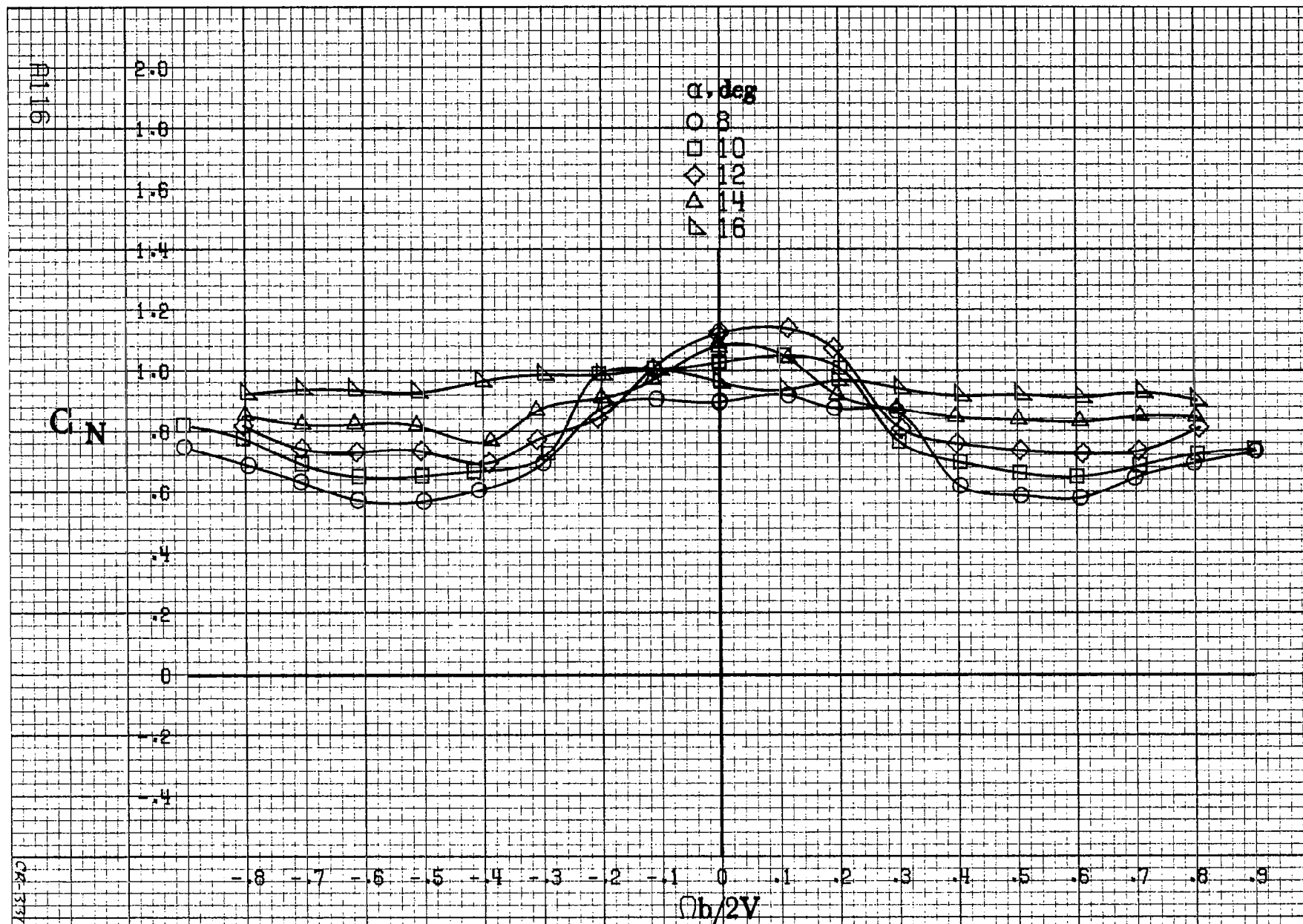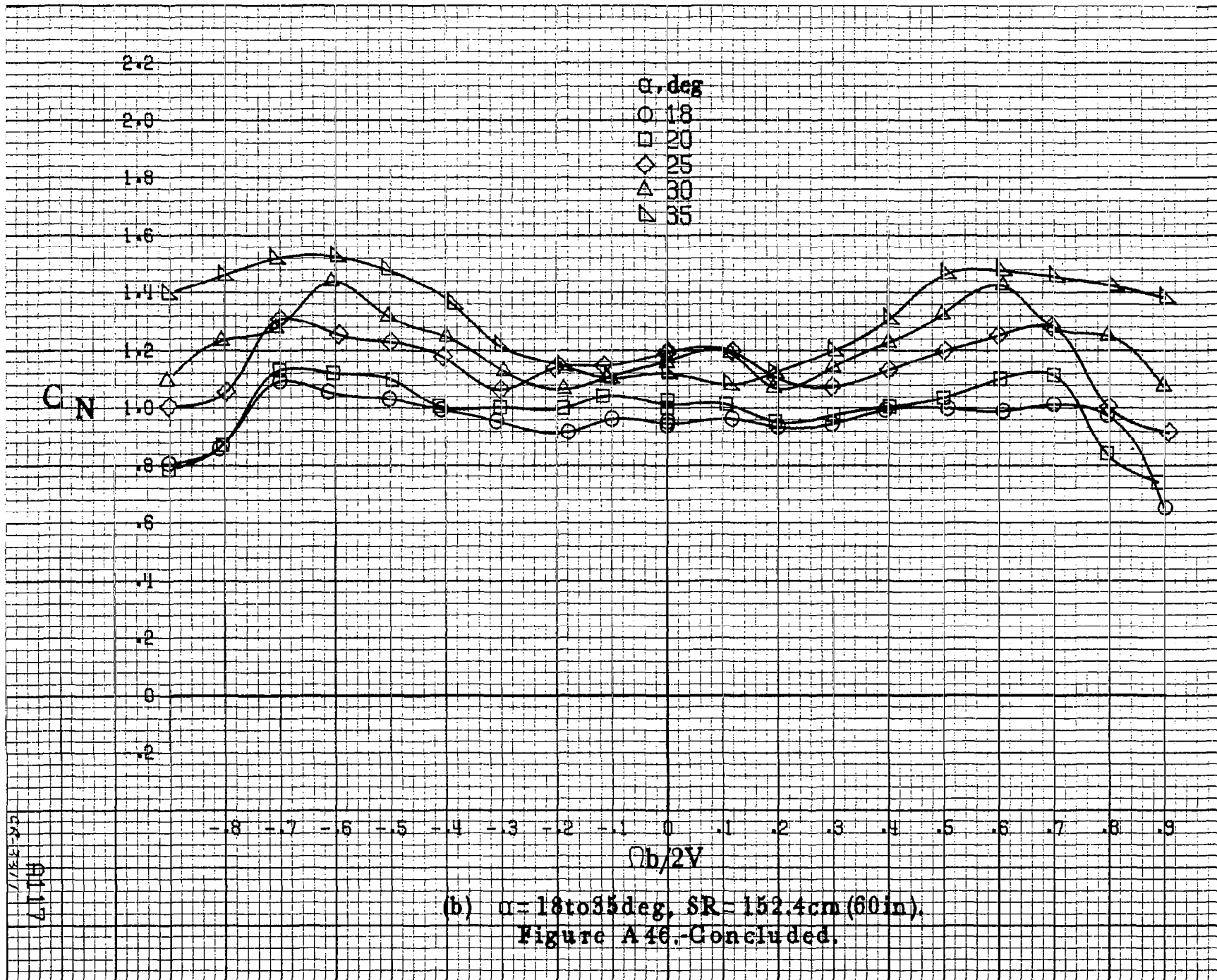(b) α = 18 to 35 deg, SR = 152.4 cm (60 in).

Figure A 42.-Concluded.

(a) α = 8 to 16 deg, SR = 152.4 cm (60 in).

Figure A43.-Effect of rotation rate and angle of attack on yawing-moment
coefficient for wing-fuselage fillet configuration. δₑ = 0°, δₐ = 0°, δᵣ = 0°.
β = 0°.
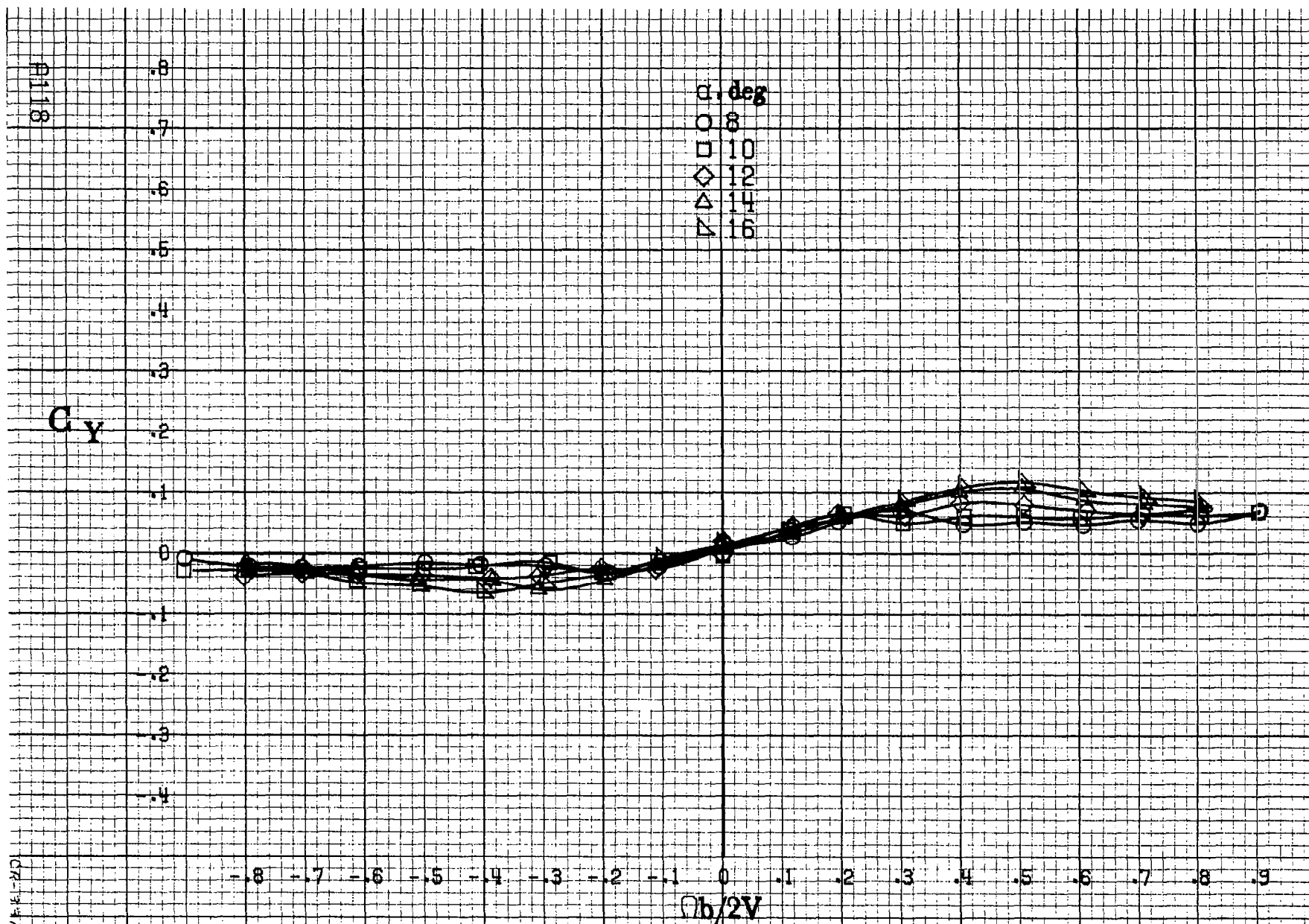
(b) α = 18 to 35 deg, SR = 152.4 cm (60 in).

Figure A43.-Concluded.

(a) α = 8 to 16 deg, SR = 152.4 cm (60 in).

Figure A44.-Effect of rotation rate and angle of attack on rolling-moment coefficient for wing-fuselage fillet configuration. δe = 0°, δa = 0°, δr = 0°. β = 0°.

(b) α = 18 to 35 deg, SR = 152.4 cm (60 in)

Figure A 44.- Concluded.
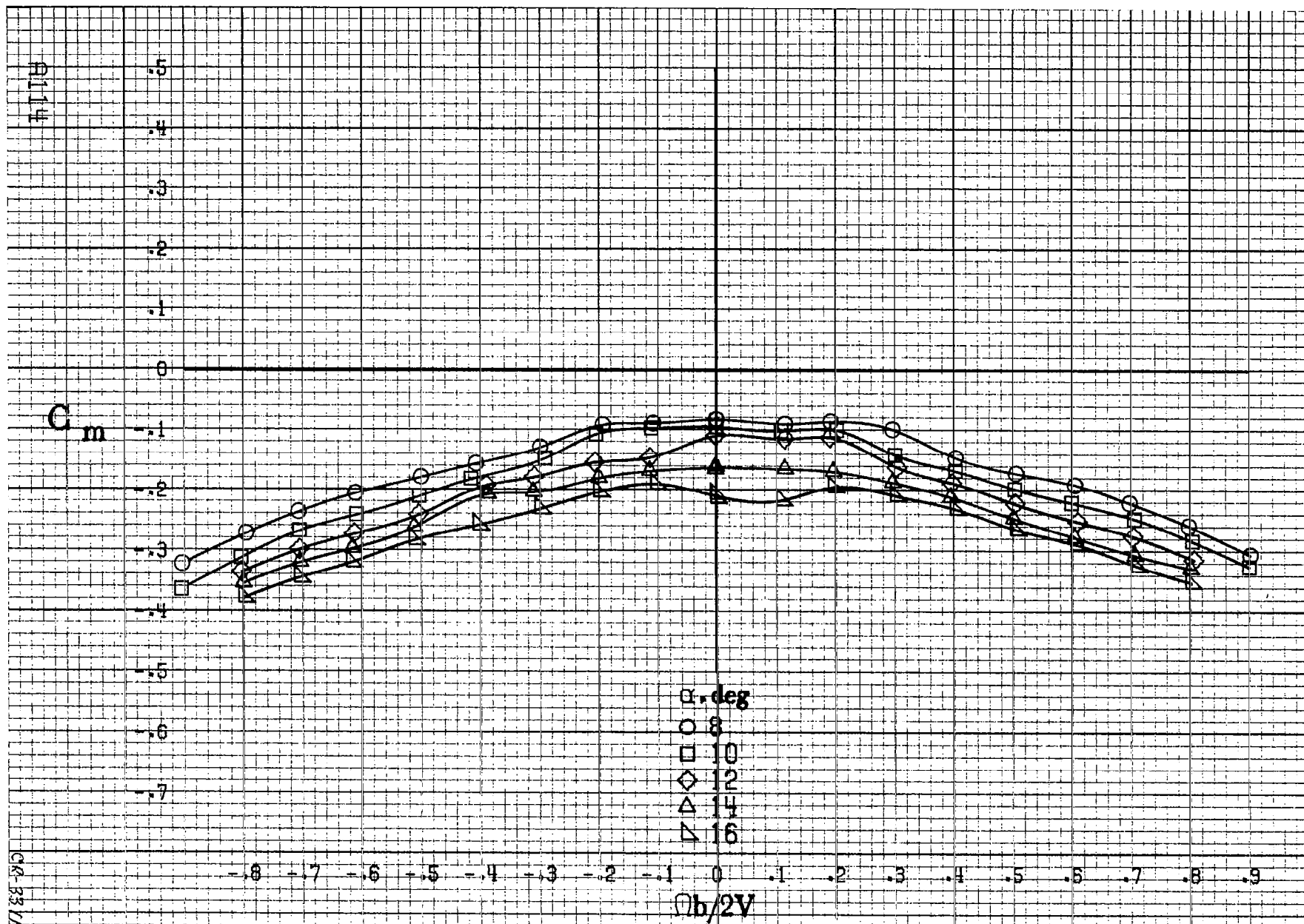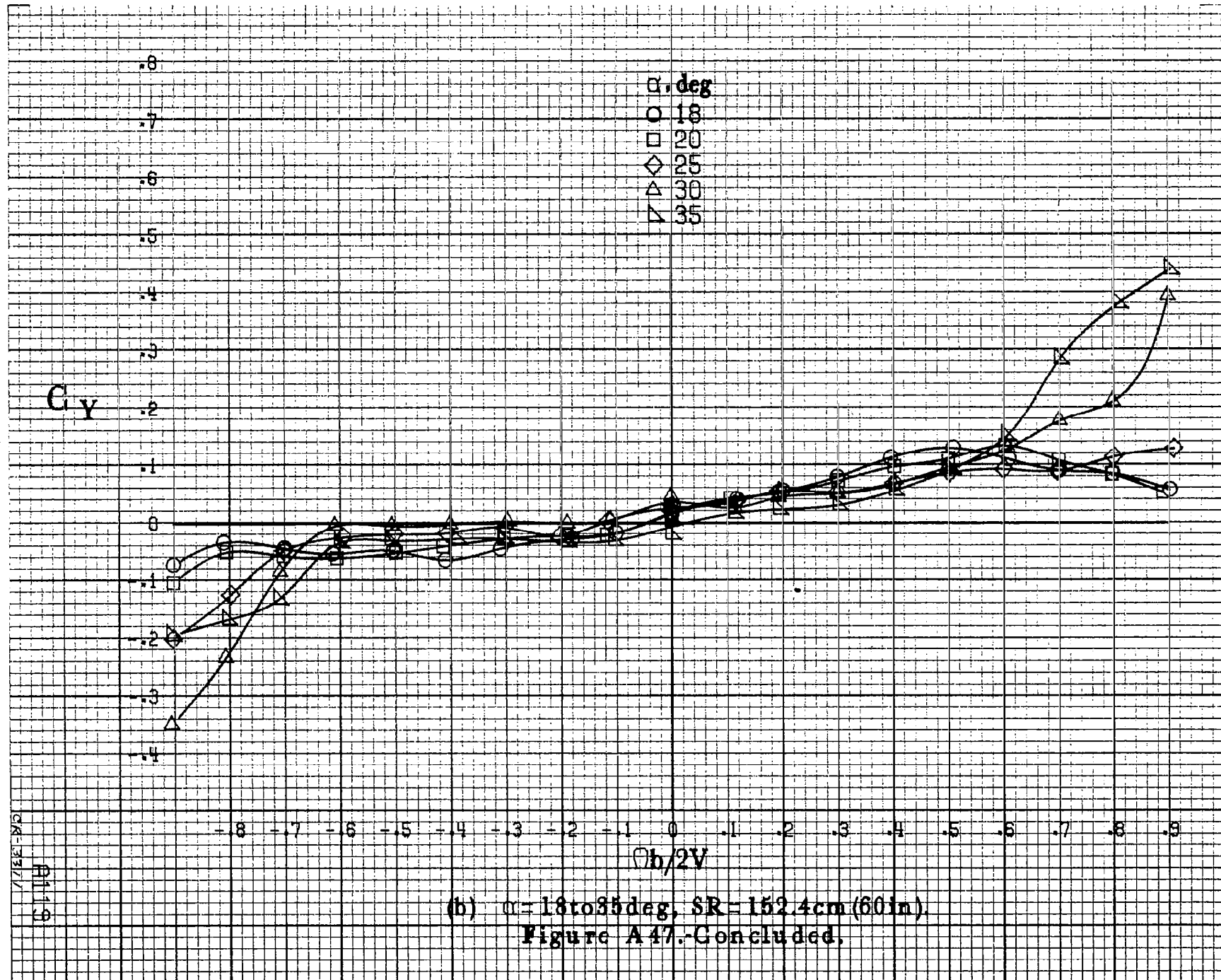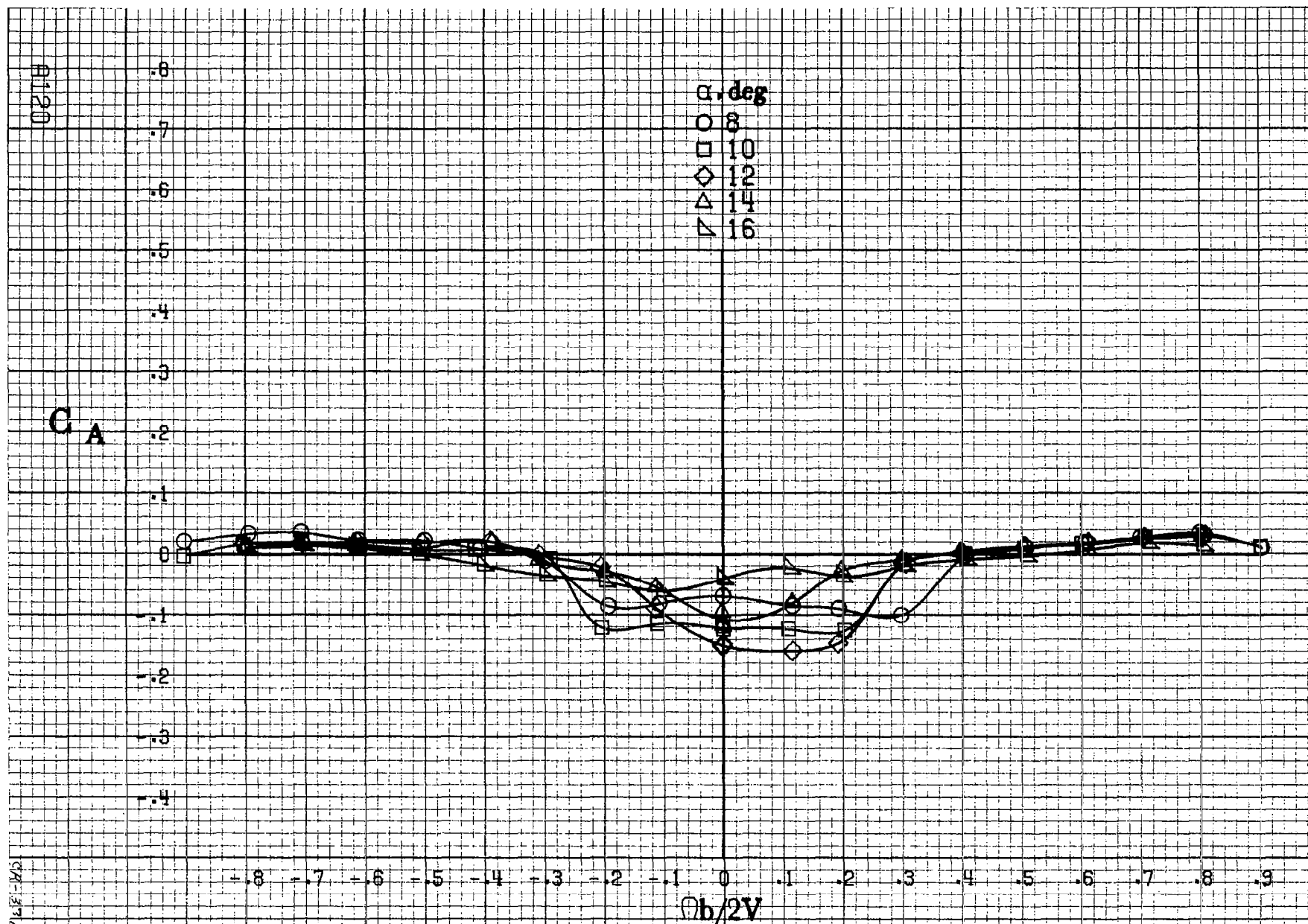
(a) $\alpha = 8$ to 16 deg, $SR = 152.4$ cm (60 in).

Figure A45.-Effect of rotation rate and angle of attack on pitching-moment coefficient for wing-fuselage fillet configuration. $\delta_e = 0°$, $\delta_a = 0°$, $\delta_r = 0°$. $\beta = 0°$.

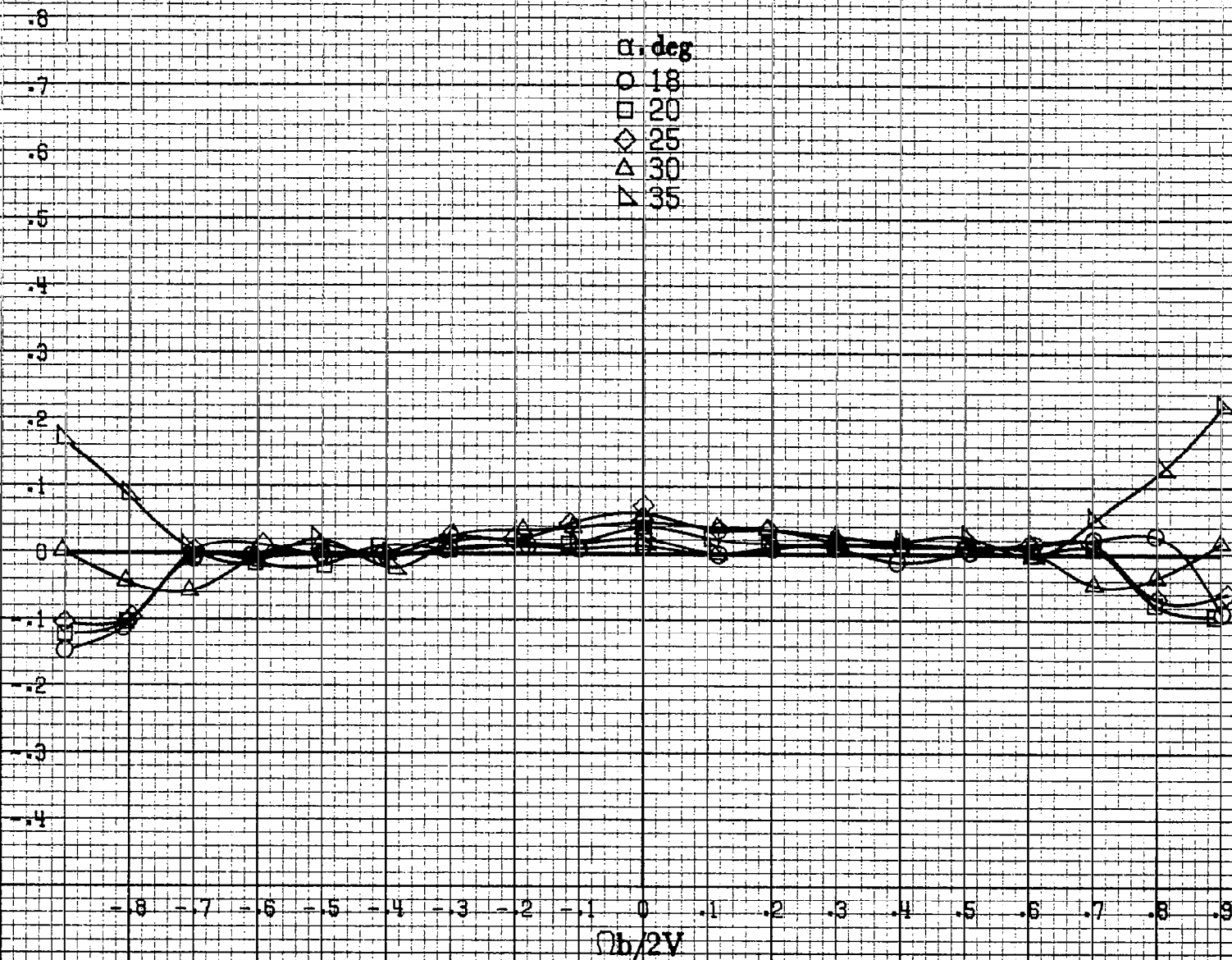(b) α = 18 to 35 deg, SR = 152.4 cm (60 in).
Figure A45.-Concluded.

(a) α = 8 to 16 deg, SR = 152.4 cm (60 in).

Figure A46.-Effect of rotation rate and angle of attack on normal-force coefficient for wing-fuselage fillet configuration. δ_e = 0°, δ_a = 0°, δ_r = 0°, β = 0°.

(b) $\alpha = 18$ to 35 deg, $SR = 152.4$ cm (60 in).

Figure A 46.-Concluded.

(a) α = 8 to 16 deg. SR = 152.4 cm (60 in).

Figure A47.-Effect of rotation rate and angle of attack on side-force coefficient for wing-fuselage fillet configuration. δe = 0°, δa = 0°, δr = 0°. β = 0°.

(b) α = 18 to 35 deg, SR = 152.4 cm (60 in).

Figure A 47.- Concluded.

(a) α = 8 to 16 deg, SR = 152.4 cm (60 in.).

Figure A48.-Effect of rotation rate and angle of attack on axial-force coefficient for wing-fuselage fillet configuration. δe = 0°, δa = 0°, δr = 0°, β = 0°.

(b)   α=18 to 35 deg, SR = 152.4 cm (60 in).

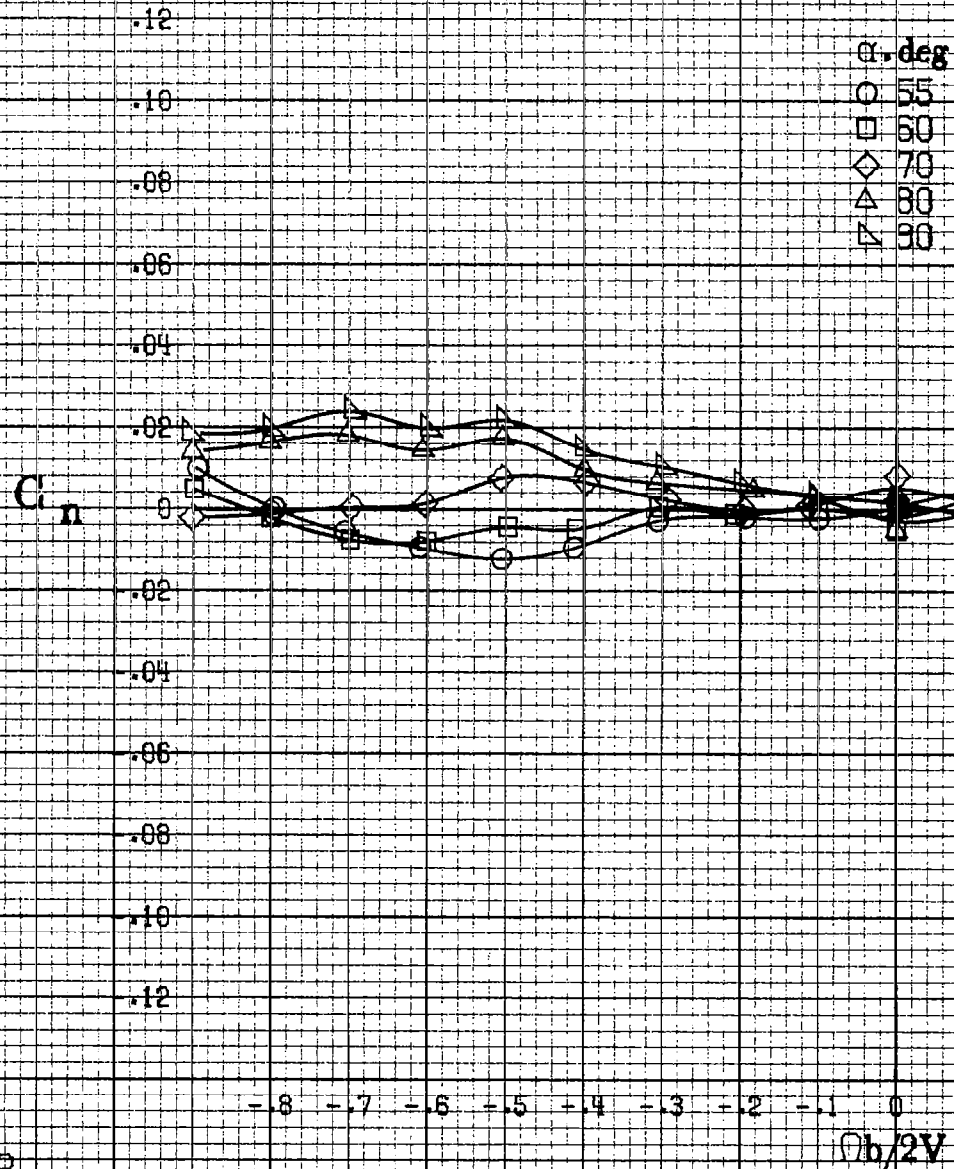Figure A48.-Concluded.

(a) α=8to16deg, SR=152.4cm(60in).
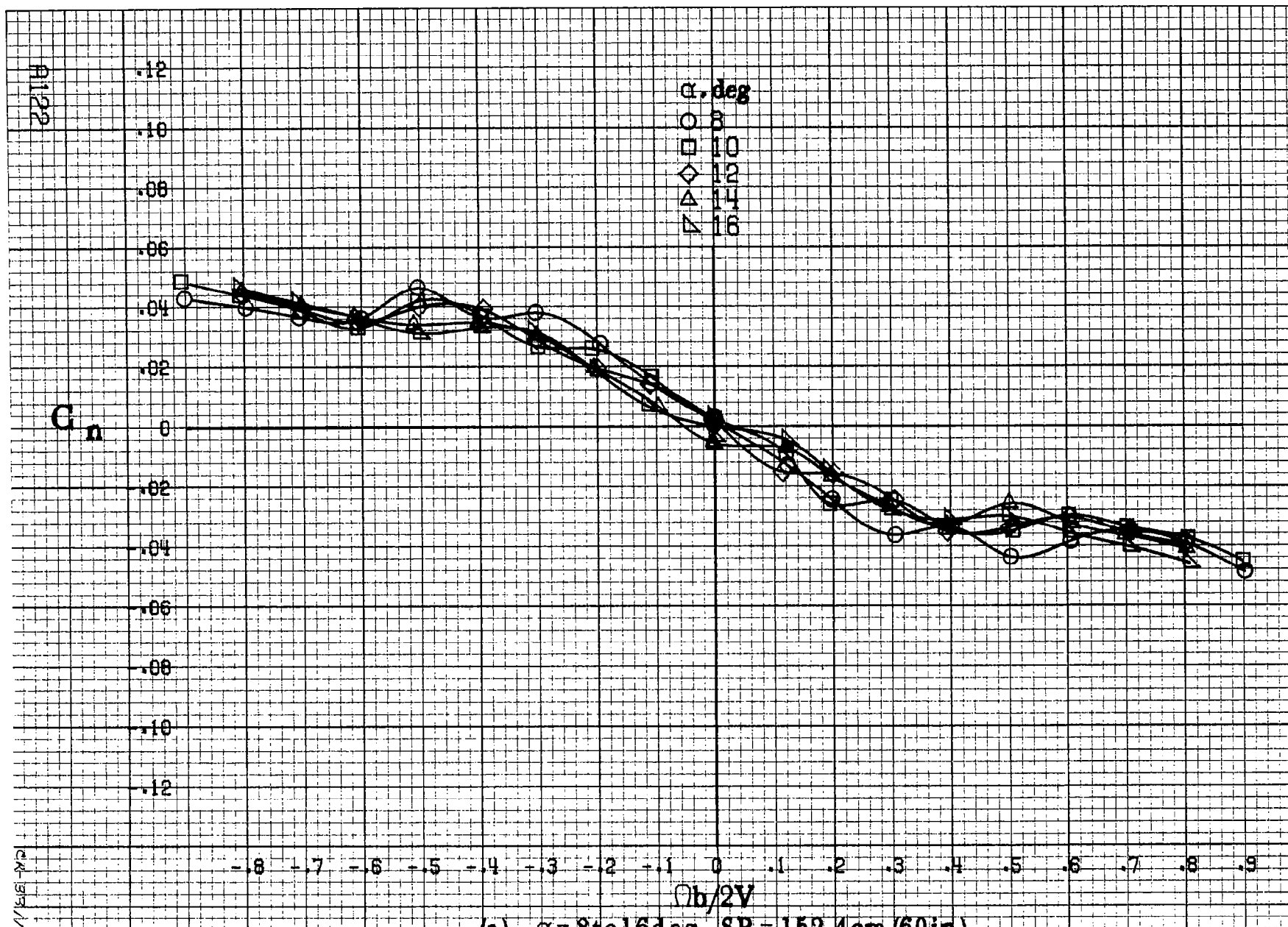
Figure A49.-Effect of rotation rate and angle of attack on yawing-moment coefficient for configuration having wing-fuselage fillet with outboard LE wing droop. δₑ=0°, δₐ=0°, δᵣ=0°. β=0°.

(b) α = 18 to 35 deg, SR = 152.4 cm (60 in).

Figure A.49.- Continued.

(c) α=30to50deg, SR=0.

Figure A49.-Continued.
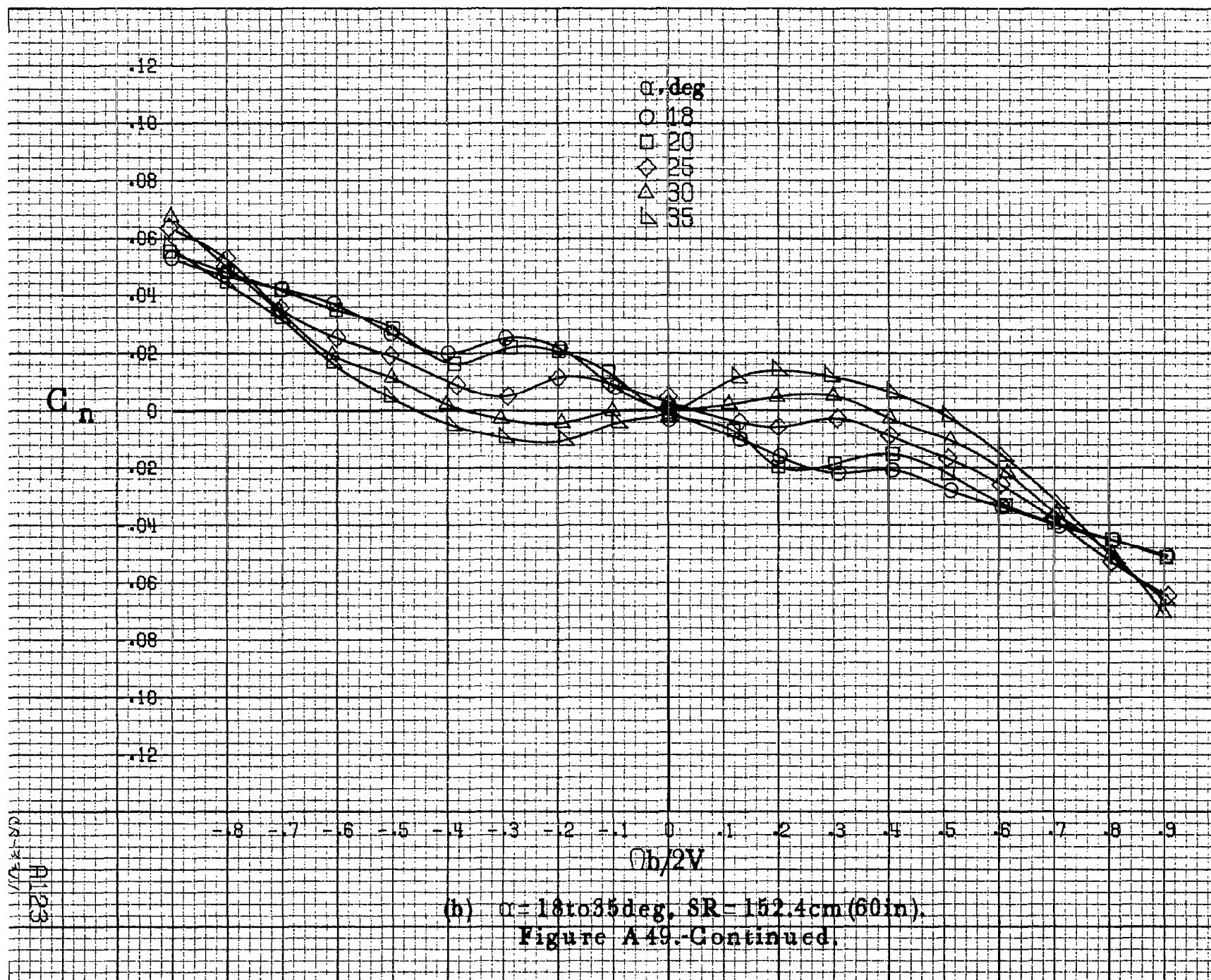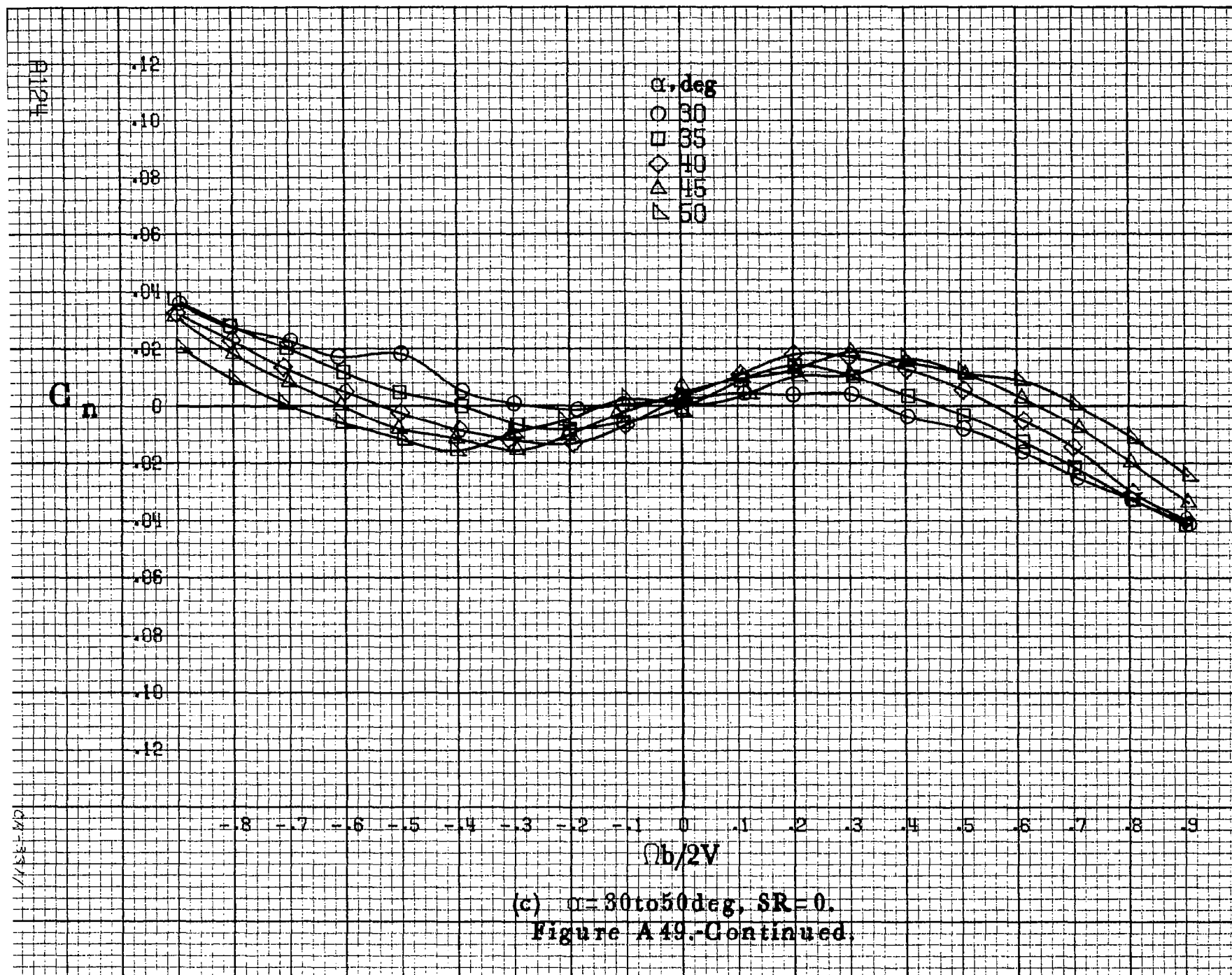
(d) α = 55 to 90 deg, SR = 0.

Figure A 49.-Concluded.

(a) α = 8 to 16 deg, SR = 152.4 cm (60 in).

Figure A50.—Effect of rotation rate and angle of attack on rolling-moment coefficient for configuration having wing-fuselage fillet with outboard LE wing droop. $\delta_e = 0°$, $\delta_a = 0°$, $\delta_r = 0°$, $\beta = 0°$.
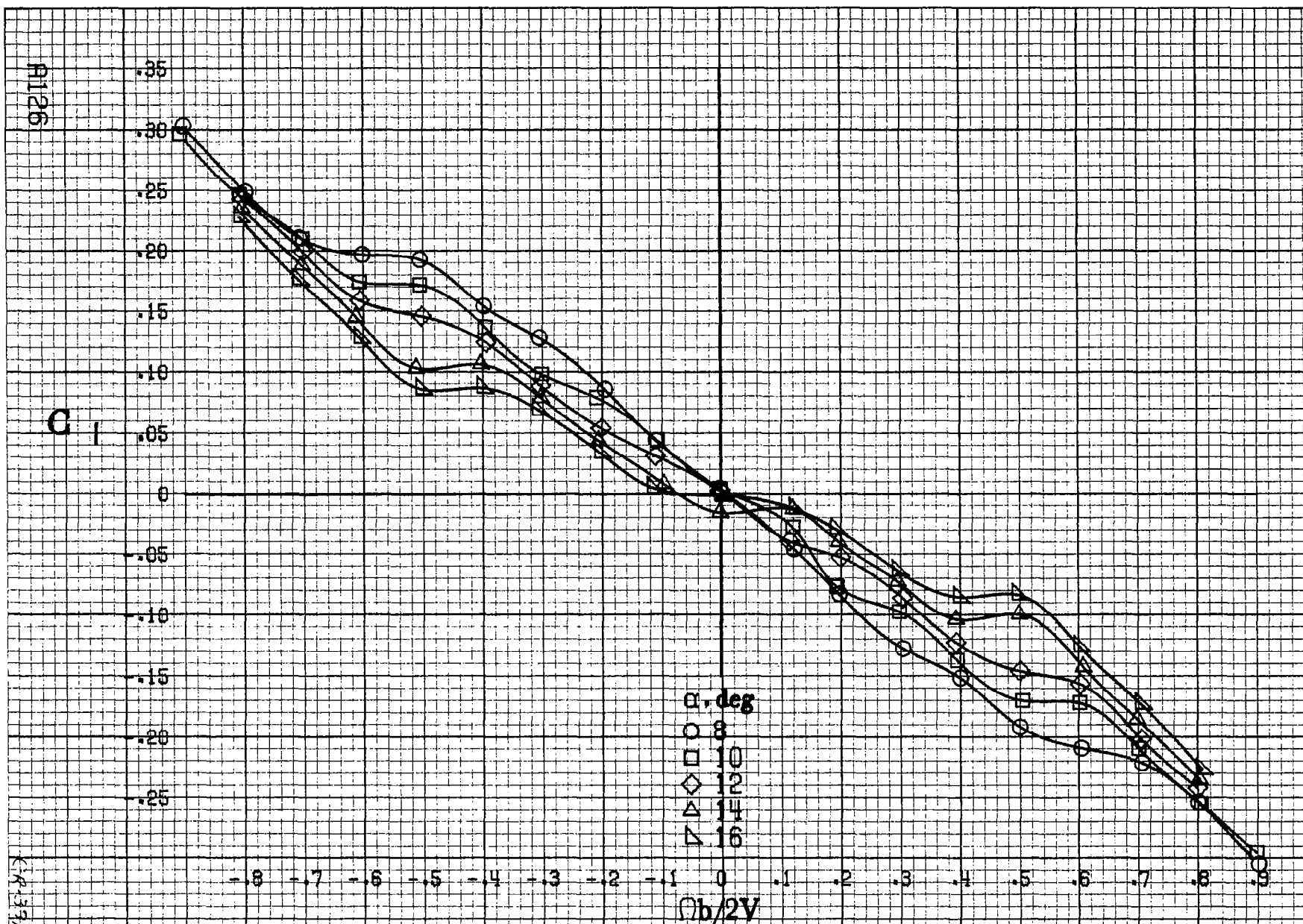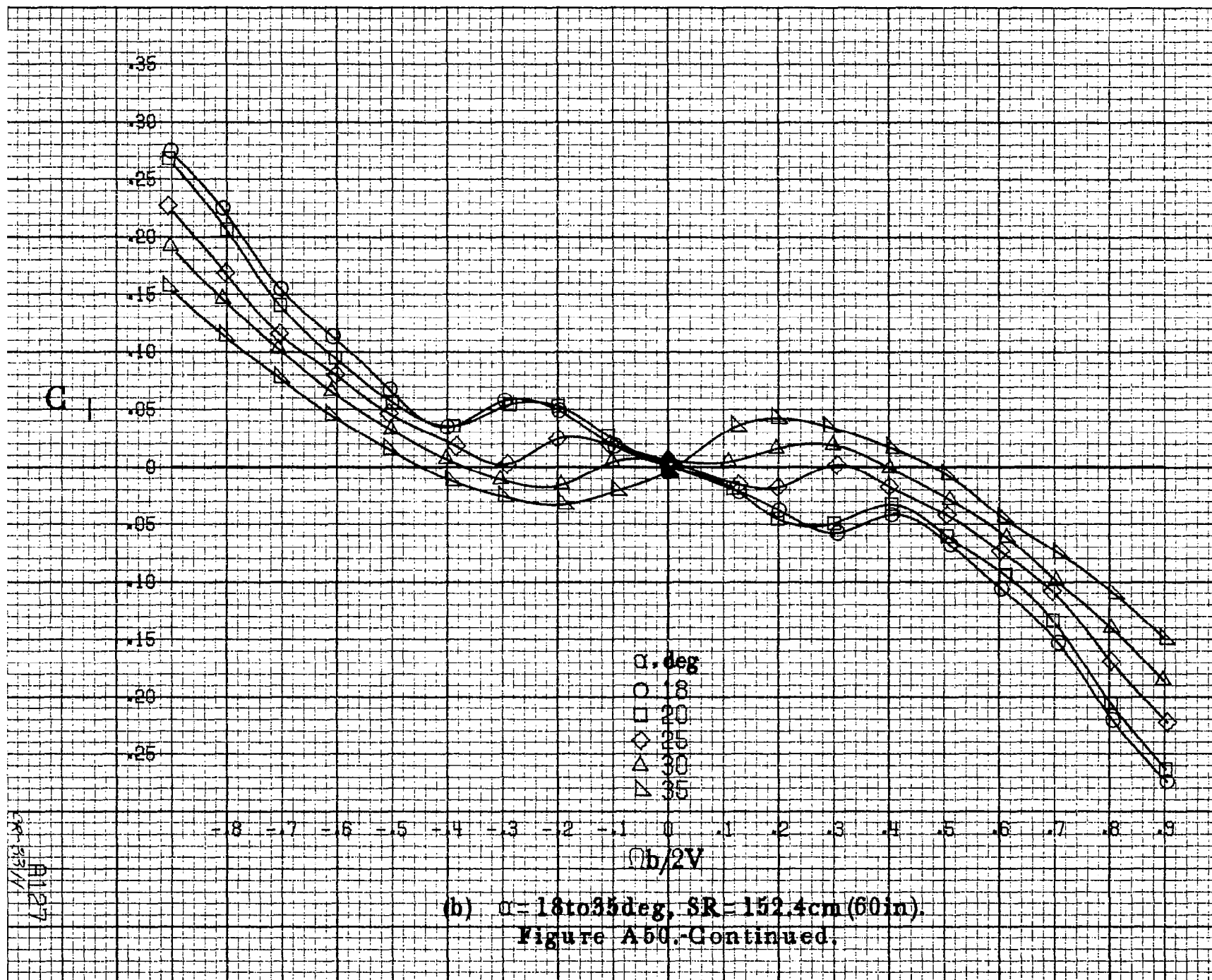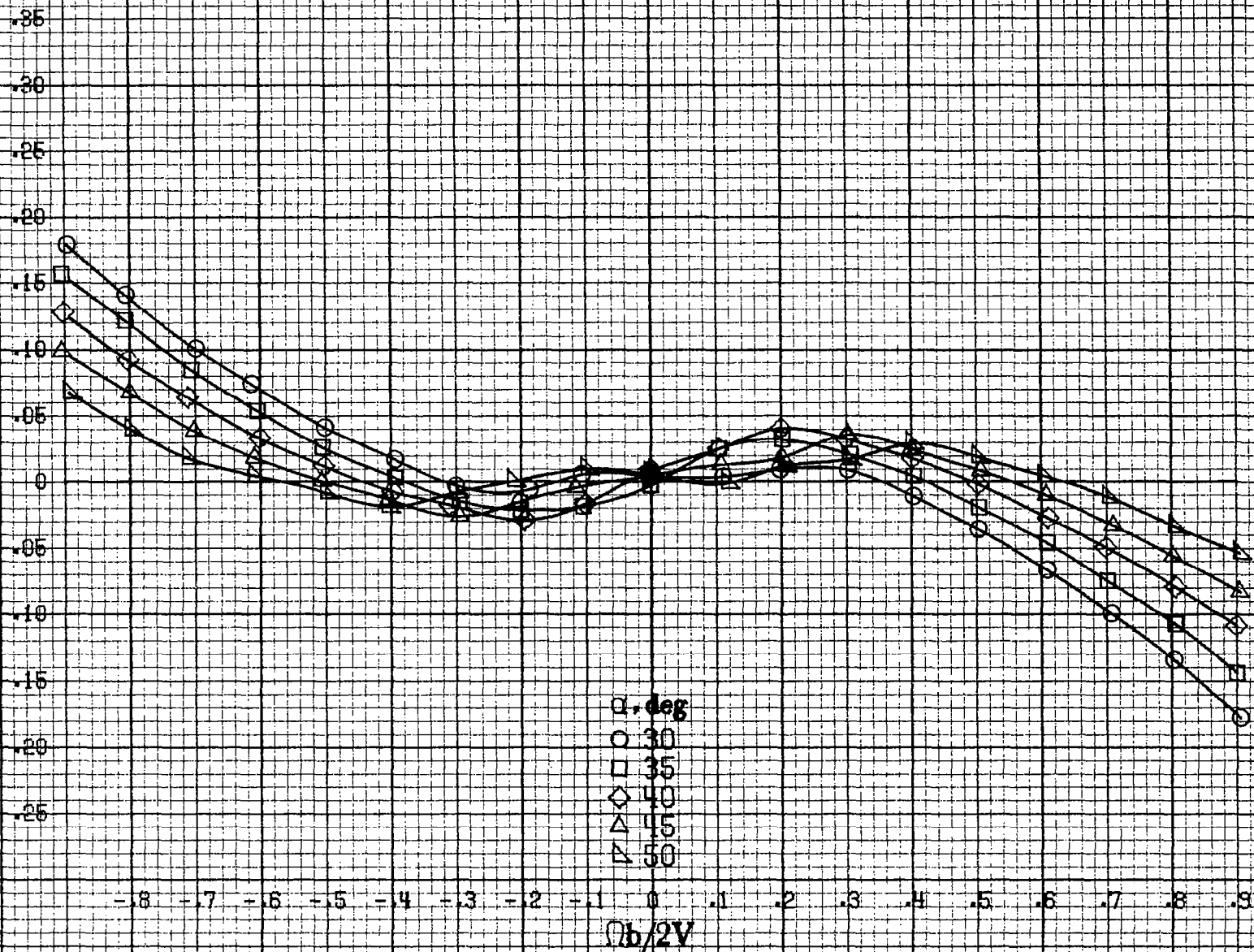
(b) α = 18 to 35 deg, SR = 152.4 cm (60 in).

Figure A50.-Continued.

(c) α = 30 to 50 deg, SR = 0.

Figure A50.-Continued.

(d) α = 55 to 90 deg, SR = 0.

Figure A50.- Concluded.
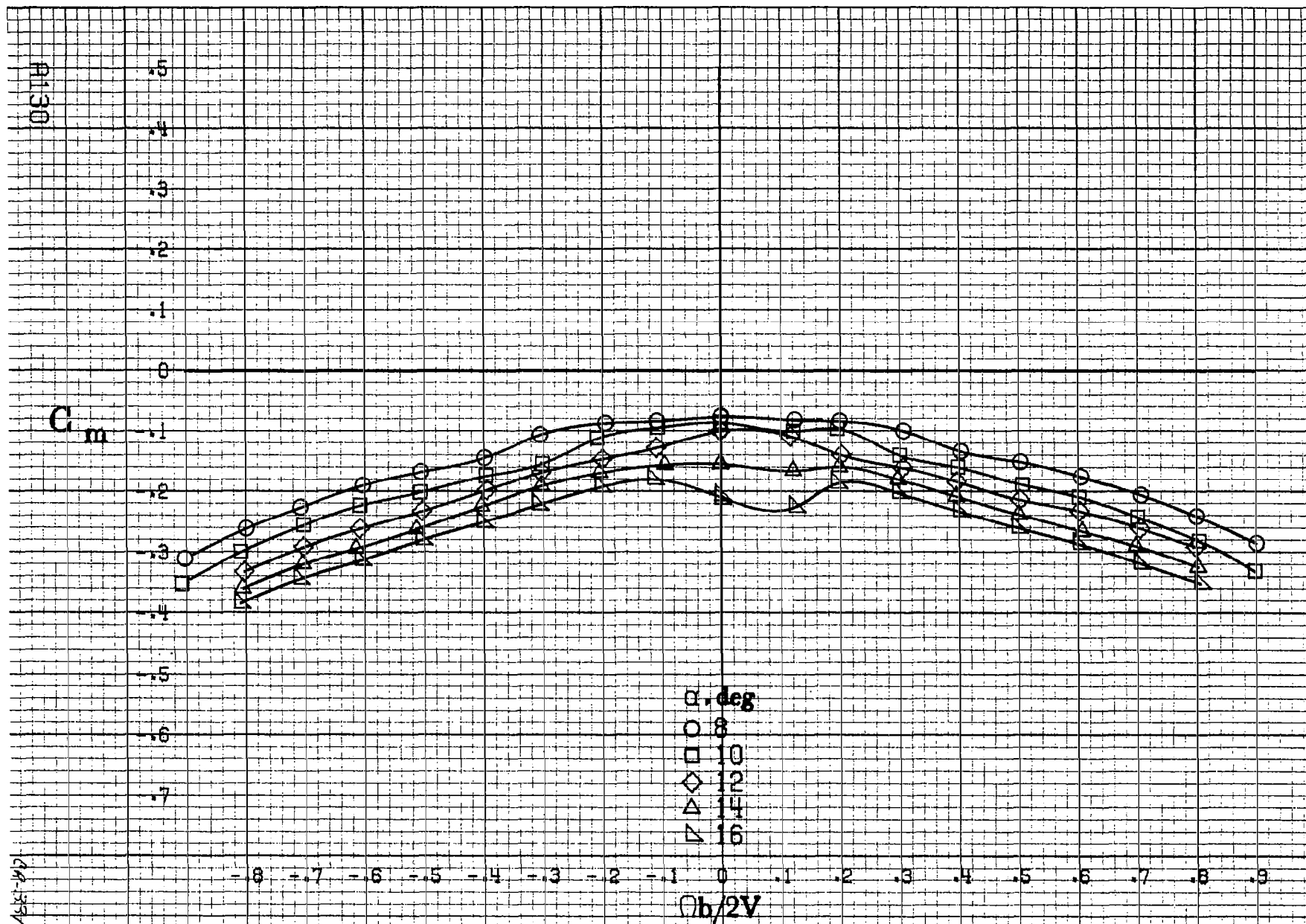
(a) α=8to16deg, SR=152.4cm(60in).

Figure A51.-Effect of rotation rate and angle of attack on pitching-moment
coefficient for configuration having wing-fuselage fillet with outboard LE
wing droop. δe =0°, δa =0°, δr =0°. β =0°.